Searching for Pulsars with the Effelsberg Telescope

Dissertation

zur

Erlangung des Doktorgrades (Dr. rer. nat.)

der

Mathematisch-Naturwissenschaftlichen Fakultät

der

Rheinischen Friedrich-Wilhelms-Universität Bonn

vorgelegt von

Ewan Daniel Barr

aus

Glasgow, Schottland

Submitted 15.11.2012

Angefertigt mit Genehmigung der Mathematisch-Naturwissenschaftlichen Fakultät der Rheinische Friedrich-Wilhelms-Universität Bonn

Berichterstatter:

Prof. Dr. M. Kramer

Prof. Dr. N. Langer

Tag der Promotion: 08.04.2013

Erscheinungsjahr: 2013

"Once we were blobs in the sea, and then fishes, and then lizards and rats, and then monkeys, and hundreds of things in between. This hand was once a fin, this hand once had claws! In my human mouth I have the pointy teeth of a wolf and the chisel teeth of a rabbit and the grinding teeth of a cow! Our blood is as salty as the sea we used to live in! When we're frightened, the hair on our skin stands up, just like it did when we had fur. We ARE history! Everything we've ever been on the way to becoming us, we still are. Would you like the rest of the story? I'm made up of the memories of my parents and my grandparents, all my ancestors. They're in the way I look, in the color of my hair. And I'm made up of everyone I've ever met who's changed the way I think."

Sir Terry Pratchett

RHEINISCHE FRIEDRICH-WILHELMS-UNIVERSITÄT BONN

Abstract

The Faculty of Mathematics and Natural Sciences

Doctor of Philosophy

by Ewan Daniel Barr

Pulsar searches have the potential to teach us much about the Universe in which we live. From the discovery of highly magnetised pulsars that enable detailed study of classical and quantum electrodynamics, to extremely stable, rapidly-rotating pulsars that will form integral parts of a timing array for the direct detection of gravitational waves, new pulsar discoveries are highly desirable.

The high sensitivity of the Effelsberg telescope makes it one of the most powerful pulsar survey instruments in existence. Yet, despite this fact, the telescope has seen limited use by pulsar searchers. This thesis marks the beginning of a new era at Effelsberg, with 13 pulsars being discovered in this work, including two rapidly-rotating millisecond pulsars. These pulsars represent the first output from a new wave of pulsar surveys that use the state-of-the-art instrumentation at Effelsberg to observe the dynamic radio sky with unprecedented time and frequency resolution.

To begin with, I present an introduction to pulsars, giving a brief overview of their observational characteristics and currently accepted evolutionary models (Chapter 1). I then go on to discuss the intricacies of performing a modern pulsar search. Here we review the techniques needed to go from a signal entering the receiver, to a pulsar discovery being made (Chapter 2). Having established the required knowledge base for the reader, I then present the methods and results of five diverse pulsar searches conducted as part of this work.

The first of these surveys, deals with the hunt for radio-loud pulsars in γ-ray sources from the *Fermi* LAT First Source Catalog. Here, we have performed sensitive radio observations of 289 γ-ray sources with no known association, leading to the discovery of the 2.65-ms pulsar J1745+1017. Through an extensive timing campaign involving three of Europe's largest radio telescopes, we have shown J1745+1017 to be a member of a new population of tight binary pulsars with very low-mass companions. Furthermore, through phase folding of the LAT γ-ray photons, we conclusively show J1745+1017 to

be a pulsed γ-ray emitter. The high number of sources observed in this survey, make it the largest exploration of the LAT sky at radio frequencies (Chapter 3).

The second survey presented, is the High Time Resolution Universe North pulsar survey (HTRU-North). This is an ambitious project to, in tandem with a partner survey using the Parkes radio telescope, perform an all-sky search for pulsars and fast transients. Here, we describe the strategy and sensitivity of our survey, and perform simulations of the expected discovery yield. This survey has already resulted in the discovery of 12 new pulsars, the timing parameters of which are presented. We close by discussing two of the survey's discoveries; PSR J1946+3414, a Galactic-disk millisecond pulsar in a highly-eccentric binary system, and PSR J2004+3427, a pulsar with a characteristic age of < 19 kyr (Chapter 4).

Finally, I describe targeted pulsar search observations of three objects of interest; 1RXS J141256.0+792204 (Calvera), an unidentified source of pulsed X-ray emission; SN 2008iz, a recent radio supernova in the M82 galaxy; and SGR 1833−0832, a recently discovered magnetar in outburst. No transient or periodic radio emission was detected from these sources. For each source, we discuss the implications of our non-detection and look at the possibilities for future observations (Chapter 5).

I close the thesis by looking at what the future holds for pulsar searching.

RHEINISCHE FRIEDRICH-WILHELMS-UNIVERSITÄT BONN

Zusammenfassung

Der Mathematisch-Naturwissenschaftlichen Fakultät

Doktorarbeit

von Ewan Daniel Barr

Die Suche nach Pulsaren hat das Potenzial, uns viel über das Universum zu lehren, in welchem wir leben. Von der Entdeckung stark magnetisierter Pulsare, welche das detaillierte Studium der klassischen und Quantenelektrodynamik ermöglichen, hin zu extrem stabilen, schnell rotierenden Pulsaren, die integraler Bestandteil eines Timing-Array für den direkten Nachweis von Gravitationswellen bilden, sind neue Pulsarentdeckungen höchst erstrebenswert.

Die hohe Empfindlichkeit des Effelsberg-Teleskopes macht es zu einem der mächtigsten existierenden Instrumente für die Pulsarsuche. Doch trotz dieser Tatsache wurde das Teleskop nur eingeschränkt für die Pulsarsuche genutzt. Diese Doktorarbeit markiert den Beginn einer neuen Ära in Effelsberg, mit 13 in dieser Arbeit entdeckten Pulsare, darunter zwei schnell rotierende Millisekunden-Pulsare. Diese Pulsare stellen die ersten Ergebnisse einer neuen Welle von Pulsarkatalogen dar, welche die state-of-the-art Instrumente in Effelsberg nutzen, um den dynamischen Radiohimmel mit beispielloser Zeit- und Frequenzauflösung zu beobachten.

Dieser Arbeit beginnt mit einer Einführung in das Thema Pulsar-Astronomie, welche aus einem kurzen Überblick über ihre Beobachtungen, Eigenschaften und momentan gültigen evolutionären Modelle besteht (Kapitel 1). Anschließend diskutiere ich die Feinheiten bei der Durchführung einer modernen Pulsarsuche. Hier beschreiben ich die erforderlichen Techniken, um von dem Signal eines Receivers zu einer Pulsarentdeckung zu gelangen (Kapitel 2). Nachdem die erforderliche Wissensbasis für den Leser hergestellt wurde, präsentiere ich die Methoden und Ergebnisse von fünf verschiedenartigen Pulsarsuchen, die als Teil dieser Arbeit durchgeführt wurden.

Die Erste dieser Studien beschäftigt sich mit der Jagd nach radiolauten Pulsaren in Gamma-Quellen aus dem *Fermi* LAT First Source Catalog. Hier haben wir empfindliche Radiobeobachtungen von 289 Gamma-Quellen mit unbekannter Herkunft durchgeführt, was zu der Entdeckung des 2,65-ms Pulsar J1745+1017 führte. Durch eine umfangreiche Timing-Kampagne mit drei der größten Radioteleskope Europas haben wir gezeigt, dass

J1745+1017 ein Mitglied einer neuen Population von engen binären Pulsaren ist, mit einem Begleiter von sehr geringer Masse. Darüber hinaus, durch Phasenfaltung der LAT Gammaphotonen, zeigen wir schließlich, dass J1745+1017 ein gepulster Gammastrahlenaussender ist. Die hohe Anzahl von beobachteten Quellen in dieser Studie, macht es zu der größten Untersuchung des LAT Himmels bei Radiofrequenzen (Kapitel 3).

Die zweite präsentierte Vermessung ist die High Time Resolution Universe North Pulsarsuche (HTRU-North). Dies ist ein anspruchsvoll Projekt in Zusammenarbeit mit dem Parkes-Radioteleskop, welches den gesamten Himmel nach Pulsaren und schnellen Transienten durchsucht. Hier beschreiben wir die Strategie und die Sensibilität unserer Suche und führen Simulationen zur erwarteten Ausbeute der Entdeckungen durch. Diese Suche führte bereits zu der Entdeckung von 12 neuen Pulsaren, dessen Timing-Parameter vorgestellt werden. Wir schließen mit der Diskussion zweier der Entdeckungen aus dieser Suche; PSR J1946+3414, ein Millisekunden-Pulsar aus der galaktischen Ebene in einem hoch-exzentrischen binären System und PSR J2004+3427, ein Pulsar mit einem charakteristischen Alter von < 19 Kilojahren (Kapitel 4).

Abschließend beschreibe ich gezielte Beobachtungen zur Pulsarsuche von drei interessanten Objekten; 1RXS J141256.0+792.204 (Calvera), eine nicht identifizierte Quelle gepulster Röntgenstrahlung; SN 2008iz, eine aktuelle Radio-Supernova in der Galaxie M82 und SGR 1833−0832, ein kürzlich entdeckter Magnetar im Ausbruch. Keine vorübergehende oder periodische Radiostrahlung wurde in diesen Quellen entdeckt. Für jede Quelle diskutieren wir die Auswirkungen unserer Nicht-Detektion und schauen nach Möglichkeiten für zukünftige Beobachtungen (Kapitel 5).

Ich schließe diese Arbeit mit einem Ausblick darüber, was die Zukunft für die Pulsarsuche bereit hält.

Acknowledgements

In the last three years, I have had the great fortune to work with an group of people who I not only consider to be fantastic scientists, but also friends. First and foremost, I would like to thank my supervisors Dr. David Champion and Prof. Dr. Michael Kramer, mainly for putting up with me, but also for guiding me and giving me the opportunity to be involved in something that I truly enjoy. In particular, I would like to thank David for teaching me many tricks of the trade and for not losing the plot at my numerous, daft questions.

I wish to extend my gratitude to all members of the Bonn pulsar group, each of whom have influenced me in one way or another. Singling out a few members in no particular order...

Thank you to Lucas Guillemot, for getting me through my first paper writing experience and being irrepressibly genial; Ramesh Karuppusamy, for teaching me the intricacies of all things digital; Joris Verbiest, for, among many other things, his phenomenal work in proof reading this thesis and providing comments; Aris Noutsos, for showing that very small changes in the initial conditions can lead a conversation anywhere (is this not the very definition of chaos?); Paulo Freire, for expanding my mind on a most bizarre and diverse range of subjects; Ralph Eatough for making sure that the bus did not leave without me; Evan Keane for not rubbing it in too hard when the Republic won the Nations Cup.

I wish to thank all the students who have kept me sane and provided banter throughout these three years. In particular, thanks to John Antoniadis, Cherry Ng, Charlotte Sobey, René Gießübel, David Mulcahy, Lijing Shao, Jana Köhler, Nicolas Caballero and Patrick Lazarus (despite his valiant attempts to make sure this thesis was never completed). Also thanks to all my footballing compatriots for providing an outlet to all that pent-up rage that is an integral part of writing pulsar searching software.

From across the channel, I would like to thank Ben Stappers and Andrew Lyne for teaching me how to solve pulsars. On a similar note, my thanks go out to Cees Bassa and Gemma Janssen, who have both provided much help in the timing of pulsars from this work.

For helping to make my transition to German life as easy as possible, I thank Gabriele Breuer, Simone Pott and Emmanouil (Manolis) Angelakis.

For fostering my love of pulsars in the first place and putting me on the path that led me to the MPIfR, I thank Graham Woan.

From the technical side of things, I would like to thank Guido Kölsch, Jan Behrend, Helge Rotmann and Walter Alef for keeping everything computer related running as smoothly as possible. Also, my thanks go out to all the telescope operators at Effelsberg.

I thank the International Max Planck Research School (IMPRS) for Astronomy and Astrophysics at the Universities of Bonn and Cologne for providing financial support for this research.

I would like to extend my thanks to John Hunter, who sadly passed away during the writing of this thesis. I have never met John, but his MATPLOTLIB package is directly responsible for the more beautiful plots throughout this thesis.

Ich wünsche allen meinen K55 mitbewohner zu danken. Ohne diese verrückten Leute, würde ich nichts über echte deutsche Kultur wissen.

Thanks to Dave Wardle, Jeff Hodgson and Bill Seites-Rundlett for never being adverse to spending their Sundays in the pub watching football.

Finally, above all else, I wish to thank Tina Konerth for giving me Pavlovian butterflies in my stomach whenever I start a long train journey.

Contents

List of Figures

List of Tables

For Mum & Dad

Chapter 1

Introduction

"Six or eight weeks after starting the survey, I became aware that on occasions there was a bit of 'scruff' on the records..."

Dame Jocelyn Bell Burnell

Proposed at the end of a 1934 paper by Baade and Zwicky (1934), neutron stars were thought to be very small, dense and, most importantly, cool bodies, that would be very difficult to detect due to a lack of any large-scale emission. Fortunately, this turned out not to be the whole story.

It would be 33 years before the accidental discovery of a highly regular, repeating pulse train in the data charts of Anthony Hewish and his research student Jocelyn Bell. The source of the pulses appeared to be celestial in nature, with the source appearing at the same sidereal time each day. A lack of measurable parallax showed the source to lie well outwith the local space, while measurements of the degree of frequency dispersion in the broadband radio pulses showed that the source was intragalactic in nature. Work by Pacini (1967), published prior to the discovery, and by Gold (1968) and Hewish et al. (1968a), published post discovery, hypothesised that the source of the observed pulses could be a rotating neutron star, with Gold going as far as to predict a slow decrease in the observed frequency of the pulses due to the emission of magnetic dipole radiation. It was around this time that journalist Anthony R. Michaelis coined the term 'pulsar', a portmanteau of pulsating and star, to describe the new discovery.

The discovery of the Crab and Vela pulsars (Large et al., 1968a; Staelin and Reifenstein, 1968) solidified the theory of pulsars as neutron stars, with both objects rotating too rapidly to be composed of anything other than degenerate neutron material and both

objects exhibiting a measurable frequency derivative, verifying the predictions of Gold (1968).

1.1 Pulsars

1.1.1 Formation

The life of a pulsar begins with the death of a star, or more specifically, a supernova explosion. During this cataclysmic event, the core of the star implodes, rapidly collapsing under its own gravity. If the mass of the core lies above the Chandresekhar limit (at which electron degeneracy pressure will halt the collapse; Chandrasekhar, 1931) but below the Tolman-Oppenheimer-Volkoff limit (at which neutron degeneracy can no longer stop the core becoming a black hole; Oppenheimer and Volkoff, 1939; Tolman, 1939), then what remains after the collapse will be a neutron star.

Through simple arguments, we are able to infer several characteristics of the newly formed star. Since the density of neutron degenerate material is of the order 4×10^{17} kg m^{-3} (Akmal et al., 1998), a neutron star of mass $\sim 1.44\ M_{\odot}$, the Chandresekhar mass[1], must have a radius of ~ 12 km. Using the mass-radius relation for massive stars (see e.g. Allen, 1999), we see that for a 10-$M_{\odot}$ progenitor, this implies a radial shrinkage of five orders of magnitude. Through conservation of angular momentum and magnetic flux, this difference in radius decreases the rotational period of the star by a factor of 10^{10} and increases the magnetic field strength at the stellar surface by a factor of 10^{10}, creating a rapidly rotating, highly magnetised body.

For the purposes of clarity in the following discussion, we shall assume the pulsar model of Goldreich and Julian (1969). Although this model does not describe a realistic scenario[2], it is useful for explaining some of the observational characteristics of pulsars. Current efforts to better understand pulsar electrodynamics via numerical simulations can be found in, for example, Spitkovsky (2004, 2011).

As the magnetic field rotates with the star, a strong local electric field is induced. This field acts to strip charged particles from the surface of the neutron star, gradually building up charge density in the magnetosphere. After some time a 'force-free' state is reached in the magnetosphere, as the electrostatic field from the charged particles cancels out the induced field from the rotation of the magnetic field (Goldreich and

[1] Through the study of binary pulsar systems, it is possible to measure the neutron star mass. The mean value for this mass is $\sim 1.4\ M_{\odot}$, agreeing well with the Chandresekhar mass (see e.g. Zhang et al., 2011).

[2] For example, in this model the spin and magnetic axes are aligned. If we assume that the beam is perfectly aligned with the magnetic axis, then this scenario would not result in pulsed emission.

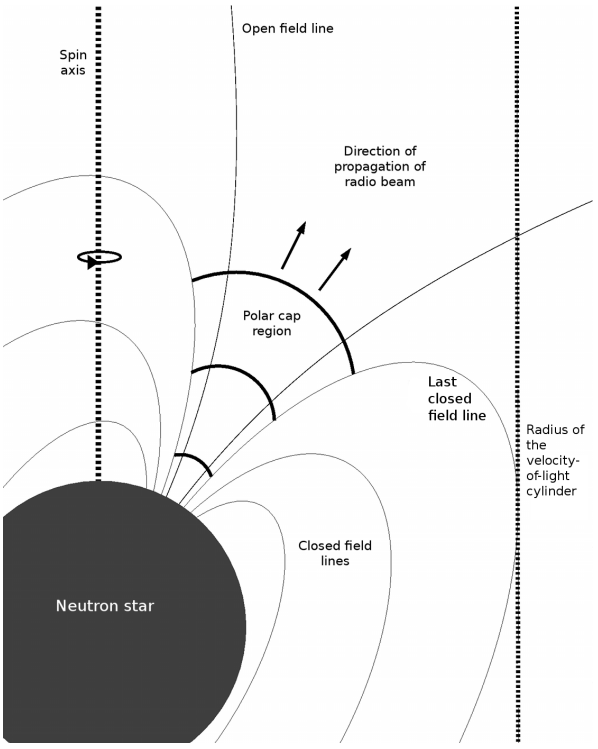

FIGURE 1.1: A simple model for radio emitting pulsars.

Julian, 1969). At this stage the magnetosphere can be thought of as an extension of the neutron star interior, with the magnetospheric plasma co-rotating with the neutron star. This co-rotation breaks down at a distance

$$r_c = \frac{Pc}{2\pi}, \tag{1.1}$$

where P is the rotational period of the pulsar. Here the speed of the magnetospheric plasma approaches the speed of light. At this distance, known as the radius of the *velocity-of-light cylinder*, the force-free state cannot be maintained, leading to a large potential difference across the boundary region. As charged particles are locked to magnetic field lines, only particles which lie on field lines which do not close within the light cylinder are accelerated in this potential (see Figure 1.1). It is in this region, known as the *polar gap*, that the relativistically-beamed, coherent[3], broadband radio emission we see from pulsars is thought to be formed. The mechanisms underlying the radio emission are poorly understood and will not be covered in this work; for an in-depth discussion of the various models for radio emission from the polar gap, see e.g. Chen and Ruderman (1993); Graham-Smith (2003); Sturrock (1971). With the onset of beamed radio emission along the magnetic axis, the pulsar enters what we will term its 'live'

[3]Pulsars have brightness temperatures of the order $\sim 10^{28}$ K, much larger than the brightness temperature achievable through incoherent synchrotron emission (see e.g. Hasan et al., 2008).

state, where, assuming it is beamed towards Earth, it will spend its radio-observable lifetime.

1.1.2 Spin evolution

Although pulsars are very stable rotators[4], their periods gradually increase over time due to the loss of rotational kinetic energy in a process known as *spin-down*. The kinetic energy may be lost through, among other things; magnetic dipole radiation (see e.g. Jackson, 1962), high energy emission (e.g. Guillemot et al., 2012a; Ransom et al., 2011) and torque from the strong particle wind from the pulsar (see e.g. Kramer et al., 2006a). Although not true for all pulsars, it is useful to assume that magnetic dipole radiation is the predominant mechanism for energy loss, as this allows us to calculate several interesting characteristic quantities.

A rotating dipole with angular frequency Ω and component of the magnetic dipole moment orthogonal to the rotation axis $\mathbf{m}_\perp$, radiates an electromagnetic wave at its rotational frequency with radiation power (see e.g. Jackson, 1962)

$$\dot{E}_{dipole} = \frac{2}{3c^3}{\mathbf{m}_\perp}^2\Omega^4. \tag{1.2}$$

If the pulsar is undergoing spin-down, then the rate of change of rotational kinetic energy, its *spin-down luminosity*, is given by (see e.g. Lorimer and Kramer, 2005)

$$\dot{E}_{rot} = -\frac{\mathrm{d}(\mathrm{I}\Omega^2/2)}{\mathrm{dt}} = -I\Omega\dot{\Omega} = 4\pi^2 I\dot{P}P^{-3}, \tag{1.3}$$

where I is the moment of inertia of the pulsar. As the internal structure of the neutron star is not well known, the moment of inertia is defined as $I = kMR^2$, where $k = 2/5$ for a solid sphere of uniform density. Assuming that magnetic dipole radiation is the only mechanism for energy loss from the pulsar, we may combine equations 1.2 and 1.3 to obtain an expected rate of slow-down,

$$\dot{\Omega} = -\frac{2}{3}\frac{{\mathbf{m}_\perp}^2}{Ic^3}\Omega^3 \tag{1.4}$$

As mentioned above, magnetic dipole radiation is not the only mechanism for rotational energy loss from the pulsar. For this reason, Equation 1.4 is usually written in power-law form

$$\dot{\Omega} = -C\Omega^n, \tag{1.5}$$

[4]PSR J0437−4715 being an extreme example, with a spin period stable to one part in 10^{15} (Verbiest et al., 2008).

or

$$\dot{P} = -CP^{(2-n)}, \tag{1.6}$$

where n is referred to as the *breaking index* of the pulsar and C is a constant. For the case of spin-down solely by energy loss through magnetic dipole radiation, n takes the value 3. The breaking index of pulsars is only measurable through the second derivative of the pulse period. Unfortunately $\ddot{P}$ measurements are only possible in young pulsars with high spin-down rates, where timing noise (Hobbs et al., 2010b) and glitches (Espinoza et al., 2011b) are common, leading to very few reliable measures of n (see Table 1 of Espinoza et al., 2011a).

1.1.3 Characteristic surface magnetic field strength

If $\mathbf{m}_\perp \simeq R^3 B_0 \sin\alpha$ (see e.g. Jackson, 1962), where B_0 is the magnetic field strength at the surface of the pulsar and α is the inclination angle between spin and magnetic axis, then rearranging Equation 1.4 leads to several useful relations.

By rearranging for B_0 and replacing angular frequency, Ω, by period, P, we get

$$B_0 = \left(\frac{3}{8} \frac{c^3}{\pi^2} \frac{kMP\dot{P}}{R^4 \sin^2\alpha} \right)^{\frac{1}{2}}. \tag{1.7}$$

This quantity is known as the *characteristic surface magnetic field strength*. By substituting the radius and mass expected from the formation mechanism described above and assuming that the neutron star has a rigid interior of uniform density, this relation may be re-written as

$$B_0 \simeq 3 \times 10^{19} (P\dot{P})^{\frac{1}{2}} \text{ Gauss}, \tag{1.8}$$

for $\alpha = 90°$, i.e. aligned magnetic and spin axes. Different assumptions for the equation of state of the neutron star will result in variations in both k and R, altering the value of the constant in Equation 1.8.

1.1.4 Characteristic age

By integrating Equation 1.6 across the lifetime of the pulsar we obtain the *characteristic age* (see e.g. Lorimer and Kramer, 2005),

$$t_{\text{char}} = \frac{P}{(n-1)\dot{P}} \left[1 - \left(\frac{P_0}{P} \right)^{n-1} \right], \tag{1.9}$$

where P_0 is the initial spin period of the pulsar. Assuming that the pulsar was born with $P_0 << P$ and has a constant breaking index determined solely by the emission of magnetic dipole radiation, i.e. $n = 3$, Equation 1.9 reduces to

$$t_{\rm char} \simeq \frac{P}{2\dot{P}}. \tag{1.10}$$

This relation should not be considered an accurate measure of the pulsar's age, as any assumptions about the initial spin period of pulsars and their breaking indices have a large intrinsic uncertainty due to the low number of measurements of n avialable (see e.g. Espinoza et al., 2011a). This relationship breaks down when considering millisecond pulsars which have undergone an prolonged phase of 'spin-up' caused by mass accretion from their companion stars (see Section 1.1.8.3), leading to several cases of pulsars with characteristic ages greater than a Hubble time (Tauris, 2012).

1.1.5 Pulse profiles

As the pulsar rotates, the beams of coherent radio emission from the polar caps sweep across the sky like the beams of a lighthouse. When one or both of these beams intersects with the Earth, then the emission presents itself as a regular train of pulses at the rotational period of the pulsar. Although there is a large variation in flux density and pulse shape on a pulse-to-pulse basis, adding many pulses together in phase, results in a characteristic pulse profile. For the majority of pulsars, the pulse profile becomes very stable after the addition of a few thousand pulses (see e.g. Liu et al., 2012). However, longer term changes in pulse shape can occur due to mechanisms such as mode switching (Timokhin, 2010), geodetic precession (Weisberg and Taylor, 2002) and, possibly, free precession (Jones, 2012). Figure 1.2 shows the pulse profile of PSR B0355+54 after averaging over 1150 pulses. At each phase the standard deviation of the pulse was calculated, showing that PSR B0355+54's first component is markedly less variable than its second component.

1.1.6 Dispersion

If space were a perfect vacuum, the broadband signal emitted by a pulsar would traverse the Galaxy unhindered, with all frequencies arriving at an observer simultaneously. This is demonstrably not the case, and was one of the first things noted by Hewish et al. (1968b) during observations of the first pulsar. They found that the observed radio pulses would be delayed when observing at lower frequencies. This effect can be explained by considering the signal to have propagated through an *interstellar medium*

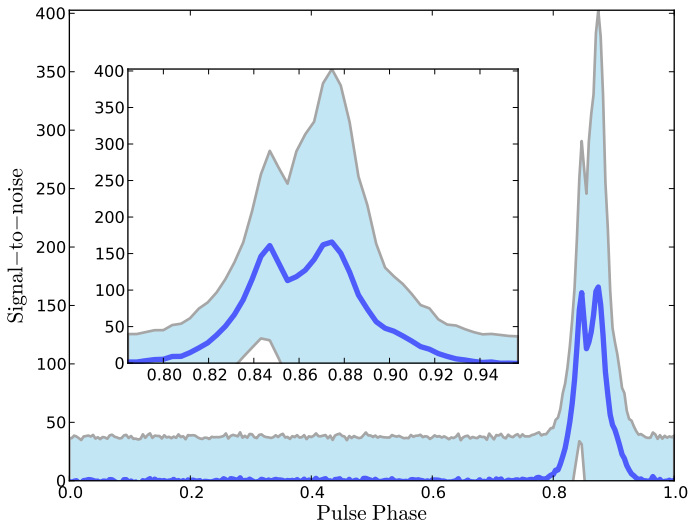

FIGURE 1.2: The average pulse profile of PSR B0355+54 after summation of 1150 individual pulses. The dark-blue line shows the pulse profile in units of signal-to-noise and the filled, light-blue area shows the standard deviation of each phase bin.

(ISM) composed of cold plasma. For an electromagnetic wave in such a medium, the group velocity is given by (see e.g. Huba, 2011)

$$v_{\mathrm{g}} = c\sqrt{1 - \left(\frac{f_{\mathrm{p}}}{f}\right)^2}, \tag{1.11}$$

where f is the frequency of the wave and f_{p} is the plasma frequency. The plasma frequency is given by (see e.g. Huba, 2011)

$$f_{\mathrm{p}} = \sqrt{\frac{e^2 n_{\mathrm{e}}}{\pi m_{\mathrm{e}}}} \approx 8.98\sqrt{\frac{n_{\mathrm{e}}}{\mathrm{cm}^{-3}}}\ \mathrm{kHz}, \tag{1.12}$$

where e is the electron charge, m_{e} is the electron mass and n_{e} is the free electron number density. From Equation 1.11, it is clear to see that in the case $f \gg f_{\mathrm{p}}$, the group velocity tends towards c, i.e. the wave will behave as if in a vacuum. However, when $f \gtrsim f_{\mathrm{p}}$ the group velocity will be significantly reduced. As the signal from a pulsar is broadband, each frequency will have a different group velocity, with lower frequencies propagating through the ISM at considerably slower rates than their higher frequency counterparts. This effect is known as *dispersion*.

By integrating the electron number density along the line of sight to a pulsar, it can be shown (see e.g. Lorimer and Kramer, 2005) that, for a path length of l, the time delay

between the arrival of an infinite frequency pulse and a pulse at frequency f is given by

$$\Delta t = \frac{e^2}{2\pi m_{\rm e} c} \frac{\rm DM}{f^2}, \tag{1.13}$$

where DM is the *dispersion measure* of the pulsar, given by

$$\rm DM = \int_0^d n_e \, dl, \tag{1.14}$$

in units of pc cm^{-3}. Filling in values for the constants in Equation 1.13, we obtain[5]

$$\Delta t \simeq 4.15 \times 10^3 \left(\frac{\rm DM}{\rm pc\ cm^{-3}}\right) \left(\frac{\rm MHz}{f^2}\right) \text{ sec.} \tag{1.15}$$

By assuming a model for the Galactic electron number density, such as the NE2001 Galactic free electron density model (Cordes and Lazio, 2002), it is possible to integrate this equation numerically to obtain the distance to a pulsar with a known DM. Distance measures obtained via this method tend to have large uncertainties (usually taken to be $\sim 20\%$ for the NE2001 model (Cordes and Lazio, 2002), but in practice the uncertainty may be much larger (see Figure 6.15 of Deller, 2009)) due to the intrinsic uncertainties in the model used. Unfortunately, for the majority of pulsars this is the only viable method of distance estimation.

1.1.7 Interstellar scattering

Another effect of propagation through the ISM, is that a pulse will become scatter broadened due to inhomogeneities in the local electron number density, and, therefore, index of refraction. These inhomogeneities result in emitted photons being bent both into and out of the line of sight across a *scattering disk* of angular width $\theta_{\rm d}$, where the angular intensity distribution across this disk is given by (see e.g. Lorimer and Kramer, 2005)

$$I(\theta) d\theta \propto \exp(-\theta^2/\theta_{\rm d}^2)\ 2\pi\theta d\theta. \tag{1.16}$$

Photons arriving from different radii of the scattering disk will be shifted in phase w.r.t. an unscattered pulse, due to the varying path lengths travelled between pulsar and observer. Such phase shifts result in a characteristic intensity variation in time, given

[5]The full value of the constant here is $(4.148808 \pm 0.000003) \times 10^3$ MHz^2 pc^{-1} cm^3 s (Lorimer and Kramer, 2005), however for the purposes of clarity this will be rounded off to three significant figures in this thesis. It should be assumed that any calculation involving DM will use the full value of this constant and not its approximation.

by (see e.g. Lorimer and Kramer, 2005)

$$I(t) \propto \exp(-t/\tau_{\rm s}), \tag{1.17}$$

where $\tau_{\rm s}$ is known as the *scattering timescale*. The scattering timescale is related to the observing frequency, f, and the distance between pulsar and observer, d, by $\tau_{\rm s} \propto d^2/f^4$.

The scattering timescale can also be expressed in terms of DM, via, for example, the empirical relation of Bhat et al. (2004)

$$\log \tau_{\rm s} = -6.46 + 0.154 \log {\rm DM} + 10.7(\log {\rm DM})^2 - 3.86 \log f \text{ s}. \tag{1.18}$$

As we will see throughout this thesis, the effects of scattering are often ignored when considering pulsar searching, as even though scattering is ultimately what determines the maximum distance at which we can detect pulsars, the scattering relation is not well understood. This is evidenced by a 2-3 order of magnitude scatter when comparing observed scattering timescales to the timescales predicted by Equation 1.18.

Figure 1.3 shows the expected deformation of a single Gaussian pulse profile at different DMs, assuming the scattering timescale is well described by Equation 1.18. For each DM the profile can simply be thought of as the convolution of the original Gaussian pulse and an exponential given by Equation 1.17.

1.1.8 The pulsar menagerie

Considering the dependence of the characteristic age and surface magnetic field strength on the period and spin-down, a plot of P vs. $\dot{P}$ becomes a useful visualisation of the overall pulsar population. This 'P-$\dot{P}$' diagram can be thought of as the pulsar analogue of the Hertzsprung-Russell diagram for stars. Figure 1.4 shows a P-$\dot{P}$ diagram created using data from the ATNF pulsar catalogue[6]. In this section we will examine the composition of the main areas on the P-$\dot{P}$ diagram.

The reader should note that the nomenclature presented here cannot be considered canonical, as one person's 'young' pulsar may be another person's 'normal' pulsar, and so on. In general, the boundaries between different pulsar classes are somewhat blurred and open to interpretation. The definitions presented here will be used throughout this thesis.

[6] `http://www.atnf.csiro.au/people/pulsar/psrcat/` (Manchester et al., 2005)

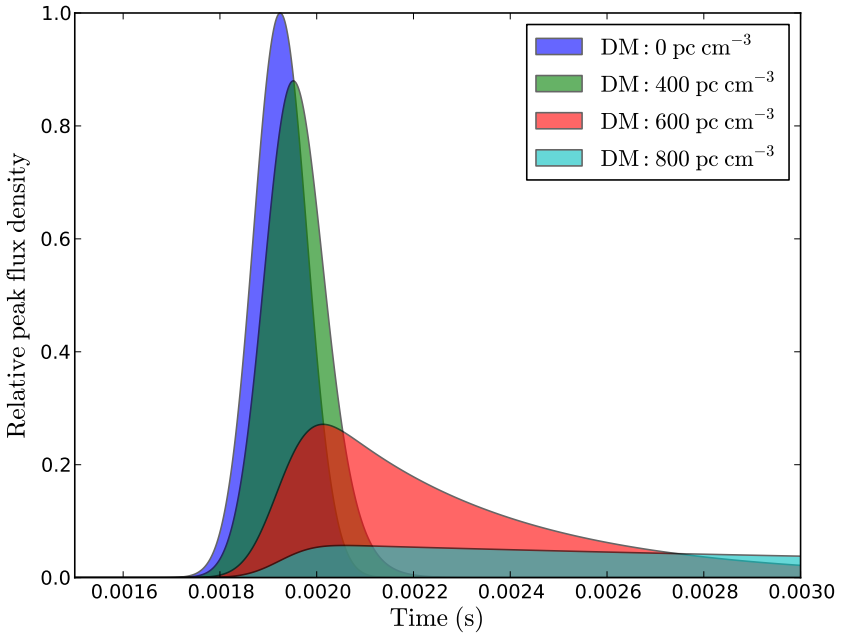

FIGURE 1.3: The deformation of a single Gaussian pulse profile at different DMs due to interstellar scattering. In all cases, the scattering timescale is given by Equation 1.17. It is important to note, that for pulsars where the scattering tail is longer than the rotational period, the pulsar effectively becomes a continuum source, with emission at all phases. However, this does not always render the pulsar undetectable, as there is still modulation in the pulse intensity as a function of phase.

1.1.8.1 Young pulsars

Occupying the top-left of the P-$\dot{P}$ diagram are the so-called *young pulsars*. These systems are named as such due to their high rates of spin-down, which correspond to characteristic ages $\lesssim 100$ kyr. A key piece of evidence suggesting that these systems are truly young, is the large number of supernova remnant (SNR) associations found for pulsars in this region of the P-$\dot{P}$ diagram (see e.g. Camilo et al., 2002a,b, 2009), as SNRs are relatively short lived phenomenon, with observable lifetimes $\lesssim 10^5$ years. These associations are expected if the formation channel for pulsars is as described in Section 1.1.1. An important benefit of associating a pulsar with an SNR, is the independent distance and age estimates that it allows (see e.g. Xu et al., 2005). This is particularly true for pulsars like J0205+6449, where there is evidence that the supernova responsible for the associated SNR occurred in 1181 A.D. (Camilo et al., 2002c), making the pulsar only 831 years old[7]. Independent pulsar age estimates allow constraints to be placed on the initial periods, magnetic fields and space velocities of pulsars. Such constraints are vital to our understanding of the physics of core-collapse supernovae and

[7]As compared to a characteristic age of 5370 years.

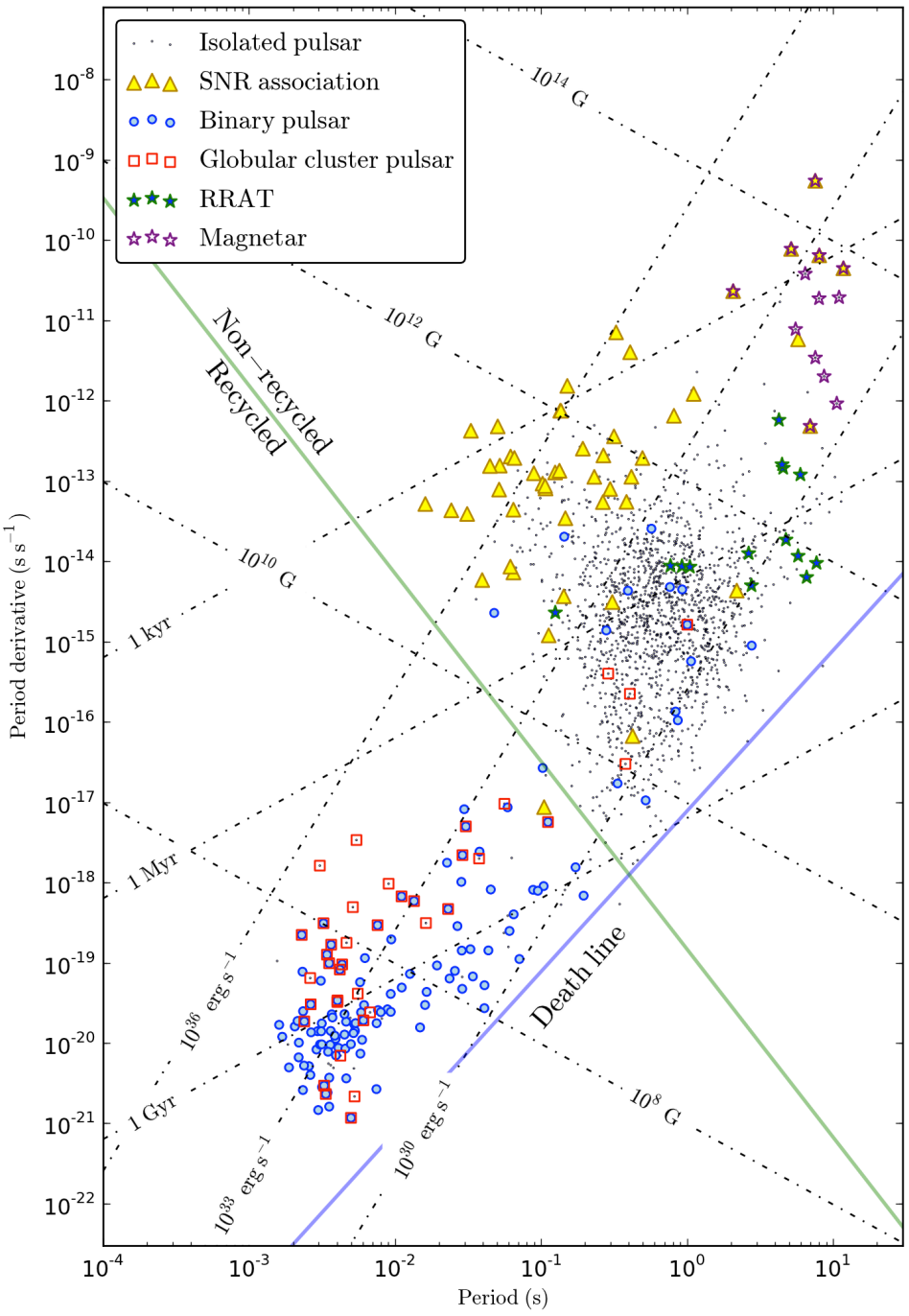

FIGURE 1.4: A P-$\dot{P}$ diagram containing 1801 pulsars from the ATNF pulsar catalogue. Lines of constant characteristic age, characteristic surface magnetic field strength and spin-down luminosity are plotted, assuming a rigid equation of state for the neutron star interior and a breaking index of 3. Also plotted, are the empirical definition for recycled pulsars, as determined by Lee et al. (2012), and the most probable pulsar 'death line', as determined by Chen and Ruderman (1993)

allow for examination of the equation of state of neutron stars through the testing of cooling models (see e.g. Umeda et al., 1994).

1.1.8.2 Normal pulsars

The term *normal pulsar* roughly refers to those pulsars with periods between ~ 100 ms and a few seconds, and characteristic ages of between ~ 100 kyr and ~ 1 Gyr. Normal pulsars constitute the largest fraction of the observed radio pulsar population. This is mainly due to the relative ease with which pulsars of this type can be found.

Despite the name, normal pulsars should not be considered boring or devoid of use[8], as they are anything but. The large number of known normal pulsars allows for comprehensive population studies (see e.g. Faucher-Giguère and Kaspi, 2006; Lorimer et al., 2006) and for in-depth analysis of their emission properties (see e.g. Burke-Spolaor et al., 2012; Weltevrede et al., 2006), providing a more complete picture of radio pulsars as a whole. Furthermore, normal pulsars are invaluable probes of the Galactic magnetic field (see e.g. Noutsos et al., 2008) and the ISM (see e.g. Bhat et al., 2004; Hill et al., 2003).

If an isolated normal pulsar is left to evolve with no external influence, it will gradually spin-down until the point where its magnetic field is no longer strong enough to maintain the mechanism that produces coherent radio emission (see e.g. Chen and Ruderman, 1993; Ruderman and Sutherland, 1975). This effect manifests itself as an emission-model-dependent 'death line' on the P-$\dot{P}$ diagram (see Figure 1.4).

For pulsars in binary systems however, death may not be as final as the name suggests, as a pulsar beyond the death line may be brought back to life through the process of recycling.

1.1.8.3 Recycled pulsars

Looking at the lower left-hand corner of the P-$\dot{P}$ diagram, we can see a clearly separate population of pulsars with periods and spin-downs much lower than those of the normal and young pulsar populations. These *recycled pulsars* can be empirically defined as any pulsar which satisfies $\frac{\dot{P}}{10^{-17}} \leq 3.23(\frac{P}{100\ \mathrm{ms}})^{-2.34}$ (Lee et al., 2012).

The presently favoured evolutionary model for recycled pulsars (see e.g. Alpar et al., 1982; Bisnovatyi-Kogan and Komberg, 1974; Smarr and Blandford, 1976) attributes the small spin period of these pulsars to angular momentum transfer through the accretion of matter from a binary companion star. This hypothesis is supported by the fact that

[8] There is no such thing as a boring pulsar.

75% of observed recycled pulsars reside in binary systems[9]. The process of increasing the spin frequency of the pulsar by this method is known as *recycling*.

If we have a binary star system with a low-mass ($\sim 1\ M_\odot$) star orbiting a higher-mass ($\sim$ 8-10 $M_\odot$) star, assuming they were formed at the same time[10], we see that the massive companion will evolve first, creating a pulsar through the formation mechanism described in Section 1.1.1. If the system is not disrupted during the supernova, then what remains will be a binary system containing a pulsar with a low mass companion. As the companion completes its life on the main sequence, it will swell, becoming a red giant. In the red giant phase, the star rapidly fills its Roche lobe, causing its outer layers to become gravitationally unbound from the core. Material from the companion now begins to flow onto the pulsar in a prolonged phase of steady mass transfer. It is at this stage that the spin period of the pulsar begins to decrease as it gains angular momentum from material drawn from its companion (see e.g. Podsiadlowski et al., 2002; van den Heuvel, 1976). Frictional heating of the in-falling matter has the effect of producing thermal X-ray emission from the neutron star (see e.g. Archibald et al., 2009; Bhattacharya and van den Heuvel, 1991; Tauris and van den Heuvel, 2006), creating a low-mass X-ray binary system. If the companion's mass is sufficiently low, it will eventually shed its outer layers, leaving a white dwarf orbiting a rapidly spinning *millisecond pulsar* (MSP)[11].

In the model described above, it is the initial mass of the companion that ultimately determines the final state of the binary system. Systems in which the companion mass is closer to the progenitor mass will evolve faster, leading to short, unstable periods of accretion and milder recycling of the pulsar. Overviews of the different evolutionary paths for recycled pulsars may be found in Stairs (2004) and Lorimer (2008).

The enormous angular momentum of MSPs makes them extremely stable rotators, with fractional stabilities rivalling those of the best atomic clocks on Earth (see e.g. Verbiest et al., 2009). Such stability has led to the creation of a time standard based entirely on pulsars (Hobbs et al., 2012), allowed for independent measurements of the mass of planets in the solar system (Champion et al., 2010) and may even be instrumental in the future spacecraft navigation systems (Bernhardt et al., 2011).

As mentioned above, the majority of MSPs are in binary systems. The measurement of the binary parameters for these systems provides a wealth of information, and can lead

[9]Compared to only 2% of normal pulsar systems residing in binaries.

[10]This is a natural assumption for stellar binaries in the Galactic disk, however this may well not be the case in globular clusters, where binaries may exchange components through N-body interactions (Ivanova et al., 2005).

[11]To give the spin frequencies of MSPs some context, we can consider a household blender. While the fastest blenders on the market spin at ∼600 Hz, the most rapidly spinning pulsar, PSR J1748-2446ad (Hessels et al., 2006), spins at 716 Hz (for the musical among us, this is somewhere between F_5 and $\mathrm{F}_5^{\#}$).

to accurate measurements of the pulsar and companion masses. Such measurements are vital in both constraining the equation of state of neutron stars (see e.g. Demorest et al., 2010) and understanding binary, and possibly trinary, evolution scenarios (see e.g. Freire et al., 2011).

1.1.8.4 Double neutron stars

If the initial binary components in the above model are both high-mass, rather than ending up as a neutron star-white dwarf binary, the system may end up as a neutron star-neutron star binary (see e.g. Stairs, 2004). These systems contain a young/normal pulsar, such as those described above, and a mildly recycled pulsar in a tight binary orbit. The discovery of these *double neutron star* (DNS) systems has given pulsar astronomy some of its most impressive results, with the discoverers of the first DNS, B1913+16 (Hulse and Taylor, 1975b), going on to be awarded a Nobel Prize for their work. DNSs are a fantastic natural laboratory for tests of general relativity (GR). This is especially true for the *Double Pulsar*, J0737−3039A/B (Burgay et al., 2003; Lyne et al., 2004), a system in which both neutron stars are pulsars which beam towards the Earth[12]. Long-term study of this system has provided some of the most stringent tests of GR and of the validity of alternative theories of gravity, ever performed (see e.g. Breton et al., 2008; Kramer et al., 2006b).

It should be noted that tests of GR and alternative theories of gravity can also be performed using neutron star-white dwarf binaries (see e.g. Antoniadis et al., 2012; Bailes et al., 2003; Lange et al., 2001), and in some cases they may even provide more stringent limits than those achievable with DNSs (Freire et al., 2012).

1.1.8.5 Magnetars

Occupying the top right of the P-$\dot{P}$ diagram is a population of pulsars which have extremely high characteristic magnetic field strengths and relatively long spin periods. These *magnetars* are different from the other pulsar populations we have looked at so far, in that the energy in their emission cannot be accounted for purely through the loss of rotational kinetic energy. Instead it is proposed that the emission seen from magnetars is powered by the decay of their ultra-strong magnetic fields (for recent reviews, see Mereghetti, 2008; Woods and Thompson, 2006). The huge magnetic fields present in these pulsars are thought to be created when conditions for efficient helical dynamo

[12]This is currently not the case, as relativistic precession has temporarily moved the beam of the 'B' pulsar out of the line of sight (Perera et al., 2010).

action are met in the first few seconds of a newly formed neutron star's life (Duncan and Thompson, 1992; Thompson and Duncan, 1993).

The magnetar population has historically been subdivided into Soft Gamma Repeaters (SGRs) and Anomalous X-ray Pulsars (AXPs). These classes are distinguished by the type of high-energy emission that they exhibit. SGRs show exceptionally bright soft γ-ray/hard X-ray bursts of energies as high as $\sim 10^{45}$ erg s^{-1} (Golenetskii et al., 1984). These bursts are separated from other types of astrophysical γ-ray burst by their lack of high energy γ-ray emission and their repeating nature (Atteia et al., 1987; Laros et al., 1986). AXPs show periodic X-ray emission with a soft spectrum and little to no long term variability. These characteristics, combined with a lack of observed orbital motion caused by a binary companion, clearly separate AXPs from compact X-ray binaries (see e.g. Mereghetti, 2008). In the last decade, the distinction between SGRs and AXPs has become blurred, with certain SGRs showing AXP like properties and vice versa (see e.g. Gavriil et al., 2004).

Prior to 2006, magnetars would not have earned a place in the menagerie of radio-emitting pulsars, having only been observed to have higher energy emission. The detection of radio emission from a known AXP XTE J1810−197 changed this, showing a link between radio emitting pulsars and magnetars (Camilo et al., 2006; Halpern et al., 2005). The subject of radio searches for magnetars will be covered in more detail in Section 5.3.

1.1.8.6 RRATs

The last class of pulsar we will look at is the Rotating Radio Transients (RRATs) (for a recent review, see Keane and Mclaughlin, 2011). First discovered by McLaughlin et al. (2006), these sources do not show continual pulsations like the majority of radio pulsars, but instead show bursty emission with pulses being seen sporadically. The time between RRAT bursts is variable, with some RRATs being detected every few seconds and others appearing once every 100-1000 seconds (Hessels et al., 2008).

The population distribution of RRATs is somewhat different from that of normal pulsars, with RRATs generally having longer periods and higher magnetic field strengths than the normal pulsar population (Keane and Mclaughlin, 2011). In particular, several RRATs lie in the region of the P-$\dot{P}$ diagram between the magnetar and normal pulsar populations. This region contains very few normal pulsars, which would naïvely suggest that RRATs and magnetars were linked. Observations of RRAT J1819-1458 have lent credence to this idea, suggesting that the pulsar may have originated in the magnetar portion of the P-$\dot{P}$ diagram before migrating to its current position (Lyne et al., 2009).

However, it should be noted that the long periods of the observed RRAT population is most likely a selection effect, caused by the fact that wider pulses generally contain greater energy, making them easier to detect. This selection effect will also skew the distribution of characteristic surface magnetic field strengths found for RRATs, as longer period pulsars generally have larger rates of spin-down (see Equation 1.8 and Figure 1.4).

Another explanation for the behaviour of RRATs is that they are simply weak/distant pulsars which have peak radio flux densities much higher than their average radio flux density. In this case, the single pulses seen from RRATs are simply the most luminous pulses emitted (Keane and Mclaughlin, 2011). If this is true, then the definition of a RRAT becomes somewhat arbitrary, as one telescope's RRAT may be another telescope's normal pulsar, depending on the minimum observable flux density achievable.

As with all classes of pulsar described here, the key to understanding RRATs is to increase the number of known systems. To this end, modern pulsar surveys routinely employ single pulse searching algorithms to increase sensitivity to such transient emission (see Section 2.2.6). An important aspect of single pulse searches is that they are sensitive to all short duration radio bursts, not just those from RRATs. This has been spectacularly demonstrated in the discovery of several, thus far unexplained, powerful radio bursts of extragalactic origin (Keane et al., 2012; Lorimer et al., 2007). Bursts such as these are a new and relatively unstudied phenomenon, and so the discovery of more of them is one of the main goals of current radio pulsar surveys.

1.2 A brief history of pulsar surveys

1.2.1 The early years

The discovery of the first pulsar in 1968, sparked a proverbial 'pulsar rush', with radio telescopes across the globe hunting for more of these enigmatic objects. In particular, searches at the Molonglo, Jodrell Bank and Arecibo radio observatories were instrumental in increasing the number of known radio pulsars (Davies and Large, 1970; Hulse and Taylor, 1974; Large et al., 1968b). The difference in processing methods employed by these three surveys is exemplary of the rapid progression of pulsar search techniques and technologies at the time. While the original Molonglo survey (Large et al., 1968b; Turtle and Vaughan, 1968; Vaughan and Large, 1970, 1972) used a pen-chart recorder to monitor the total power in the receiver, the first Jodrell Bank survey (Davies and Large, 1970; Davies et al., 1970, 1972, 1973) went a step further by employing a computer to perform automatic detection of bright single pulses. Although bright pulse searches were shown to be a capable method of detecting new pulsars, they were inherently insensitive

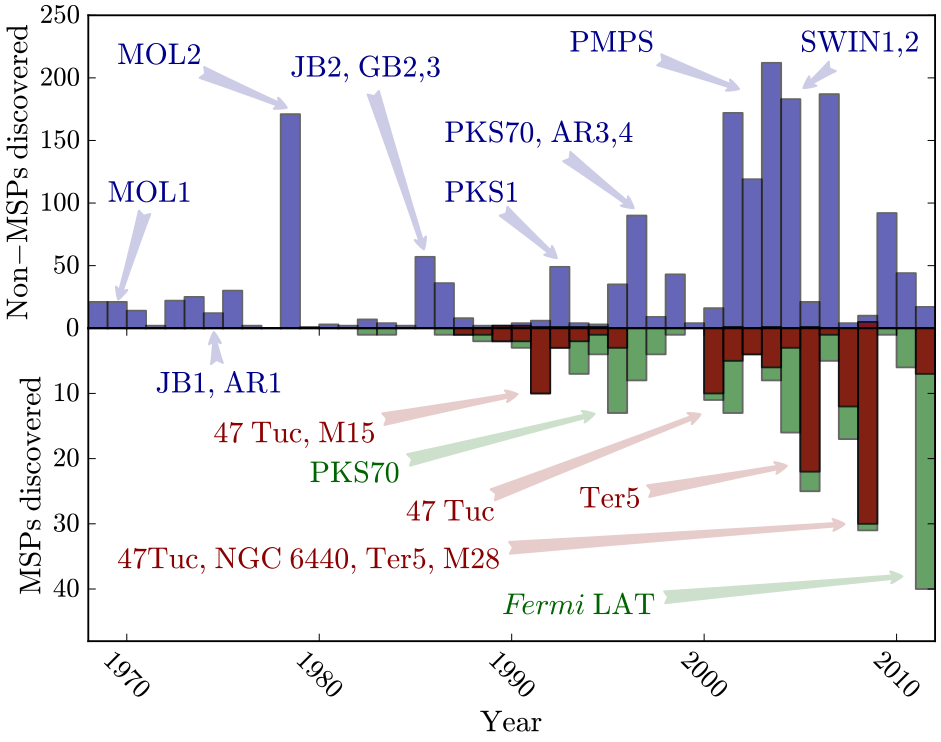

FIGURE 1.5: The number of pulsars discovered each year, from 1968 to 2012. Here, to reflect the difficulty in their detection, we define MSPs as any pulsar with $P < 30$ ms. For years in which a significant number of pulsars were discovered, either the main contributing surveys and/or search targets are indicated. Pulsars in the Galactic disk are shown in blue (normal pulsars) and green (MSPs), while pulsars discovered in globular clusters are shown in red. *Top panel (left to right):* The first Molongolo (MOL1; Large et al., 1968b; Turtle and Vaughan, 1968; Vaughan and Large, 1970, 1972), Jodrell Bank (JB1; Davies and Large, 1970; Davies et al., 1970, 1972, 1973) and Arecibo surveys (AR1; Hulse and Taylor, 1974, 1975a). The second Molonglo (MOL2; Manchester et al., 1978) and Jodrell Bank surveys (JB2; Clifton and Lyne, 1986). The second and third Green Bank surveys (GB2,3; Dewey et al., 1985; Stokes et al., 1985). The first Parkes survey (PKS1; Johnston et al., 1992). The Parkes 70-cm survey (PKS70; Lyne et al., 1998; Manchester et al., 1996) (also in the lower panel). The third and fourth Arecibo surveys (AR3,4; Camilo et al., 1996a,b; Foster et al., 1995; Nice et al., 1995). The Parkes Multibeam Pulsar Survey (PMPS; Faulkner et al., 2004; Hobbs et al., 2004; Kramer et al., 2003; Lorimer et al., 2006; Manchester et al., 2001; Morris et al., 2002). The Swinburne intermediate latitude pulsar surveys (SWIN1,2; Edwards et al., 2001a; Jacoby et al., 2009). *Bottom panel:* Messier 15 (M15; see e.g. Anderson et al., 1990). 47 Tucanae (47Tuc; see e.g. Camilo et al., 2000; Manchester et al., 1991). NGC 6440 (see e.g. Freire et al., 2008). Terzan 5 (Ter5; see e.g. Ransom et al., 2005). Messier 28 [M28; see e.g. `http://www.naic.edu/~pfreire/GCpsr.html`]. *Fermi* Large Area Telescope (LAT) unassociated γ-ray point sources (see Chapter 3 and references therein).

to pulsars with peak flux densities below or comparable to the noise level of the receiver used. To probe the sky for weaker pulsars than had previously been searched for, the first Arecibo survey (Hulse and Taylor, 1974, 1975a) made use of Fourier techniques (Burns and Clark, 1969; Taylor and Huguenin, 1969), leading to 40 new discoveries, including the relativistic binary system PSR B1913+16 (see Section 1.1.8.4). Many of the techniques used in the Arecibo survey are still used today, highlighting how far pulsar searching advanced during its first decade.

By 1975, more than 140 pulsars had been discovered. Although not all had been thoroughly studied, the observed sample had reached the size where strong inferences could be made about the overall spatial and luminosity distributions (Davies et al., 1977; Taylor and Manchester, 1977), suggesting a total Galactic population of $\sim 10^5$ pulsars[13]. However, the size of the available sample would soon be spectacularly increased thanks to the second Molonglo pulsar survey (Manchester et al., 1978). This hugely successful survey observed the entire southern sky below a declination of $+20°$, using techniques pioneered by earlier surveys to discovered 155 new pulsars, more than doubling the known population at the time. The high yield of this survey would remain unrivalled until the arrival of the hugely successful Parkes Multbeam Pulsar Survey (PMPS) at the turn of the millennium (see Section 1.2.3).

1.2.2 The dawn of the MSP

In the six years following the second Molonglo survey, the pulsar discovery rate dropped significantly. Despite this lull, it was during this time that one of the most important pulsar discoveries was made, PSR B1937+21 (Backer et al., 1982), the first MSP. Spinning once every 1.56 ms, this pulsar would have been invisible to earlier surveys that typically used sampling times of the order ~ 10 ms. Importantly, PSR B1937+21 was one of the most luminous pulsars yet discovered, suggesting that many more such MSPs should exist in the Galaxy (Backer, 1984). This revelation was the motivation for the commencement of new pulsar surveys using the Arecibo and Lovell radio telescopes, that employed backends with significantly higher time resolution than had previously been used in pulsar search observations (Clifton and Lyne, 1986; Stokes et al., 1985). While these surveys were successful in the sense that they discovered significant numbers of new pulsars, they failed to discover any new MSPs, probably due to the deleterious effects of interstellar scattering, dispersion and scintillation being exacerbated by relatively coarse frequency resolution and small bandwidths. Although the known Galactic MSP population would remain sparse for many years, the overall MSP population would

[13]This value, despite the low number statistics, is remarkably similar to the total Galactic population of 155000 ± 6000 predicted by Lorimer et al. (2006) almost 30 years later.

steadily climb thanks to successful targeted searches, namely those looking at globular clusters (GCs).

The proposal of an evolutionary model linking MSPs to X-ray binaries (Alpar et al., 1982), the latter of which had already been identified to exist in large numbers in GCs (Clark, 1975), provided an enticing reason to perform deep radio observations of GCs in the hunt for recycled pulsars. While the first discovery of these new surveys would come from observations of M28 (Lyne et al., 1987), it would be observations of 47 Tucanae (47Tuc) in the early 90s, that would truly show the potential of targeted GC searches, with 11 MSPs being discovered there (Manchester et al., 1990, 1991).

In the same year that such success was being found in observations of 47Tuc, Johnston and Bailes (1991) produced a study exploring the Galactic MSP population based on the results of several high-time-resolution searches of the the Galactic plane. Their study suggested that the only way to significantly increase the known Galactic disk population of MSPs was to perform all-sky surveys[14]. Several such surveys were undertaken with the Arecibo (Camilo et al., 1996a,b; Foster et al., 1995; Nice et al., 1995) and Parkes (Lyne et al., 1998; Manchester et al., 1996) radio telescopes during the mid 90s, successfully increasing the known Galactic MSP population by a factor ~ 5. However, it would be the commencement of a series of pulsar surveys using the Parkes telescope in 1998 that would usher in a new era in pulsar astronomy, discovering almost half of all known pulsars.

1.2.3 The Parkes Multibeam Pulsar Survey

During the mid 90s, the Australian National Telescope Facility, began construction of a 7-beam receiver with 100-MHz bandwidth, intended for extragalactic HI surveys using the Parkes telescope. Thanks to extra money in the available budget and some cajoling from prominent members of the pulsar astronomy community, the number of beams in the receiver was increased to 13, with each beam having an improved bandwidth of 288 MHz. These improvements would make this a truly impressive instrument, and arguably the best receiver available for pulsar surveys at the time.

Soon after the completion of the receiver, several new pulsar surveys began at the Parkes telescope (see Lyne et al., 2008, for a review). The most prolific of these surveys was, without a doubt, the Parkes Multibeam Pulsar Survey (PMPS) (Faulkner et al., 2004; Hobbs et al., 2004; Kramer et al., 2003; Lorimer et al., 2006; Manchester et al., 2001;

[14]This, while being true for low frequency surveys (where dispersive smearing and scattering are most problematic), is not true for higher frequency surveys with extremely sensitive telescopes, as the projection effect of the Galaxy means that at larger distances the MSP population (and pulsar population as a whole) will generally tend to lower Galactic latitudes.

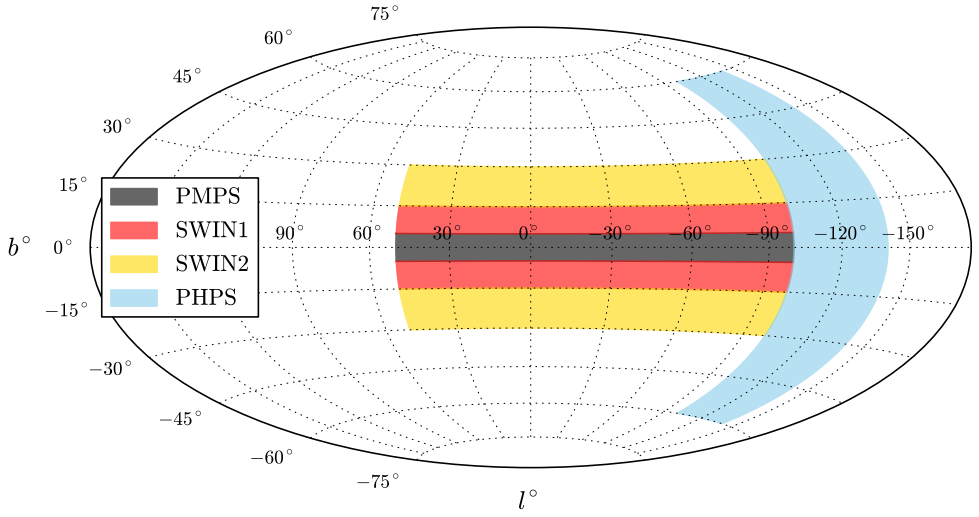

FIGURE 1.6: Projection of the Galaxy showing the observed regions of the Parkes Multi-beam Pulsar Survey (PMPS), the Swinburne intermediate latitude surveys (SWIN1, SWIN2) and Parkes High latitude Pulsar Survey (PHPS). See text for descriptions of each survey.

Morris et al., 2002). This survey observed a narrow strip of the Galactic plane between $260° < l < 50°$ and $|b| < 5°$ in 2800, 35-minute pointings. The long integration times, in combination with a high observing frequency of 1374 MHz and fast sampling rate of 250 μs, allowed the PMPS to probe much deeper into the Galaxy than its predecessors, with stunning results. By the end of its first processing, the PMPS had resulted in the discovery of a phenomenal 742 new pulsars, a number that has been subsequently increased to more than 800 by the successful reprocessing of the data with new search algorithms (see e.g. Eatough et al., 2009; Keane et al., 2010). Highlights from these discoveries include three DNSs systems (Faulkner et al., 2005; Keith et al., 2009; Lyne et al., 2000a) and the class of pulsar known as RRATs (see Section 1.1.8.6).

With the PMPS probing deep into the Galactic plane, other surveys at Parkes took the opportunity afforded by the new receiver to explore the intermediate and high Galactic latitudes for new pulsars. The Swinburne Intermediate Latitude Pulsar Survey (Edwards et al., 2001a) and its extension (Jacoby et al., 2009) observed the region between $50° < l < 260°$ and $5° < |b| < 30°$ with 4.5-minute pointings, in the hope of detecting bright MSPs. This resulted in the discovery of more than 100 pulsars, of which 15 were recycled. The high percentage yield of recycled pulsars from this survey clearly demonstrates the value of performing relatively shallow surveys at higher Galactic latitudes, as although there is a large amount of sky to observe, some of the most fascinating pulsars reside at these latitudes. The clearest illustration of this point comes from the third survey

conducted at the time, the Parkes High Latitude Pulsar Survey (PHPS; Burgay et al., 2006). The PHPS observed the region between $220^\circ < l < 260^\circ$ and $|b| < 60^\circ$, and while the number of pulsars it discovered was relatively low, this was the survey that discovered the Double Pulsar (see Section 1.1.8.4), arguably the most important pulsar discovery since PSR B1937+21[15]. Figure 1.6 shows the observation regions of each of the aforementioned surveys.

1.2.4 In the meantime...

While the PMPS was swiftly swelling the known pulsar population, the hunt for GC pulsars did not cease. On the contrary, new deep observations of 47Tuc, using the Parkes 21-cm receiver, resulted in the discovery of a further 12 pulsars (Camilo et al., 2000; Lorimer et al., 2003), bringing the total number in the cluster up to 23[16].

The early 2000s also saw the completion of the Robert C. Byrd Green Bank Telescope (GBT), the largest fully-steerable single dish radio telescope on Earth. With a bore-sight gain of 2 K Jy^{-1} at 21-cm wavelengths, this instrument was, and still is, well suited to deep observations of GCs, being able to reach much lower flux density limits in a shorter amount of time than possible with the Parkes telescope. This was comprehensively proven through observations of the cluster Terzan 5 (Ter5). Even though Ter5 had previously been extensively searched with the Parkes telescope (Lyne et al., 1990, 2000b), it had only been found to host two MSPs. Observations by Ransom et al. (2005) using the GBT, found an astonishing 21 MSPs in this cluster. This fantastic result has led to further searches of Ter5 with the GBT, bringing the total number of MSPs in the cluster up to 32. For reviews of GC searches, see Ransom et al. (2008) and Camilo and Rasio (2005).

So far the only targeted searches[17] we have looked at, have been those observing GCs in the hope of detecting MSPs. In truth, GC searches are only one of many types of targeted search performed in the hunt for new pulsars, with much success being had in, for example, searches of SNRs (see e.g. Camilo et al., 2002a,b, 2009). It should be noted that the first MSP, B1937+21, was itself found through targeted observations of an unidentified, steep-spectrum radio source (Backer et al., 1982). Such targeted searches are vital to our understanding of the pulsar population, as they allow us to

[15]It should be noted that the Double Pulsar, J0737-3039A/B, was actually discovered in the Galactic plane, at a latitude of $b = -4.5^\circ$. Its location was previously observed in the PMPS survey, but the pulsar was not detected due to its high acceleration.

[16]A comprehensive list of GC pulsars is maintained by Paulo Freire, and can be found at `http://www.naic.edu/~pfreire/GCpsr.html`.

[17]i.e. searches for which a particular position on the sky is selected to be observed based on some prior information suggesting a high probability of finding a pulsar there.

probe specific regions of the sky down to much lower sensitivity limits than achievable in a large survey. A good example of this comes from the recent boom in the Galactic MSP population caused by targeted radio searches of unassociated γ-ray point sources discovered by the *Fermi* LAT (see Chapter 3).

1.2.5 What about Effelsberg?

In all our discussions of the history of pulsar searching, mention of the Effelsberg radio telescope has been conspicuously absent. Considering that Effelsberg was the largest fully-steerable radio telescope on Earth between 1972 and 2000, this begs the question: Why?

A possible explanation for the lack of pulsar searching performed with Effelsberg, was that the telescope was under constant demand from other radio astronomy disciplines, mainly due to the telescopes ability to perform sensitive observations at high radio frequencies, leading to a lack of time allocated for such projects. This is not to say that Effelsberg was never used for pulsar searches. Prior to the deep GC observations which led to the discovery of pulsars in M28 and 47Tuc, Seiradakis and Graham (1980) had used Effelsberg to perform a series of deep observations of various objects of interest, including several SNRs, GCs and X-ray sources. These observations were ultimately unsuccessful in discovering new pulsars, most likely due to the use of processing methods which only retained sensitivity to pulsars with periods greater than 320 ms. As noted by Lorimer (2000), these periodicity limitations meant that the observations of Seiradakis and Graham narrowly missed out on discovering the 289-ms pulsar B1745−20 in NGC 6440 (Manchester et al., 1989). Such a discovery would have undoubtedly changed the way time was allocated to pulsar searching with Effelsberg. As it was, Effelsberg would be made to wait until the end of the 1990s for its first pulsar discovery.

During 1998, with the first hints of the success of the PMPS coming to the fore, a group of pulsar astronomers at the Max-Planck-Institut für Radioastronomie in Bonn, led by Duncan Lorimer and Michael Kramer, decided to perform a small survey of a 2-deg^2 strip of the northern Galactic plane between $28^\circ < l < 30^\circ$ and $|b| < 0.5^\circ$ (Lorimer et al., 1999). As the data taking hardware available at the time was rather limited, with an available bandwidth of only 4×4 MHz, these observations were primarily designed as a proof of concept for a larger pulsar survey using a 100-MHz bandwidth receiver. In this respect, the survey performed perfectly, detecting seven pulsars, of which four were previously unknown. The survey would have undoubtedly also discovered high-DM PSRs J1843−0355 (Morris et al., 2002) and J1844−0256 (Crawford et al., 2001), the only other (non-RRAT) radio pulsars currently known in the volume, were it not for

the poor frequency resolution available at the time. Regardless of these non-detections, the survey provided a much-needed confirmation of the capabilities of the Effelsberg telescope as a pulsar searching instrument and laid the groundwork for the searches presented throughout this thesis.[18]

1.2.6 Where are we now?

Looking at this very brief history of pulsar surveys, it is easy to see that periods of abundant pulsar discovery correlate with either a revelation in our theoretical understanding of pulsars or with an improvement in the technology available to observe them. The former can be seen in the theoretical triggers that led to deep observations of GCs in the search for recycled pulsars, while the latter can be seen in the PMPS; a survey that covered a region of sky that had already been thoroughly searched several times, but did so at higher frequency, with a wider bandwidth, faster sampling and deeper pointings, all of which were facilitated by improvements in receiver design, data transport and storage, and computing capabilities.

Recent technological developments have led to a new wave of pulsar surveys, implementing even larger bandwidths, smaller channel sizes and faster sampling rates than the PMPS. Ongoing surveys of note include, the Pulsar Arecibo L-band Feed Array survey (P-ALFA; Cordes et al., 2006; Deneva et al., 2009b), the Green Bank Nothern Celestial Cap survey (GBNCC), the Survey for Pulsars At Nançay (SPAN512), the High Time Resolution Universe survey (HTRU; Bates et al., 2011a; Burke-Spolaor et al., 2011, 2012; Keith et al., 2010, 2012) and the High Time Resolution Universe North survey (HTRU-North) which will be presented in Chapter 4. A summary of the observing parameters of these surveys is presented in Table 1.1.

The observant reader will notice that several of the pulsar surveys shown in Table 1.1 show significant overlap in their survey regions. At first glance, this would seemingly make all but the most sensitive survey in a given region obsolete. However, this is far from the case, with the surveys complementing each other by probing different aspects of the pulsar population. For example, while the HTRU-North and GBNCC survey cover the same area of sky, the HTRU-North survey is capable of penetrating much deeper into the Galaxy with its higher frequency observations. Conversely, the GBNCC

[18]It is worth noting, that Effelsberg has been used to perform high frequency observations of the Galactic centre in the search for radio pulsars (Klein, 2004). The high observing frequency of these observations, 8.3 and 5 GHz, allowed for the survey to probe the regions very close to the Galactic center, where interstellar scattering is at its most detrimental. These surveys narrowly missed out on the discovery of three pulsars, which would be subsequently discovered in observations with Parkes telescope (J1745-2912, J1746-2856; Johnston et al., 2006) and the GBT (J1746-2850; Deneva et al., 2009a).

TABLE 1.1: Observing parameters for a selection of currently ongoing pulsar surveys.

Survey	Telescope	Region[a]	Frequency (MHz)	$S_{\nu,\mathrm{min}}$[b] (mJy)
P-ALFA (centre)	Arecibo	$32^\circ \lesssim l \lesssim 77^\circ$, $\lvert b\rvert \lesssim 5^\circ$	1400	0.02
P-ALFA (anti-centre)	Arecibo	$168^\circ \lesssim l \lesssim 214^\circ$, $\lvert b\rvert \lesssim 5^\circ$	1400	0.03
GBNCC	GBT	$\delta \gtrsim -45^\circ$	350	0.8
SPAN512	Nançay	$74^\circ \lesssim l \lesssim 77^\circ$, $3.5^\circ \lesssim \lvert b\rvert \lesssim 5^\circ$	1400	0.06
HTRU (low-lat)	Parkes	$-80^\circ \leqslant l \leqslant 30^\circ$, $\lvert b\rvert \leqslant 3.5^\circ$	1352	0.08
HTRU (mid-lat)	Parkes	$-120^\circ \leqslant l \leqslant 30^\circ$, $\lvert b\rvert \leqslant 15^\circ$	1352	0.2[c]
HTRU (high-lat)	Parkes	$\delta \leqslant +10^\circ$, $\lvert b\rvert \geqslant 15^\circ$	1352	0.3
HTRU-North (low-lat)	Effelsberg	$\delta \geqslant -20^\circ$, $\lvert b\rvert \leqslant 3.5^\circ$	1360	0.05
HTRU-North (mid-lat)	Effelsberg	$\delta \geqslant -20^\circ$, $\lvert b\rvert \leqslant 15^\circ$	1360	0.1
HTRU-North (high-lat)	Effelsberg	$\delta \geqslant -20^\circ$, $\lvert b\rvert > 15^\circ$	1360	0.2

[a] Shown in terms of declination (δ), Galactic latitude (b) and Galactic longitude (l).
[b] Rough limiting flux density estimation assuming a 10% pulse duty-cycle (see Chapter 4).
[c] Assuming a spectral index of -1.8 (Maron et al., 2000), this corresponds to a limiting flux density of ~ 0.08 mJy as 1.4 GHz.

survey is more sensitive to pulsars that are nearby and that have steep spectral indices. Although the HTRU-North and the GBNCC will result in some duplicate discoveries, many interesting systems will only be observable by one or the other of these surveys. Similarly, the SPAN512 survey will observe a small strip of the Galactic plane covered by the HTRU-North survey, but will do so with twice the sensitivity, probing the low-luminosity pulsar population in this region. Finally, by observing the same regions of sky multiple times using different telescopes, frequencies and integration lengths, we reduce the probability of missing pulsars due to, among other things; scintillation, RRAT-like behaviour, intermittency, variable scattering, bursting behaviour (as seen in magnetars), eclipsing, RFI, high accelerations and unfavourable pointing positions[19]. Together, these surveys will allow us to build the clearest ever picture of the dynamic radio sky on short timescales.

1.2.7 Why We Search

Despite the fact that we now know of more than 2000 pulsars, there are still many open questions in pulsar astronomy. The goal of all pulsar searches is to provide the means by which we can answer these questions. Below, I present a small selection of open[20] questions in pulsar astronomy.

[19] Survey pointings are usually tiled such that there is a maximum sensitivity drop of 50% for a pulsar that falls between two adjacent beams.
[20] Or, perhaps, ajar.

The Galactic distribution of pulsars

With every new population study produced (see e.g. Johnston and Bailes, 1991; Lorimer et al., 2006; Manchester et al., 1978), those who determine the distributions must extrapolate to contend with various selection biases present in pulsar observations. Increased frequency- and time-resolution backends, in combination with new or improved receivers, allow each successive generation of pulsar surveys to reduce the effects of many of these selection biases. As such, current pulsar surveys are probing the Galaxy to greater distances and with greater sensitivity than has ever been achieved before (see e.g. Chapter 4). The discoveries from these surveys will be invaluable in producing accurate models of the Galactic pulsar distribution. Such models have a plethora of uses, from enabling predictions of the binary-neutron-star merger rate (an essential part of understanding the observable event rates for gravitational wave detectors, see e.g. Abbott et al., 2008; Kalogera et al., 2004), to the examination of the spatial velocity of neutron stars (which has implications for the prevalence of supernovae types and their asymmetries, see e.g. Hobbs et al., 2005).

The origin of magnetars

The boundary between the magnetars and the high B-field normal pulsars (see Figure 1.4) is not fully understood (see e.g. Lin and Zhang, 2004; Pivovaroff et al., 2000). The discovery of a magnetar showing pulsed radio emission in 2006 (Camilo et al., 2006), brought several interesting questions to the fore, namely: Are all magnetars radio emitters (and if not, what is the trigger mechanism for the production of radio emission) and do all high B-field pulsars exhibit magnetar-like behaviour? The small number of known magnetars makes these questions particularly difficult to answer. However, the ability of new pulsar surveys to detect objects such as the radio emitting magnetar J1622−4950 (Levin et al., 2010), will bring us closer to understanding whether magnetars are simply an evolutionary stage for radio pulsars or something else entirely. An expansion of the known magnetar population will also allow for detailed study of plasma under some of the most extreme conditions in the known universe (see e.g. Harding and Lai, 2006; Heyl and Hernquist, 2005).

The evolution of MSPs

Despite almost 15% of MSPs not belonging to binary systems, the formation mechanism for isolated MSPs is still not fully understood. The predominant theory, is that the particle wind from pulsars in tight binary orbits ($P_b < 24$ hrs) with low mass companions ($M_c < 0.05\ M_\odot$)[21], the so-called 'Black Widow' systems (see e.g. Roberts, 2011), can evaporate their binary companions through ablation (see e.g. Bhattacharya and van den

[21]Such systems should constitute a significant fraction of pulsar binaries (Podsiadlowski et al., 2002).

Heuvel, 1991). Prior to 2009, only three Black Widow binaries were known in the Galactic disk, with observations of these systems suggesting mass-loss rates much smaller than would be required for evaporation of the companion within a Hubble time (see e.g. Stappers et al., 1996). While this result would seemingly rule out evaporation as a formation channel for isolated MSPs, the low-number statistics involved restricts any strong conclusions from being drawn from this result. The recent discovery of ten Black Widow systems (Ray et al., 2012b), of which PSR J1745+1017 (see Section 3.6) is one, may provide the means by which we can examine companion evaporation in more detail. There are several alternatives to the evaporation theory presented above. For example, it has been suggested that isolated MSPs may be a possible final product of hierarchical triple systems (Freire et al., 2011; Portegies Zwart et al., 2011) or could even be formed through the core collapse of a white dwarf in a Type Ia supernova (Chen et al., 2010). By discovering many isolated and binary MSPs, current and future pulsar surveys will provide the missing pieces in the isolated MSPs formation puzzle and will, undoubtedly, provide new insight in to all aspects of binary and stellar evolution.

Neutron star characteristics

The discovery of pulsars at the edges of the distribution, whether extremely massive, light, fast, slow, magnetic, young or energetic, is a key goal of current pulsar surveys. These systems are important, as they allow us to rule out certain pulsar and neutron star models. An example of this can be seen in the many equation-of-state models ruled out through mass measurement of PSR J1614-2230 (see Figure 3 of Demorest et al., 2010). Similarly, the discovery of the fastest spinning pulsar, J1748-2446ad (Hessels et al., 2006), seemingly rules out neutron star radii of greater than 16 km, for a 2-$M_{\odot}$ pulsar[22]. As the orbit of J1748-2446ad is almost perfectly circular and the pulsar's emission is very faint, it is, unfortunately, not possible to constrain the mass of the pulsar through pulsar timing. The hypothetical discovery of a similar system to J1748-2446ad, in which both the pulsar's mass and radius could be tightly constrained, would give the strongest yet indication as to the mass-radius relation for neutron stars and, thus, teach us much about the behaviour of supra-nuclear matter.

Pulsar-black hole binary systems

Known throughout the pulsar searching community as simply the 'Holy Grail', the discovery of a pulsar-black hole (PSR-BH) system (see e.g. Narayan et al., 1991) is, arguably, the most exciting and enticing prospect of current and future pulsar surveys. These systems are thought to be formed through several channels (see e.g. Bethe and

[22]For a pulsar mass of 1.4 $M_{\odot}$, this drops to 14.4 km.

Brown, 1998; Pfahl et al., 2005; Voss and Tauris, 2003), with the largest number of PSR-BH systems expected to be composed of a normal pulsar in a tight binary with a low-mass black hole. The formation rate of such systems is still a matter of debate (see e.g. Bethe and Brown, 1998; Pfahl et al., 2005; Sipior et al., 2004), with the more optimistic rates suggesting one PSR-BH system for every 1,500-10,000 field pulsars (Sipior et al., 2004).

A different kind of PSR-BH system may be found by looking for a pulsar orbiting the black hole in the centre of our Galaxy, Sagittarius A* (Sgr A*). For example, Pfahl and Loeb (2004) suggest a population of ~ 1000 pulsars in < 100 year orbits around Sgr A*, with 1-10 of these expected to be detectable with current radio telescopes. Although pulsar searches towards the Galactic centre are limited by scatter broadening and high background temperatures, several such searches have been performed, albeit with limited success (see e.g. Deneva et al., 2009a; Johnston et al., 2006).

The discovery of a PSR-BH system would be a landmark scientific moment, providing a peerless natural laboratory for the study of general relativity and black hole physics (Kramer et al., 2004).

Dececting gravitational waves

Perhaps the most impressive application for the MSP population, is as a timing array for directly detecting gravitational waves (Foster and Backer, 1990). Pulsar timing arrays offer a means by which correlated variations in the signal from pulsars at different positions on the sky may be measured, variations that would be indicative of the presence of a gravitational wave (Jenet et al., 2005)[23]. Several collaborations of pulsar astronomers are currently working on being the first to directly detect gravitational waves (see e.g. Demorest et al., 2012; Ferdman et al., 2010; Hobbs et al., 2010a; Yardley et al., 2011). However, for pulsar timing arrays to work, they require a fairly even distribution of precisely timed pulsar across the sky. Surveys with high time and frequency resolution are therefore vital for finding suitable pulsars for the timing array. Although the existence of gravitational waves has been inferred through measurements of orbital shrinkage of the Hulse-Taylor pulsar (Taylor and Weisberg, 1989), a direct detection of gravitational waves has so far eluded the scientific community. Pulsar timing arrays are expected to be sensitive to low-frequency gravitational waves (10^{-9} to 10^{-7} Hz), such as may be produced by coalescing supermassive black holes, cosmic superstrings and relic gravitational waves from the big bang (see e.g. Jaffe and Backer, 2003; Maggiore, 2000).

[23]Pulsar timing arrays are also a vital tool for, among other things, providing independent constraints on the masses of the planets in the Solar System (Champion et al., 2010) and for the development of a pulsar-based time standard (Hobbs et al., 2012).

Extragalactic bursts

Perhaps the most intriguing result in recent years, has been the discovery of several bright, highly-dispersed radio bursts of extragalactic origin (Keane et al., 2012; Lorimer et al., 2007, Thornton et al., in prep.), made possible by the use of high time- and frequency-resolution instrumentation. The discovery of these bursts has been a revelation in itself, giving a clear example of the value of looking at data in new ways and with new algorithms. The origins of these bursts are currently unclear, with proposed theories including double-neutron-star binary mergers and radio emission from expanding supernova shells (Keane et al., 2012)[24]. If the former, these bursts could be used as a post-event trigger for gravitational wave detectors such as LIGO (Abramovici et al., 1992), while if the latter, they may be used as probes of magnetic field evolution in supernovae shells. As such, the discovery of more bursts like these is highly desirable.

1.3 Thesis outline

This thesis deals with current efforts to discover new pulsar systems with the 100-m Effelsberg radio telescope, providing the means by which the above questions may be answered. The methods and techniques of pulsar searches will be described and the results of several surveys, both large and small, will be presented.

In **Chapter 2** we examine the techniques, methods and instrumentation used in modern-day pulsar searches with particular focus on those techniques used on data taken with the 100-m Effelsberg radio telescope.

In **Chapter 3** we present "*Pulsar searches in Fermi unassociated sources with the Effelsberg telescope*", a targeted search of 289 γ-ray point sources, which resulted in the discovery of MSP J1745+1017.

In **Chapter 4** we present "*The High Time-Resolution Universe North: System configuration and initial results*", on the all-sky pulsar survey conducted with the 100-m Effelsberg radio telescope. In this chapter we present 12 newly discovered pulsars with complete timing solutions.

In **Chapter 5** we present three smaller scale targeted pulsar searches performed with the Effelsberg telescope.

In **Chapter 6** we present conclusions and future research plans.

[24] Other theories include giant pulse type emission and annihilating black holes, although it should be noted that both of these explanations require the source of the burst to be Galactic in nature.

Chapter 2

Pulsar searching

"In every branch of knowledge the progress is proportional to the amount of facts on which to build, and therefore to the facility of obtaining data."

James Clerk Maxwell

While the fundamental principles behind pulsar searching have not changed for the past 40 years, the techniques, algorithms and hardware available to perform such searches have advanced significantly. The ever increasing power and decreasing cost of computing resources, in combination with advances in data storage and transport techniques, have allowed modern-day pulsar surveys to explore the sky at much higher time and frequency resolution than has previously been achievable. In this chapter we describe the instrumentation and algorithms used in a modern-day pulsar search, namely the High Time Resolution Universe North survey (see Chapter 4).

2.1 Instrumentation

Pulsars are very weak radio sources, with observed flux densities in the Jy to μJy range at 1.4 GHz (Manchester et al., 2005). While it is possible to observe pulsars using small radio telescopes and long integration times, to achieve sensitivity to the weakest pulsars within reasonable timeframes[1], we require telescopes with large collecting areas. The high instantaneous sensitivity of such systems is also vital for the observation of weak radio bursts of astrophysical origin, a major aspect of current pulsar surveys (see Section

[1]Being able to achieve high signal-to-noise ratios in short observations is important in simplifying the task of searching for pulsars in binary systems (see Section 2.2.4.7).

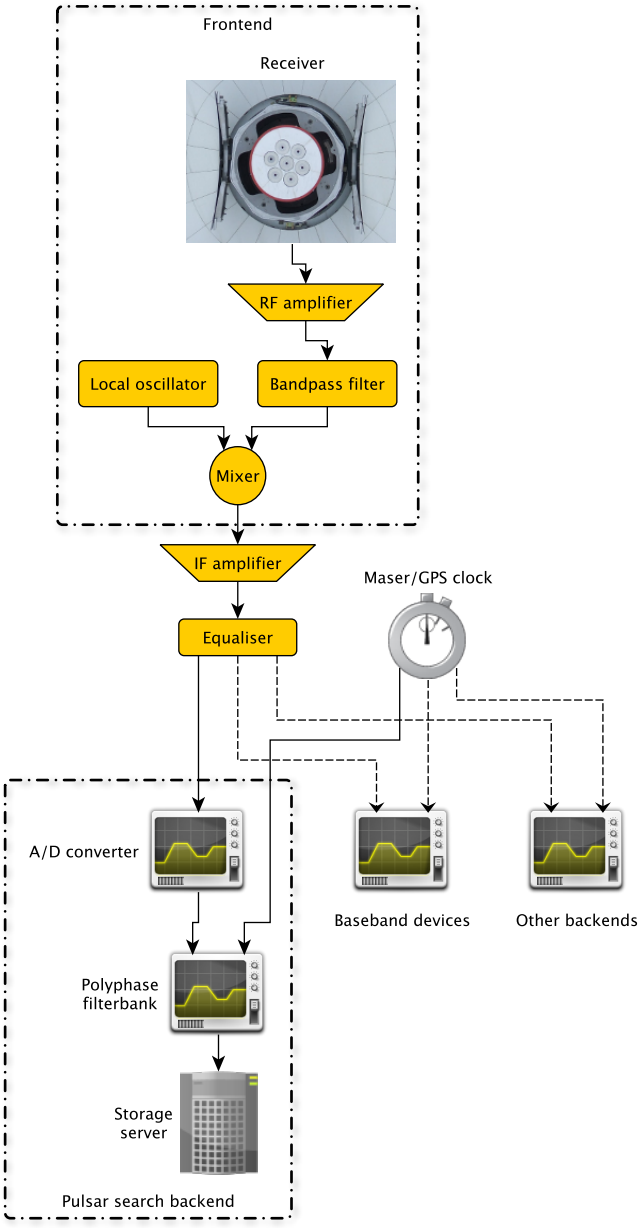

FIGURE 2.1: Schematic representation of a generic single-dish pulsar observing system.

2.2.6). Several large telescopes exist that are well suited to pulsar search observations. These include the 100-m Effelsberg radio telescope, the 64-m Parkes radio telescope, the 105-m Robert C. Byrd Green Bank Telescope (GBT) and the 300-m Arecibo radio Telescope, all of which are currently performing large-scale pulsar searches (see Table 1.1).

Figure 2.1 shows a schematic of a generic observational setup for single-dish pulsar observations. In the following sections, we will review each stage of the signal chain.

2.1.1 Frontend

The term *frontend* generally refers to those parts of the observing system which deal with the signal at the incoming radio frequency (RF). For most observing systems, the frontend is composed of a feed horn, low-noise amplifier, bandpass filter and mixer (Léna et al., 2012).

Radiation focused by the dish onto the receiver enters the feed horn, where standing waves at select RFs are allowed to form. The electric fields created by these standing waves are then sampled by a probe in two orthogonal polarisations (see e.g. Burke and Graham-Smith, 2009). As the signal paths for the two sampled polarisation senses (usually orthogonal linear or dual circular) are identical, we shall from here on refer to only a single signal path.

After being sampled by the probe, the weak radio signal is amplified in a low-noise amplifier (LNA) with a specific frequency response centred on the middle of the observing band. This amplification stage represents the major noise contribution in high-frequency radio observations ($\gtrsim 1$ GHz)[2]. To limit the thermal noise in the system, the LNAs and the probe are usually housed in a cryogenic Dewar flask which is kept at temperatures of the order of a few tens of Kelvin. The amplified signal is then passed through a filter that suppresses known strong, persistent radio-frequency interference (RFI) signals in the band.

The last stage in the frontend involves frequency conversion from the incident RF to a lower intermediate frequency (IF). Frequency conversion is achieved through the process of heterodyning, wherein the RF signal is 'beat' with a lower-frequency signal from a local oscillator, in a device known as a mixer. As the characteristic impedance of a transmission line decreases with decreasing frequency (see e.g. Huba, 2011), the drop in frequency acts to reduce losses during transmission of the signal from the frontend to where the backends are housed.

Between the frontend and the backend, the IF signal undergoes a final amplification stage. Like the RF amplifier the IF amplifier also has a specific frequency response range, which is the width of the desired band. Before entering the backend, the signal is passed through an equaliser to remove any frequency-dependent artifacts caused by propagation effects in the cabling used to carry the signal from the frontend.

For more information on frontend systems for radio telescopes, see e.g. Léna et al. (2012).

[2] At lower observing frequencies, the major noise contribution comes from Galactic synchrotron emission. For this reason the true switch frequency between the two regimes is dependent on Galactic longitude and latitude.

2.1.2 Pulsar search backend

The term *backend*, refers to the end of the signal chain, in which the signal is digitised, processed and stored. Here we will specifically look at the type of backend that is most commonly used in modern pulsar search observations, the polyphase filterbank.

As the IF signal enters the backend, it is Nyquist-sampled and digitised using an analogue-to-digital converter (ADC). The ADC maps out the IF signal to an n-bit number with nano-second-scale sampling before passing the digitised data stream to a digital filterbank.

In the simplest terms, the digital filterbank contains a field-programmable gate array (FPGA) which performs fast Fourier transforms (FFT, see Section 2.2.4.2) of discrete blocks of data to produce a spectrum every few microseconds. Spectral leakage in the FFT stage can cause strong signals at specific frequencies to spread their power over several adjacent Fourier bins in the power spectrum. To reduce the effects of spectral leakage, modern-day backends employ polyphase filtering techniques (see e.g. Lyons, 2010) . These techniques purify the signal response by weighting overlapping sections of data with a sinc function pre-FFT. The combination of polyphase filter and FPGA is referred to as a *polyphase filterbank*[3].

The length and sampling rate of the data undergoing FFT are determined by the number of filterbank channels desired and the overall bandwidth. To achieve a 512-channel filterbank over a bandwidth of 300 MHz, would require a 1024-point FFT of data sampled at 600 MHz, i.e. a 1024-point FFT every ~ 1.7 μs. Such a high rate of sampling is not desired for search observations, as we only require a sampling rate two or more times higher than the frequency of the fastest pulsar for which we are searching. This means it is theoretically possible to detect a pulsar with a spin frequency of 1 kHz using a sampling of only 2 kHz. In reality we require a larger number of samples across the pulse period, as the period is *a priori* unknown and any strong blue-noise[4] components in the data can potentially mask out the pulsar signal. For this reason the spectra produced in the polyphase filterbank are integrated to give sampling rates of several tens of microseconds, more than enough to detect the fastest pulsars known.

As we do not require any polarisation information for the purposes of pulsar searching, a quadrature sum of the output from each polarisation channel is performed.

In the final step performed by the backend, the data are formatted and the resultant files are written to disk for processing.

[3] A short, useful guide to polyphase filterbank techniques can be found at `https://casper.berkeley.edu/`

[4] i.e. noise which is stronger at higher temporal frequencies.

2.2 Pulsar search methodology

Figure 2.2 shows a generic pulsar searching pipeline. In this section we will review each of the steps in this pipeline, with focus on the techniques implemented in recent pulsar searches with the Effelsberg radio telescope.

2.2.1 Data formats

It is initially useful to examine the common data formats used in pulsar searching. As noted in Section 2.1.2, pulsar search backends generally output data in a native format. To reduce the need to write software that can handle each data type from each backend, native-backend-format data are usually converted to a more common format for processing and long-term storage.

The two most common data formats used for pulsar search data are *filterbank format*[5] and PSRFITS (Hotan et al., 2004). The essential difference between these formats is the method by which observational metadata are stored, with PSRFITS providing a much more dynamic and extensible system to store such information, it itself being based on the well-known Flexible Image Transport System (FITS, Pence et al., 2010). Although PSRFITS, or something similar, is likely to be the common standard in the future, pulsar searching software is still catching up with the complexity it brings to data access, meaning that filterbank format is currently the most widely used data format, and is the format that is used for the majority of work in this thesis.

In brief, filterbank format consists of a binary header containing keyword value pairs pertaining to certain metadata, such as the number of filterbank channels, the sampling time and the start time of the observation. After the header comes a stream of n-bit numbers which represent the data in time-major order, where the i^{th} data point in the stream belongs to channel $i \bmod N_{\text{chans}}$ and sample $\lfloor i/N_{\text{chans}} \rfloor$, where $\lfloor x \rfloor$ is the floor of x.

2.2.2 Radio-frequency interference excision

For radio astronomers, the continual advancement of communication technology creates a problem, as more and more individuals, companies and governments require access to certain RF bands. Communication satellites, mobile phones and wireless modems, along with a plethora of other electronic devices, all produce signals, collectively known in the radio astronomy community as RFI, which are harmful to sensitive pulsar observations.

[5]For a full description of this format, see `http://sigproc.sourceforge.net/sigproc.pdf`.

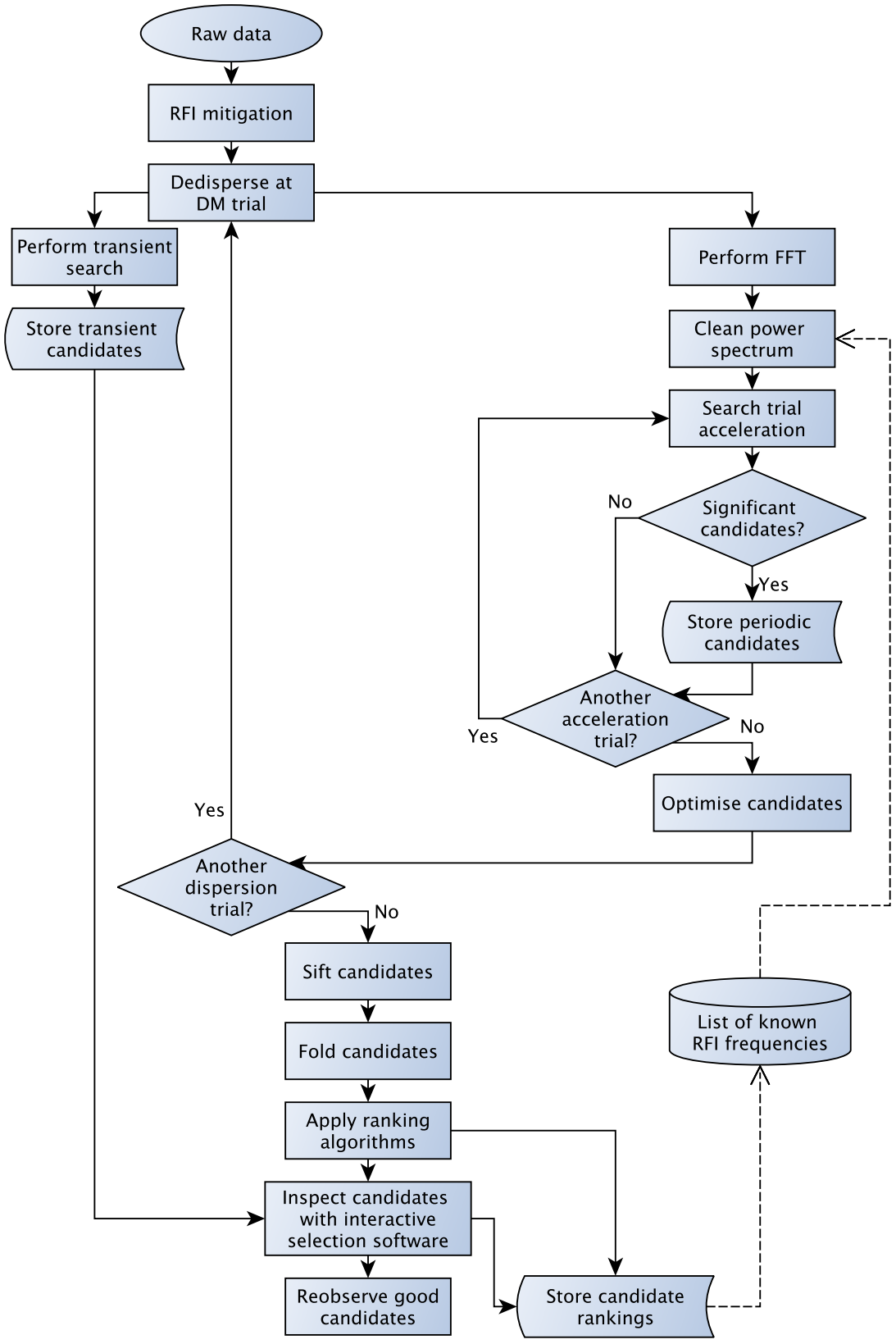

FIGURE 2.2: A schematic representation of a standard pulsar searching pipeline. Solid lines show the control flow for processing of a single observation, while dashed lines show optional steps that can be performed after many observations have been processed.

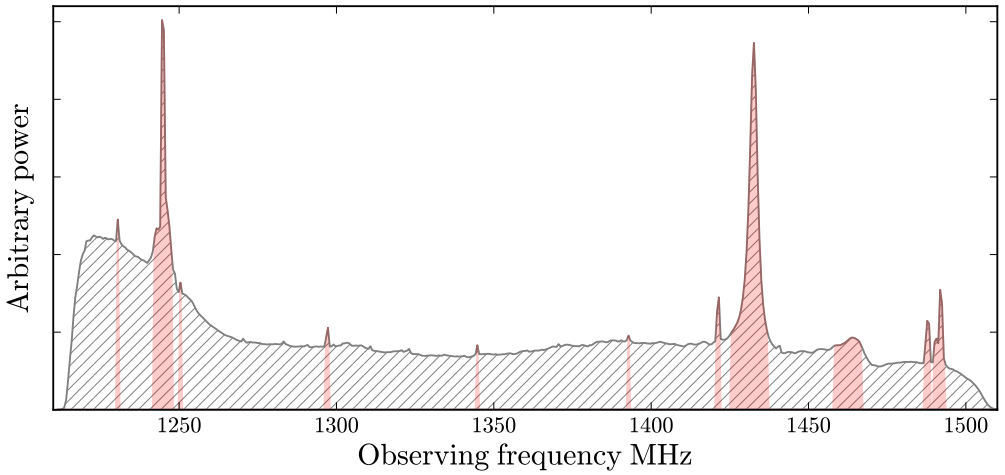

FIGURE 2.3: The bandpass of the 21-cm Effelsberg multi-beam receiver's central beam. Red areas show 'bad' observing frequencies which have been flagged by automatic spike finding algorithms. It should be noted that such automatic algorithms are not infallible, ocasionally flagging a channel that is unaffected by RFI. This can clearly be seen at $\sim$ 1465 MHz, where the local bandpass shape has produced a spurious RFI detection.

Therefore, it is imperative that the first stage of any pulsar search should attempt to suppress or remove these unwanted signals from the data.

Here we review several techniques used to mitigate the effects of RFI. Generalised versions of these techniques are described in (Fridman and Baan, 2001). We will only consider cases applicable to pulsar search observations.

2.2.2.1 Frequency domain techniques

By integrating all frequency channels across the length of the observation, a bandpass is obtained showing the distribution of power throughout the spectral channels. The data in channels identified as containing excess power can be replaced with zeros to suppress the effects of **persistent narrowband RFI**. The selection of channels to be replaced with zeros can be done either dynamically, using algorithms which process the bandpass to identify significant power levels, or statically, using a list of observing frequencies known to be contaminated by RFI. Figure 2.3 shows an example bandpass of the 21-cm multi-beam receiver at Effelsberg and its RFI affected channels.

2.2.2.2 Time domain techniques

By integrating all time samples across the observing bandwidth, a time series is obtained at a DM of zero, the so-called *zero-DM* time series. Performing a statistical analysis on

this time series allows for the identification of signals generated by **strong impulsive RFI**. The data in each channel of a sample identified as being contaminated by RFI can then be replaced by Gaussian noise indistinguishable from the data in the adjacent samples, or clipped such that its power is greatly reduced.

A variant of the above method, known as *zero-DM filtering*, has been used to good effect in re-processing the PMPS (Eatough et al., 2009). In this technique, each time sample in the original filterbank is normalised by subtraction of its average across all frequency channels. While this method has been shown to be an excellent method of RFI removal in single-bit data, trials using multi-bit data have been met with limited success.

2.2.2.3 Fourier domain techniques

A powerful method of mitigating against **period RFI** in an observation, is to examine it in the Fourier domain. Using prior knowledge of the local RFI environment, it is possible to remove power from Fourier bins likely to be contaminated by RFI. To do this, the discrete Fourier transform (DFT, see Section 2.2.4.2) of the zero-DM time series is taken. Fourier frequencies which have been identified as containing periodic RFI can then be zeroed or replaced with noise such that they do not influence candidate selection or acceleration searching procedures at later stages of data processing.

2.2.2.4 Multi-beam techniques

Through the use of multi-beam (or multi-pixel) receivers, the above techniques may be applied dynamically, significantly enhancing their ability to nullify the effects of man-made interference.

Unlike the signal from a pulsar, RFI is not usually detected in only a single beam of a pointing. Instead RFI tends to show in some or all beams simultaneously. By examining the spatial distribution and temporal coherence of an incident signal, it is possible to determine if a signal is RFI, down to much lower thresholds than possible via other methods.

By first understanding the noise statistics of each frequency channel in the data, the detection significance of temporally coherent data points may be compared and thresholded. For example, in a seven-beam receiver the probability of a single data point having a significance of 3-σ is 0.26%, assuming the data are purely Gaussian noise. However, considering that all beams are observing simultaneously, the same 3-σ data point cannot be considered independent of data points taken by other beams at the same time. The

probability of having a 3-σ or greater detection in all beams is therefore 10^{-18}%. Mitigating against impulsive RFI therefore becomes a case of selecting a threshold number of beams in which a signal must be detected above a given significance in a single time bin[6]. Signals which satisfy these criteria may be replaced by Gaussian noise based on the statistics of the surrounding data.

A similar methodology may be applied to mitigate against multi-beam RFI in the Fourier domain. In this case, the data from each beam may be examined in the Fourier domain, with Fourier bins which have power above some threshold in multiple beams, being removed. For a discussion on thresholds for signals in the Fourier and time domain see Sections 2.2.4.6 and 2.2.5.2.

As part of this work, we have developed a system to perform multi-beam RFI excision using all of the methods outlined above. In particular, this is the first system to implement multi-beam RFI filtering using the full time and frequency resolution of the incoming data. This system has been used to good effect in the processing of data from the High Time Resolution Universe North pulsar survey (see Chapter 4).

Other, arguably more elegant, forms of multi-beam RFI excision exist, such as the method proposed by Kocz et al. (2012), which considers the covariance matrix for each time sample of the observation. Unfortunately, this method, however powerful, is currently limited by the amount of computation it requires.

2.2.3 De-dispersion

After RFI has been removed from the observational data, the next step of processing is the removal of the dispersive delays described in Section 1.1.6. To do this, the delay relative to the top of the band is calculated for the centre of each frequency channel, i.e. Equation 1.15 becomes

$$\Delta\mathrm{bin_i} = \left\lfloor 4.15 \times 10^3 \left(\frac{\mathrm{sec}}{\mathrm{t_{samp}}}\right)\left(\frac{\mathrm{DM}}{\mathrm{pc\ cm^{-3}}}\right)\left(\frac{\mathrm{MHz}}{f_\mathrm{i}^2} - \frac{\mathrm{MHz}}{f_\mathrm{top}^2}\right)\right\rceil, \tag{2.1}$$

where $\Delta\mathrm{bin_i}$ is an integer number of time samples by which to shift a channel at frequency f_i with respect to the top of the band, f_top, and $\lfloor x \rceil$ is the nearest integer to x. The data are then collapsed in frequency to create a *de-dispersed time series* where the j^th element $\mathcal{T}_j$ is given by

$$\mathcal{T}_j = \sum_{i=0}^{N_\mathrm{chans}} \mathcal{F}_{(j+\Delta\mathrm{bin_i})\times\mathrm{N_{chans}}+\mathrm{i}} \tag{2.2}$$

[6]While the statistical significance of a noise detection is unaffected by the sensitivity differences between beams, the same cannot be said of RFI. Having one or more beams with significantly lower sensitivity to the rest, will result in a lower rejection rate for RFI signals.

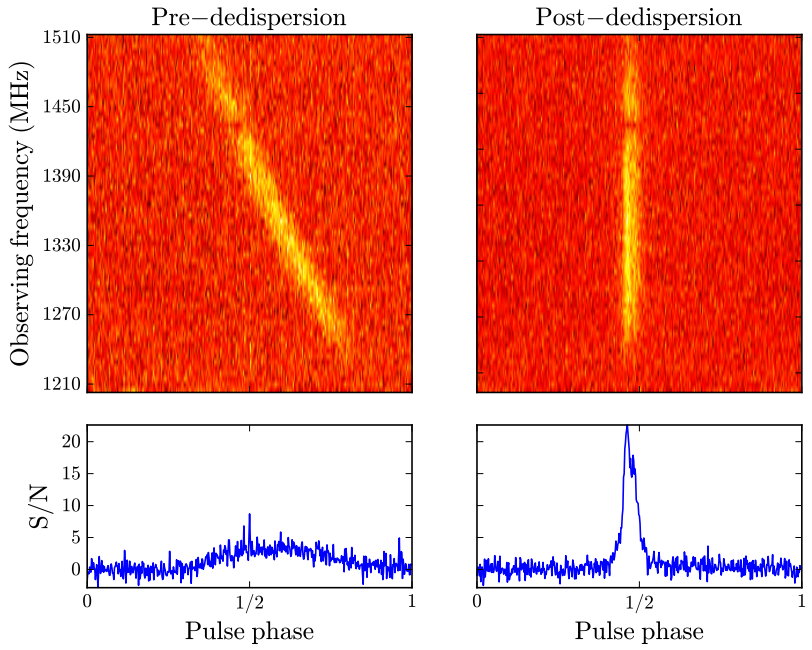

FIGURE 2.4: An example single pulse from PSR B0355+54. *Left-hand panels:* Subband plot and pulse profile without taking into account the pulsar's DM. *Right-hand panels:* Subband plot and pulse profile after de-dispersion at the correct DM.

where $\mathcal{F}$ is a stream of filterbank data containing $N_{\rm chans}$ channels and $> j + \Delta{\rm bin}_{\rm N_{chans}}$ time samples. This process is known as *standard incoherent de-dispersion* and is the most common form of de-dispersion used for pulsar search observations. Figure 2.4 shows a frequency-resolved pulse before and after de-dispersion.

The method described above is the simplest realisation of the de-dispersion algorithm. A different realisation of this algorithm can be found in *tree de-dispersion* (Taylor, 1974). Although tree de-dispersion is computationally faster than the method described above, it requires that the dispersive delay across the band be treated as a linear function. Such an effect can be achieved by the simple addition of extra channels to the filterbank data, as was shown to good effect in the first PMPS processing (Manchester et al., 2001). Despite this, the power of modern computer processors has rendered tree de-dispersion somewhat obsolete, with speed improvements being generally outweighed by the added complexity the tree algorithm brings to any processing pipeline.

Standard incoherent de-dispersion is often split into two steps through the process of *subbanding*. Here the data are initially de-dispersed in groups of channels to form a set of de-dispersed subbands. The subbanded data may simply be thought of as a reduced-frequency-resolution filterbank file in which each channel is a de-dispersed time series. By adding subbands together with appropriate time delays (see Equation 2.1), further de-dispersion to DMs similar to the DM of the subbands can be quickly performed.

When performing a search for unknown pulsars, we must de-disperse the data at many *trial DMs* to retain sensitivity to pulsars at all DMs. The choice of DMs to de-disperse to is an important factor in the processing pipeline, as using too many trial DMs will result in unnecessary computation, whereas using too few trial DMs will result in a lack of sensitivity to fast pulsars, especially at high DMs. To optimise the number and separation of the DM trials used in a pulsar survey, we must consider the deformation of a standard pulse profile due to instrumental and ISM effects.

The effective width, $W_{\rm eff}$, of a pulse can be given by the quadrature sum of a series of geometrical factors, Δt, which act to widen that pulse (see e.g. Manchester et al., 2001). For a pulsar of intrinsic width $W_{\rm int}$,

$$W_{\rm eff} = \sqrt{W_{\rm int}^2 + \Delta t_{\rm scatter}^2 + \Delta t_{\rm dispersion}^2 + \Delta t_{\rm sampling}^2}, \tag{2.3}$$

where $\Delta t_{\rm scatter}$ is the scattering timescale (see Section 1.1.7), $\Delta t_{\rm dispersion}$ is the dispersive timescale and $\Delta t_{\rm sampling}$ is the timescale of the intrinsic smearing associated with sampled data.

Although $\Delta t_{\rm sampling}$ ultimately determines the resolution of the pulse at 0 DM, its effect at higher DMs is negligible and thus the term may be safely ignored. The scattering timescale may be given by the empirical relation of Bhat et al. (2004) (see Equation 1.18). By this relation, scattering should be the dominant delay at high DMs. However, we note that the intrinsic scatter of delay estimates about this relation is several orders of magnitude. For this reason, scattering is normally not taken into account when determining optimal trial DM values. Therefore, the only remaining term is the dispersive smearing across the full band, given by (see e.g. Lorimer and Kramer, 2005)

$$\Delta t_{\rm dispersion} = 4.15 \times 10^3 \left(\frac{\rm MHz}{f_{\rm bottom}^{-2}} - \frac{\rm MHz}{f_{\rm top}^2} \right) \left(\frac{\rm DM}{\rm pc\ cm^{-3}} \right)\ {\rm sec}, \tag{2.4}$$

where $f_{\rm bottom}$ and $f_{\rm top}$ are the frequencies at the bottom and top of the band, respectively.

A logical choice for a DM step therefore becomes the DM for which the degree of smearing across the band is equal to the sampling time of the observation, i.e.

$$\Delta{\rm DM} = 2.41 \times 10^{-4} \left(\frac{t_{\rm samp}}{\rm sec} \right) \left(\frac{\rm MHz}{f_{\rm bottom}^{-2}} - \frac{\rm MHz}{f_{\rm top}^2} \right)\ {\rm pc\ cm^{-3}} \tag{2.5}$$

In this case the $i^{\rm th}$ DM trial is given by $i \times \Delta{\rm DM}$.

At higher DMs the dispersive smearing in individual channels becomes the dominant contribution to the effective pulse width. Considering that the channel bandwidth is

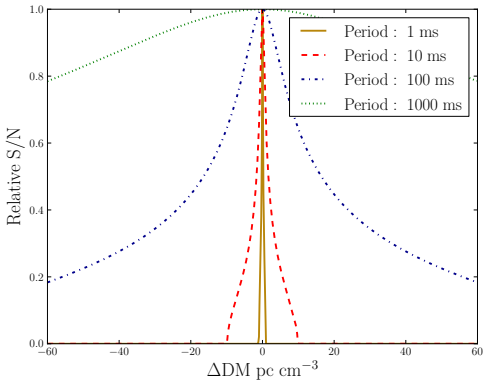

FIGURE 2.5: Relative S/N as a function of DM for a selection of pulsar periods. $\Delta\text{DM} = 0$ at the true DM of the pulsar. All pulsars shown have a 5% duty-cycle.

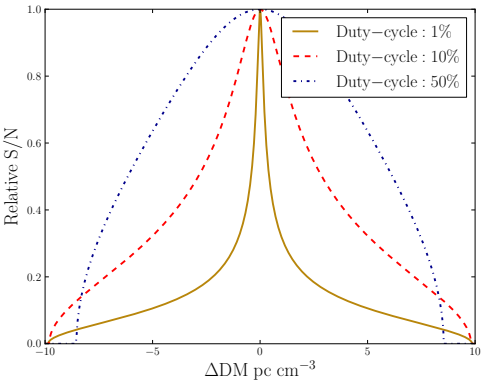

FIGURE 2.6: Relative S/N as a function of DM for a selection of pulsar duty-cycles. $\Delta\text{DM} = 0$ at the true DM of the pulsar. All pulsars shown have a 10 ms period.

much smaller than the total bandwidth, we may represent the smearing in a single channel, $\Delta t_{\text{channel}}$, of width Δf, by the derivative of Equation 1.15,

$$\Delta t_{\text{channel}} = 8.3 \times 10^3 \left(\frac{\Delta f}{\text{MHz}}\right)\left(\frac{\text{MHz}}{f^3}\right)\left(\frac{\text{DM}}{\text{pc cm}^{-3}}\right) \text{ sec.} \tag{2.6}$$

In the case where $\Delta t_{\text{channel}} \geq n t_{\text{samp}}$, the so-called *diagonal DM*, the data are oversampled and may be reduced in time resolution by a factor of n, where $n \in \mathbb{Z}$ and $n \geq 2$. To do this, the data in each frequency channel are averaged over n adjacent samples. As the sampling time is increased through the re-sampling, the DM step size may be recalculated through Equation 2.5.

To examine how the choice of DM step will affect the signal-to-noise ratio, S/N, of a pulsar with period P, we may use Equation 1 of Dewey et al. (1985),

$$S/N \propto \sqrt{\frac{P - W_{\text{eff}}}{W_{\text{eff}}}}. \tag{2.7}$$

Combining the above equation with Equations 2.3 and 2.4 we can calculate the S/N behaviour of a pulsar at ΔDM away from its optimal DM. Figure 2.5 shows the DM evolution of the relative S/N of 1-, 10-, 100- and 1000-ms pulsars with duty-cycles of 5%. Figure 2.6 shows the DM evolution of the relative S/N of three, 10-ms pulsars with 1%, 10% and 50% duty-cycles, respectively.

For each trial DM, a de-dispersed time series is created which is then searched for periodic and accelerated signals.

2.2.4 Periodicity searches

2.2.4.1 Barycentring

In the first stage of periodicity searching, the observation is transformed into the reference frame of the Solar System barycentre (SSB). This process, known as *barycentring*, is important in longer search observations as it removes any Doppler shift induced by the rotation of the Earth and its motion around the Sun. For shorter search observations, especially those employing techniques to search for accelerated pulsars, barycentring does not change the detectability of celestial pulsed signals and can be skipped[7]. A complete description of the barycentring process may be found in Lorimer and Kramer (2005). A description of the barycentring process as applied to pulsar timing observations can be found in Section 2.3.3.

2.2.4.2 Discrete Fourier transform

The fastest way to search for periodic signals in a uniformly sampled time series is to examine it in the Fourier domain (see e.g. Burns and Clark, 1969; Taylor, 1974). As the time series is both non-continuous and finite, we must use the discrete Fourier transform (DFT) to convert the time series from the time domain to the Fourier domain.

For a time series, $\mathcal{T}_k$, the value of the j^{th} bin of its DFT is defined as (see e.g. Bracewell, 2000)

$$\mathcal{F}_j = \frac{1}{N}\sum_{k=0}^{N-1}\mathcal{T}_k e^{-i2\pi j\frac{k}{N}}, \tag{2.8}$$

where N is the number of sampled points and $i = \sqrt{-1}$. As $\mathcal{T}_k$ is uniformly sampled, by Nyquist sampling theory, the frequency of bin $\mathcal{F}_j$ is given by $\nu_j = j/(Nt_{\text{samp}}) = j/t_{\text{obs}}$ with a maximum frequency $\nu_{\text{Nyquist}} = 1/(2t_{\text{samp}})$, where t_{obs} is the length of the observation and t_{samp} is the sampling interval. Each Fourier bin therefore has a width of $1/t_{\text{obs}}$.

[7] Assuming an observatory on the Earth's equator, we can roughly determine the minimum length of observation for which barycentring is required. Assuming the radius of the Earth at the equator to be $R \simeq 6.38 \times 10^6$ m, we determine the maximum radial acceleration at the Earth's surface to be $a \simeq 0.035$ m s^{-2} (here we ignore the effects of the Earth's motion around the Sun). By considering the Doppler effect and making a constant acceleration approximation, we see that for an observation of length t_{obs}, this acceleration will cause a change in a pulsars apparent spin frequency of $\Delta\nu = a\nu t_{\text{obs}}^2/c$, where ν is the intrinsic spin frequency of the pulsar (see Section 2.2.4.7). For an observation to require barycentring, the spin frequency of a given pulsar must drift by at least one Fourier bin over the course of the observation, i.e. $\Delta\nu \leqslant 1/t_{\text{obs}}$, where $1/t_{\text{obs}}$ is the width of a Fourier bin (see Section 2.2.4.2). Putting everything together we find $t_{\text{obs}} = \sqrt[3]{c/(a\nu)}$. Assuming we wish to remain sensitive to 1000 Hz pulsars, an observation must only be barycentred when it is has a length $\gtrsim 206$ sec.

Performing a DFT through brute-force calculation of Equation 2.8 is computationally expensive, requiring $O(N^2)$ arithmetical operations. To reduce the number of operations, and, therefore, the amount of time required to calculate the DFT, we make use of the fast Fourier transform (FFT) algorithm (Cooley and Tukey, 1965). The FFT is a highly efficient algorithm which requires only $O(N \log N)$ operations to calculate an N-point real DFT. Furthermore the FFT may itself be sped up by realisation that $\mathcal{T}_k \in \mathbb{R}$, meaning that the DFT is symmetric about $\nu_{\rm Nyquist}$, with the value of $\mathcal{F}_{N-j}$ simply being the complex conjugate of $\mathcal{F}_j$. Currently the fastest free-ware FFT library available is FFTW[8]. FFTW has become the standard FFT library used in pulsar search software in recent years due to its portability, speed[9] and ease of use.

In the case of bright normal pulsars, we may detect them through simple examination of the power in each Fourier bin. This is done by creating a *power spectrum*, where $\mathcal{P}_j = \mathbb{R}(\mathcal{F}_j)^2 + \mathbb{I}(\mathcal{F}_j)^2$. However, in the case of weak pulsars, especially those with long periods or narrow pulse profiles, we must use several techniques to improve the response of the DFT to pulsar-like signals.

2.2.4.3 Improving DFT frequency response

One of the largest problems associated with using the DFT, is that it has a non-uniform frequency response. For signals with frequencies which fall in the center of a Fourier bin, $\nu = \nu_j$, the response is maximised, whereas for signals which fall on the edge of a Fourier bin, $\nu = \nu_j \pm 1/(2t_{\rm obs})$, the response is minimised. In the worst case scenario the degree of amplitude degradation can be as high as 36% (see e.g. Ransom et al., 2002), meaning that methods should be used to recover this power before searching for periodic signals in the power spectrum.

Through the use of *zero-padding*, we may increase the spectral resolution of the DFT. In zero-padding, the time series to be transformed is padded with $N_{\rm pad}$ data points of mean value, until the frequency resolution of the DFT output, $1/(t_{\rm samp}[N + N_{\rm pad}])$, reaches a desired level. The addition of such a noiseless stream of constant-valued data to the time series will produce a uniform offset in the amplitude and phase of the Fourier components (see e.g. Bracewell, 2000). As a consequence, the limiting factor in zero-padding is the compute speed and memory usage required to perform very long FFTs.

[8] `http://www.fftw.org/`

[9] FFTW maintains speed by using a variety of different algorithms depending on the size and shape of the data set to be transformed. The algorithm with the lowest number of operations, the so called 'split-radix' algorithm (Johnson and Frigo, 2007), is sped up by the ability to factor the data using small prime numbers. It is therefore fastest to perform FFTs on data sets which are a power of two in length.

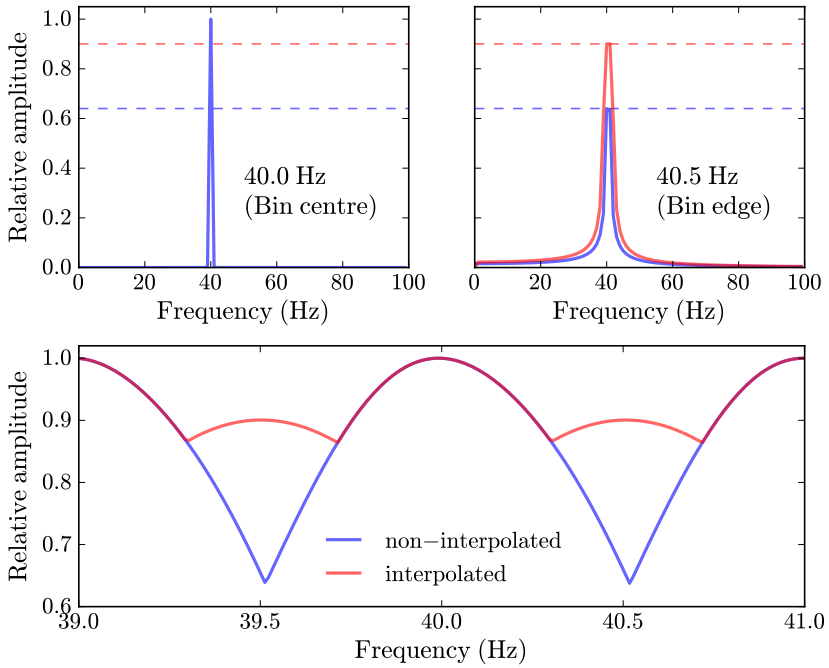

FIGURE 2.7: The frequency response of the DFT. *Top-left:* The response for a signal with a frequency that falls in the centre of a Fourier bin. *Top-right:* The response for a signal with a frequency that falls halfway between adjacent Fourier bins (*solid, blue line*) and the recovered response after application of Equation 2.9 (*solid, red line*). *Bottom:* The response as a function of frequency, before (*solid, blue line*) and after (*solid, red line*) application of Equation 2.9. Here the width of a Fourier bin is 1 Hz.

Another method of recovering signals that fall off the bin centre, is to compare the power in each bin with that of its two nearest neighbours. By this method, the power in the j^{th} Fourier component is given by (see e.g. Lorimer and Kramer, 2005),

$$\mathcal{P}_j = \max\left(\frac{|\mathcal{F}_{j-1} + \mathcal{F}_j|^2}{2}, |\mathcal{F}|^2, \frac{|\mathcal{F}_j + \mathcal{F}_{j+1}|^2}{2}\right). \tag{2.9}$$

Here, any power from a signal which lies on a bin edge is reconstructed into its nearest whole bin.

The above methods are not mutually exclusive and are often used in tandem when analysing pulsar search data. In certain circumstances, it is useful to pad the time series up to a power-of-two length before processing, as this both increases resolution and can, with certain FFT algorithms, speed up the DFT calculation. After the spectrum has been created, it is always useful to compare neighbouring bins, regardless of the increased spectral resolution.

2.2.4.4 Spectral whitening

If the observation is predominantly Gaussian noise, then the output of the DFT should also be predominantly Gaussian noise. However, gain fluctuations in the receiver, combined with strong, long-period RFI or backend instabilities, can produce large power contributions at the low-frequency end of the Fourier spectrum (Israel and Stella, 1996). Such excess *red noise*, significantly alters the statistical properties of the spectrum and can act to mask long-period pulsars from the data. It is therefore necessary to apply methods to whiten the spectrum prior to searching it for periodic signals.

The first step in any whitening procedure is to zero the first bin, the *DC bin*, in the Fourier spectrum. The value of this bin is simply the mean of the transformed time series[10] and contains, at least for our purposes, no useful information. Dependent on the degree of red-noise power, it is often useful to perform brute-force suppression of the lowest frequency components in the data. In this case the spectrum is zeroed up to the minimum frequency which is to be searched for pulsed signals. Typically this is done up to a frequency of ~ 0.1 Hz, although it should be noted that for longer observations the red noise components in the data may be more easily modelled, allowing for this limit to be reduced.

After the lowest frequency components have been dealt with, the spectrum may be whitened by subtraction of a running mean or median (see e.g. Israel and Stella, 1996; Ransom et al., 2002). Although calculation of a running mean is computationally faster than calculation of a running median, the running median is used more often due to its lack of sensitivity to outlying data points. Special care must be taken in selection of the window sizes for the median filter, as signals which drift in frequency spread their power over a number of adjacent Fourier bins. In cases where the filter window is comparable in size to the number of Fourier bins over which a signal has drifted, the application of the filter can result in suppression of the signal. As signals which drift in frequency are characteristic of pulsars in binary systems, the filter window size is often chosen to have frequency-dependent width, with windows at higher frequencies being larger than those at lower frequencies.

After the whitening process the Fourier components will have a mean of zero. By further normalising the spectrum such that it has a variance of one, the S/N of any signal in the power spectrum is simply its Fourier amplitude, $\sqrt{\mathcal{P}_j}$.

[10] If we look at Equation 2.8, in the case of the first Fourier bin (i.e. $k = 0$), the last term becomes $e^{-i2\pi j \frac{0}{N}} = 1$, making $\mathcal{F}_0 = \frac{1}{N} \sum_{k=0}^{N-1} \mathcal{T}_k$.

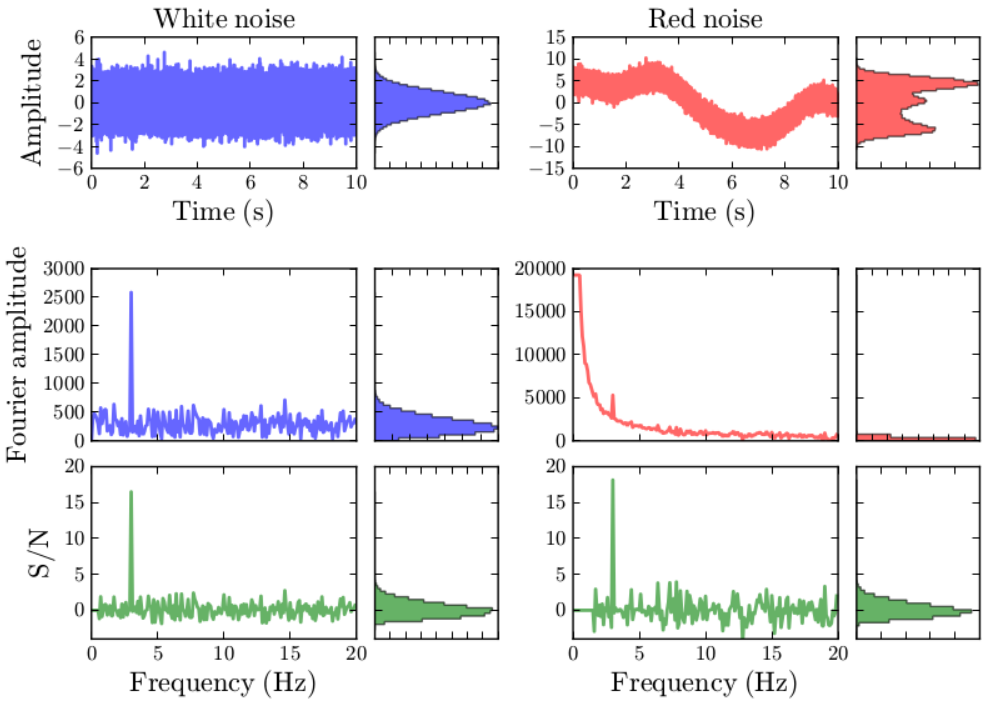

FIGURE 2.8: A comparison of spectral whitening using a running median filter for a 3 Hz sine wave in white (Gaussian) and red noise. *Top panels:* Two time series containing a 3 Hz sine wave. Both time series are composed of Gaussian noise, with the right-hand time series containing strong low-frequency noise. *Middle panels:* The Fourier spectrum of each time series. *Lower panels:* The result of the application of a running median filter with frequency dependent width. At 0 Hz the filter width is 3 bins, while at 5 Hz the filter width is 13 bins. A brute-force suppression of the power below 1.0 Hz is also performed.

2.2.4.5 Harmonic summing

Of the pulsars with measured pulse widths in the ATNF pulsar catalogue[11], only 1% have duty-cycles greater than 30%. A consequence of these narrow duty-cycles is that the signals from pulsars are not a clean tones in the Fourier spectrum. Instead, the power from the pulse is spread over the fundamental and a number of harmonics.

To examine the distribution of power throughout the harmonics, we shall consider the behaviour of a pulsed signal with a 10% duty-cycle and a profile given by a 'top-hat' function. The Fourier transform of this top-hat function is proportional to $\mathrm{sinc}(\pi\delta)$ (see e.g. Bracewell, 2000), where δ is the duty-cycle of the pulse. Similarly the Fourier transform of a train of top-hat pulses will be a train of delta functions modulated by the shape of the transform of a single pulse. Figure 2.9 shows the modulation of harmonics for our pulsed signal in the case where it has a fundamental frequency of 10 Hz. It is clear to see from Figure 2.9 that the harmonic envelope has its first null at $f = 1/(P\delta) = 1/W$,

[11] `http://www.atnf.csiro.au/people/pulsar/psrcat/` (Manchester et al., 2005)

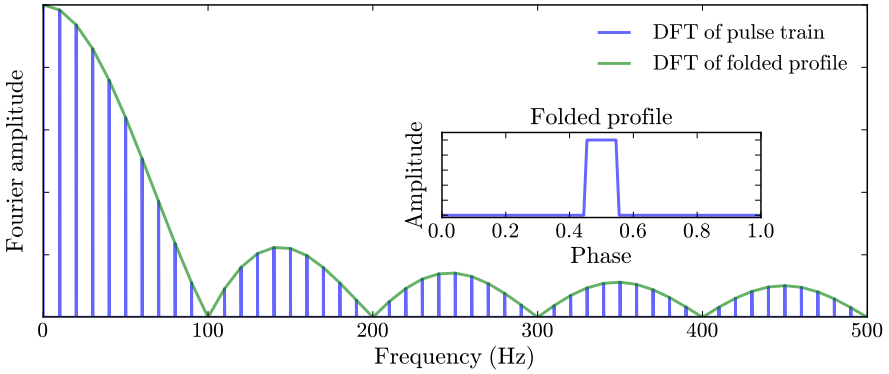

FIGURE 2.9: The modulation of harmonics from a noiseless top-hat pulse with a duty-cycle of 10% and fundamental frequency of 10 Hz

where W is the width of the pulse. If we consider only harmonics up to the first null, then we can say that a top-hat signal of duty-cycle δ and period P, spreads its power over $1/\delta$ harmonics, spaced by $1/P$.

To recover the power distributed in these harmonics, the process of *incoherent harmonic summing* (Taylor and Huguenin, 1969) is used. Here, the spectrum is summed with a stretched copy of itself such that all second harmonics are added to their corresponding fundamentals. In the case of the noiseless signal shown in Figure 2.9, this results in almost a doubling of the Fourier amplitude. In reality there will be significant Gaussian noise in the observation. As the summation of two Gaussian distributions with standard deviation σ, is another Gaussian distribution with standard deviation $\sqrt{2}\sigma$, the net increase in S/N achieved through a single incoherent harmonic sum is of the order $\sqrt{2}$ (Taylor and Huguenin, 1969). By repeating the summing process for both even and odd harmonics, we may recover a significant portion of the power distributed throughout the spectrum. It should be noted that for wider-profile pulsars, such as the majority of MSPs, summing up to the higher-order harmonics will not significantly improve the signal. In this case the higher-order harmonics will simply add noise to the signal. For each harmonic fold performed, we search the resultant spectrum for statistically significant signals.

2.2.4.6 Identifying significant signals

To determine which periodic signals are statistically significant, we must first consider the statistical properties of the Fourier power spectrum. Groth (1975) showed that, for a time series composed of both signal and Gaussian noise, the PDF of its Fourier power

spectrum, after n harmonic sums, may be described by

$$p(\mathcal{P}) = \frac{\mathcal{P}^{n-1}}{\Gamma(n)} \exp^{-\mathcal{P}}, \tag{2.10}$$

where the Fourier powers have been normalised such that the total power is zero (i.e normalisation by $N\bar{\mathcal{T}_k}$, where N is the number of samples in time series $\mathcal{T}_k$ (see e.g. Ransom et al., 2002)) and $\Gamma(n) = (n-1)!$. By integrating this relation between our lowest significant power $\mathcal{P}_{\rm min}$ and infinity we find

$$p(\mathcal{P} > \mathcal{P}_{\rm min}) = \sum_{j=1}^{n} \frac{\mathcal{P}_{\rm min}^{j-1}}{\Gamma(j)} \exp^{-\mathcal{P}_{\rm min}}, \tag{2.11}$$

where $p(\mathcal{P} > \mathcal{P}_{\rm min})$ is the probability that the power in a given Fourier bin exceeds $\mathcal{P}_{\rm min}$ for n harmonic folds. By setting this probability such that it gives only a single false positive in $n_{\rm trials}$ independent Fourier trials, we may estimate a minimum significant power level for a pulsar search.

This approach may also be extended to searches which work with Fourier amplitudes rather than powers. It can be shown (see e.g. Lorimer and Kramer, 2005) that in this case the minimum significant S/N is given by

$$\mathrm{S/N_{min}} = \frac{\sqrt{\ln\left[\mathrm{n_{trials}}\right]} - \sqrt{\pi/4}}{\sqrt{1-\pi/4}}. \tag{2.12}$$

For signals which exceed $\mathrm{S/N_{min}}$ or $\mathcal{P}_{\rm min}$, a secondary measurement of their significance can be obtained by reconstruction of the time domain pulse (see e.g. Manchester et al., 2001). This is done by performing the inverse DFT of only those Fourier bins which contain the signal, its harmonics and their complex conjugates. As the reconstructed profile considers the phase of the signal, the effects of random RFI superpositions on the signal's harmonics are suppressed. By the same logic, the reconstructed profile also selects against sinusoidal signals in the data, as very little signal will be present in the harmonics being back-transformed. This effect can be both desirable and detrimental, as while many RFI signals are sinusoidal in nature, the reconstructed profile also selects against pulsars with wide pulse profiles. The S/N of the reconstructed profile can be measured using standard techniques (see Section 2.2.5.2).

2.2.4.7 Acceleration searching

So far, all the methods described to enhance and detect periodic signals in a time series have only considered signals which have approximately uniform frequency throughout

the course of an observation. However, many of the most interesting pulsars we know of reside in binary systems. In such systems, changes in the line-of-sight velocity due to the orbital motion of the pulsar, creates a time-varying Doppler correction to its intrinsic frequency. This correction takes the form $\nu(t) = \nu_0(1 + v_t/c)$, where $\nu(t)$ is the frequency of the pulsar at time t, ν_0 is the intrinsic frequency of the pulsar and v_t is the line-of-sight velocity of the pulsar at time t, where $v_t << c$. The change in apparent frequency across an observation is therefore given by $\Delta\nu = a\nu_0 t_{\rm obs}/c$, assuming that the line-of-sight acceleration, a, is constant (an approximation which is valid for observations where $t_{\rm obs} \lesssim P_{\rm orb}/10$ (Ransom et al., 2003)). By expressing $\dot{\nu}$ in terms of a number of Fourier bins, Z, we find that a pulsar of intrinsic period P will spread its power over $Z = |at^2_{\rm obs}/Pc|$ Fourier bins during an observation of integration time $t_{\rm obs}$. Applying methods which can recover power spread across multiple Fourier bins allows us to detect pulsars in relativistic binary systems.

For all acceleration searches in this thesis, we apply the 'correlation technique' of matched filtering in the Fourier domain (Ransom et al., 2002). Here the Fourier amplitudes are cross-correlated with an analytically predicted signal response function of width Z. The correlation is therefore maximised when the pulsar has an acceleration $|a| = ZPc/t^2_{\rm obs}$. To make our search sensitive to a range of possible accelerations, matched filters are applied multiple times with different values of Z.

2.2.4.8 Candidate improvement

Having found significant accelerated or non-accelerated signals in the Fourier domain, it is possible to improve the frequency response of the DFT using *Fourier interpolation*. For a hypothetical signal at a frequency ν_r, which is less than half a Fourier bin from frequency ν_k, the DFT response can be shown (see e.g. Ransom et al., 2002) to be

$$\mathcal{F}_r = \mathcal{F}_k \mathrm{sinc}[\pi(\mathrm{k} - \mathrm{r})]. \tag{2.13}$$

As this response is sinc-like, the majority of the power from the signal will be distributed among Fourier bins local to $\mathcal{F}_k$. By correlating the nearest bin to r with a predicted response function for the signal, the true frequency of the signal may be recovered (Ransom et al., 2002). Typically the response function covers only a small number of bins (~ 32) around the nearest bin to r. This technique may also be extended to account for power distributed throughout higher harmonics.

2.2.4.9 Candidate sifting

After periodicity searching, the candidates are sifted to remove duplicates and to attempt to ensure that all detected signals are of the fundamental frequency. Furthermore, when periodicity searches have been performed for all trial DMs, the candidates can be sifted to remove signals which exhibit RFI-like behaviour. This can be signals which do not appear at a minimum number of adjacent DM trials, signals which appear strongest below a threshold DM[12] or signals which are at known RFI periods. A true pulsar signal should appear at multiple DM trials, with the S/N in each DM trial being dependent on the true DM of the pulsar, its pulse width and its rotational period (see figures 2.5 and 2.6). At this stage the candidates may be examined graphically or ranked on significance, or S/N, to be passed to a phase-folding algorithm.

2.2.5 Candidate folding

Candidates which remain after the sifting procedure are phase-folded to allow for closer examination of the signal. In the folding process, the observation is displayed as a function of the phase of the candidate signal, i.e. for a time series $\mathcal{T}_j$ the j^{th} sample has phase

$$\phi_j = \nu_0 t_j \left(1 + \frac{a_0 t_j}{2c}\right), \tag{2.14}$$

for a signal of spin frequency ν_0 with constant acceleration a_0, where $t_j = j t_{\text{samp}}$. Figure 2.10 shows folded subintegrations for a simulated 5-ms pulsar both with and without correction for acceleration in the folding procedure.

While phase-folding a time series will produce a pulse profile for the signal and a measure of its persistence in time, it lacks frequency information. As the dispersed, broadband nature of a pulsar signal is one of the key factors that distinguishes it from man-made interference, it is useful to fold the original filterbank data to obtain a pulse profile with both time and frequency information. Figure 2.11 shows a real-world example of a phase-folded observation of PSR J2206+6152, a newly discovered pulsar from this work. Shown are several diagnostic plots, including a pulse profile, subintegration and subband plot. The examination of plots such as these is the primary way by which we may distinguish between real pulsar signals, RFI and Gaussian noise.

[12]Typically, DM thresholds are chosen to be ~ 2 pc cm^{-3}. The choice of threshold should be dependent on the local RFI environment and the forms of RFI excision used on the observation.

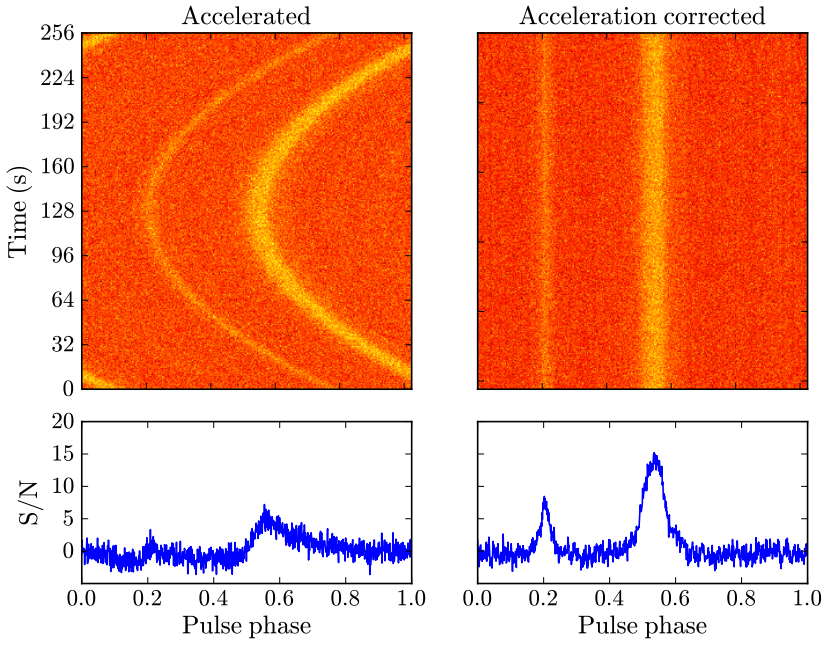

FIGURE 2.10: A simulated observation of a 5-ms pulsar experiencing a constant acceleration of 100 m s^{-2}. *Left-hand panels:* Subintegration plot and integrated pulse profile without taking into account the pulsar's acceleration. *Right-hand panels:* Subband plot and integrated pulse profile after correcting for the accelerated motion.

2.2.5.1 Fold optimisation

Having phase-folded a candidate, it is possible and desirable to further improve its period and DM. Optimisation of these parameters is important for correctly identifying pulsars in the data and for producing more accurate initial ephemerides for the purpose of pulsar timing.

A candidate which has been found with a period $P_{\rm disc}$, will exhibit a drift in phase across the course of an observation of (following e.g. Lorimer and Kramer, 2005)

$$\Delta\phi_P = \frac{t_{\rm obs}}{P_{\rm disc}}\left(\frac{P_{\rm opt}}{P_{\rm disc}} - 1\right), \tag{2.15}$$

where $P_{\rm opt}$ is the true period of the pulsar to within

$$\Delta P_{\rm opt} = \frac{P_{\rm opt}^2}{n_{\rm bins} t_{\rm obs}}, \tag{2.16}$$

where $n_{\rm bins}$ is the number of phase bins across the a folded profile.

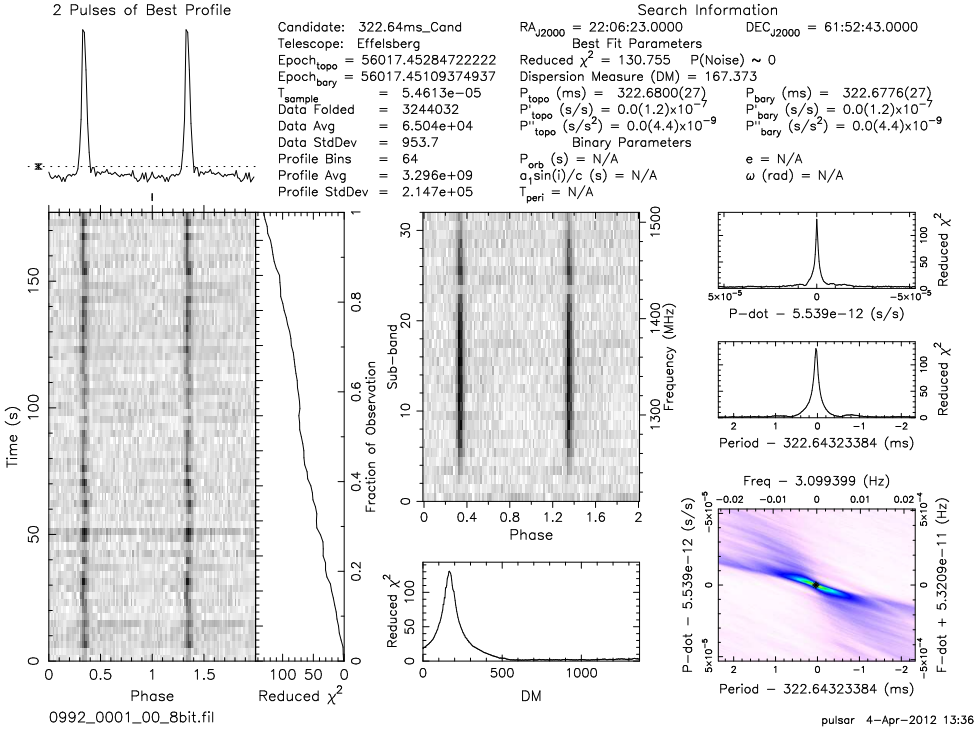

FIGURE 2.11: The discovery observation of PSR J2206+6152, found through the High Time Resolution Universe North pulsar survey (see Chapter 4). *Top-left:* The pulse profile, shown twice. *Bottom-left:* A subintegration plot showing the behaviour of the pulse profile with time. *Middle:* A subband plot showing the behaviour of the profile with frequency. *Middle-bottom:* A plot of reduced χ^2 as a function of DM. *Top-right:* A plot of reduced χ^2 as a function of period. *Middle-right:* A plot of reduced χ^2 as a function of period-derivative. *Bottom-right:* A period, period-derivative space mapping.
This figure was created using the PRESTO software package (see Section 2.2.7.1)

Similarly, a pulsar which has been found with a DM of $\mathrm{DM_{disc}}$, will exhibit a drift in time across its bandwidth of (following e.g. Lorimer and Kramer, 2005)

$$\Delta t_{\mathrm{DM}} = 4.15 \times 10^3 \left(\frac{1}{f_{\mathrm{bottom}}^2} - \frac{1}{f_{\mathrm{top}}^2} \right) (\mathrm{DM_{opt}} - \mathrm{DM_{disc}}) \text{ sec}, \tag{2.17}$$

where $\mathrm{DM_{opt}}$ is the true DM of the pulsar to within

$$\Delta \mathrm{DM_{opt}} = 1.2 \times 10^{-3} \frac{P f^3}{\mathrm{n_{bins}} \Delta f} \text{ pc cm}^{-3}. \tag{2.18}$$

By applying phase rotations to individual subbands or subintegrations, we may examine the signal strength at a range of trial phase offsets in both DM and period to obtain the characteristic *period* and *DM curve* for the signal. Both period and DM curve are shown in Figure 2.11.

2.2.5.2 Folded profile significance

An important measure of a folded profile is its S/N or significance. As the sum of multiple Gaussian distributions is itself a Gaussian distribution, the probability of a signal having a S/N greater than $\mathrm{S/N_{min}}$ is given by,

$$p(\mathrm{S/N} > \mathrm{S/N_{min}}) = \frac{n_{\mathrm{bins}}}{2}\ \mathrm{erfc}\left(\frac{\mathrm{S/N_{min}}}{\sqrt{2}}\right), \tag{2.19}$$

where n_{bins} is the number of bins in the folded profile and erfc is the complimentary error function,

$$\mathrm{erfc}(x) = \int_x^\infty e^{-t^2}\mathrm{d}t. \tag{2.20}$$

Although S/N is not a defining feature of the signal from a pulsar, low signal-to-noise ratios tend to indicate that a signal is the product of random noise processes. For example, in a 1024-bin profile dominated by white noise, the probability of any bin having a $\mathrm{S/N} > 2$ is $\sim 2300\%$. By comparison, for a good pulsar detection we expect $\mathrm{S/N} \gtrsim 8$. The probability of such a detection being from Gaussian noise processes is of the order $10^{-11}\%$.

For a folded profile p_i, the S/N can be defined as (following e.g. Lorimer and Kramer, 2005)

$$\mathrm{S/N} = \frac{\sqrt{W_{\mathrm{eq}}}}{\sigma_{\mathrm{off}}}(\bar{S}_{\mathrm{on}} - \bar{S}_{\mathrm{off}}), \tag{2.21}$$

where $\bar{S}_{\mathrm{on}}$ and $\bar{S}_{\mathrm{off}}$ are the mean on- and off-pulse flux densities, σ_{off} is the off-pulse standard deviation and W_{eq} is the equivalent width of a 'top-hat' function of the same area and peak height as the pulse. In the case of a known pulsar, the S/N is relatively simple to calculate, as the pulse width is already known, making it trivial to determine the on- and off-pulse regions of the profile. However, when the pulse width is unknown, we must apply methods which can accurately determine the on- and off-pulse phases. Such methods often have varying effectiveness for different pulse shapes, making the process of finding the true on-pulse region difficult. A good estimate for the off-pulse standard deviation can be found by considering the noise statistics of the data prior to folding, as the raw data should be dominated by Gaussian noise of standard deviation $\sigma_{\mathcal{T}}$. For a time series which has been folded $n_{\mathrm{folds}} = t_{\mathrm{obs}}/P$ times, the standard deviation of the resulting off-pulse portion of the profile will be $\sqrt{n_{\mathrm{folds}}}\sigma_{\mathcal{T}}$. Further normalising the profile by dividing each phase-bin by the number of points folded into it, we find $\sigma_{\mathrm{off}} = \sigma_{\mathcal{T}}/\sqrt{n_{\mathrm{folds}}} = \sigma_{\mathcal{T}}/\sqrt{(P/t_{\mathrm{obs}})}$.

It is also possible to use the probability-value of the χ^2 statistic of the profile to obtain a significance in terms of σ (i.e. a measure of the profiles deviation from pure Gaussian noise, see e.g. Leahy et al., 1983). This method is well suited to use on binned data as

well as sampled data. However, It should be noted that for highly significant signals, the probability rapidly approaches zero. This imposes a limit on numerically calculated values of σ for the most significant signals (i.e. for signals of > 40-σ significance, the true significance cannot be easily calculated numerically).

After optimisation and determination of the S/N or σ value of all candidates, the folded data are stored for later analysis by eye or by automatic pulsar selection algorithms (see Section 4.6.3.5).

2.2.6 Transient searches

The discovery of RRATs (see Section 1.1.8.6) as well as the discovery of some intriguing, and as of yet unexplained, one-time-only radio bursts (Keane et al., 2012; Lorimer et al., 2007), has shown the value of performing transient searches as part of a modern-day pulsar survey. The principal method for performing such a search (see e.g. Burke-Spolaor and Bailes, 2010; Cordes and McLaughlin, 2003), is to smooth the time series with box-car filters of a range of widths, before thresholding each smoothed time series at some minimum S/N. A signal of width W will therefore have a maximised S/N in a time series smoothed by a filter of width W.

The S/N of a pulse may be measured via Equation 2.21, assuming that the time series contains predominantly Gaussian noise with a mean of zero. Calculation of an appropriate S/N threshold is important in keeping the number of candidates created through single-pulse searches at a manageable level. For a time series which has been smoothed with a filter of width W, the probability that any signal will have a S/N greater than $\mathrm{S/N_{min}}$ is simply

$$p(\mathrm{S/N} > \mathrm{S/N_{min}}) = \frac{1}{2}\,\mathrm{erfc}\left(\mathrm{S/N_{min}}\sqrt{\frac{W}{2}},\right), \tag{2.22}$$

assuming that the original, unsmoothed time series was normalised such that it had a mean of zero and variance of one. By setting an acceptable number of noise detections N_{noise}, the S/N threshold becomes

$$\mathrm{S/N_{min}} = \sqrt{\frac{2}{W}}\,\mathrm{erfc}^{-1}\left(\frac{2N_{\mathrm{noise}}}{N_{\mathrm{samples}}}\right), \tag{2.23}$$

where erfc^{-1} is the inverse complementary error function.

By performing transient searches at all DM trials, we may build a map of S/N as a function of time and DM for each beam of an observation. Figure 2.12 shows an example of such a map for PSR B0355+54. Through visual inspection of these maps,

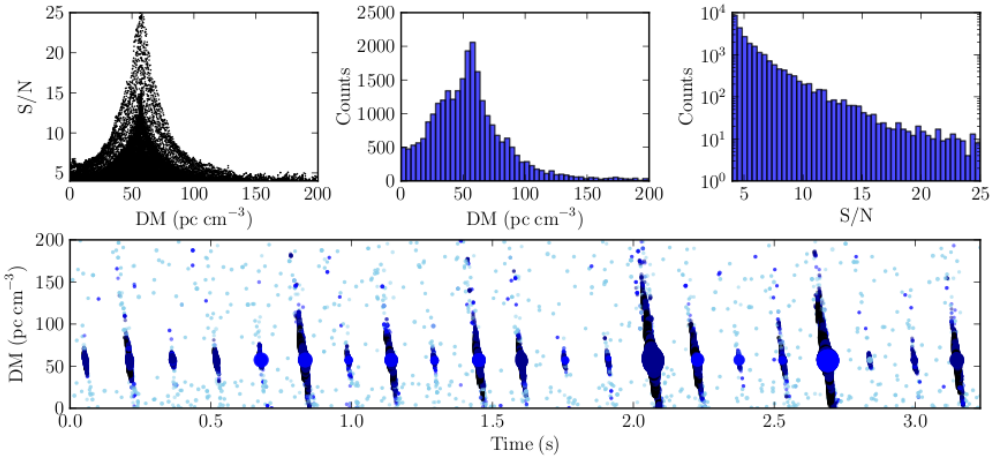

FIGURE 2.12: Detection of single pulses from PSR B0355+54. Plot shows the distribution of S/N values with DM (*upper left*), the number of detections at each DM (*upper middle*) and the distribution of S/N values for all detections (*upper right*). The bottom plot shows time vs. DM, with the diameter of the plotted circles indicating their S/N values (larger S/N gives wider diameters) and the colour of the circles indicating the box car width with which the detection was made (lighter blues indicate narrower box cars). The slopes seen in the detections in the lower plot are an artifact of the filterbank data being dispersed w.r.t. the highest observing frequency. It should be noted that no downsampling has been performed above the diagonal DM.

it is relatively simple to identify detections that are both temporally coherent and that have a maximum S/N at a single DM trial. Candidate signals which meet these criteria are further examined through conversion of the raw filterbank data to an image that covers the duration of the pulse. This allows for simple discrimination between signals which show a cold-plasma dispersion relation (see Equation 1.15) and those which do not. This is the most important test that any transient signal must pass before it is accepted as being celestial in nature.

An in-depth look at the theory behind transient searching can be found in Keane (2012). Also see Burke-Spolaor and Bailes (2010) for a discussion of a modern, transient-searching pipeline implementation.

2.2.7 Pulsar searching software

There are currently two main software packages used in the analysis of pulsar search data. Here we will briefly review these packages.

2.2.7.1 PRESTO

The **P**ulsa**R** **E**xploration and **S**earch **TO**olkit (PRESTO[13], Ransom (2001)), is a large suite of analysis software designed primarily to efficiently detect highly accelerated pulsars in long data sets. PRESTO implements several novel techniques which make use of the DFT response to accelerated signals in the data. First and foremost of these is the 'correlation technique' (Ransom et al., 2002) outlined in Section 2.2.4.7. PRESTO also implements RFI rejection algorithms and candidate folding and optimisation routines.

Due to its ease of use and memory efficiency, PRESTO is used in the majority of processing pipelines described in this thesis.

2.2.7.2 SIGPROC

SIGPROC[14] is a large and diverse pulsar data analysis package. SIGPROC is simple to use, implementing a stdin/stdout input/output system which allows the programs to be easily combined with normal Unix command line code. This simplicity makes SIGPROC a good development platform for new pulsar software. An example of this can be seen in the DEDISPERSE_ALL (Keith et al., 2010) program and its extensions (Burke-Spolaor and Bailes, 2010), which use the full processing capability of multi-core processors to speed up both de-dispersion and transient searching algorithms.

The ease of development using SIGPROC has also become its major flaw, as a lack of code standardisation and commenting guidelines has led to severe bloating of the inner workings of the package as more new code is tacked onto old code.

As part of this work, I have tried to modernise the SIGPROC package by re-coding it using an object oriented programming paradigm. In this manner it is easier to control code, perform unit testing and to abstract complex procedures from developers who do not need them. This new package, which is currently under the working title of SIGPYPROC, will be covered in Appendix A.

2.3 Follow-up timing

Discovering pulsars through radio searches is no longer, on its own, enough to bring interesting and publishable scientific results. If we wish to explore the nature of any new discoveries made through a given search, the new pulsars must be repeatedly observed

[13] `http://www.cv.nrao.edu/~sransom/presto/`
[14] `http://sigproc.sourceforge.net/`

and analysed using *pulsar timing* techniques. Pulsar timing is an expansive field, and the vast majority of it lies outwith the scope of this thesis. Here we will only review those techniques which allow us to perform initial timing, i.e. going from a rough knowledge of period and DM to a well-understood, phase-coherent model of a pulsar's rotation that takes into account period, spin-down, position and any potential binary motion.

2.3.1 Acquiring timing data

The first step in timing a new pulsar is to produce an initial ephemeris from the discovery observation. This should be done after fold optimisation (see Section 2.2.5.1) to achieve the best guess for the pulsar's parameters prior to timing observations. Next the discovery position is re-observed using a backend designed to handle pulsar timing observations.

Current pulsar timing backends differ from their searching counterparts, in that they perform both de-dispersion and folding (see Sections 2.2.3 and 2.2.5) online and in real-time. While older backends perform de-dispersion via application of passband dependent software or hardware delays based on Equation 2.1, newer backends use *coherent de-dispersion* (Hankins and Rickett, 1975) to resolve the pulse more accurately. In brief, coherent de-dispersion applies a chirp-function to the phase of the incoming voltages from the frontend. As dispersion can be thought of as a 'phase-only' filter, this acts to phase align the pulsar at all observing frequencies. De-dispersion in this manner removes the effects of intra-channel dispersive smearing, enabling us to resolve features of the pulse profile which may otherwise be obscured. It should be noted that the benefits of coherent de-dispersion become negligible at large distances, where interstellar scattering is the predominant pulse broadening mechanism.

After the observation has been folded and de-dispersed using an initial guess at the pulsar's ephemeris, the observation may again be optimised to determine the period and DM at the current observing epoch. When several such timing observations have been successfully completed, pulse times-of-arrival (TOAs) are generated.

2.3.2 Generating TOAs

The TOA is the basis of all pulsar timing. Each TOA relates the arrival time of the pulse to a reference observation, known as a *template*. To obtain the absolute arrival time, the observed pulse profile is cross-correlated with the template. In simple terms,

the TOA is given by

$$\mathrm{TOA} = \mathrm{MJD}_{\mathrm{obs}} + \arg\max_t(\mathcal{P} \star \mathcal{T})(t) \tag{2.24}$$

where $\mathcal{P}$ is the folded pulse profile from an observation, $\arg\max_t$ is an operator that returns the value of t which maximises the value of the correlation, $\mathcal{T}$ is the template, which is a scaled, offset and noiseless version of the pulse profile, and $\mathrm{MJD}_{\mathrm{obs}}$ is the start time of the observation which generated $\mathcal{P}$. For the purposes of initial timing the template profile is created from the highest S/N observation available. Assuming a template which accurately represents the true pulse shape, the uncertainty on each TOA is given by $\sigma_{\mathrm{TOA}} \simeq W/(\mathrm{S/N})$, where W is the profile width. It should be noted, that by the above equation, the TOA is given by the arrival time of the first pulse in the observation.

2.3.3 Frame correction

At this stage, all TOAs are referenced to the local time at the observatory at which they were taken. As the observatory frame cannot be considered inertial w.r.t. the pulsar, TOAs must be transferred to the nearest approximation we have to an inertial reference frame, the SSB. This transformation from *topocentric* to *barycentric* reference frames can be considered as the sum of several time delays which alter the arrival time of a pulse at the SSB w.r.t. the arrival time at the observatory. For a topocentric arrival time of t_{topo}, the corresponding barycentric arrival time is given by (see e.g. Lorimer and Kramer, 2005)

$$t_{\mathrm{bary}} = t_{\mathrm{topo}} + t_{\mathrm{corr}} - \Delta t_{\mathrm{DM}} + \Delta t_{\mathrm{R}_\odot} + \Delta t_{\mathrm{S}_\odot} + \Delta t_{\mathrm{E}_\odot}. \tag{2.25}$$

Below we give a brief account of each term in Equation 2.25, for a deeper look at calculation of each delay, see Lorimer and Kramer (2005). The first term, t_{corr}, is an observatory-dependent clock correction factor which takes into account any offsets in the observatory clock from a managed time standard such as International Atomic Time (TAI). Δt_{DM} is simply the dispersive delay from infinite frequency, and can be calculated via Equation 1.15. The *Römer delay*, $\Delta t_{\mathrm{R}_\odot}$, is the classical light-travel-time difference between arrival time at the telescope and at the SSB, for a pulse emitted at infinite distance. The *Shapiro delay*, $\Delta t_{\mathrm{S}_\odot}$, is a relativistic time delay caused by deviations in the curvature of space-time due to massive bodies in the path of the pulse. Such deviations alter the null geodesic length, and therefore the distance light must travel between pulsar and observatory, and pulsar and SSB. The final term is the *Einstein*

delay, $\Delta t_{\mathrm{E}_\odot}$, which is a combination of time dilation from the motion of the Earth in its orbit and gravitational redshift caused by massive bodies in the Solar System.

The calculation of the last three delays requires an accurate knowledge of the positions of all massive bodies in the solar system. This is done through use of a *Solar System ephemeris*, such as a current Jet Propulsion Laboratory Development Ephemeris[15] (i.e. DE200, DE405, DE414 etc.).

2.3.4 Fitting pulsar models

With the observation frames corrected to the SSB, TOA phases should be predominantly determined by a combination of the motion of the pulsar and uncertainty in the pulsar's position. This being the case, it is now possible to attempt to fit a selection of the pulsar's parameters.

2.3.4.1 Isolated pulsars

For isolated pulsar systems, we can express the pulsar spin frequency as a Taylor expansion

$$\nu(t) = \nu_0 + \dot{\nu_0}(t - t_0) + \ldots, \tag{2.26}$$

where ν_0 and $\dot{\nu_0}$ are the spin frequency and its derivative at reference epoch t_0. As the spin frequency can be simply thought of as the rate of change of pulse phase, we may integrate Equation 2.26 to obtain

$$\phi(t) = \phi_0 + \nu_0(t - t_0) + \frac{1}{2}\dot{\nu_0}(t - t_0)^2 + \ldots, \tag{2.27}$$

where ϕ_0 is the pulse phase at t_0. Through the use of least squares fitting, we may accurately determine both ν_0 and $\dot{\nu_0}$. In least squares fitting the TOAs, we attempt to minimise the expression

$$\chi^2 = \sum_{i=0}^{N_{\mathrm{TOA}}} \left(\frac{\phi(t_i) - \lfloor \phi(t_i) \rceil}{\sigma_i} \right)^2, \tag{2.28}$$

where N_{TOAs} is the number of TOAs, $\phi(t_i)$ is the phase of the i^{th} TOA, $\lfloor \phi(t_i) \rceil$ is $\phi(t_i)$ rounded to the nearest integer and σ_i is the TOA uncertainty in units of phase.

In practice, minimisation of Equation 2.28 is done in stages. Initially we take a set of observations which are close enough in time that the spin frequency error calculated

[15] `http://ssd.jpl.nasa.gov`

through the fold optimisation of a single observation is less than a single pulse period over the time between observations. By taking ϕ_0 as the pulse phase from the one or other of the observations and setting $\dot{\nu} = 0$, we may fit for ν across our observation pair. Repeating this process, adding in consecutive observations with each new fit, will begin to give a very accurate measure of the pulsar's spin frequency. The quality of the fit will not improve linearly, as with longer timing baselines the effects of spin-down will come into play. Refitting the data for both ν and $\dot{\nu}$ will allow continued timing of the pulsar by taking into account its spin-down. Similarly for longer timing baselines, the effects of positional uncertainty will become apparent through incorrect calculation of $\Delta t_{\mathrm{R}_\odot}$. Such an effect is easily seen as a year long sinusoid in the offsets of all TOAs from the best-fit model for the pulsar's rotation, otherwise known as the *timing residuals*. Figure 2.13 shows a graphical representation of the solving of an isolated pulsar. For initial timing of isolated pulsars, it is enough to fit for only the spin frequency, spin-down and position, assuming that the pulsar shows no significant timing irregularities. For binary systems the process is markedly more complicated, as the orbital motion of the pulsar introduces many more free parameters to the pulsar model.

2.3.4.2 Binary pulsars

Assuming a simple binary system that shows no strong relativistic effects, the orbit may be described by five parameters (see e.g. Lorimer and Kramer, 2005). These are P_b, the orbital period of the pulsar; T_0, the epoch of periastron passage; ω, the longitude of periastron passage; e, the eccentricity of the orbit; and $a \sin i$, the projected semi-major axis, where i is the inclination of the orbital plane w.r.t. the line of sight. All these parameters are contained within the classical *Römer delay*, $\Delta t_{\mathrm{R}_{\mathrm{binary}}}$, caused by the motion of the pulsar in its orbit. Blandford and Teukolsky (1976) show this delay to be

$$\Delta t_{\mathrm{R}_{\mathrm{binary}}} = x(\cos E - e)\sin\omega + x \sin E \sqrt{1-e^2}\cos\omega, \tag{2.29}$$

where $x = a \sin i/c$ and E is the *eccentric anomaly* as given by

$$E - e \sin E = \frac{2\pi}{P_b}(t - T_0), \tag{2.30}$$

to first order. E may be solved-for numerically using a root-finding algorithm such as the Newton-Raphson method. By fitting for our five orbital parameters, the intrinsic spin frequency and spin-down, we may determine a phase-coherent timing solution for the pulsar.

Due to the high number of degrees of freedom, we require accurate initial guesses at the binary parameters prior to fitting. To estimate the binary parameters, we observe

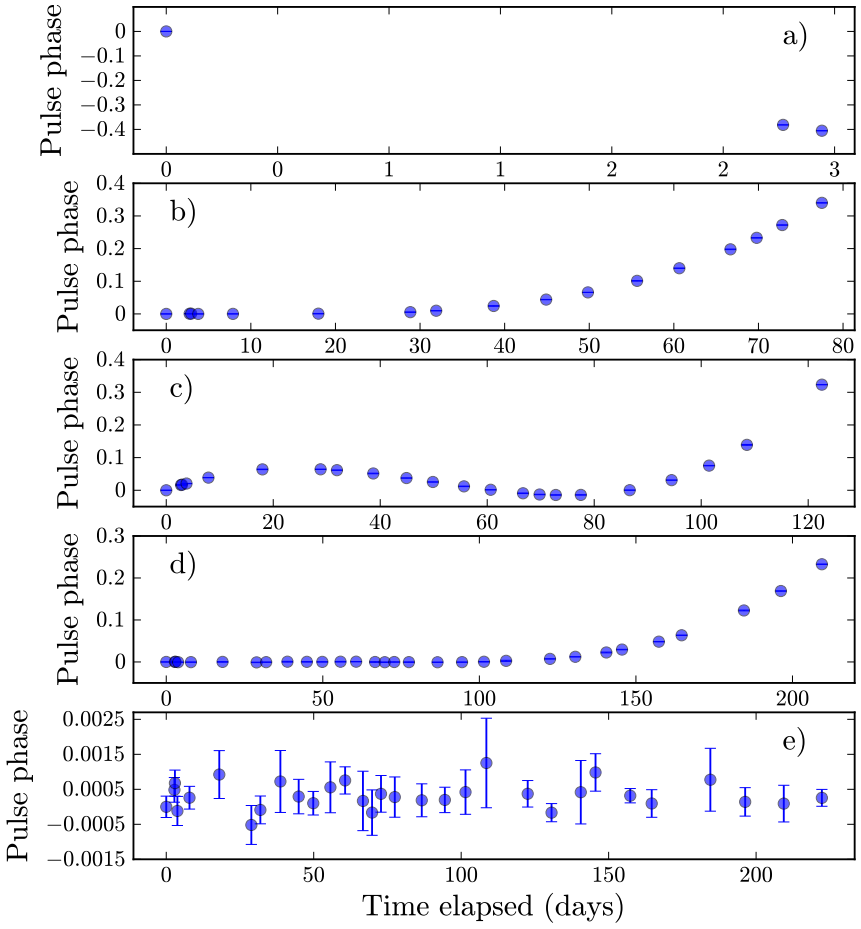

FIGURE 2.13: A step-by-step solving of the 922-ms, isolated pulsar J0425+4936. Panel a) shows the first three TOAs acquired. By fitting these TOAs for spin frequency, we can roughly predict the behaviour of the pulsar for ∼80 days, before we lose phase connection. This is shown in panel b). By further fitting the data in panel b) for a constant period derivative (panel c)), right ascension offset (panel d)) and declination offset (panel e)) we obtain a phase-coherent timing solution for the pulsar, which covers almost 250 days of timing.

the period evolution of the pulsar. As seen in Section 2.2.4.7, the Doppler correction to the spin frequency of a pulsar in a binary system is given by $\nu(t) = \nu_0(1 - v_t/c)$. Expressing the line-of-sight velocity, $v_{\mathrm{l.o.s.}}$, in terms of the position of the pulsar in its orbit we obtain (see e.g. Lorimer and Kramer, 2005)

$$\nu(t) = \nu_0(1 - v_{\mathrm{l.o.s.}}(A_{\mathrm{T}})/c) \tag{2.31}$$

where $A_{\rm T}$ is the *true anomaly*, which describes the position of a body in a Keplerian orbit. The true anomaly is given by

$$A_{\rm T}(E) = 2\arctan\left[\sqrt{\frac{1+e}{1-e}}\ \tan\frac{E}{2}\right]. \tag{2.32}$$

If the line-of-sight velocity is given by (see e.g. Lorimer and Kramer, 2005)

$$v_{\rm l.o.s.}(A_{\rm T}) = \frac{2\pi}{P_b}\frac{a\sin i}{\sqrt{1-e^2}}[\cos(\omega + A_{\rm T}) + e\cos\omega], \tag{2.33}$$

then by least-squares fitting the changes in observed spin frequency, we may generate estimates for all our binary parameters.

In practice we start by assuming all binary parameters to be zero and fit for the intrinsic spin frequency of the pulsar. With a good estimate for this value we may then attempt to fit for P_b and $a\sin i$, while keeping $e = 0$, i.e. assuming a perfectly circular orbit. If the χ^2 from the fit starts to become large when adding in more period measurements, then the data may be further fit with e, ω and T_0 to determine if the orbit is eccentric.

With suitably accurate estimates for the binary parameters, the process of solving the system follows closely the methodology used for isolated pulsars, with Equation 2.27 changed to

$$\phi(t) = \phi_0 + \nu_0(t - t_0) + \frac{1}{2}\dot{\nu_0}(t - t_0)^2 + \Delta t_{\rm R_{binary}}, \tag{2.34}$$

where $\Delta t_{\rm R_{binary}}$ is a function of binary phase and the orbit is Keplerian.

It should be noted that in the case of highly circular orbits (i.e. $e \simeq 0$), Equation 2.29 reduces to

$$\Delta t_{\rm R_{binary}} = x\sin(E + \omega). \tag{2.35}$$

Timing models based on this equation are unable to decouple the covariance of ω and T_0, leading to large uncertainties in these quantities. By redefining the orbit of the pulsar in terms of three new parameters; $T_{\rm asc}$, the time of ascending node; η, the first Laplace-Lagrange parameter; and κ, the second Laplace-Lagrange parameter, where

$$\eta = e\ \sin\omega, \tag{2.36}$$

$$\kappa = e\ \cos\omega, \tag{2.37}$$

$$T_{\rm asc} = T_0 - \frac{\omega P_b}{2\pi}, \tag{2.38}$$

Lange et al. (2001) developed a timing model by which ω and T_0 may be decoupled. Here, the Römer delay is redefined as

$$\Delta t_{\mathrm{R_{binary}}} \simeq \left(\sin\phi + \frac{\kappa}{2}\sin 2\phi - \frac{\eta}{2}\cos 2\phi\right), \tag{2.39}$$

where

$$\phi = \frac{2\pi}{P_b}(t - T_{\mathrm{asc}}). \tag{2.40}$$

This timing model, known as the *ELL1* model, is important for precision timing of low-eccentricity binaries, such as the majority of MSPs. The application of this model may be seen in Chapter 3, in the timing of PSR J1745+1017.

2.3.5 Pulsar timing software

There exist many software applications designed to aid in the timing of pulsars. Here we will mention two such packages which have been heavily used in the timing of pulsars found from searches in this thesis.

2.3.5.1 PSRCHIVE

PSRCHIVE[16] is an open-source, object-oriented software package designed for the manipulation of pulsar data in several formats. PSRCHIVE is written in C++ and has both its own shell environment and Python bindings to enable interactive use. Although not strictly a pulsar timing software package, PSRCHIVE is used heavily in the manipulation of timing observations to generate TOAs.

2.3.5.2 TEMPO2

TEMPO2[17] is a pulsar timing package written in C/C++, which contains least-squares fitting algorithms for the generation of phase-coherent timing solutions. Through the use of user developed 'plug-ins', TEMPO2 allows for interactive examination of timing data, simplifying the process of generating timing solutions for new pulsars. For this reason, TEMPO2 has been used for the timing of all newly discovered pulsars presented in this thesis.

[16] `http://psrchive.sourceforge.net/` (Hotan et al., 2004)
[17] `http://www.atnf.csiro.au/research/pulsar/tempo2/` (Hobbs et al., 2006)

Chapter 3

Pulsar searches of *Fermi* unassociated sources with the Effelsberg telescope

E. D. Barr,[1,2] L. Guillemot,[1,3] D. J. Champion,[1] M. Kramer,[4,1] R. P. Eatough,[1] K. J. Lee,[1] J. P. W. Verbiest,[1] C. G. Bassa,[4] F. Camilo,[5,6] Ö. Çelik,[7,8,9] I. Cognard,[10] E. C. Ferrara,[7] P. C. C. Freire,[1] G. H. Janssen,[4] S. Johnston,[11] M. Keith,[11] A. G. Lyne,[4] P. F. Michelson,[12] P. M. Saz Parkinson,[13] S. M. Ransom,[14] P. S. Ray,[15] B. W. Stappers,[4] K. S. Wood[15]

[1] *Max-Planck-Institut für Radioastronomie, Auf dem Hügel 69, 53121 Bonn, Germany*

[2] *email: ebarr@mpifr-bonn.mpg.de*

[3] *email: guillemo@mpifr-bonn.mpg.de*

[4] *Jodrell Bank Centre for Astrophysics, School of Physics and Astronomy, The University of Manchester, M13 9PL, UK*

[5] *Columbia Astrophysics Laboratory, Columbia University, New York, NY 10027, USA*

[6] *Arecibo Observatory, HC3 Box 53995, Arecibo, PR 00612, USA*

[7] *NASA Goddard Space Flight Center, Greenbelt, MD 20771, USA*

[8] *Center for Research and Exploration in Space Science and Technology (CRESST) and NASA Goddard Space Flight Center, Greenbelt, MD 20771, USA*

[9] *Department of Physics and Center for Space Sciences and Technology, University of Maryland Baltimore County, Baltimore, MD 21250, USA*

[10] *Laboratoire de Physique et Chimie de l'Environnement, LPCE UMR 6115 CNRS, F-45071 Orléans Cedex 02, and Station de radioastronomie de Nançay, Observatoire de Paris, C NRS/INSU, F-18330 Nançay, France*

[11] *CSIRO Astronomy and Space Science, Australia Telescope National Facility, Epping NSW 1710, Australia*

[12] *W. W. Hansen Experimental Physics Laboratory, Kavli Institute for Particle Astrophysics and Cosmology, Department of Physics and SLAC National Accelerator Laboratory, Stanf ord University, Stanford, CA 94305, USA*

[13] *Santa Cruz Institute for Particle Physics, Department of Physics and Department of Astronomy and Astrophysics, University of California at Santa Cruz, Santa Cruz, CA 95064, USA*
[14] *National Radio Astronomy Observatory (NRAO), Charlottesville, VA 22903, USA*
[15] *Space Science Division, Naval Research Laboratory, Washington, DC 20375-5352, USA*

Abstract:
Using the 100-m Effelsberg radio telescope, operating at 1.36 GHz, we have performed a targeted radio pulsar survey of 289 unassociated γ-ray sources discovered by the Large Area Telescope (LAT) aboard the *Fermi* satellite and published in the 1FGL catalogue (Abdo et al., 2010a). This survey resulted in the discovery of millisecond pulsar J1745+1017, which resides in a short-period binary system with a low-mass companion, $M_{c,min} \sim 0.0137\ M_{\odot}$, indicative of 'Black Widow' type systems. A two-year timing campaign has produced a refined radio ephemeris, accurate enough to allow for phase-folding of the LAT photons, resulting in the detection of a dual-peaked γ-ray light curve, proving that PSR J1745+1017 is the source responsible for the γ-ray emission seen in 1FGL J1745.5+1018 (2FGL J1745.6+1015; Nolan et al., 2012). We find the γ-ray spectrum of PSR J1745+1017 to be well modelled by an exponentially-cut-off power law with cut-off energy 3.2 GeV and photon index 1.6. The observed sources are known to contain a further 10 newly discovered pulsars, which were undetected in this survey. Our radio observations of these sources are discussed and in all cases limiting flux densities are calculated. The reasons behind the seemingly low yield of discoveries are also discussed.

3.1 Introduction

The detection of pulsed γ-ray emission from the Crab Pulsar in the early 1970's (Grindlay, 1972; Vasseur et al., 1970), the first of its kind, brought new light to the study of pulsar emission physics and high-energy emission physics in general. Gamma-ray photons of energies greater than 100 keV are created in processes involving nuclear or other non-thermal reactions, and as such become important when exploring the Universe at its most energetic. The current model for the creation of γ-ray photons that we see from pulsars is that charged particles stripped from the surface are accelerated to relativistic energies in the pulsar's strong electric field. As these particles travel along curved magnetic field lines, they produce γ-ray photons via synchrotron radiation, curvature radiation (e.g. Ruderman and Sutherland, 1975) and inverse Compton scattering from lower-energy photons (e.g. Daugherty and Harding, 1986). The study of these processes gives insight into the structure and composition of the magnetospheres of pulsars.

Prior to 2008, the most successful space-based γ-ray experiment was the Compton Gamma-Ray Observatory (CGRO), which was in orbit for nine years and carried the

Energetic Gamma-Ray Experiment Telescope (EGRET, Kanbach et al., 1989). EGRET was sensitive to γ-ray photons in the range 20 MeV – 30 GeV, and during its lifetime brought the known number of γ-ray emitting pulsars up to at least six (Thompson, 2008). However, the legacy of EGRET for the radio community was not the pulsars it detected, but rather those sources for which it could make no positive association. Targeted radio searches of these 169 γ-ray sources, unassociated with either pulsars or blazars, were performed, leading to several pulsar discoveries (e.g. Champion et al., 2005; Keith et al., 2008).

The Large Area Telescope (LAT) (Atwood et al., 2009) aboard the *Fermi* Gamma-ray Space Telescope, represents a significant improvement upon EGRET, providing a greater energy range and sensitivity, allowing for better measurements of source characteristics and localisations. With a host of new sources discovered, including many active galactic nuclei (AGNs) and pulsars, the *Fermi* telescope is the most successful GeV γ-ray observatory to date. As with EGRET, it is those sources which *Fermi* cannot immediately provide an association for that have piqued the interest of the pulsar searching community. A catalogue of 1451 γ-ray sources detected above 100 MeV was created from the first 11 months of LAT data. Of these sources, 630 were unassociated with known astrophysical objects (AGNs, pulsars, etc.; Abdo et al., 2010a). Multi-wavelength observations of the unassociated sources were encouraged so as to determine their natures, with many radio observatories searching for radio pulsations in the *Fermi* observational error-ellipses (e.g. Cognard et al., 2011; Keith et al., 2011; Ransom et al., 2011).

While *Fermi* LAT data have already been proved to contain a wealth of pulsars, with more than 100 pulsars detected through blind periodicity searches and phase-folding of LAT photons using known pulsar ephemerides (Ray and Saz Parkinson, 2011), low photon counts introduce strong selection biases in the detection of pulsars through blind searches of the LAT data. This is due to the large amount of computation required to perform wide-parameter-space searches of sparse photon data sets. For this reason, blind searches of the LAT data currently have great difficulty in detecting millisecond pulsars (MSPs) or pulsars in binary systems.

Radio pulsation searches are subject to different biases and thus are an important alternate method for identifying LAT unassociated sources as pulsars. At the time of this writing, there have been 47 radio-loud pulsars discovered through searches of these sources, of which 41 are MSPs likely to be associated with their corresponding LAT source (Ray et al., 2012a). These discoveries highlight the importance of targeted radio searches of LAT γ-ray sources, as these pulsars were most likely undetected in more general surveys due to shorter integration times or lack of searching for binary motion.

Of the MSPs discovered, 10 are thought to be in 'Black Widow' systems where the companion star has a very low mass due to ablation from the strong wind of the pulsar (Fruchter et al., 1988). Before *Fermi*, only three of these systems were known to exist outside globular clusters (Burgay et al., 2006; Fruchter et al., 1988; Stappers et al., 1996), which stresses the importance of investigating this new population of pulsars uncovered by the LAT. Those MSPs discovered that are not in Black Widow systems may also be of great use to current and future pulsar timing arrays for gravitational wave detection (Foster and Backer, 1990), which benefit from an even distribution of precisely timed pulsars across the sky.

In this paper we present a targeted search of 289 unassociated *Fermi* LAT sources using the 100-m Effelsberg telescope operating at 1.36 GHz. The search has resulted in the discovery of a 2.65-ms pulsar, PSR J1745+1017, in a 17.5-hour binary orbit with a 0.016-$M_\odot$ companion. The positions of 10 pulsars found in other targeted searches of unassociated LAT sources are contained within the 289 sources observed. For these sources, we discuss possible reasons for our non-detections and provide flux density limits where applicable.

This paper is structured as follows. In Section 3.2 we discuss selection criteria for sources to be observed. In Section 3.3 we discuss the observational methods and data processing. In Section 3.4 we discuss the survey sensitivity. In Section 3.5 we discuss simulations of the survey. In Section 3.6 we discuss the results of the survey. In Section 3.7 we discuss the source selection and detection rate. In Section 3.8 we present our conclusions.

3.2 *Fermi* catalogue source selection

All the sources searched for this paper were selected either from the *Fermi* LAT First Source catalogue (1FGL) (Abdo et al., 2010a) or from an unpublished update to the 1FGL that covered the first 18 months of *Fermi* observations.

The 1FGL contains 630 sources unassociated with any known astrophysical object, in the 100 MeV to 100 GeV energy range. The catalogue includes source localisations defined in terms of an elliptical fit to the 95% confidence level, power-law spectral fits, monthly light curves and flux measurements in 5 energy bands for each source. A full description of the 1FGL can be found in Abdo et al. (2010a). To narrow down the number of potentially observable sources, those below -20° declination, and those for which a known association existed were ignored. For all sources, the pointing position was chosen to coincide with the centre of the error ellipse. As better source localisations

became available, pointing positions were altered such that they coincided with the center of the updated error ellipse.

The remaining sources were ranked using an application of the Gaussian-mixture model as outlined in Lee et al. (2012). The best pulsar candidates exhibit significantly curved emission spectra and little γ-ray flux variability over time, in contrast with e.g. blazars and AGNs (see e.g. Figure 17 of Nolan et al., 2012).

The top 250 ranked candidates from the 1FGL catalogue were selected to be observed. A further 39 highly ranked sources from the 18-month update to the 1FGL were also selected to be observed, giving a total of 289 target sources.

3.3 Observational method and data processing

All search data presented in this paper were taken with the 100-m Effelsberg radio telescope at a centre frequency of 1.36 GHz between November 2009 and July 2010, using the central horn of the new Effelsberg multi-beam receiver with 300-MHz bandwidth.

The 289 sources selected for this survey were observed in three different observing campaigns. Initially all sources were observed with between 10- and 16-minute integrations. These integrations allowed for a preliminary shallow sweep of all sources such that the brightest pulsars, those likely to have been of the greatest use for timing applications, could be found. The second observing campaign was comprised of 32-minute integrations on 78 sources, with special focus given to covering as many of the highest ranked sources as time allowed. Finally, in the third campaign, 70 highly ranked sources were observed with between 60- and 76-minute integrations, with 32 of these sources observed multiple times. Observing in this manner reduced the effects of scintillation and of man-made radio-frequency interference (RFI), as most sources were observed multiple times with different integration times at different observing epochs.

Data were recorded over 512 filterbank channels of 585.3-kHz width, with a sampling rate of 53 μs. Initially all data were sampled at 32 bits by the digitisers before being brought down to 8 bits and written to high-capacity magnetic tape for transportation and storage.

To meet the processing demands imposed by the 5.5 TB of data created in the survey, a 22-node, 168-core computing cluster situated in the MPIfR was used for all data analysis. The PRESTO software package (Ransom, 2001) was used for data processing.

In the first stage of the processing pipeline, data underwent RFI treatment in which a time- and frequency-dependent mask was created to be applied at a later stage. As the

1FGL catalogue contains no distance information, each beam was de-dispersed at 2760 trial dispersion measures in the range 0–997 pc cm^{-3} to mitigate against the frequency-dependent delay in the pulsar signal due to dispersion by free electrons along the line of sight. Our choice of such a fine sampling in dispersion space allows for the retention of the data's maximum possible time resolution at all dispersion measures. The effect of this was a heightened sensitivity to millisecond and potential sub-millisecond pulsars.

All de-dispersed time series were fast-Fourier-transformed (FFT) and the resulting power spectra were de-reddened and known RFI frequencies were removed. To reconstruct power distributed throughout harmonics in the Fourier domain, the process of incoherent harmonic summing was used. Here the original spectra are summed with versions of themselves that have been stretched by a factor of two such that all second-order harmonics are added to their corresponding fundamental. This process was repeated four times, such that all power distributed in even harmonics up to the 16^{th} harmonic was incoherently added to the fundamental (see e.g. Lorimer and Kramer, 2005). The spectra from each stage of the summing process were searched for accelerated and non-accelerated signals.

At this stage the number and size of the FFTs required to achieve sensitivity to fast binaries becomes computationally too expensive for the longest pointings. To deal with this, the processing of the data was split into two stages. Initially all data were analysed at full length with a moderate acceleration search in the Fourier domain. This analysis is very sensitive to isolated and mildly accelerated pulsars in the data. The second processing stage involves splitting the data into 10-minute blocks and re-analysing with a much more intensive acceleration search. Although this stage uses shorter integrations, it is more sensitive to highly accelerated binary systems in the data. The details of the acceleration search can be found in Section 3.4.

Upon completion of the processing, all candidate signals underwent a sifting routine that removed any signals which were likely to be RFI. Finally, for the top 50 candidates, a set of diagnostic plots were created for visual inspection (e.g. Eatough et al., 2010). In cases where there were more than 50 candidates with greater than 8-σ significance, the pointing was considered to be contaminated by RFI and was flagged for re-observation.

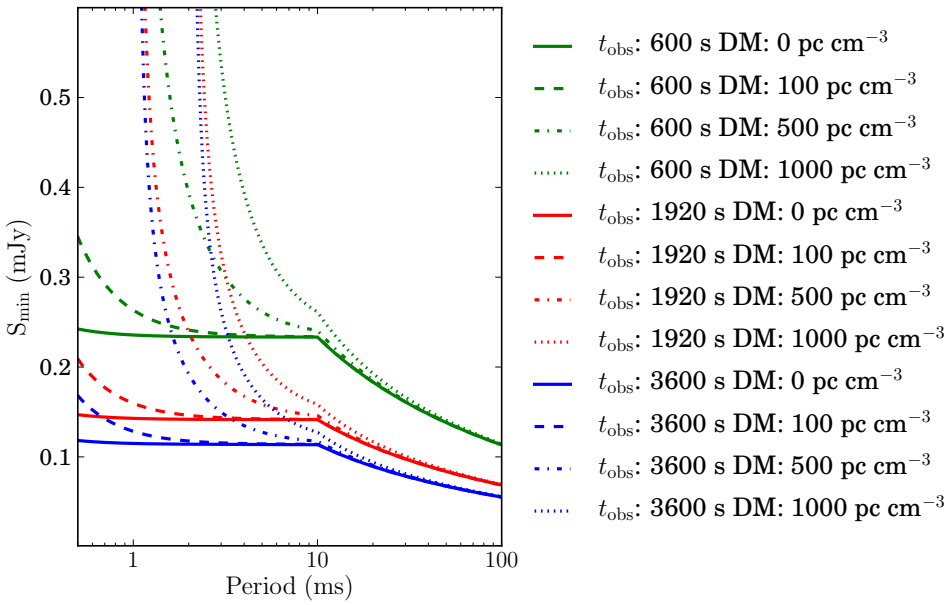

FIGURE 3.1: Theoretical minimum detectable flux densities ($S_{\rm min}$) vs. spin period for three integration regimes. A minimum detectable signal-to-noise of 8 was imposed. The break point at 10 ms occurs due to the assumption that the pulse duty-cycle scales as period$^{-0.5}$ with a maximum value of 1/3 (Kramer et al., 1998).

3.4 Sensitivity

To estimate the sensitivity of our survey setup we used the radiometer equation (see e.g. Lorimer and Kramer, 2005),

$$S_{\rm min} = \beta \frac{S/N_{\rm min} T_{\rm sys}}{G\sqrt{n_p t_{\rm obs} \delta f}} \left(\frac{P_{\rm cycle}}{1 - P_{\rm cycle}} \right)^{\frac{1}{2}}, \tag{3.1}$$

where the constant factor β denotes signal degradation due to digitisation, which for 8-bit digitisation is $\sim 1\%$, giving $\beta = 1.01$ (Kouwenhoven and Voûte, 2001). $T_{\rm sys}$ is the system temperature of the receiver. From flux density calibration measurements we found $T_{\rm sys} = 25$ K. G is the antenna gain (1.5 KJy^{-1} at 1.36 GHz), $P_{\rm cycle}$ is the pulse duty cycle, $t_{\rm obs}$ is the length of the observation, δf is the effective bandwidth of the receiver (240 MHz) and n_p is the number of polarisations summed, which for this survey is always 2. The factor $S/N_{\rm min}$ is the minimum signal-to-noise ratio with which we can make a detection. Based on false alarm statistics, we chose $S/N_{\rm min} = 8$.

Figure 3.1 shows the minimum detectable flux density as a function of pulsar period for four dispersion measures; 0, 100, 500, and 1000 pc cm^{-3}. Assuming a pulsar of typical duty cycle 5%, we achieve a minimum detectable flux density of 0.02 mJy for a 76-minute pointing and 0.06 mJy for a 10-minute pointing.

In a binary system, due to the Doppler effect, the apparent spin frequency of the pulsar drifts with time, spreading the pulsar's power in the Fourier domain. To reconstruct Fourier power smeared across multiple bins, we employed PRESTO's *accelsearch* routine which uses the 'correlation technique' of template matching in the Fourier domain as outlined in Ransom et al. (2002). The relationship between the largest range of Fourier bins over which to search for drifted signals, $Z_{\rm max}$, and the acceleration to which the search is sensitive, a_0, can be described by

$$a_0 = \frac{Z_{\rm max} P c}{t_{\rm obs}^2}, \tag{3.2}$$

where P is the spin period of the pulsar being searched for, $t_{\rm obs}$ is the integration time and c is the speed of light in a vacuum.

By assuming a 1-ms pulsar in a binary system, we may determine the sensitivity of the search at the extreme limit of the pulsar population. For the first processing pass, where the data were analysed in full length, we used $Z_{\rm max} = 50$ to achieve sensitivity to accelerations of up to $|a_0| \sim 42$ m s^{-2} and $|a_0| \sim 1$ m s^{-2} for 10- and 76-minute integrations, respectively. For the second processing pass, where data were analysed in 10-minute blocks, we used $Z_{\rm max} = 600$ to achieve sensitivity to accelerations of up to $|a_0| \sim 500$ m s^{-2}. For all systems which fall inside the acceleration limits for their integration lengths, the minimum detectable flux density may be calculated via Equation 3.1.

3.5 Simulations

As with any survey that contains many pointings, we may assume that the chance detection probability for pulsars unassociated with the LAT sources targeted is non-negligible. In order to determine this probability, simulations of the normal pulsar and MSP populations were made based on the model presented in Lorimer et al. (2006), using the PSRPOP[1] software. As the population distributions for MSPs and normal pulsars differ, separate simulations were performed for pulsars with rotational periods above and below 40 ms.

To simulate the normal pulsar population, input model parameters were chosen as follows:

- An empirical period distribution taken from the probability density function of the known population.

[1] http://psrpop.phys.wvu.edu/index.php

- A log-normal luminosity distribution, with mean and variance in log space of -1.1 and 0.9, respectively (Faucher-Giguère and Kaspi, 2006).
- A Gaussian distribution of spectral indices, with mean of -1.6 and variance of 0.5.
- An exponential distribution for the height above the Galactic plane, with a scale height of 0.33 kpc (Lorimer et al., 2006).
- A radial distribution as described in Lorimer et al. (2006).
- The NE2001 Galactic free electron density model (Cordes and Lazio, 2002).

To simulate the MSP population, the same model parameters were used with the Galactic scale height increased to 0.5 kpc to better match the known MSP distribution (Lorimer et al., 2006).

The number of pulsars simulated was such that the cumulative number of pulsars discovered in simulated versions of the Parkes Multibeam Pulsar Survey (Manchester et al., 2001), the Swinburne Intermediate Latitude Pulsar Survey (Edwards et al., 2001a) and its extension (Jacoby et al., 2009), and the Parkes High Latitude Survey (Burgay et al., 2006), matched the real discovery numbers.

Each observation of the 289 sources in the survey was then compared against the simulated pulsar distribution to determine if a chance detection could have been made. The Galactic pulsar population was simulated 1000 times and comparisons repeated with each simulation. We find a mean detection rate of 0.4 normal pulsars and 0.04 MSPs in the 289 pointings. While not ruling out the possibility of a chance MSP detection, these figures suggest that any MSP found in this survey will be associated to the LAT source targeted, at 96% confidence.

3.6 Results

3.6.1 PSR J1745+1017

3.6.1.1 Radio analysis

The main result of this work is the discovery of the radio pulsar PSR J1745+1017 in LAT source 1FGL J1745.5+1018 (2FGL J1745.6+1015). Initially discovered as a mildly accelerated candidate in a 10-minute data segment, PSR J1745+1017 has a period of 2.65 ms and a period derivative of 2.72×10^{-21}, making it the first MSP discovered with the Effelsberg telescope.

Upon discovery, PSR J1745+1017 was the subject of an intensive timing campaign involving the Effelsberg, Lovell and Nançay radio telescopes. Pulse times of arrival (TOAs) were analysed with the TEMPO2 software package (Hobbs et al., 2006) to create a phase-connected timing solution for the first two years of radio observations. The pulsar ephemeris and a selection of derived properties are displayed in Table 3.1.

From period and period derivative measurements we infer a characteristic age of 16.9 Gyr. Combined with the rapid spin period of PSR J1745+1017, this implies that the pulsar has undergone an extensive period of accretion-induced spin-up due to mass transfer from a companion star. This hypothesis is supported by the timing solution, which shows PSR J1745+1017 to be in a low-eccentricity binary system with an orbital period of 17.5 hr and a low-mass companion. Using the definition for the binary mass function,

$$f(m_1, m_2) = \frac{4\pi^2}{G}\frac{(a\sin i)^3}{P_b^2} = \frac{(m_2 \sin i)^3}{(m_1 + m_2)^2}, \tag{3.3}$$

where m_1 and m_2 are the masses of the pulsar and companion respectively; G is Newton's gravitational constant; $a \sin i$ is the projected semi-major axis of the system, where i is the inclination angle of the binary (defined such that $i = 90^\circ$ is edge on); and P_b is the orbital period, we obtain $f(m_1, m_2) = 1.4 \times 10^{-6} M_\odot$. Assuming an average pulsar mass of 1.35 $M_\odot$, this gives minimum and median companion masses of 0.014 and 0.016 $M_\odot$, respectively.

This small range of low companion masses strongly suggests that PSR J1745+1017 is a 'Black Widow' system with a white dwarf companion that has been heavily ablated by the strong particle wind from the pulsar. Unlike Black Widow systems such as PSR B1957+21 (Fruchter et al., 1988) and PSR J2051−0827 (Stappers et al., 1996), PSR J1745+1017 exhibits neither eclipsing behaviour nor DM variations across orbital phase, implying a low inclination angle. If the inclination is low, then the companion mass is likely to be larger than the presented value. As noted by Lorimer and Kramer (2005), the probability of observing a binary system with an inclination less than i_0 for a random distribution of orbital inclinations is $p(i) = 1 - \cos(i_0)$. This relation suggests that the inclination angle is greater than 26°, at 90% confidence. We therefore place an upper limit of 0.032 $M_\odot$ on the mass of the companion, to the same confidence level.

From proper motion measurements of PSR J1754+1017, we find a transverse velocity of $\sim 48 \pm 9$ km s^{-1}. The small dispersion-measure-inferred distance to this pulsar, $d \sim 1.3$ kpc, suggests that the Shklovskii effect (Shklovskii, 1970) contribution to the measured period derivative will be non-negligible. For a pulsar with transverse velocity v_t, the Shklovskii effect acts to increase the intrinsic period derivative of the pulsar by a factor

Pv_t/cd (see Camilo et al., 1994), where c is the speed of light in a vacuum. We find a contribution to the period derivative of $5 \pm 2 \times 10^{-23}$, or $\sim 18\%$ of the measured value.

Assuming a moment of inertia of 10^{45} g cm^2 and using the Shklovskii-corrected period derivative, we derive the spin-down luminosity of PSR J1745+1017 to be $\dot{E} = 4\pi^2 I \dot{P}/P^3 = 4.7 \times 10^{33}$ ergs s^{-1}, a value which makes this pulsar a good candidate for pulsed γ-ray emission (Abdo et al., 2010a).

3.6.1.2 Gamma-ray analysis

In order to characterize the γ-ray emission of PSR J1745+1017, we selected *Fermi* LAT data recorded between 2008 August 4 and 2012 March 7, with reconstructed energies larger than 0.1 GeV, directions within a circular region of interest (ROI) of 15° radius around the pulsar's position, and zenith angles smaller than 100°. We further restricted the dataset to 'Source' class events of the P7_V6 instrument response functions, and rejected times when the rocking angle of the LAT exceeded 52° or when the Earth's limb infringed upon the ROI. The selected γ-ray events were finally phase-folded using the ephemeris given in Table 3.1 and the *Fermi* plug-in distributed with TEMPO2 (Ray et al., 2011).

Initial pulsation searches using standard data selection cuts yielded marginal detections only. For instance, selecting photons found within 1° of the pulsar and with energies larger than 0.1 GeV, we found an H-test parameter (de Jager and Büsching, 2010) of 15.6, which translates to a significance of $\sim 3.1\sigma$. Nonetheless, pulsation searches can be made more sensitive by weighting the photons by the probability that they originate from the pulsar. These probabilities can be computed through a spectral analysis of the pulsar and the neighbouring sources (Guillemot et al., 2012b; Kerr, 2011).

The γ-ray spectrum of PSR J1745+1017 was measured by fitting sources in the ROI using a binned likelihood method, with the *pyLikelihood* module included in the *Fermi* Science Tools [2]. The source model used for the analysis included the spectral parameters of the 78 sources of the *Fermi* LAT Second Source Catalogue (2FGL Nolan et al., 2012) found within 20° of the pulsar. The spectrum of PSR J1745+1017 was represented by an exponentially-cut-off power-law of the form $dN/dE = N_0 \left(E/1 \text{ GeV}\right)^{-\Gamma} \exp\left(-E/E_c\right)$, where N_0 is a normalization factor, Γ is the photon index, and E_c is the cut-off energy. The extragalactic diffuse emission and the residual instrument background were modelled using the *iso_p7v6source* template, and the Galactic diffuse emission was modelled using the *gal_2yearp7v6_v0* map cube. The spectral parameters of the sources within 5° of

[2] http://fermi.gsfc.nasa.gov/ssc/data/analysis/scitools/overview.html

TABLE 3.1: PSR J1745+1017 ephemeris created from TOAs taken with the Nançay, Effelsberg and Lovell telescopes over the course of 22 months. Numbers in parentheses represent twice the formal 1-σ uncertainties in the trailing digit as determined by TEMPO2. The dispersion-measure-derived distance was calculated using the NE2001 Galactic electron density model (Cordes and Lazio, 2002), giving a likely uncertainty of 20%. The mass function calculation assumes an average mass of 1.35 $M_\odot$ for the pulsar. The characteristic age, spin-down luminosity and surface magnetic field strengths were calculated using the Shklovskii-corrected period derivative. All parameters are determined for the given reference epoch. These parameters were determined with TEMPO2, which uses the International Celestial Reference System and Barycentric Coordinate Time. Refer to Hobbs et al. (2006) for information on modifying this timing model for observing systems that use TEMPO format parameters.

PSR J1745+1017 ephemeris	
Fitted timing parameters	
Right Ascension (R.A. J2000) (hh:mm:ss)	17:45:33.8371(7)
Declination (Decl. J2000) ($^\circ$:′:″)	+10:17:52.523(2)
Proper motion:	
in R.A. ($\mu_\alpha \cos(\text{decl.})$) (mas yr^{-1})	6(1)
in Decl. (μ_δ) (mas yr^{-1})	-5(1)
Period (s)	0.00265212967108(3)
Period derivative ($\times 10^{-21}$)	2.73(1)
Dispersion measure (pc cm^{-3})	23.970(2)
Orbital period (days)	0.730241444(1)
Projected semi-major axis (lt-s)	0.088172(1)
Epoch of ascending node (MJD)	55209.968794(2)
κ ($\equiv e\cos\omega$) ($\times 10^{-5}$)	0(2)
η ($\equiv e\sin\omega$) ($\times 10^{-5}$)	0(2)
Fixed parameters	
Reference epoch (MJD)	55400
Clock correction procedure	TT(TAI)
Time system	TCB
Solar system ephemeris model	DE414
Binary model	ELL1 (Lange et al., 2001)
Derived parameters	
Frequency (Hz)	377.05547013813(5)
Frequency derivative (Hz s^{-1} $\times 10^{-16}$)	-3.88(2)
Orbital eccentricity ($\times 10^{-5}$)	0(2)
Epoch of periastron passage (MJD)	55210.3(4)
Galactic longitude (J2000) (deg)	34.8693081(3)
Galactic latitude (J2000) (deg)	19.2536887(5)
Mass function ($M_\odot$)	1.38(1)$\times 10^{-6}$
Minimum companion mass ($M_\odot$)	0.0137
Median companion mass ($M_\odot$)	0.0158
Dispersion measure-derived distance (kpc)	1.3(2)
Shklovskii-corrected	
period derivative ($\times 10^{-21}$)	2.22(5)
Characteristic age (Gyr)	18.9
Spin-down luminosity ($\times 10^{33}$ ergs s,$^{-1}$)	4.7
Surface magnetic field ($\times 10^7$ G)	7.7
rms residual (μs)	5.05
Further parameters	
Median flux density at 1.36 GHz (mJy)	0.3
Maximum flux density at 1.36 GHz (mJy)	4.4
Span of timing data (MJD)	55225 - 56026
Number of TOAs	156

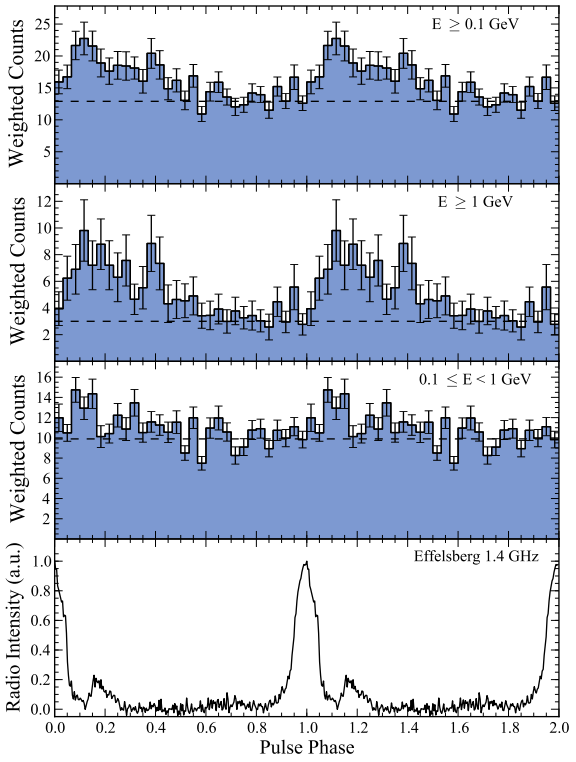

FIGURE 3.2: Multi-wavelength light curves of PSR J1745+1017. The bottom panel shows the 1.4-GHz radio profile recorded with the Effelsberg radio telescope. The upper panels show probability-weighted γ-ray light curves in different energy ranges, with 30 bins per rotation. Horizontal dashed lines show the estimated γ-ray background levels. For clarity, two rotations are shown.

the pulsar as well as the normalizations of the diffuse models were re-fit, while the parameters of other sources were fixed at the 2FGL catalogue values.

We found no evidence of significant emission from the pulsar in the phase range [0.6; 1]. In order to increase the signal-to-noise ratio of the pulsar we thus restricted the dataset to photons with reconstructed pulse phases between 0 and 0.6 (the γ-ray light curve of PSR J1745+1017, presented below, is indeed compatible with showing emission only in this phase range). The best-fitting spectral parameters of PSR J1745+1017 are listed in Table 3.2, along with the integrated photon and energy fluxes above 0.1 GeV derived from these results. Systematic uncertainties were calculated by running the same analysis as described above, but using bracketing IRFs for which the effective area has been perturbed by ±10% at 0.1 GeV, ±5% near 0.5 GeV, and ±10% at 10 GeV, with linear interpolations in log space between.

Using the best-fitting spectral model for the ROI obtained from the analysis described above, we could calculate probabilities that the photons in the ROI originate from PSR J1745+1017. Selecting events found within 5° and with calculated probabilities larger than 0.01, we obtained a weighted H-test parameter (see Kerr, 2011) of 58.0,

TABLE 3.2: Measured γ-ray light curve and spectral parameters for PSR J1745+1017. First quoted uncertainties are statistical, and the second are systematic. Details on the determination of the systematic uncertainties are given in Section 3.6.1.2.

Parameter	Value
First peak position, Φ_1	0.14 ± 0.04
First peak full width at half-maximum, FWHM_1	0.20 ± 0.16
Second peak position, Φ_2	0.39 ± 0.03
Second peak full width at half-maximum, FWHM_2	0.10 ± 0.10
Radio-to-γ-ray lag, δ	0.14 ± 0.04
γ-ray peak separation, Δ	0.26 ± 0.06
Photon index, Γ	$1.6 \pm 0.2^{+0.1}_{-0.1}$
Cutoff energy, E_c (GeV)	$3.2 \pm 1.2^{+0.2}_{-0.1}$
Photon flux (> 0.1 GeV), F_{100} (10^{-8} cm^{-2} s^{-1})	$1.1 \pm 0.3^{+0.1}_{-0.1}$
Energy flux (> 0.1 GeV), G_{100} (10^{-12} erg cm^{-2} s^{-1})	$9.3 \pm 1.2^{+0.3}_{-0.6}$
Luminosity, L_γ / f_Ω (10^{33} erg s^{-1})	$1.8 \pm 0.6^{+0.6}_{-0.6}$
Efficiency, η / f_Ω	$0.3 \pm 0.1^{+0.1}_{-0.1}$

corresponding to a pulsation significance of 6.5σ. Figure 3.2 shows probability-weighted light curves for PSR J1745+1017 in different energy bands. The background levels shown in Figure 3.2 were calculated by summing the probabilities that selected γ-ray events do not originate from the pulsar, as described in Guillemot et al. (2012b). Statistical error bars were obtained by calculating $\sqrt{\sum_i w_i^2}$, where w_i represents the photon probability and i runs over photons falling in the same phase bin (Pletsch et al., 2012). As can be seen from Figure 3.2, the γ-ray profile of PSR J1745+1017 shows evidence for two distinct peaks, at phases ~ 0.14 and ~ 0.39. Fits of the two γ-ray peaks with Lorentzian lines above 0.3 GeV yielded the peak positions Φ_i and the full widths at half maxima FWHM_i listed in Table 3.2. We also attempted to fit the light curve with one asymmetric Lorentzian line, and found that the model with two peaks is slightly preferred, at the $\sim 1\sigma$ level. The radio-to-gamma-ray lag $\delta = \Phi_1 - \Phi_r$ (where $\Phi_r = 0$ is the phase of the maximum of the radio profile shown in Figure 3.2) and the γ-ray peaks separation $\Delta = \Phi_2 - \Phi_1$ are found to be $\delta = 0.14 \pm 0.04$ and $\Delta = 0.26 \pm 0.06$ (see Table 3.2). The uncertainty on the radio-to-gamma-ray lag due to the error on the measurement of the DM parameter is estimated to be $\Delta(\delta) = \Delta(\mathrm{DM})/(Kf^2)$ where $K = 2.410 \times 10^{-4}$ MHz^{-2} cm^{-3} pc s^{-1} is the dispersion constant. We find $\Delta(\delta) \sim 10^{-3} \times P$, which is very small compared to the statistical error bar. Such values of δ and Δ are relatively common amongst other known γ-ray pulsars (see Figure 4 of Abdo et al., 2010b), and match the predictions of theoretical models that place the high-energy emission from pulsars at high altitudes in the magnetosphere (Romani and Yadigaroglu, 1995).

The ephemeris used for phase-folding the γ-ray data considered in this analysis is based on radio timing taken after 2010 January 30 (MJD 55226). In an attempt to determine whether the ephemeris describes the rotational behaviour of the pulsar over the entire

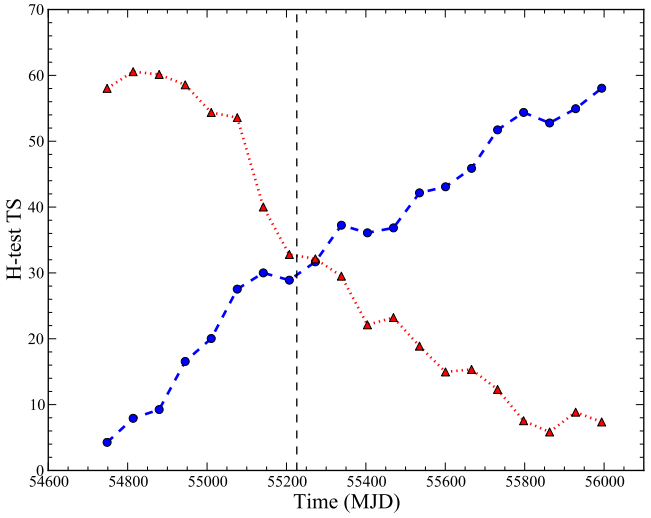

FIGURE 3.3: Evolution of the weighted H-test Test Statistic (TS) as a function of time. The blue, dashed line shows the weighted H-test parameter with increasing time, using data taken from 2008 August 8. The red, dotted line shows the weighted H-test parameter when going backwards in time, using data taken before 2012 March 7. The vertical dashed line indicates the formal start of the ephemeris validity interval.

Fermi LAT dataset accurately, we analysed the evolution of the weighted H-test parameter as a function of time. The results of this analysis are shown in Figure 3.3. First of all, because the H-test depends linearly on the number of photons for a given pulsed signal fraction, the linear increase of the H-test parameter as a function of the dataset length provides further evidence that the pulsed γ-ray signal from PSR J1745+1017 is real. Moreover, the increase of the H-test parameter when going forward or backward in time is monotonic outside the formal ephemeris validity interval, which indicates that the ephemeris given in Table 3.1 provides a good description of the pulsar's rotational behaviour across the entire LAT dataset.

From the energy flux G_{100} measured from the spectral analysis, we calculated the γ-ray luminosity above 0.1 GeV using $L_\gamma = 4\pi f_\Omega G_{100} d^2$, where f_Ω is a geometrical correction factor depending on the beaming angle of the pulsar and the viewing geometry (Watters et al., 2009). Using the distance derived from the NE2001 model of $d = 1.3 \pm 0.2$ kpc, we get the γ-ray luminosity $L_\gamma / f_\Omega \sim 1.8 \times 10^{33}$ erg s^{-1} and the γ-ray efficiency, $\eta / f_\Omega = L_\gamma / \dot{E} \sim 0.3$. This value for the efficiency lies well within the distribution of γ-ray efficiencies seen for other LAT-detected MSPs (Abdo et al., 2010b).

From the measurement of the γ-ray energy flux and the proper motion of the pulsar, we can put an upper limit on the distance derived from the inequality $L_\gamma < \dot{E}$ (see Equation 2 of Guillemot et al., 2012b). Assuming $I = 10^{45}$ g cm^2 and $f_\Omega = 1$ (a typical value for other gamma-ray MSPs, see e.g. Venter et al., 2009), we get $d \leqslant 1.9$ kpc.

3.6.2 Radio pulsar non-detections

During the course of the observations, other observatories discovered six radio-emitting pulsars associated with the sources observed in this survey. These pulsars were not detected in this survey due to a combination of reasons, such as limited flux density, local RFI conditions and source position redefinitions. Further information on all sources observed in this work may be found in Appendix B.

3.6.2.1 PSR J2030+3641

PSR J2030+3641 (Camilo et al., 2012), initially undetected in our data processing, exhibits a rotational frequency which is similar to the 10^{th} sub-harmonic of the 50 Hz local mains frequency. Unfortunately signals which are similar in frequency to harmonics of the mains are often lost in noise or excised from the data in the process of Fourier RFI excision, wherein known RFI signals are removed from the power spectrum of the observation prior to pulse detection. It should be noted that this pulsar was discovered using the Robert C. Byrd Green Bank Telescope in the US, where the mains frequency is 60 Hz.

Reprocessing of these data with the published ephemeris yielded a detection of the pulsar at signal-to-noise 6.4, a value that lies below the detection threshold of this survey. Using Equation 3.1, we found a corresponding estimated flux density of 0.08 mJy. This value is half that of the published flux density at 1.5 GHz, a discrepancy which may be attributed to the extra noise induced by the oscillations of the mains electricity at the folding period. It should be noted, that the derived position of J2030+3641 is coincident with the position observed in this survey.

3.6.2.2 PSRs J1646−2142, J1816+4510 and J1858−2218

PSRs J1646−2142, J1858−2218 (Ray et al., 2012a) and J1816+4510 (Kaplan et al., 2012) were all discovered at LAT positions that were significantly different from the position determined in the 1FGL catalogue. Because of this, the discovery position of these pulsars is a half-beamwidth or more away from the position observed in this work, and so no detection is expected.

3.6.2.3 PSRs J0307+7443 and J1828+0625

PSRs J0307+7443 and J1828+0625 (Ray et al., 2012a) were both discovered at positions coincident with sources observed in this survey. Both pulsars were detected at low radio

PSR	Pointing offset (°)	$S_{\rm min}$ (mJy)	Reference
J0734−1559	0.05	0.1	Saz Parkinson (2011)
J1803−2149	0.05	0.1	Pletsch et al. (2012)
J2030+4415	0.02	0.08	Pletsch et al. (2012)
J2139+4716	0.04	0.09	Pletsch et al. (2012)

TABLE 3.3: Limiting flux densities ($S_{\rm min}$) for LAT detected pulsars coincident with sources observed in this work. All pulsars are assumed to have a radio pulse with a 10% duty-cycle and scattering effects are ignored. It should be noted that the upper radio flux limits presented here are higher than those published in Pletsch et al. (2012), due to the use of an increased detection threshold of signal-to-noise 8.

frequency and appear to be weak radio emitters. Assuming similar profile characteristics at both 1.36 GHz and at the discovery frequency, we found upper limits of 0.1 and 0.2 mJy on the radio flux densities at 1.36 GHz for PSRs J0307+7443 and J1828+0625, respectively.

3.6.3 Gamma-ray pulsar non-detections

Through blind searches of *Fermi* LAT photons, a further four pulsars associated with the sources observed have since been discovered (Pletsch et al., 2012; Saz Parkinson, 2011). No radio detection has so far been made for these pulsars, therefore in Table 3.3 we present our upper limits on their radio flux densities at 1.36 GHz.

A simple model for the telescope beam was used to adjust limiting flux densities for position offsets between the pointing and true position of the source. Limiting flux densities were divided by a Gaussian factor q, given by $q = e^{-(\theta/\phi)^2/1.5}$, where θ is the pointing offset and ϕ is the beam half-width at half maximum, to return the true limiting flux density at 1.36 GHz ($S_{\rm min}$).

3.7 Discussion

Considering the success that other surveys of unassociated *Fermi* LAT sources have had (Camilo et al., 2012; Cognard et al., 2011; Keith et al., 2011; Ransom et al., 2011), we must consider the reasons behind our relatively small yield of discoveries.

Sources observed in this work were selected based on information provided in the 1FGL catalogue. However, in the recently published 2FGL catalogue, many of these sources are no longer listed. A detailed description of the possible causes for this can be found in Section 4.2 of Nolan et al. (2012). Using the 2FGL catalogue to examine the 289 sources selected for observation, we find:

- 106 sources that are no longer listed.
- 46 sources that have moved by more than half the FWHM of the telescope beam.
- 22 sources marked as potentially spurious.

Selecting against these sources and choosing only sources for which the entire updated 95% confidence region was contained within the FWHM of the telescope beam, we are left with 72 sources for which observations adequately cover the LAT source targeted.

This would suggest that the detection rate for the survey is ∼1.4%. However, as noted by Camilo et al. (2012), a large number of pulsar surveys at radio wavelengths have focused on observing the Galactic plane at low latitudes, introducing a strong bias against the discovery of new radio-emitting pulsars in this volume. Selecting only those 58 sources that lie in the region $|b| > 3.5°$, we find the detection rate to be 1.7%.

We note that the strategy employed by other surveys of LAT unassociated sources has generally been to select a small number of sources and observe with long integration times, often at lower frequencies (e.g. Ransom et al., 2011). By contrast, we have selected a large number of sources and observed at various integration lengths at higher frequency. Although this strategy has lacked the discoveries that other searches have made, it has provided the most complete picture yet of the LAT sky at high radio frequencies.

The results of our survey suggest that future surveys of unassociated LAT sources would benefit from lower observing frequencies, as wider beam-widths will increase the LAT error ellipse coverage, which, when combined with the decrease in LAT error ellipse size due to increasing observation depth, will significantly reduce the problems associated with source redefinitions. Furthermore, we note that the majority of pulsars discovered through radio searches of the LAT data have been found at low frequencies. This suggests that this population of pulsars may have particularly steep spectral indices. Continued multi-frequency study of pulsars discovered in unassociated LAT sources will deny or confirm this hypothesis.

3.8 Conclusion

We have performed repeated observations of 289 unassociated sources from the First *Fermi* LAT catalogue of γ-ray sources, resulting in the discovery of PSR J1745+1017.

PSR J1745+1017 has a 2.65 ms spin period and orbits a very low mass companion with an orbital period of 17.5 hours. The low mass of the companion suggests that

PSR J1745+1017 is a 'Black Widow' system, however a two-year timing campaign has thus far found no evidence of eclipses, dispersion measure variations across orbital phase or Shapiro delay. By performing weighted-probability analysis of LAT photons in the region of interest around PSR J1745+1017, we also detected γ-ray pulsations from the source. This gives a clear indication that PSR J1745+1017 is responsible for the γ-ray emission seen from 1FGL J1745.5+1018 (2FGL J1745.6+1015).

The observed sample contains three radio pulsars, newly discovered through similar searches performed by other observatories, and four γ-ray selected, radio-quiet pulsars, found through blind searches of *Fermi* LAT data.

No radio detection was made for the four γ-ray selected pulsars contained in our sample. The upper limits on their radio flux densities at 1.36 GHz were calculated. These limits can be found in Table 3.3.

Of the three newly-discovered radio pulsars coincident with LAT sources searched in this survey, only PSR J2030+3641 was detected using the known timing solution. PSRs J0307+7443 and J1828+0625 were suspected to have radio flux densities at 1.36 GHz lower than the limiting flux density of our observations.

Acknowledgements

This work was carried out based on observations with the 100-m telescope of the MPIfR (Max-Planck-Institut für Radioastronomie) at Effelsberg.

The *Fermi*-LAT Collaboration acknowledges generous ongoing support from a number of agencies and institutes that have supported both the development and the operation of the *Fermi*-LAT as well as scientific data analysis. These include the National Aeronautics and Space Administration and the Department of Energy in the United States, the Commissariat à l'Energie Atomique and the Centre National de la Recherche Scientifique/Institut National de Physique Nucléaire et de Physique des Particules in France, the Agenzia Spaziale Italiana and the Istituto Nazionale di Fisica Nucleare in Italy, the Ministry of Education, Culture, Sports, Science and Technology (MEXT), High Energy Accelerator Research Organization (KEK), and Japan Aerospace Exploration Agency (JAXA) in Japan, and the K. A. Wallenberg Foundation, the Swedish Research Council, and the Swedish National Space Board in Sweden.

Additional support for science analysis during the operations phase is gratefully acknowledged from the Istituto Nazionale di Astrofisica in Italy and the Centre National d'Études Spatiales in France.

The Nançay Radio Observatory is operated by the Paris Observatory, associated with the French Centre National de la Recherche Scientifique(CNRS)

JPWV acknowledges support by the European Union under Marie-Curie Intra-European Fellowship 236394.

PCCF and JPWV acknowledge support by the European Research Council under ERC Starting Grant Beacon (contract no. 279702).

We would like to thank Matthew Kerr for his input regarding initial source selection.

Chapter 4

The Northern High Time Resolution Universe Pulsar Survey I: Initial setup and discoveries

E. D. Barr,[1] D. J. Champion,[1] M. Kramer,[2,1] R. P. Eatough,[1] P. C. C. Freire,[1] R. Karuppusamy,[1,2] K. J. Lee,[1] A. G. Lyne,[2] B. Stappers,[2] J. P. W. Verbiest,[1]

[1] *Max-Planck-Institut für Radioastronomie, Auf dem Hügel 69, 53121 Bonn, Germany*
[2] *Jodrell Bank Centre for Astrophysics, School of Physics and Astronomy, The University of Manchester, M13 9PL, UK*

Abstract:
We report on the initial setup and discoveries of the Northern High Time Resolution Universe survey for pulsars and fast transients in the northern hemisphere, the first major pulsar survey conducted with the 100-m Effelsberg radio telescope and the first pulsar survey in 20 years to observe the whole northern sky at high radio frequencies. Using a newly developed 7-beam receiver system coupled with a state-of-the-art polyphase filterbank, we record a 300-MHz passband in 512 channels centered on 1.36 GHz with a time resolution of 54 μs. Such fine time and frequency resolution increases our sensitivity to millisecond pulsars and fast transients, especially at large distances, where previous surveys have been limited due to intra-channel frequency dispersion. To optimise observing time, the survey is split into three integration regimes dependent on Galactic latitude, with 1500-s, 180-s and 90-s integrations for latitude ranges $|b| < 3.5°$, $|b| < 15°$ and $|b| > 15°$, respectively. The survey has so far resulted in the discovery of 12 radio pulsars, including a pulsar with a characteristic age $\lesssim 19$ kyr, PSR J2004+3427, and a highly-eccentric,

binary millisecond pulsar out of the Galactic plane, PSR J1946+3414. All newly discovered pulsars are timed using the 76-m Lovell radio telescope at the Jodrell Bank observatory and the 100-m Effelsberg radio telescope. We present timing solutions for all newly discovered pulsars and discuss potential supernova remnant associations for PSR J2004+3427.

4.1 Introduction

It could be argued, that no other astophysical object has the ability to provide insight into as many fields of pyhsics and astrophysics as the pulsar. The extreme conditions found in and around these objects make them unique natural laboratories for the study of subjects such as the equation of state of supra-nuclear matter (Demorest et al., 2010), the behaviour of gravity in the strong-field regime (Kramer et al., 2006b), the formation and evolution of binary systems (Stairs, 2004) and the existence and properties of gravitational waves (Foster and Backer, 1990). Therefore the discovery of new pulsars systems, through targeted or blind surveys, holds great scientific potential.

Pulsar surveys will in general always increase our understanding of the underlying source distribution and its properties, but it is the potential for the detection of rare and exciting systems, such as a hypothesised pulsar-black hole system (Narayan et al., 1991), that is the major driving force behind modern-day pulsar surveys. Several examples of such exciting discoveries can be found in surveys conducted within the last two decades. These include the discovery of the so-called 'Diamond-planet pulsar', PSR J1719−1438 (Bailes et al., 2011), with its Jupiter-mass CO white dwarf companion; of PSR J0437−4715 (Johnston et al., 1993), a pulsar which rotates with a fractional stability of one part in 10^{15}; of PSR J1903+0327 (Champion et al., 2008), a rapidly rotating pulsar in a highly-eccentric orbit, which has shed light on the evolution of hierarchical triple-systems (Freire et al., 2011); and perhaps most impressively, of the 'Double pulsar', PSR J0737−3039A/B (Burgay et al., 2003), which consists of two pulsars orbiting each other in a highly-relativistic binary system. Studies of this unique system have led to the most stringent tests of gravity in the strong-field regime ever conducted (Kramer et al., 2006b), tests which are currently impossible anywhere else in the known universe.

While targeted pulsar surveys, such as those which observe globular clusters (e.g. Ransom et al., 2005) or γ-ray point sources (e.g. Cognard et al., 2011; Keith et al., 2011), tend to have a high discovery rate, they can not produce an unbiased measure of the underlying population. To achieve a more complete picture of the true population distribution and the exotic systems it may hide, we must perform all-sky surveys.

In the past, blind surveys have been successful in detecting many new and exciting pulsar systems. Good examples can be found in the many blind surveys (e.g. Burgay et al., 2006; Edwards et al., 2001a; Manchester et al., 2001) conducted using the 20-cm multi-beam receiver system of the Parkes radio telescope over the last 20 years. These surveys have been remarkably successful, not only discovering almost 60% of all known pulsars, but also some unique and fascinating objects. As well as the discovery of the aforementioned Double pulsar, these surveys have discovered six of the ten known double neutron star systems (DNS); the pulsar with the highest magnetic field (Levin et al., 2010), the most massive companion (Stairs et al., 2001) and the largest glitch (Manchester and Hobbs, 2011). Furthermore, reprocessing of the data from these surveys has led to the discovery of Rotating Radio Transients (RRATs McLaughlin et al., 2006), a new class of pulsars that display bursty radio emission on varying timescales (see Keane et al., 2011, for a recent review).

The above surveys used a 96×3 MHz channel analogue filterbank with a 250-μs sampling time. This coarse frequency and time resolution resulted in a diminished searchable volume for narrow-pulse-width transients and millisecond pulsars (MSPs), due to dispersion smearing within individual channels. These limitations were compounded by a 1-bit digitisation scheme employed by the analogue filterbank. While 1-bit digitisation provides a crude real-time radio-frequency interference (RFI) filter, its limited dynamic range acts to decrease the signal-to-noise (S/N) ratio of any pulsed or transient signals by 30% (Manchester et al., 2001). While these surveys were state-of-the-art at their conception, affordable technology now exists to significantly improve on them. Recent improvements in field-programmable gate array (FPGA) technology combined with advancements in data transfer and storage techniques, have allowed for the use of tunable polyphase filterbanks capable of providing large numbers of high-resolution frequency channels and high sampling rates. These improvements, combined with the development of a state-of-the-art 1.36-GHz multi-beam receiver for the 100-m Effelsberg telescope, has led to the High Time Resolution Universe (HTRU) survey, the motivation behind which is understanding of the Galactic population of (MSPs) and characterising the transient sky down to timescales of a few tens of microseconds. Using the 100-m Effelsberg telescope in the northern hemisphere and the 64-m Parkes telescope in the southern hemisphere, the HTRU survey aims to achieve complete sky coverage at varying integration depths, with the deepest integrations along the Galactic plane.

The southern half of the HTRU survey (Keith et al., 2010) has been underway for several years, resulting in the discovery of more than 100 new pulsars, several of which are high-dispersion-measure MSPs (Bates et al., 2011a; Keith et al., 2012), undetectable in previous surveys of this region due to intra-channel dispersive smearing.

In this paper we present the setup and initial results of the northern half of the HTRU survey, from here on referred to as HTRU-North.

In Section 4.2 we desribe the observing strategy used in the HTRU-North survey. In Section 4.3 we describe the front and backend systems used at the Effelsberg radio telescope. In Section 4.4 we present analytical and empirical estimates of the survey sensitivity. In Section 4.5 we consider the expected pulsar yield as determined through Monte Carlo simulations of the Galactic pulsar population. In Section 4.6 we describe the data processing pipeline from acquisition to candidate selection. In Section 4.7 we present the discoveries made by HTRU-North thus far.

4.2 Strategy

The HTRU-North survey will be comprised of more than 1.5 million observed positions on the sky, making the efficient scheduling of observations of paramount importance. To optimise the usage of our observing time, the HTRU-North survey is split into three complementary parts based on Galactic latitude.

The **high-latitude** section covers the sky at Galactic latitudes of $|b| > 15^\circ$ with short integrations of 90 s. The majority of sky covered by the high-latitude section has remained unsurveyed for 20 years, and so with the technical advances implemented by HTRU-North, we expect to discover a wealth of bright pulsars, which do not require long integration times to detect, and both Galactic and extragalactic transients (see Section 4.6).

The **mid-latitude** section covers Galactic latitudes of $|b| < 15^\circ$ with 180-s integrations. This section of the survey probes the regions of the Galaxy most likely to contain bright MSPs necessary for gravitational wave detection by pulsar timing arrays (Foster and Backer, 1990). In the mid-latitude section, we also perform a shallow sweep of the Galactic plane. These observations are expected to discover many bright normal pulsars.

Finally, the **low-latitude** section covers Galactic latitudes of $|b| < 3.5^\circ$ with long integrations of 1500 s. Here we search for faint pulsars deep in the Galactic plane. This section gives the greatest hope of discovering exotic systems such as double neutron stars and pulsars orbiting black holes, as the long integration times make this the deepest ever large-scale survey of the Galactic plane as seen from the northern hemisphere, and because these systems are expected to be close to their birth locations, given their relatively low ages (Manchester et al., 2001).

TABLE 4.1: Observational parameters of each latitude region of the HTRU-North survey.

Survey	High	Mid	Low
Region	$\|b\| > 15°$	$\|b\| < 15°$	$\|b\| < 3.5°$
τ_{obs} (s)	90	180	1500
N_{beams}	1066135	375067	87395
T_{samp} (μs)	53	53	53
$\Delta\nu$ (MHz)	240	240	240
$\Delta\nu_{chan}$ (kHz)	585.9375	585.9375	585.9375
N_{chans}	410	410	410
$N_{samples}$ ($\times 10^6$)	1.6	3.3	27.4
Data/beam (GB)	0.8	1.6	13.4
Data (total) (TB)	818.1	575.6	1117.76

For all latitude regimes, the integration times were chosen such that the limiting flux densities of the northern and southern portions of the HTRU survey were comparable. Table 4.1 shows integration times, data volumes and observational parameters for all parts of the HTRU-North survey.

4.3 Instrumentation

All searching was perfomed using the 100-m Effelsberg radio telescope owned by the Max-Planck-Institut für Radioastronomie in Bonn, Germany. Below, we describe both the receiver and backend systems used to acquire observational data.

4.3.1 The 21-cm Effelsberg multi-beam receiver

The 21-cm Effelsberg multi-beam receiver consists of seven horns at the prime focus of the Effelsberg telescope. The horns are arranged in a close-packed hexagonal pattern around the central beam, with a beam separation of 0.25°. The central beam is circular with a beam-width (FWHM) of 0.16°, while the outer beams have slight ellipticity with a corresponding circular beam-width of 0.166°. Each of the seven horns has an effective bandwidth of 240 MHz and two polarisation channels, left- and right-hand circular for the central horn and orthogonal linear for the outer horns. Signals from the 14 channels are amplified in extreme low-noise amplifiers, before undergoing down-conversion from 1210-1510 MHz to an intermediate frequency of 80-220 MHz via heterodyning.

During the course of an observation the parallactic angle of the beam pattern on the sky changes with the telescope's azimuth-elevation position. To keep the outer beams at constant Galactic latitude, the receiver box is rotated to maintain a constant parallactic angle.

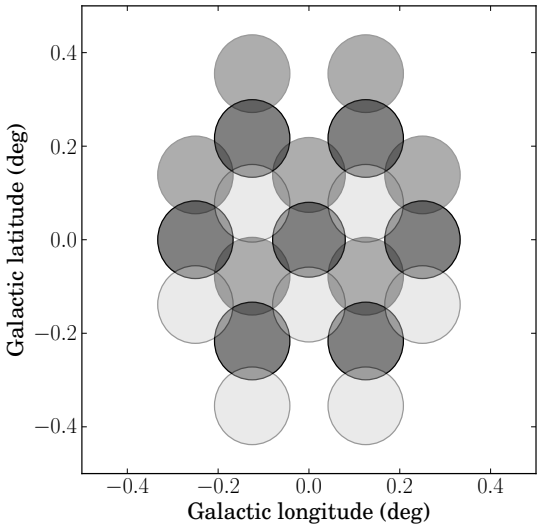

FIGURE 4.1: The beam pattern of the 21-cm Effelsberg multi-beam receiver on the sky. Shown are three pointings interleaved to make up a single tessellation unit for the survey. Circle diameters are given by the FWHM of each beam.

The laboratory-measured receiver temperature of the central horn is 21 K, with the outer horns having temperatures of between 13 and 18 K. The receiver temperatures for each horn, plus further information about the receiver system, can be found at http://www.mpifr-bonn.mpg.de/effelsberg.

The layout of the beam pattern on the sky and the tessellation unit for the survey can be seen in Figure 4.1.

4.3.2 The PFFTS backend

Signals entering the PFFTS[1] pulsar search backend are initially digitised with with nanosecond resolution before being passed to a polyphase filterbank providing 512×586-kHz channels sampled every 1.67 μs. To reduce data flow, samples are integrated in blocks of 32 to provide an effective sampling time of 54 μs. Observational data are written to disk as 32-bit floats in native format.

[1]The PFFTS is a modified version of the AFFTS system used at Effelsberg for continuum observations, for futher information on the AFFTS, see Klein et al. (2012)

4.4 Sensitivity

4.4.1 Analytical sensitivity

To estimate the sensitivity of our survey setup we use the modified radiometer equation (see e.g. Lorimer and Kramer, 2005),

$$S_{\rm min} = \beta \frac{S/N_{\rm min} T_{\rm sys}}{G\sqrt{n_p t_{\rm obs} \delta f}} \left(\frac{P_{\rm cycle}}{1 - P_{\rm cycle}} \right)^{\frac{1}{2}}, \tag{4.1}$$

where the constant factor β denotes signal degradation caused by digitisation, which for 8-bit sampling is $\sim 1\%$, giving $\beta = 1.01$ (Kouwenhoven and Voûte, 2001). $T_{\rm sys}$ is the system temperature of the receiver, where $T_{\rm sys} = T_{\rm rec} + T_{\rm sky}$. From flux density calibration measurements we find $T_{\rm rec} = 21$ K for the central horn. G is the antenna gain of the Effelsberg 100-m telescope (1.5 K Jy^{-1} at 1.36 GHz), $P_{\rm cycle}$ is the pulse duty cycle, $t_{\rm obs}$ is the length of the observation, δf is the effective bandwidth of the receiver (240 MHz) and n_p is the number of polarisations summed, which for this survey is always 2. The factor $S/N_{\rm min}$ is the minimum S/N ratio with which we can confidently make a detection. Based on false alarm statistics, $S/N_{\rm min} = 8$.

Figure 4.2 shows sensitivity curves for four DM regimes for each region of the survey.

4.4.2 Pulsar redetections

Thus far, observations have been concentrated on the mid-latitude portion of the HTRU-North survey. Processing of these observations has led to the redetection of 93 known pulsars. To obtain an empirical confirmation of our survey sensitivity, observed S/N ratios were compared to S/N ratios predicted using published flux densities taken from the ATNF pulsar catalogue [2].

Using the sky temperature model of Haslam et al. (1982), scaled with a spectral index of -2.4, and published pulsar positions taken from the ATNF pulsar catalogue, we calculated the expected S/N ratio for all redetections through rearranging equation 4.1. As the redetections did not lie in the centre of their discovery beam, S/N values were multiplied by a Gaussian offset factor, $q = e^{-(\theta/\phi)^2/1.5}$, where θ is the pointing offset in degrees and ϕ is the beam half-width at half maximum.

To make the comparison more robust, only redetections that were within one beamwidth of the observed position were used. Redetection observations were also cleaned of RFI

[2] http://www.atnf.csiro.au/research/pulsar/psrcat/ (Manchester et al., 2005)

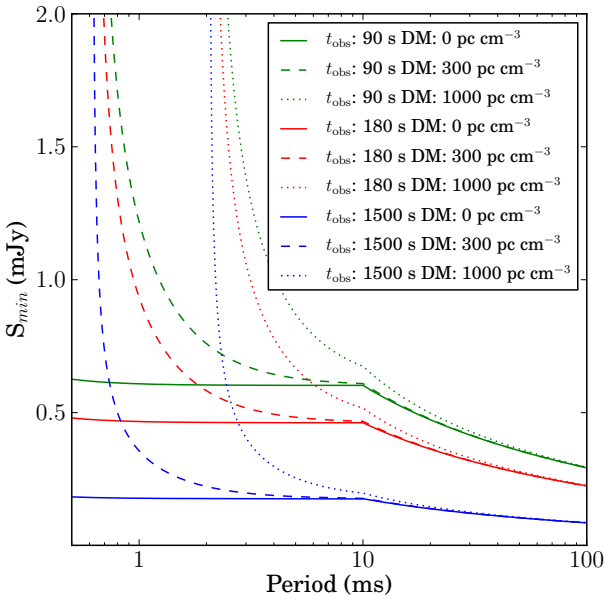

FIGURE 4.2: Theoretical minimum detectable flux densities ($S_{\rm min}$) vs. spin period for high-latitude, mid-latitude and low-latitude regions of the survey. For each region, the lines from left to right represent dispersion measures of 0, 300 and 1000 pc cm^{-3} respectively. The break point at period $\sim$ 10 ms occurs due to the assumption that the pulse duty-cycle scales as period$^{-0.5}$ with a maximum value of 1/3 (Kramer et al., 1998). To determine the best-case sensitivity, $T_{\rm sky}$ is taken to be 4 K. A minimum detectable S/N ratio of 8 is imposed. Due to intra-channel dispersive smearing, our survey sensitivity is DM dependent

prior to S/N measurement. Figure 4.3 shows the observed S/N versus the expected S/N for the remaining sample of redetections.

As an independent test for sensitivity losses in the backend, timing observations from the Lovell telescope were used to obtain S/N ratio measurements for the newly discovered pulsars from this survey. In all cases the S/N ratio measurements from the Effelsberg observations agreed with the S/N ratio measurements obtained from the Lovell telescope timing data to within 1σ.

To verify that no pulsar had been missed by the survey, all pointings for which a known pulsar was within one beam-width were examined. S/N ratios for these pulsars were estimated using the method outlined above. Of the pulsars with estimated S/N ratios above 8, five were undetected in the initial processing of the data. Folding the data for these pulsars with published ephemerides led to detections for two of the pulsars with S/N ratios below our detection limit. The three remaining pulsars which were undetected all have periods in excess of 2.5 s. Long period systems such as these, are often difficult to detect in short observations, as wider Fourier bins and large red-noise components in the data act to suppress the pulsar signal. It should be noted that although these three

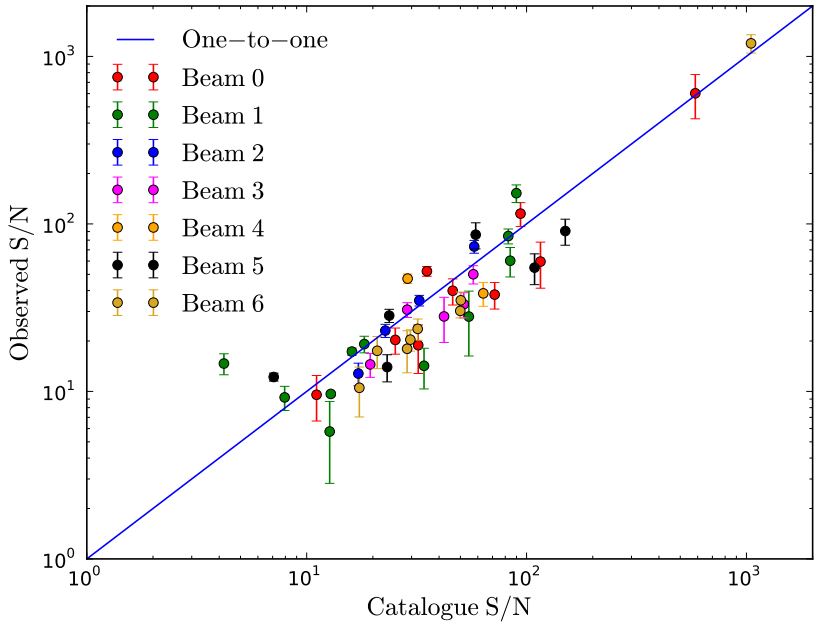

FIGURE 4.3: Observed S/N vs. expected S/N for redetected HTRU-North pulsars. Estimated S/N values are calculated using published flux densities taken from the ATNF pulsar catalogue, with a scaling factor for the offset of the pulsar from the bore-sight of the beam.

pulsars were undetected in periodicity searches, one was detected through single-pulse analysis.

These results suggest that the observing system is performing as expected, with no loss of sensitivity.

4.5 Simulations

To estimate the discovery rate of the HTRU-North survey, Monte-Carlo simulations of the Galactic MSP and normal pulsar populations were performed using the model outlined in Lorimer et al. (2006), with the PSRPOP[3] software. To simulate the normal pulsar population, input model parameters were chosen as follows:

- Empirical period distribution taken from the PDF of the known population.
- A log-normal luminosity distribution, with mean and variance in log space of -1.1 and 0.9, respectively (Faucher-Giguère and Kaspi, 2006).
- A Gaussian distribution of spectral indices, with mean of -1.6 and variance of 0.5.

[3]http://psrpop.phys.wvu.edu/

TABLE 4.2: Simulated pulsar yields for all parts of the HTRU-North survey. Numbers in parenthesis assume a prior pass of the volume in the mid-latitude portion of the survey.

Survey	Non-MSPs		MSPs	
	Total	New	Total	New
High-lat	108	80	18	8
Mid-lat	524	310	41	32
Low-lat	681	515(211)	40	31(16)

- An exponential distribution for the height above the Galactic plane, with a scale height of 0.33 kpc (Lorimer et al., 2006).
- A radial distribution as described in Lorimer et al. (2006).
- The NE2001 Galactic free electron density model (Cordes and Lazio, 2002).

The number of pulsars simulated was such that the discovery rates of simulated versions of the Parkes Multibeam Pulsar Survey (Manchester et al., 2001), the Swinburne Intermediate Latitude Pulsar Survey (Edwards et al., 2001a) and its extension (Jacoby et al., 2009) and the Parkes High Latitude Survey (Burgay et al., 2006), matched that of their real counterparts.

To simulate the MSP population, the same model parameters were used with the Galactic scale height increased to 0.5 kpc to better match the known MSP distribution (Lorimer et al., 2006).

Table 4.2 shows the results of the simulations for both MSPs and normal pulsars. The simulations suggest that the HTRU-North survey will discover $\sim$ 600 normal pulsars and $\sim$ 50 MSPs. We note that the predicted number of pulsars represents the extreme best case scenario, with simulations ignoring the effects of RFI, scintillation and pulsar intermittency.

4.6 Data analysis

Processing of data collected by HTRU-North is currently performed both on-site at the Effelsberg observatory and at the Max-Planck-Institut für Radioastronomie in Bonn. Data undergoes pre-processing and RFI treatment before being processed twice, once in a 'quick-look' pipeline that is sensitive to the majority of normal pulsars in the data, and once in a full pipeline that incorporates searches for pulsars in binary systems. Below we describe all stages in the processing and archiving of data from HTRU-North. It should be noted that the data analysis procedure reported here is only valid for medium- and

high-latitude pointings from the survey. The analysis procedure for the low-latitude pointings will be presented elsewhere.

4.6.1 Pre-processing

Initially, data written in 32-bit format by the PFFTS backend are down-converted to 8-bit format for storage, transportation efficiency and software compatibility. During the conversion, the data in each frequency channel are clipped at the 3-σ level, allowing the data to be mapped to 8 bits with minimal loss in dynamic range. A by-product of this process is that noisy channels are down-weighted and quiet channels are up-weighted with respect to one another. For purposes of RFI mitigation and completeness in the data archiving system, the original 32-bit data bandpass shape is stored.

4.6.2 RFI excision

Before the data can be searched for pulsars, they must be treated with several RFI excision methods to remove spurious signals of man-made origin.

In the first stage of RFI removal, frequency channels with average power levels 3σ or more above the normalised mean across the original 32-bit bandpass are replaced with zeros. This reduces our sensitivity to weak, persistent, narrow-band RFI.

The multi-beam nature of the receiver allows for the application of a spatial filtering system to mitigate against impulsive RFI in the data. Assuming all RFI that enters the multi-beam receiver is temporally coherent, we may apply a simple thresholding scheme to each data point to identify interference which exhibits itself in multiple beams.

As the PFFTS is an adapted version of the AFFTS backend (Klein et al., 2012), which is used for continuum observations at Effelsberg, the individual beam servers do not begin recording simultaneously at the start of each observation. As the lag between the first and last beam server to begin recording can be up to a few milliseconds, data must be cross-correlated to determine an absolute reference sample before performing multi-beam impulsive RFI excision. This process inherently relies on the presence of a multi-beam signal in the data which will produce a strong feature in the cross-correlation. In the cases where no such signal exists the impulsive masking section of the RFI excision is bypassed.

After an absolute reference has been determined for each pointing, each data point is compared across the seven beams. If the data point has a significance of 1.5σ in four or more beams, it is replaced with Gaussian noise indistinguishable from the surrounding

data and is written to file for further analysis. Assuming that each channel is composed of white noise, the chance probability of removing a single 'good' data point is 0.03%. The value of 1.5σ was chosen based on the RFI environment as determined by empirical tests of the mitigation procedure.

Once all beams have been compared, the data points flagged as RFI are histogrammed both by time sample and by frequency channel. By examining the number of bad data points in each frequency channel, we can isolate channels which have persistent impulsive noise. If the percentage of 'bad' data points in a given channel is greater than 0.2%, the data in that channel are replaced by zeros. Similarly if more than 10% of the channels in a given time sample are 'bad', then all channels in the time sample are replaced by Gaussian noise, unless they have been previously replaced by zeros.

To identify periodic signals in the pointing, the 'clean' data are collapsed along their frequency axis, with the resultant 'zero-DM' time series analysed in the Fourier domain (see Section 4.6.3.2). Fourier frequencies which appear in four or more beams with a 2-σ or greater significance are written to a 'zaplist' file which is used during periodicity searching and candidate sorting in the processing pipelines.

4.6.3 Processing pipeline

Here we cover the main stages of the full processing pipeline used to analyse HTRU-North data. The pipeline is based on the PRESTO data analysis package (Ransom, 2001). A 'quick-look' pipeline is also used to analyse data with reduced resolution. This is described in Section 4.6.4.

4.6.3.1 De-dispersion

As the broadband signal from a pulsar travels through the interstellar medium, the frequency-dependent refractive index of the free electrons along the propagation path acts to delay the signal such that components at lower frequencies become delayed with respect to those at higher frequencies. As the degree to which the signal from an unknown pulsar is dispersed, its dispersion measure (DM), is not known *a priori*, we search 3240 trial DMs in the range 0-978 pc cm^{-3}. Such a large number of trail DMs allows for retention of the data's highest possible time resolution at all DMs. As the number of DMs searched is currently hardware limited, future processing will probe the data to much higher DMs. At this stage in the analysis, the data are barycentred to remove the effects of the Earth's rotation and motion in the Solar System.

4.6.3.2 Periodicity searching

Each of the 3240 time series created in the de-dispersion stage of the pipeline must be searched for periodic signals from isolated pulsars and pulsars in binary systems. To this end, the time series are discrete Fourier transformed to create a power spectrum for each DM trial. Often the power spectra contain strong low-frequency noise from long period RFI or gain fluctuations in the receiver. To mitigate against this, the power spectra are de-reddened through subtraction of an interpolated red-noise curve. At this stage, Fourier frequencies which have been found to contain RFI through the excision process are suppressed in the spectra.

To reconstruct power distributed through harmonics in the Fourier domain, the process of incoherent harmonic summing is used. Here the original spectra are summed with versions of themselves that have been stretched by a factor of two such that all second-order harmonics are added to their corresponding fundamental. This process is repeated four times such that all power distributed in even harmonics up to the 16^{th} harmonic may be added to the fundamental (see e.g. Lorimer and Kramer, 2005).

To identify non-accelerated signals in the data, the spectra from each stage of the harmonic summing are searched for significant peaks.

In the case of pulsars in binary systems, the Doppler effect causes the apparent spin frequency of the pulsar to drift with time, spreading the pulsar's power in the Fourier domain. To reconstruct Fourier power smeared across multiple Fourier bins, we employ the 'correlation technique' of matched filtering in the Fourier domain as outlined in Ransom et al. (2002).

The number of Fourier bins drifted by the signal, $N_{\rm drift}$, and the binary acceleration of the pulsar, a_0, are related by $a_0 = N_{\rm drift} Pc/t_{\rm obs}^2$. To achieve sensitivity to accelerations of $\sim |250|$ m s^{-2}, for a 1-ms pulsar, we search values of $N_{\rm drift}$ up to 27 for medium-latitude pointings and 7 for high-latitude pointings.

4.6.3.3 Candidate sifting

To reduce the large quantity of candidates that periodicity searching produces, we apply a selection of thresholds and excision criteria. Initially, duplicate candidates are removed. As the DM behaviour of real pulsars is well understood, we can excise candidates based on their DM characteristics. Candidates that are found at a DM lower than 2 pc cm^{-3} or do not show up at two or more consecutive DM trials are removed. Candidates that are lower significance harmonics of other candidates are also removed. Finally all candidates are sorted by significance to be passed to the folding algorithm.

4.6.3.4 Folding and optimisation

To determine if a candidate is truly a pulsar, the data are phase-folded and de-dispersed at the period and DM found through candidate sifting. After the data are folded, both the period and the DM of the candidate can be optimised through searching a small range of values around the discovery values. The optimisation is tailored such that for higher-frequency candidates, smaller ranges in DM and period are searched. To reduce sensitivity to RFI, long period candidates do not undergo DM optimisation.

All candidates with greater than 8-σ significance are folded. The top 50 candidates with greater than 6-σ significance are also folded.

4.6.3.5 Candidate viewing and ranking

To deal with the >80 million candidates the survey will produce, a suite of interactive plotting software coupled with a MySQL[4] database has been developed. For each folded candidate, the database stores all the relevant statistics of that candidate. Through use of the viewing software, users may query the database to select candidates which satisfy certain criteria, before viewing those candidates in the phase space of their choice. User rankings of each candidate are stored in the database, with highly ranked candidates marked for re-observation.

For someone with experience in candidate selection, taking on average two seconds to view each candidate, it would take five years without pause to view all candidates produced by the survey. To reduce the volume of candidates that must be inspected, we implement both an artificial neural network (ANN) and an automatic ranking algorithm in post-processing.

The PEACE software package (Lee et al. 2012 in prep.) is used to generate automatic rankings for each candidate. Here, the software weights and combines a selection of scores, determined through analysis of the folded data, to generate and overall 'likeliness-of-pulsar' measure for each candidate. As the PEACE software is designed to detect pulsars that display expected properties, it is subject to selection bias against atypical systems.

ANNs are a class of computational techniques which attempt to emulate the decision making behaviour of a human mind. ANN have been successfully applied to candidate selection (e.g. Eatough et al., 2010; Keith et al., 2010) and have been shown to reduce the number of candidates required to be looked at by several orders of magnitude. To

[4] www.mysql.com

train the ANN, it is provided with a vector of 'scores', in this case generated by the PEACE software, for each candidate from a selection of real pulsar signals and RFI. The use of ANNs must be treated with extreme care, as their sensitivity to pulsars which do not exhibit typical behaviour (e.g. pulsars which are intermittent, in binary systems or highly scintillating) is highly dependent on the composition of the data set used in training.

Although the PEACE software is currently stronger at discriminating between real pulsar signals, RFI and noise, the use of an ANN can be seen as long term project, with its effectiveness increasing with the size of training sets available to it. Although both ANNs and PEACE are effective in determining whether a candidate is a pulsar or not, direct visual inspection of the candidates is still the primary method of pulsar identification. The rankings generated through visual inspection act as an absolute reference for all automatic ranking systems.

4.6.4 Quick-look pipeline

The aim of the quick-look pipeline is to process data faster than it can be observed and to perform transient searching. By keeping up-to-date with the observed data, we are able to monitor the performance of the receiver and backend systems, as well as maintain up-to-date knowledge of the RFI environment at the Effelsberg telescope.

Data passed to the quick-look pipeline are initially downsampled by factors of four and two in time and frequency, respectively. Although downsampling reduces our sensitivity to short period pulsars, $P \leq 30$ ms, it increases the throughput of the pipeline by a factor of eight, allowing processing to be performed with limited resources at 1.6× real-time. The data are then de-dispersed to 406 trial dispersion measures in the range 0-2975 pc cm^{-3}. To perform multiple de-dispersions efficiently, we employ the method outlined in Keith et al. (2010), with the caveat that we must first reduce the data to 7-bit resolution to avoid integer overflow in the output data.

For each trial DM, two searches are performed, a Fourier-domain search for periodic, unaccelerated signals and a time-domain search for isolated pulses. The Fourier domain search closely follows the methodology outlined for the full pipeline with the exception that no acceleration searching is performed.

4.6.4.1 Transient searching

To search for isolated pulses in the time domain, we follow a similar methodology to that outlined in (Burke-Spolaor and Bailes, 2010). Here, we use matched filtering to

identify significant impulsive signals of varying widths. Signals with significance greater than 4σ are collated and compared across all DMs to determine whether a candidate obeys the cold plasma dispersion relation and to determine that candidate's optimal dispersion measure. As the data have already undergone spatial/temporal coincidence filtering during pre-processing, no event matching is required across beams.

Candidate detections from the transient search are viewed on a beam-by-beam basis with the GPlotter toolkit available in the SigPyProc[5] software package. GPlotter provides interactive filterbank viewing routines which simplify the task of determining if a candidate is a real astrophysical signal or not.

The remaining steps of the quick-look pipeline follow the same process as the full pipeline, with the exception that candidates are stored independently of the MySQL database.

4.7 New pulsar discoveries

Here we present the initial pulsar discoveries of the HTRU-North survey. All discoveries originate from the processing of the first 9% of the mid-latitude region of the survey.

Upon discovery, each new pulsar is timed by the Lovell radio telescope at the Jodrell Bank observatory. Pulse times-of-arrival (TOAs) are analysed with the tempo2 software package (Hobbs et al., 2006) to create phase-connected timing solutions for each pulsar. Table 4.3 shows the new pulsar discoveries with current timing solutions. Figure 4.4 shows stacked pulse profiles from coherently de-dispersed observations with the Lovell telescope.

[5] https://github.com/ewanbarr/SigPyProc

TABLE 4.3: Timing solutions for the first discoveries of the HTRU-North survey. Numbers parentheses represent twice the formal 1-σ uncertainties in the trailing digit as determined by TEMPO2. The dispersion measure-derived distances are calculated using the NE2001 Galactic electron density model (Cordes and Lazio, 2002), giving a likely uncertainty of 20%. All parameters are measured w.r.t. reference epoch MJD 56000. These parameters were determined with TEMPO2, which uses the International Celestial Reference System and Barycentric Coordinate Time. Refer to Hobbs et al. (2006) for information on modifying this timing model for observing systems that use TEMPO format parameters.

PSR	R.A. (hh:mm:ss.ss)	Decl. ($^\circ$:′:″)	Period (ms)	Period derivative (s/s)	Dispersion measure (pc cm^{-3})	Mean flux density at 1.5 GHz (mJy)
J0325+5239	03:24:55.5(9)	+52:39:30(2)	336.62022692(1)	$3.9(3) \times 10^{-16}$	119	0.19(4)
J0425+4936	04:26:06.384(6)	+49:33:37.6(1)	922.474390132(8)	$3.9347(3) \times 10^{-14}$	88	0.19(5)
J1913+3733	19:13:27.98(3)	+37:32:13.4(7)	851.0789363(4)	$1.48(2) \times 10^{-15}$	69	0.38(5)
J1946+3414	19:46:25.121(3)	+34:17:14.62(1)	3.17013922762(5)		110	0.29(6)
J1959+3618	19:59:38.4(1)	+36:20:30.9(8)	406.08118072(4)	$4(2) \times 10^{-17}$	273	0.4(1)
J2004+3427	20:04:48.7(2)	+34:28:49(20)	240.950861(4)	$2.063(5) \times 10^{-13}$	351	0.11(4)
J2005+3549	20:05:47(1)	+35:51:28(55)	307.94289(2)	$2(1) \times 10^{-15}$	445	0.21(7)
J2036+2834	20:36:46.33(6)	+28:35:10.9(4)	1358.7267451(2)	$2.06(5) \times 10^{-15}$	99	0.15(6)
J2206+6152	22:06:17.9(2)	+61:51:57(1)	322.6735469(4)	$3.6(5) \times 10^{-16}$	167	0.8(2)
J2216+5800	22:16:05.74(5)	+57:59:51.5(7)	419.10166792(3)	$6.909(2) \times 10^{-14}$	176	0.23(6)
J2320+6415	23:19:35.0(4)	+64:11:26.2(5)	216.0182774(3)	$1.5(4) \times 10^{-16}$	246	0.27(7)
J2334+6152	23:33:19.46(2)	+61:45:29.8(2)	756.89937191(2)	$1.182(9) \times 10^{-15}$	98	0.47(7)

4.7.1 Orion-spur observations

To achieve complete coverage and statistics for a sample portion of the survey, mid-latitude pointings were targeted on the region $64.1° < l < 71.9°$, $|b| < 15°$. In this direction the line-of-sight lies along the axis of the Orion spur up to a distance of ~ 3 kpc, and intersects with the Perseus arm and Outer arm at distances of ~ 6 kpc and ~ 10 kpc respectively. These hydrogen-rich regions are known for star formation, and as such make excellent targets for pulsar searches.

The only survey of comparable sensitivity to have covered this volume is the on-going P-ALFA survey (Cordes et al., 2006). Although this survey discovered four new pulsars in the region, the declination limit of $+38°$ imposed by the Arecibo telescope limited the coverage of the region. The Effelsberg telescope has no upper declination limit and so is capable of observing the entire volume.

Data were processed in both quick-look and full pipelines and all candidates with detection significance greater than 6σ were viewed by eye. This has resulted in the discovery of six previously unknown radio pulsars including the eccentric binary MSP J1946+3414 and young pulsar J2004+3427.

Figure 4.5 shows the comparison between the newly discovered pulsars from this work and the known population in the region with measured flux densities at 1.4 GHz. It is clear to see that the pulsars discovered in this work have considerably lower flux densities at 1.4 GHz than their known counterparts. We also note that three of the newly discovered pulsars have DMs greater than 250 pc cm^{-3}. The only other blind survey to have found pulsars in this region at such high DMs in the P-ALFA survey, which stresses the importance of using backends with high frequency resolution. This is especially true for PSR J1946+3414, which, with a DM 110 pc cm^{-3} and a period of 3.17 ms, would have been rendered virtually undetectable for any survey with channel bandwidths greater than a few MHz.

Below we discuss potential supernova remnant (SNR) associations for PSR J2004+3427 and possible formation mechanisms for PSR J1946+3414. PSR J1946+3414 will be presented in greater detail in Barr et al. (in prep.).

4.7.2 PSR J2004+3427

PSR J2004+3427 was initially discovered as an 11-σ candidate in a 3-minute pointing analysed with the quick-look pipeline. The pulsar has a spin period of 241 ms and a DM of 352 pc cm^{-3}. We note that PSR J2004+3427's profile shows two components

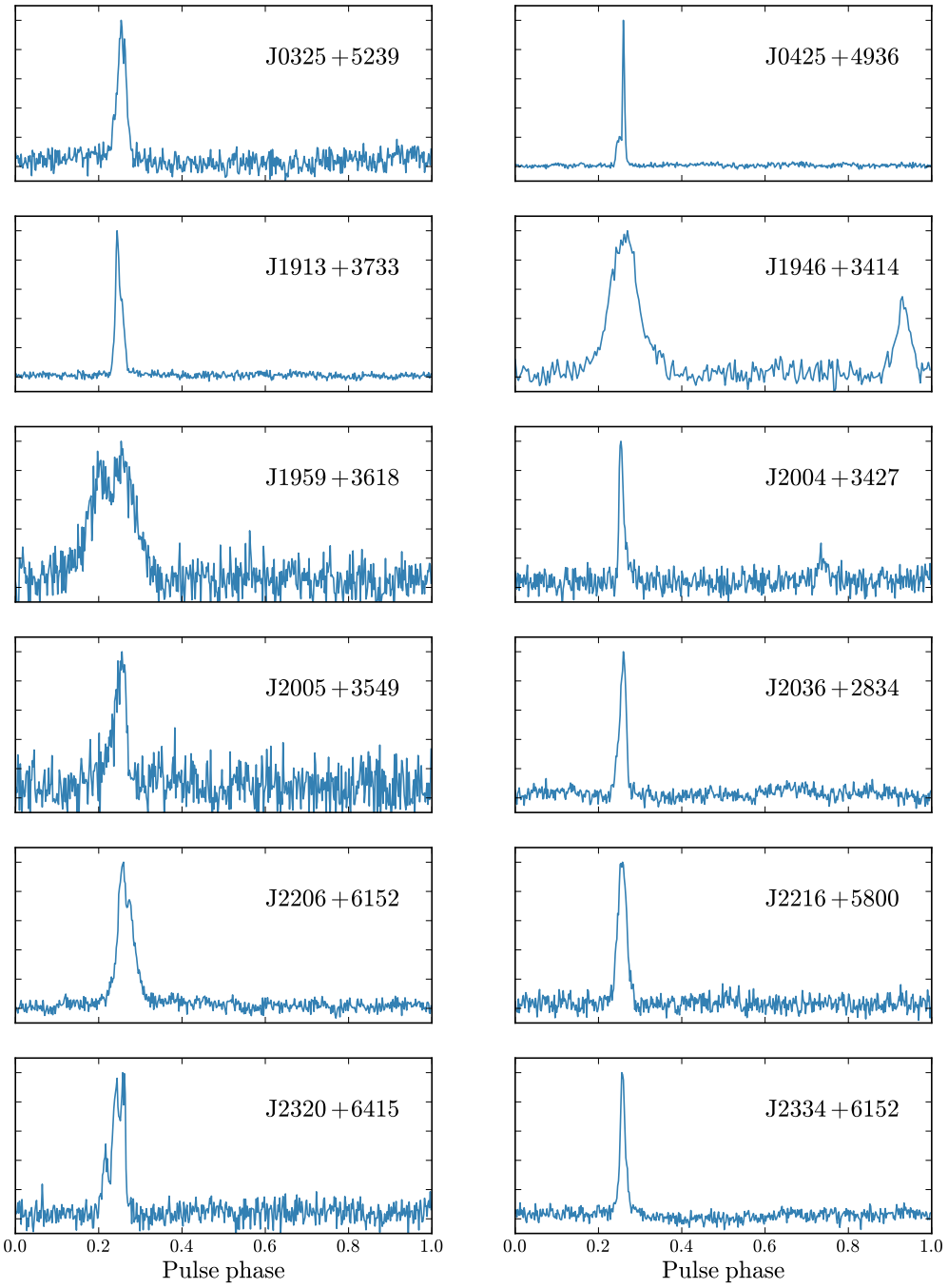

FIGURE 4.4: Stacked pulse profiles for the 12 newly discovered pulsars of the HTRU-North survey. Individual profiles were phase aligned prior to stacking using the ephemeris determined through timing of the pulsar.

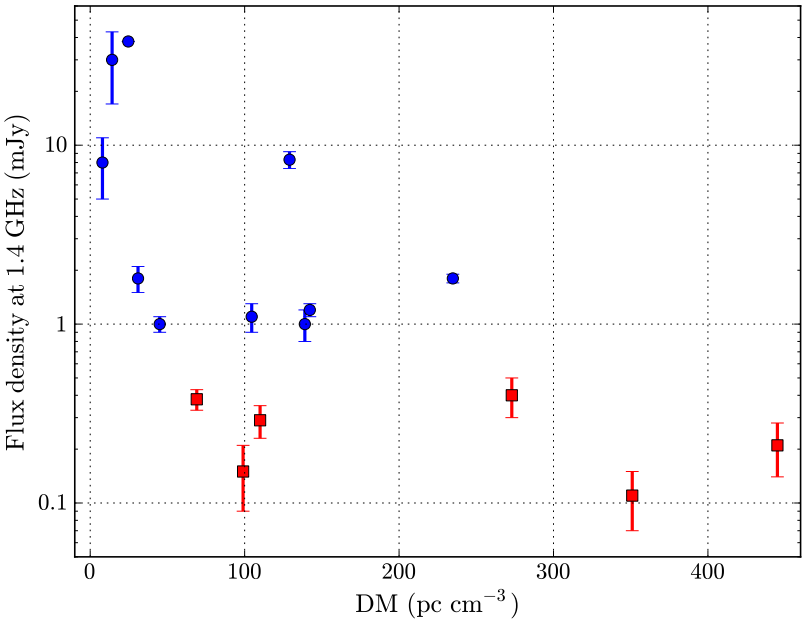

FIGURE 4.5: Comparison of known pulsar population in the Orion-spur region, to pulsars discovered in this work. Blue circles show previously known pulsars with measured flux densities at 1.4 GHz. Red triangles show pulsars discovered in this work.

separated by 180° (see Figure 4.4), suggesting that the pulsar may be an orthogonal rotator. Using the NE2001 Galactic electron density model (Cordes and Lazio, 2002) we estimate a distance to the pulsar of $11.4 \pm^{4.2}_{2.6}$ kpc. Analysis of pulsar distance measures by Verbiest et al. (2012), suggests that this distance is likely overestimated, with the real distance lying closer to 10 kpc. Timing with the Lovell radio telescope has led to a phase-coherent timing solution for PSR J2004+3427 that shows it to have a large period derivative of 2×10^{-13}. Assuming that the measured spin-down is purely caused by the emission of magnetic dipole radiation (i.e. a braking index of 3), we find the pulsar to have a *characteristic age* of ~ 18.5 kyr.

4.7.2.1 SNR associations

Considering the young age of PSR J2004+3427, it is natural to consider that it may be associated with an SNR. Using the SIMBAD astronomical data archive[6], we find three published SNRs within a 2-degree radius of PSR J2004+3427; SNRs G069.7+01.0 (Kothes et al., 2006), G070.7+01.2.(Cameron and Kulkarni, 2007; Kulkarni et al., 1992) and G069.4+01.2 (Yoshita et al., 2000). We note that the field also contains the candidate SNR G070.0+02.0 (Mavromatakis et al., 2009). SNR G070.0+02.0 will not be considered in the following discussion due to a lack of information related to the source.

[6] http://simbad.u-strasbg.fr/simbad/

Small distance estimates to SNRs G070.0+02.0, < 1 kpc (Mavromatakis et al., 2009); G069.4+01.2, ~ 2.5 kpc (Yoshita et al., 2000) and G070.7+01.2, 4.5 ± 1 kpc (Bally et al., 1989) appear to rule out any possible association with PSR J2004+3427. Using a revised Σ-D relation, which relates the surface brightness or SNRs to their distances, Case and Bhattacharya (1998) estimated a distance of ~ 14.4 kpc to SNR G069.7+01.0. This distance is consistent with the DM distance calculated for PSR J2004+3427. Such a large inferred distance is also consistent with the findings of Kothes et al. (2006) who note that SNR G069.7+01.0 is unpolarised at 1.42 GHz, possibly due to a large distance resulting in high beam depolarisation.

We calculate the separation of PSR J2004+3427 and SNR G069.7+01.0 to be $360\pm^{131}_{82}$ pc, assuming that SNR G069.7+01.0 is located at the DM distance of PSR J2004+3427. For PSR J2004+3427 to have originated in SNR G069.7+01.0 would therefore require, assuming that the characteristic age is a close approximation of the true age, that the pulsar has a transverse velocity of the order 10^4 km s^{-1}. Using the model for the pulsar velocity distribution as found by Hobbs et al. (2005), we find the probability of PSR J2004+3427 having such a high transverse velocity to be consistent with zero. We therefore find it highly unlikely that PSR J2004+3427 originated in SNR G069.7+01.0. Through continued timing of PSR J2004+3427, it should be possible to measure any significant proper motion, allowing any potential connection between SNR G069.7+01.0 and PSR J2004+3427 to be re-evaluated.

4.7.3 PSR J1946+3414

PSR J1946+3414 is the most recent MSP discovery of the HTRU-North survey. Initially seen as an unaccelerated 7-σ candidate from the full processing pipeline, PSR J1946+3414 has a spin period of 3.17 ms and a DM of 110 pc cm^{-3}. Follow-up timing with the Lovell and Effelsberg radio telescopes has revealed PSR J1946+3414 to be part of a highly eccentric binary system ($e \approx 0.134$) with a low-mass companion.

By calculating the mass function of the system via the method outlined in Section 3.6, we infer minimum and median companion masses of 0.21 and 0.25 $M_\odot$, respectively for a pulsar mass of 1.35 $M_\odot$. This mass is consistent with either a low-mass white dwarf or low-mass main sequence star, but makes it unlikely that the companion is a neutron star, as such a high companion mass would require very specific orbital configurations.

As seen in Section 1.1.8.3, rapidly spinning pulsars such as PSR J1946+3414 are expected to have been spun-up through the accretion of matter from a donor star. A by-product of this process is the circularising of the orbit due to tidal friction (Bhattacharya and

van den Heuvel, 1991). Therefore, the high eccentricity of PSR J1946+3414 is somewhat of a puzzle, as it does not fit to the generally accepted model for MSP formation.

4.7.3.1 Formation mechanisms

Here we will consider three possible formation channels which may describe the observed parameters of PSR J1946+3414. First, we consider that the pulsar has not undergone classical accretion-powered spin-up, but has instead been formed with a rotational period close to the currently observed value. Second, we consider that the pulsar has been recycled in a globular cluster (GC), before being ejected through a three-body interaction into the Galactic disk. Finally we consider that PSR J1946+3414 has been, or is currently, a primordial hierarchical triple (HT) system.

Although we cannot rule out that the pulsar has been formed rotating rapidly, we find it to be the most unlikely of the proposed formation mechanisms. While there are several pulsars with periods of tens of milliseconds known to be associated with supernova remnants, none are known to have periods comparable to PSR J1946+3414[7] and none are known to have binary companions. Unfortunately, due to the short timing baseline available, it is currently impossible to decouple the covariance of position and spin-down in the PSR J1946+3414 timing data. It is not until the spin-down is accurately measured that we may infer a characteristic surface magnetic field strength for the pulsar, allowing us to explore the allowable parameters of the progenitor in this 'born-fast' scenario.

A more likely formation mechanism for PSR J1946+3414, is that it was born and recycled in a GC before being ejected into the Galactic disk. In this case the currently observed companion is not the star responsible for spinning-up the pulsar, but is instead a more massive star that has ejected the original companion through a chaotic three-body interaction. It is this interaction, or one similar, which provides the ejection mechanism from the GC and produces the eccentricity which we observe today (see e.g. Ivanova et al., 2008). That there are no GCs near to PSR J1946+3414's position on the sky does not currently present a problem to this formation channel, as without an age estimate for either pulsar or companion, or a proper motion measurement, it is possible that PSR J1946+3414 has travelled a large distance from any potential progenitor GC.

A formation mechanism which involves PSR J1946+3414 having been part of an HT system is currently the most favoured, as this is the most likely formation mechanism for PSR 1903+0327 (Champion et al., 2008; Freire et al., 2011), the only other published eccentric binary MSP in the Galactic disk. In this scenario, the neutron star was formed in a close binary with a low-mass main sequence star, the currently observed companion

[7]The fastest being the 16-ms pulsar, PSR J0537−6910 (Marshall et al., 2004).

being further out in a wide orbit. The neutron star is then spun-up to a rapid period by the evolving inner companion. At this stage the inner star is removed from the system via ejection in a chaotic three-body interaction caused by the widening of the inner orbit due to mass transfer (Freire et al., 2011). What remains is an eccentric binary containing the MSP and the outer companion, albeit in a tighter orbital configuration than before. In a variation on this scenario, the inner companion will not be ejected, but will be evaporated by the newly formed MSP. With higher precision timing, it may be possible to determine if there is still a very light inner companion in orbit around the PSR J1946+3414.

4.8 Conclusion

We have described the instrumentation, observing strategy, sensitivity and expected results of the High Time-Resolution Universe North pulsar survey (HTRU-North), the first major search for radio pulsars ever conducted with the 100-m Effelsberg radio telescope and the most sensitive survey ever to observe the entire region above +30° declination. The survey has thus far resulted in the discovery of 13 radio pulsars, of which 12 have been found above +30° declination.

Of the newly discovered pulsars, two are of particular note. PSR 1946+3414 is a highly eccentric MSP binary located in the Galactic field. This system will be presented in detail in Barr et al. (in prep.). PSR J2004+3427 is a young pulsar with a characteristic age of 19 kyr. We currently rule out that PSR J2004+3427 is associated with nearby SNR G069.7+01.0, due to the high transverse velocity required to place the pulsar at its current position with respect to the remnant, in the time scale suggested by its characteristic age.

Chapter 5

Targeted pulsar searches with the Effelsberg Telescope

While previous chapters have focused on large-scale projects that require a considerable amount of observing time and access to high-quality processing hardware, there is plenty of science that can be achieved by spending relatively small amounts of observing time on targets previously identified as containing objects of potential interest. Examples of such searches can be found in the numerous searches of γ-ray point sources (see e.g. Champion et al., 2005; Keith et al., 2008; Kerr et al., 2012)[1], globular clusters (see e.g. Ransom et al., 2008, 2005) and supernova remnants (see e.g. Camilo et al., 2002a,b,c).

In this chapter we present three targeted searches for radio pulsars and transients conducted with the 100-m Effelsberg radio telescope.

5.1 1RXS J141256.0+792204 (Calvera)

5.1.1 Background

The enigmatic source 1RXS J141256.0+792204 (Rutledge et al., 2008) was discovered during a targeted search of sources from the *ROSAT* All-sky Survey Bright Source Catalog (Voges and Aschenbach, 1999) using the X-ray Telescope (XRT) and Ultraviolet/Optical Telescope instruments aboard NASA's *Swift* satellite (Gehrels et al., 2004). A high X-ray-to-optical flux ratio, suggested that the source was a compact object, with Rutledge et al. (2008) noting the source's similarity to the known population of X-ray

[1]The reader should note that the search presented in Chapter 3 is unusual in its scale, with the majority of targeted searches of γ- and X-ray sources focusing on a smaller selection of sources.

Dim Isolated Neutron Stars (XDINSs) (Haberl, 2007; Turolla, 2009), a sub-class of isolated neutron stars that do not emit at radio wavelengths and show a purely thermal X-ray spectra with peak flux in the soft X-ray portion of the electromagnetic spectrum. This similarity led to 1RXS J141256.0+792204 being dubbed 'Calvera', as it would be the eighth XDINS to be discovered, with those discovered prior to it being collectively known as 'The Magnificent Seven'. Even with the similarity in X-ray spectrum to the known XDINS population, Rutledge et al. (2008) noted that Calvera could be potentially associated with a number of different source classes including AXPs (see Section 1.1.8), central compact objects (CCO, e.g. De Luca, 2008) and radio-emitting MSPs.

If Calvera were to be a radio emitting MSP, the measured X-ray properties would suggest that it was very nearby, at a distance of between 80 and 260 pc (Rutledge et al., 2008). Such a pulsar could be of use for current and future pulsar timing arrays (Foster and Backer, 1990) and would present an interesting target for ground-based gravitational wave detectors (Horowitz, 2010). However, a targeted radio search at the position of Calvera using the Westerbork Synthesis Radio Telescope (WSRT), discovered no radio emission from the source down to flux densities of 4 mJy at 385 MHz and 0.3 mJy at 1.38 GHz (Hessels et al., 2007). This result implied that if Calvera is a radio emitter, then it is most likely not beamed towards the Earth.

A multi-wavelength follow-up study of Calvera has resulted in the discovery of 59-ms pulsations in the object's X-ray and γ-ray emission (Zane et al., 2011). While the γ-ray detection of Calvera has since been called into question (Halpern, 2011), the X-ray analysis has allowed for the application of pulsar timing techniques to determine a spin period, $P = 59.1982$ ms, and a 3-σ upper limit on the period derivative, $\dot{P} < 9 \times 10^{-15}$ (Zane et al., 2011). While the short period seemingly rules out Calvera as an AXP, the weak constraint on the period derivative leaves a number of valid source classes, including CCOs and mildly-recycled pulsars. It should be noted that if Calvera is a CCO, it would be the first 'orphaned' CCO, as there is no observed SNR remnant nearby on the sky (Zane et al., 2011).

As a potential way to positively identify Calvera's nature, deep radio observations were performed using the 100-m Effelsberg radio telescope. These observations would, in the case of a detection, allow for an accurate measure of the period derivative of Calvera, ruling out several source classes and providing a more robust determination of the source's X-ray efficiency through an inferred DM distance.

5.1.2 Observations and processing

Observations were performed using the receiver and backend systems described in Chapter 4, with the observing band similarly centred on 1.36 GHz. Beam 4 of the 21-cm Effelsberg multi-beam receiver was used due to the larger bandwidth of 240 MHz that was available only in this beam at the time.

Calvera was observed a total of five times, with four 78-minute integrations on MJD 55330 and a further 60-minute integration on MJD 55337. Observations were centred on J2000 coordinates R.A. = $14^{\rm h}12^{\rm m}55^{\rm s}.84$ and Decl. = $79°22'03''.7$. These coordinates were determined by X-ray astrometry performed using data from the *Chandra* X-ray Observatory (Zane et al., 2011). We note that the quoted uncertainty on these coordinates, $0.6''$ to 90% confidence, is several orders of magnitude smaller than the FWHM of the telescope beam at 1.36 GHz ($9.4''$).

To determine if Calvera had been detected at radio wavelengths, the observed data were phase-folded (see Section 2.2.5) using the ephemeris determined through X-ray timing observations. As the period derivative of Calvera from X-ray timing was poorly determined, the folded data were searched over a range of periods around the X-ray timing period. Similarly, as the true DM of Calvera was unknown, the folded data were searched over trial DMs in the range 0-1000 pc cm^{-3}. Although a DM of 1000 pc cm^{-3} is much larger than the maximum expected DM in the line of sight (42 pc cm^{-3}, see Section 5.1.3), the process of searching to higher DMs is computationally cheap and allows us to rule out higher DMs for Calvera, as previous observations had only considered DMs < 100 pc cm^{-3} (Hessels et al., 2007).

To negate any biases introduced through folding using the X-ray ephemeris, the data were also blind searched in the DM range 0-1000 pc cm^{-3}. The processing steps in the blind search closely followed those presented in Section 4, with the exception that no multi-beam RFI removal was performed. To mitigate against RFI, the RFIFIND program from the PRESTO package (see Section 2.2.7.1) was used. As the X-ray observations of Calvera showed no indication of binary motion, no acceleration searching (see Section 2.2.4.7) was performed on the data.

All candidate periodicities produced from the blind search were examined by eye to identify any signals which may have originated from Calvera. Special attention was paid to signals at low DM, where confusion due to RFI was an important factor in reducing the significance of discovered candidates. Any potentially interesting candidates were phase-folded and optimised over small ranges of period and DM.

The data were also searched for transient signals using matched filtering techniques (see Section 2.2.6). This was done both with and without RFI mitigation to reduce the chance of any low-DM pulse being accidentally removed by the RFIFIND code. Single pulse output plots were examined by eye to identify transient signals. Particular attention was given to any transient event which showed peak S/N at DM < 10 pc cm^{-3}. As the majority of RFI had peak S/N between 0 and 2 pc cm^{-3}, the chance of identifying any low-DM transient burst as being associated with Calvera was low. At higher DMs the effects of RFI confusion became negligible.

5.1.3 Results and discussion

Examination of the period and DM curves (see Section 2.2.5.1) generated through searching of the folded data, resulted in no significant detections at any DM for a signal of similar period to that given by the X-ray timing of Calvera. This was also true for the blind search, which found no evidence of pulsed celestial radio signals in the direction of Calvera. Furthermore, no pulsed signals displaying pulsar-like properties were discovered in the output of the single pulse search. We must therefore consider the reasons for our radio non-detection of Calvera.

As noted in Section 5.1.1, the hypothesis of Calvera as a radio pulsar requires that the source lies at a distance of between 80 and 260 pc (Rutledge et al., 2008). Using the NE2001 Galactic free electron density model (Cordes and Lazio, 2002), we find these distances correspond to DMs of between 1 and 3 pc cm^{-3}. Assuming that Calvera is Galactic in nature, we find a maximum DM, DM$_{\rm max}$, in the line of sight, to be ~ 42 pc cm^{-3}. At this DM, the scattering delay is $\Delta t_{\rm scat} \simeq 0.1$ μs and the intra-channel dispersion delay is $\Delta t_{\rm chan} \simeq 81.2$ μs. Considering that the combined delay from these terms, $\sqrt{\Delta t_{\rm chan}^2 + \Delta t_{\rm scat}^2}$, is only 0.13% of a pulse period, it seems most unlikely that intra-channel dispersive smearing and/or interstellar scattering are the reason for our non-detection of Calvera.

The small expected distance to Calvera suggests that the source should show strong scintillation (see e.g. Rickett, 1990). Using the NE2001 model, we find a scintillation timescale, Δt_s, and decorrelation bandwidth, Δf_s, of $\Delta t_s \simeq 1.2^{+0.2}_{-0.1}$ days and $\Delta f_s = 4.0^{+2.5}_{-1.3}$ THz for a distance of 80 pc and $\Delta t = 1.7^{+0.5}_{-0.3}$ hours and $\Delta f_s = 3.7^{+4.3}_{-1.6}$ GHz for a distance of 260 pc, assuming a source velocity of 100 km s^{-1} and an ISM well described by a Kolmogorov spectrum. These results suggest that for small source distances, we cannot rule out scintillation as a cause of our non-detection of Calvera, as the decorrelation bandwidth is much larger than the observing bandwidth and the scintillation timescale is longer than our total integration time.

Another possible reason for not detecting Calvera at radio wavelengths is simply that it does not beam radio emission towards the Earth. Assuming that the beaming fraction is proportional to $P^{-1/2}$ (Kramer et al., 1998), we find it probable that Calvera has a beaming fraction $\sim 40\%$. We can therefore not rule out unfavourable beaming as a cause for our non-detection of Calvera.

In the case that Calvera is beaming towards Earth and was not strongly scintillating during our observations, we can place strong upper limits on the radio flux density at 1.36 GHz. Following the method presented in Section 4, we find an upper limit on the flux density of $S_{1360} \leq 0.11$ mJy at 1.36 GHz for pulsed radio emission from Calvera, assuming a 20% pulse duty-cycle. This limit is a considerable improvement on the previous limit at this frequency of $S_{1380} \leq 0.3$ mJy (Hessels et al., 2007)[2]. Assuming a source distance, $d = 250$ pc, we may convert our limit on the flux density to a pseudo luminosity ($L \equiv Sd^2$) limit. We find $L \simeq 6.8(d/250 \text{ pc})^2$ μJy kpc^2 at 1.36 GHz. Using the ATNF catalogue, we find our pseudo luminosity limit to be almost an order of magnitude lower than that of the least luminous pulsar known.

5.1.4 Conclusion

In conclusion, we have performed the most sensitive radio observations yet of the mysterious X-ray source 1RXS J141256.0+792204 (Calvera). No radio emission was detected from Calvera down to a flux density of 0.11 mJy at 1.36 GHz[3]. Assuming a distance of 250 pc to Calvera, we calculate its pseudo luminosity to be dimmer than that of any known pulsar, strongly suggesting that if Calvera is a radio emitter, it is not beamed towards Earth. Our observations imply that future observations are also unlikely to find radio emission from this source, although we note that future radio observations at very low frequency may be useful, as they will provide a higher degree of DM discrimination and also perhaps observe parts of the radio beam not seen at higher frequency (Cordes, 1978).

With no radio detection, the source class of Calvera is still open to interpretation. Extended X-ray timing observations should be able to place strong limits on the period derivative of Calvera, indicating whether or not the source is a mildy-recycled pulsar, CCO or something else as yet unknown.

[2]This limit is subject to interpretation, as the pulse duty-cycle used in its calculation has been omitted from the final publication.

[3]Assuming a pulse duty-cycle of 20%

5.2 SN 2008iz

5.2.1 Background

In May 2008, a bright radio source was detected in 22-GHz Very Large Array observations of the nearby ($\sim$ 3.6 Mpc) galaxy Messier 82 (M82) (Brunthaler et al., 2009a). Although the source was initially found with a flux density of $\sim$ 90 mJy, follow-up observations in early 2009 showed the flux density to have decreased by almost 90%, to $\sim$ 11 mJy. Several explanations were put forward for the gradual fading, with the most likely being that the source was a radio supernova (Brunthaler et al., 2009c). This hypothesis would be confirmed through the observation of a rapidly expanding ring-like structure around the position of the source, earning it the designation SN 2008iz (Brunthaler et al., 2009b).

As even the most sensitive radio telescopes cannot currently detect emission from extragalactic Type-Ia supernovae (Beswick, 2006), we can safely assume that SN 2008iz was a core-collapse supernova. If we accept the neutron star/pulsar formation mechanism presented in Chapter 1, the positive identification of a core-collapse supernova represents an exciting opportunity to observe a pulsar directly after its birth. The theory that a pulsar may have been formed in SN 2008iz was bolstered by the discovery of a potential steep-spectrum compact core (Brunthaler et al., 2010). With the potential for direct measurement of the intergalactic medium (IGM) density through the dispersion measure of a pulsar in an external galaxy, we embarked upon an observation campaign of SN 2008iz using the Effelsberg telescope.

5.2.2 Observations and processing

Observations were performed using the 6-cm (4.85 GHz) single-pixel secondary-focus receiver of the Effelsberg telescope in combination with the back-end system described in Chapter 4. The high observing frequency was chosen to reduce the effect of scattering in the IGM/ISM and because the 6-cm receiver had the largest bandwidth of any receiver available at the time.

SN 2008iz was observed a total of five times with 55-minute integrations, spread between MJDs 55489 and 55490. Observations were centred on J2000 coordinates R.A. = $09^{\mathrm{h}}55^{\mathrm{m}}51^{\mathrm{s}}.551$ and Decl. = $69°40'45''.792$, as determined by Brunthaler et al. (2009c). We note that these coordinates were determined through very long baseline interferometry, and as such have uncertainties several orders of magnitude smaller than the FWHM of the Effelsberg telescope beam at 4.85 GHz ($146''$).

Given that M82 lies at the large distance of ∼3.6 Mpc (Freedman et al., 1994), the potential for the detection of periodic radio pulsations from any pulsar there is low. Using the ATNF catalogue, we find the highest pseudo luminosity for any known pulsar is $L \simeq 9.7$ Jy kpc^2 (PSR B0736−40, Large et al., 1968b) at 1.4 GHz. Scaling this value to our observing frequency using a typical spectral index of −1.8 (Maron et al., 2000), we find $L \simeq 1.3$ Jy kpc^2 at 4.85 GHz. Assuming PSR B0736−40 to be at the distance of M82 and ignoring any potential intra-channel dispersive smearing or multi-path scattering, we can translate this luminosity into a flux density at the Earth of $S \simeq 100$ nJy at 4.85 GHz. As it is not feasible to observe such weak signals with the Effelsberg telescope, no periodicity searching was performed on our observations of SN 2008iz.

To determine if any transient radio burst had been observed from the core of SN 2008iz, each observation was de-dispersed (see Section 2.2.3) to a number of trial DMs in the range 0-6000 pc cm^{-3}. Each de-dispersed time series was then searched for significant signals using matched filtering techniques (see Section 2.2.6). As the RFI environment of the Effelsberg telescope is relatively quiet at 4.85 GHz, no RFI excision was performed. Single pulse output plots were examined by eye, with interesting signals being followed-up through examination of their frequency and time behaviour in the raw data.

5.2.3 Results and discussion

No transient radio signals of astrophysical nature were detected in the direction of SN 2008iz during 275 minutes of observations. Here we will consider the physical implications of this non-detection.

By assuming a minimum detectable S/N, S/N$_{\rm min}$, of 6 (see Section 2.2.6), we can place an upper limit on the flux density of any transient radio signal emitted from SN 2008iz during our observations. It can be shown (see e.g. Cordes and McLaughlin, 2003), that the minimum detectable flux density for a radio burst is given by

$$S_{\rm min} = \beta \frac{\rm S/N_{min}\, T_{sys}}{G\sqrt{n_p \Delta f W}}, \tag{5.1}$$

where the constant factor β denotes signal degradation caused by digitisation, which for 8-bit sampling is $\sim 1\%$, giving $\beta = 1.01$ (Kouwenhoven and Voûte, 2001). $T_{\rm sys}$ is the system temperature of the receiver, where $T_{\rm sys} = T_{\rm rec} + T_{\rm sky}$. From flux density calibration measurements we find $T_{\rm rec} = 12$ K. G is the antenna gain (1.55 K Jy^{-1} at 4.85 GHz for the 100-m Effelsberg telescope), W is the width of a given transient burst, Δf is the effective bandwidth of the receiver (1 GHz) and n_p is the number of polarisations summed, 2 for our observations. Taking $T_{\rm sky} \ll T_{\rm rec}$ (Haslam et al., 1982), we find $S_{\rm min} = 1.1\ \sqrt{1\ \mu{\rm s}/{\rm W}_{\mu{\rm s}}}$ mJy. It is useful to express this limit in terms of pulse

energy (ϵ), as unlike peak flux density, the pulse energy is insensitive to pulse shape. As we can only resolve pulses which are longer than our sampling time ($t_{\rm samp} \simeq 64$ μs), our minimum detectable pulse energy is found to be $\epsilon_{\rm min} \simeq 8.8$ mJy μs.

To understand how this limit compares with the most energetic transient radio emission observed from pulsars in the Milky Way, we will consider the 'giant' pulses emitted by the Crab pulsar (see e.g. Cordes et al., 2004). To make the following discussion distance-independent, we define Φ to be the *intrinsic pulse energy* at emission. Here, $\Phi = \epsilon D^2$, where D is the distance to the source. For reference, the distance to the Crab pulsar is $\simeq 2$ kpc and the distance to M82 is $\simeq 3.6$ Mpc.

At a width of less than 0.4 ns, Hankins and Eilek (2007) showed that the narrowest of the Crab giant pulses can reach peak flux densities of 2 MJy at 9.25 GHz. Scaling this to our observing frequency of 4.85 GHz using a spectral index of -1.44 (Karuppusamy et al., 2010), we find this translates to an intrinsic pulse energy of ~ 8 kJy μs kpc^2. Even though this is one of the brightest pulses ever observed from the Crab pulsar, it is certainly not the most energetic, with Bhat et al. (2008) observing pulses of up to $\sim$264 kJy μs kpc^2 at 1.3 GHz and Soglasnov (2007) observing a 0.1-μs pulse with a peak flux density of 7.3 MJy at 2.2 GHz, giving $\Phi \simeq 2920$ kJy μs kpc^2. Scaling these values to our observing frequency, we find that they correspond to intrinsic pulse energies of ~ 84 kJy μs kpc^2 and ~ 936 kJy μs kpc^2, respectively. Converting $\epsilon_{\rm min}$ to a minimum detectable intrinsic pulse energy for a source in M82 ($\Phi_{\rm min}$), we find $\Phi_{\rm min} \simeq 114$ kJy μs kpc^2.

Assuming negligible scattering and dispersive smearing, this sensitivity suggests that we would be able to detect the brightest and most energetic pulses, such as those presented in Soglasnov (2007). However, We note that the probability of observing pulses with such high energies is dependent on the length of time observed. This probability has been shown to follow a power law (see e.g., Bhat et al., 2008; Karuppusamy et al., 2010; Popov and Stappers, 2007) of the form $p(\epsilon > \epsilon_0) \propto \epsilon_0^{\alpha}$. Following on from this definition, we find the probability of observing a pulse of energy greater than ϵ_0 in an observing run of cumulative length $t_{\rm obs}$, to be given by

$$p(\epsilon > \epsilon_0) = k \frac{t_{\rm obs}}{P_{\rm Crab}} \epsilon_0^{\alpha}, \tag{5.2}$$

where $P_{\rm Crab}$ is the period of the crab pulsar and k is a scaling factor. Through fitting of the cumulative pulse energy distribution of Crab giant pulses, both Bhat et al. (2008) and Majid et al. (2011) determined $\alpha \simeq -1.9$ in the high pulse energy regime, with Bhat et al. (2008) quoting a corresponding k value of 4.42 for their 1.3 GHz observations. Figure 5.1 shows the pulse rate as a function of intrinsic pulse energy (i.e. a distance scaled version of Equation 5.2 in the case that $p(\epsilon > \epsilon_0) = 1$) using the values of α and k as determined by Bhat et al. (2008), with the k value scaled to our observing frequency

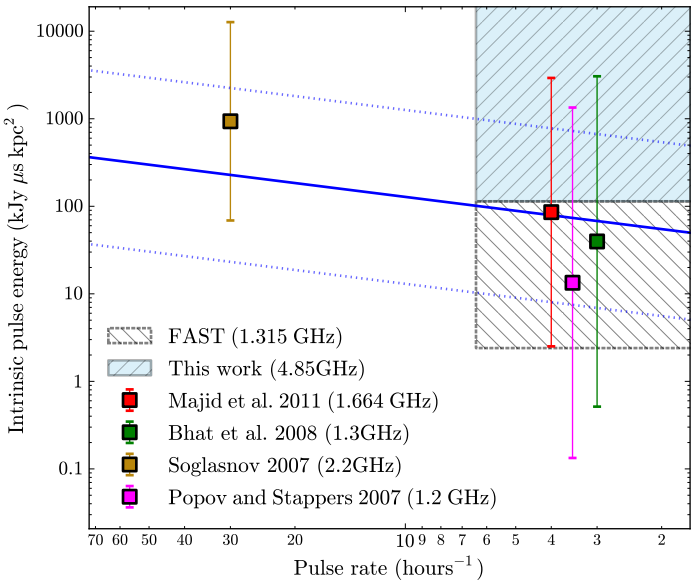

FIGURE 5.1: Predicted pulse rate as a function of intrinsic pulse energy. The blue, solid line shows the expected observation time required to observe a pulse at or below a given intrinsic energy threshold. The dotted, blue lines show the upper and lower uncertainty bounds on the frequency scaling of k (see text). The hatched, blue area shows the sensitivity limits for our observations. The scatter points show a selection of the highest-energy pulses from the literature. Each pulse was the most energetic in its observation session. Uncertainties on the scatter points are also given by the uncertainty in the spectral index used for frequency scaling. By way of comparison, the white, hatched area shows the sensitivity limits for a hypothetical observation of the same length with FAST (see Section 5.2.4).

of 4.85 GHz. Also plotted are the sensitivity limits probed by our observations and four of the most energetic pulses taken from the literature. The uncertainties on the rate relation and on the intrinsic energy of the four pulses are derived from the uncertainty on the spectral index, γ, used to convert from the published frequency to our observing frequency ($\gamma = -1.44 \pm 3.3$; Karuppusamy et al., 2010)[4]. From Figure 5.1, we can see that the observations presented in this work are sensitive to pulses with shallower spectral indices than ~ -1.44 in the range $\Phi \gtrsim 114$ kJy μs kpc^2. We note that the highest energy pulse we can expect to be emitted during our observations lies outside of our energy range for a spectral index of -1.44. However, if the spectral index for specific giant pulses is as high as ~ 1.9 (the 1-σ upper limit from Karuppusamy et al. (2010)), we may expect pulses with intrinsic energies up to ~ 1200 kJy μs kpc^2.

So far we have only considered pulses which are unaffected by intra-channel dispersive smearing and multi-path scattering. In reality these effects will considerably increase our

[4]The uncertainty/variability of the spectral indices of giant pulses was another reason to choose wider bandwidth over lower observing frequency when selecting which receiver to perform our observations with.

minimum detectable flux density, and therefore our minimum detectable pulse energy at high DMs. As our sampling rate is much longer than the width of the most energetic giant pulses in the literature, a useful number to calculate is the DM at which the total ISM broadening (defined here as the quadrature sum of the intra-channel dispersion delay and the multi-path scattering delay) is equal to our sampling time, $t_{\rm samp}$. Using the scattering relation of Bhat et al. (2004) and the dispersion relation given in section 2.2.3, we find that we retain our maximum sensitivity out to a DM of ~ 225 pc cm^{-3}, for a pulse of width $W \ll t_{\rm samp}$. To put this DM in the context of SN 2008iz, we can estimate the minimum DM for any signal originating in M82. Using the NE2001 Galactic free electron density model (Cordes and Lazio, 2002), we find a maximum DM contribution from the Milky Way of ~ 41 pc cm^{-3} in the direction of SN 2008iz. By assuming an intergalactic medium in which all baryons are fully ionised, we may place a lower limit on the expected DM of any transient radio bursts from the M82 galaxy. Following the method presented in Lorimer et al. (2007), we see that the intergalactic DM contribution should scale with red-shift, z, as DM $\sim 1200z$ pc cm^{-3}. Using the relation $z \approx H_0 d/c$, where H_0 is the Hubble constant, taken as 71 km s^{-1} Mpc^{-1}, we obtain an intergalactic DM contribution of only $\sim$1 pc cm^{-1}. This value implies a minimum DM for any radio signal originating from M82 of ~ 42 pc cm^{-3}. We therefore find that our observations retain maximum sensitivity up to a DM depth of 180 pc cm^{-3} into M82. Figure 5.2 shows the total ISM delay as a function of DM for our observations of SN 2008iz. Also plotted are the maximum DM searched, DM$_{\rm max} = 6000$ pc cm^{-3}; the sampling rate (which defines our best resolution and therefore our best sensitivity), $\Delta t_{\rm samp} \simeq 64$ μs; and the maximum DM contribution from the Milky Way in the direction of SN 2008iz, 41 pc cm^{-3}. From Figure 5.2, we see that close to maximum sensitivity is retained up to a DM of ~ 225 pc cm^{-3}, at which point our minimum detectable pulse energy begins to rapidly increase. At a DM of 1000 pc cm^{-3}, the total delay due to the ISM is ~ 9.7 ms. For a short duration pulse, this would result in an increase in minimum detectable pulse energy by a factor of ~ 12, giving $\epsilon_{\rm min} \simeq 106$ mJy μs ($\Phi_{\rm min} \simeq 1370$ kJy μs kpc^2). We note, however, that the scattering relation used has an intrinsic spread of 2-3 orders of magnitude (shown as the blue, shaded area in Figure 5.2). If we decrease the scattering delay by a factor of 1000, we find that for a short duration pulse our minimum detectable pulse energy will only be decreased by a factor of ~ 2, giving $\epsilon_{\rm min} \simeq 17.6$ mJy μs ($\Phi_{\rm min} \simeq 228$ kJy μs kpc^2).

As we have minimal knowledge of the distribution of free electrons in M82 we can place no strong upper limit on the possible DM of SN 2008iz. We note, however, that the near edge-on orientation of M82, combined with the proximity of SN 2008iz to its kinematic centre (Weliachew et al., 1984), suggests that its DM may be > 1000 pc cm^{-3}.

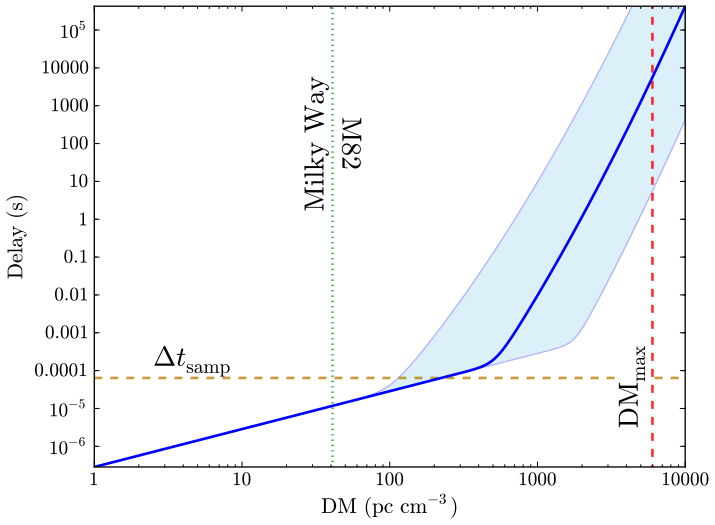

FIGURE 5.2: Total ISM/IGM delay as a function of DM. The blue line shows the delay as calculated via Equation 2.3, with the shaded, blue area showing the maximum and minimum extent of the delay given a three order of magnitude uncertainty on the scattering component. The dashed, red line shows the maximum DM to which the data was searched for radio bursts. The dashed, golden line shows the sampling time, and therefore best resolution, of our observations. The dotted, green line shows the maximum DM contribution from the Milky Way in the direction of SN 2008iz. To the right of this line it is assumed that any signal has originated in M82.

Finally, while the large distance to M82 rules out strong scintillation as a cause of our non-detection, we cannot, through the same logic shown in our discussion of Calvera (see Section 5.1), rule out the possibility that any radio burst from SN 2008iz is simply not beamed towards Earth.

5.2.4 Future prospects

Our observations, while possibly sensitive to the most energetic pulses predicted and reported in the literature, could easily be improved upon through the use of larger telescopes employing wider-bandwidth receivers and backends with higher sampling rates. The future Five hundred meter Aperture Spherical Telescope (FAST; NAN et al., 2011) fits all these requirements, and as such would be a good instrument with which to re-observe SN 2008iz. Using FAST operating at 1.315 GHz, where we will assume an observing system with a gain of 16.5 K Jy^{-1}, bandwidth of 400 MHz, sampling time of ~ 32 μs and system temperature of ~ 20 K[5], we find a minimum detectable pulse

[5]These parameters are taken from Smits et al. (2009), with the exception that we have decreased the sampling rate by a factor of three to reflect the fact that this would be a small scale targeted search and large data rates would not be a limiting factor.

energy of $\epsilon_{\rm min} \simeq 0.19$ mJy μs ($\Phi_{\rm min} \simeq 2.4$ kJy μs kpc^2), scaled to our observing frequency of 4.85 GHz. As can be seen from Figure 5.1, this limit represents a significant improvement, with very good prospects of detecting any giant pulse.

The future Square Kilometer Array (SKA) will also be a fantastic instrument for searching for transient radio signals from nearby galaxies. Unfortunately, observations of SN 2008iz with the SKA will not be possible due to the physical location of the SKA site. However, assuming an analogous event to SN 2008iz, in a nearby galaxy observable from the southern hemisphere, we can examine the sensitivity limit achievable with the SKA in its Phase 1 configuration. Observing at a centre frequency of 2 GHz, the SKA Phase 1 should have[6] a system equivalent flux density of ~ 2.8 Jy, a bandwidth of ~ 2 GHz and a sampling rate of ~ 50 μs. This translates to a minimum detectable pulse energy of $\epsilon_{\rm min} \simeq 0.21$ mJy μs ($\Phi_{\rm min} \simeq 2.8$ kJy μs kpc^2), scaled to our observing frequency of 4.85 GHz.

5.2.5 Conclusion

In conclusion, we have performed radio observations of recent radio supernova SN 2008iz in M82, in the hope of detecting transient radio emission from a newly formed pulsar. No transient radio signals were detected in the direction of SN 2008iz in 385 minutes of radio observations at 4.85 GHz with the 100-m Effelsberg telescope. This result implies that no radio burst of intrinsic energy $\gtrsim$114 kJy μs kpc^2 was beamed towards Earth, from M82, during our observations.

We find that future observations of this source with the FAST should be capable of detecting Crab-like giant pulse emission from M82.

5.3 SGR 1833−0832

5.3.1 Background

On the 19$^{\rm th}$ of March 2010, the *Swift* Burst Alert Telescope triggered on a short soft X-ray burst from deep in the Galactic plane (Gelbord et al., 2010). Rapid follow-up observations made with the *Swift* XRT, identified a previously unknown bright X-ray source to be the cause the trigger (Barthelmy et al., 2010). The properties of the X-ray emission, in combination with the low Galactic latitude of the source, led to initial speculation that the source may be an SGR (Gelbord et al., 2010). The SGR nature of

[6]The system parameters here are taken from the SKA science working group's white paper.

the source was rapidly confirmed through the determination of a 7.57-s periodicity in its X-ray emission using the *Swift* XRT and the *Rossi X-ray Timing Explorer*, earning the source the designation SGR 1833−0832 (Esposito et al., 2010; Göğüş et al., 2010a,b).

As seen in Chapter 1, SGRs are thought to belong to the magnetar class of neutron stars. Until 2006 magnetars were not known to produce pulsed radio emission. However the discovery of such emission from AXP XTE J1810−197 (Camilo et al., 2006) and variable X-ray source 1E 1547.0−5408 (Camilo et al., 2007b) changed this, hinting at a strong link between magnetars and radio pulsars. Interestingly, XTE J1810−197 was not thought to be a radio emitter prior to its only known X-ray burst (Halpern et al., 2005; Ibrahim et al., 2004). The idea that the pulsar's radio emission is somehow linked to its X-ray activity is strengthened by observations showing a correlation in the X-ray and radio flux on long timescales (Camilo et al., 2006, 2007c; Gotthelf and Halpern, 2007). More recently the first magnetar to be discovered via its radio emission (Levin et al., 2010) was found in the High Time Resolution Universe pulsar survey with the Parkes telescope (Keith et al., 2010). Considering these radio detections, a newly discovered magnetar, known to be in outburst, presents a viable target for deep search observations at radio wavelengths. We therefore conducted an observing campaign of SGR 1833−0832 using the 100-m Effelsberg telescope.

5.3.2 Observations and processing

Observations were performed using the 6-cm (4.85 GHz) single-pixel secondary-focus receiver of the Effelsberg telescope in combination with the PFFTS backend system described in Chapter 4. Due to hardware limitations, the maximum achievable bandwidth for these observations was 256×488 kHz. The 6-cm receiver was chosen to reflect the fact that the known radio magnetars all have relatively flat or inverted spectra and, as such, are likely to be brighter at higher frequencies.

SGR 1833−0832 was observed four times on MJD 55278; three times for 60 minutes and once for 35 minutes. Observations were centred on J2000 coordinates R.A. = $18^{\rm h}33^{\rm m}44^{\rm s}.3$ and Decl. = $-08^{\circ}31'05''.6$, taken from Gelbord et al. (2010). We note that the uncertainty on the position was $6.7''$ to 90% confidence, considerably smaller than the telescope beamwidth at 4.85 GHz ($146''$).

Initially observations were phase-folded using the period determined from X-ray analysis of SGR 1833−0832. To account for the possibility of a change in its period due to possible binary motion or a very large period derivative, the folded data were also searched over a small range of periods around the discovery period. As the DM of SGR 1833−0832

is unknown and, given its position in the Galactic plane, could well be very large, the folded data were also searched over trial DMs in the range 0-10000 pc cm^{-3}.

The data were also searched blindly in the DM range 0-6000 pc cm^{-3}. The processing steps in the blind search closely followed those presented in Section 4, with the exception that no multi-beam RFI removal was performed. To mitigate against periodic RFI, the RFIFIND program from the PRESTO package (see Section 2.2.7.1) was used. To retain search sensitivity to other potential pulsed radio sources in the field of view, the DM step size (see Section 2.2.3) was chosen such that the dispersive smearing across the bandwidth did not exceed our sampling time ($t_{\rm samp} \simeq 64$ μs). We note however that the DM step size required to retain sensitivity to pulsations with the period of SGR 1833−0832 is of the order $\sim$ 1000 pc cm^{-3}. This may be taken advantage of to significantly speed-up any future re-processing of our observations (i.e. re-processing with better RFI and/or red noise excision).

All candidates from the blind search were examined by eye to identify any periodicities close to, or harmonics of, the period of SGR 1833−0832. Any potentially interesting candidates were phase-folded and optimised over small ranges of period. A by-product of strong RFI at zero-DM, is that the folded profile of a long period candidate may often show a more significant χ^2 at zero DM than at its optimal DM. For this reason, no DM optimisation was performed on the folded data.

The data were also searched for transient signals using matched filtering techniques (see Section 2.2.6). As with the periodicity search, a fine sampling of DM space was chosen such that the search would be sensitive to any narrow single-pulse emission in the DM range 0-6000 pc cm^{-3}. Single pulse output plots were examined by eye to identify any potentially interesting signals. Signals with high significance which peaked at DM $>$ 2 pc cm^{-3} were examined in the raw data to determine if they were of celestial origin.

The publication of an X-ray timing ephemeris for SGR 1833−0832 spanning 225 days (Esposito et al., 2011), has allowed for refolding of the data with more accurately determined spin parameters. As with the previous folds, the folded data were searched in the DM range 0-10000 pc cm^{-3} for significant pulse profiles. Unlike the previous folds, the folded data were not searched in period, to eliminate the potential for the fold to optimise on nearby, long-period RFI.

5.3.3 Results and discussion

Examining both sets of folded data, we find no significant pulse profiles at the period of SGR 1833−0832 for any DM in the range 0-10000 pc cm^{-3}. No periodicities similar to,

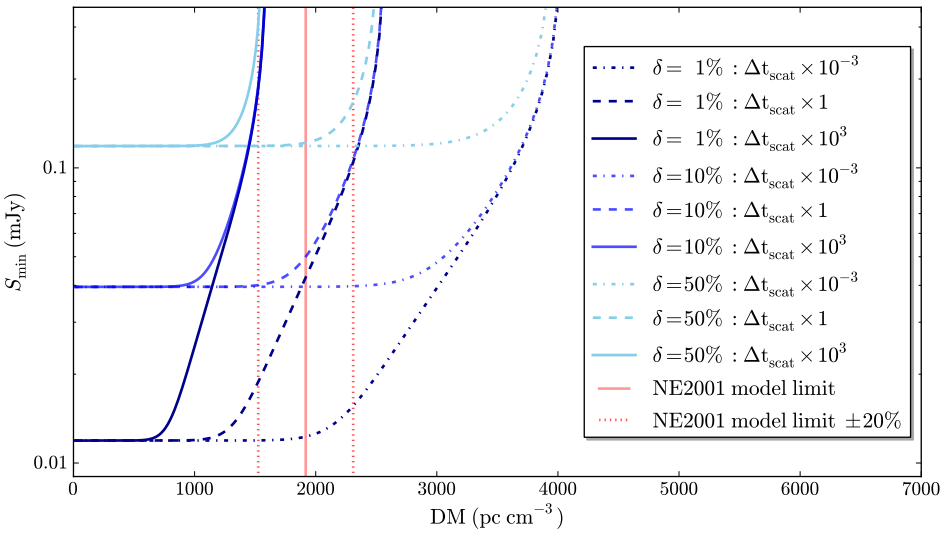

FIGURE 5.3: Minimum detectable flux density for periodic signals ($S_{\rm min}$) at 4.85 GHz, as a function of DM for intrinsic pulse duty-cycles (δ) of 1, 10 and 50%. For each duty-cycle, three regimes of scattering are shown, indicating the intrinsic uncertainty on the scattering delay (Bhat et al., 2004). Also shown is the predicted DM limit in the line of sight, as determined from the NE 2001 Galactic free electron density model (Cordes and Lazio, 2002).

or harmonics of, the X-ray timing period were found in the blind search of the data and no radio bursts of celestial origin were found in the results of our transient search.

Through application of the radiometer equation (see Equation 4.1) we can put limits on the flux density of SGR 1833−0832 at 4.85 GHz. Using the receiver and backend parameters presented in Section 5.2.3, with a reduced bandwidth of 125 MHz, we find a minimum detectable flux density of $S_{\rm min} \simeq 0.03$ mJy at 4.85 GHz, assuming that the radio profile of SGR 1833−0832 has a duty-cycle of 10%. To examine how $S_{\rm min}$ will behave with increasing DM, we can use Equation 2.3 to calculate the broadening of a pulse of duty-cycle δ, due to dispersive smearing and multi-path scattering. Figure 5.3 shows $S_{\rm min}$ as a function of DM for assumed pulse duty-cycles of 1, 10 and 50%. The curves for all duty-cycles are calculated for three regimes of scattering, to represent the intrinsic 2-3 orders of magnitude spread on the Bhat et al. (2004) scattering relation (as in Figure 5.2). Putting these flux density limits in the context of the three known radio-emitting magnetars, we find our observations would be easily capable of detecting all three sources, assuming their flux densities at discovery.

Following the method outlined in Section 5.2.3, we can place an upper limit on the flux density of any transient radio emission from SGR 1833−0832, during our observations, of $\mathcal{S}_{\rm min} \simeq 3\ \sqrt{1\ \mu{\rm s}/{\rm W}_{\mu{\rm s}}}$ mJy. This corresponds to a minimum detectable pulse energy of $\epsilon_{\rm min} \simeq 24$ mJy μs (i.e. the energy of the shortest pulse we can resolve such that it has

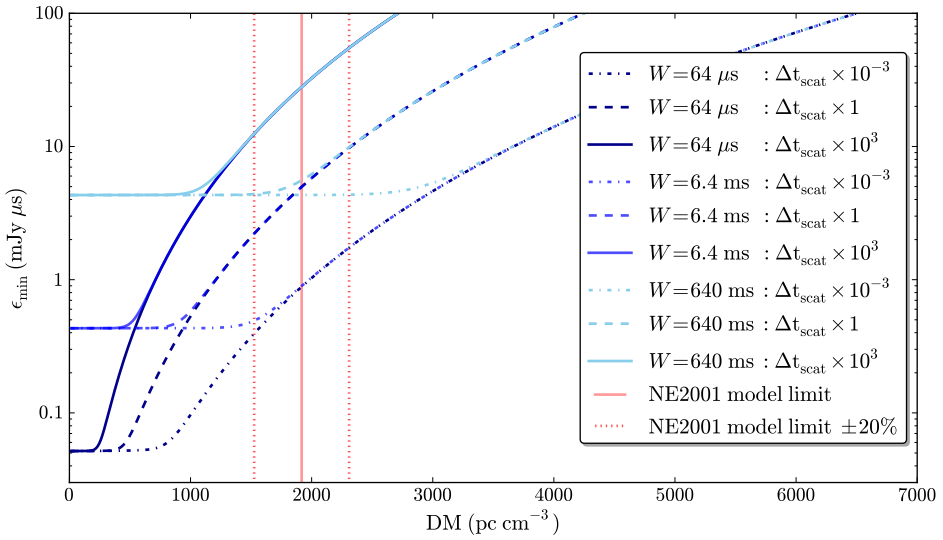

FIGURE 5.4: Minimum detectable pulse energy ($\epsilon_{\rm min}$) at 4.85 GHz as, a function of DM for intrinsic pulse widths (W) of 64 μs, 6.4 ms and 640 ms. For each width, three regimes of scattering are shown, indicating the intrinsic uncertainty on the scattering delay (Bhat et al., 2004). Also shown is the predicted DM limit in the line of sight, as determined from the NE 2001 Galactic free electron density model (Cordes and Lazio, 2002).

a flux density $\geq \mathcal{S}_{\rm min}$). Figure 5.4 shows the DM evolution of $\epsilon_{\rm min}$ assuming the pulse broadening to be determined by Equation 2.3.

The radio emitting magnetars exhibit distinctly different behaviour to the normal pulsar population. In all cases, these sources show highly variable emission properties, with XTE J1810−197 showing large changes in pulse profile on short timescales and a gradual decrease in flux on long timescales (Camilo et al., 2007a). Similarly PSR J1622−4950 shows variable flux densities and profile shapes on short timescales (Levin et al., 2010). For this reason, the limiting flux densities presented here may only be considered valid for the duration of our observations. To provide a clearer picture of any potential radio emission from SGR 1833−0832 on longer timescales, archival observations from the Parkes Multibeam Pulsar Survey (PMPS; Manchester et al., 2001) and the Methanol Multibeam Pulsar Survey (MMB; Bates et al., 2011b) were folded to search for significant pulse profiles. In both cases the closest survey beam on the sky was used and limiting flux densities were scaled to the telescope bore sight assuming a Gaussian beam shape. Table 5.1 shows the limiting flux density calculated for each observation. Also shown are the flux density limits determined through observations of SGR 1833−0832 with the WSRT (Göğüş et al., 2010a) and the Parkes radio telescope (Burgay et al., 2010).

As with our observations of Calvera (see Section 5.1) and SN 2008iz (see Section 5.2)

TABLE 5.1: Recent and archival upper radio flux density limits for SGR 1833−0832. The flux density limits presented are only valid for their respective observing frequency.

Survey	Observing frequency (GHz)	Observation date (MJD)	$S_{\nu,10\%}$[a] (mJy)	$S_{\nu,50\%}$[b] (mJy)
PMPS	1.37	51298	0.2	0.5
MMB	6.59	54313	0.4	1.2
WSRT[c]	2.28	55278	0.2	0.6
WSRT[c]	1.38	55278	0.1	0.3
This work	4.85	55278	0.03	0.09
WSRT[c]	1.38	55279	0.1	0.3
Parkes[d]	1.40	55279	0.1	0.3
WSRT[c]	1.38	55282	0.1	0.3

[a] Flux density limit assuming a 10% duty-cycle.
[b] Flux density limit assuming a 50% duty-cycle.
[c] Göğüş et al. (2010a)
[d] Burgay et al. (2010)

we cannot rule out unfavourable beaming as a reason for our non-detection of SGR 1833−0832.

5.3.4 Conclusion

In conclusion, we have performed deep radio observations at 4.85 GHz, of recently discovered SGR 1833−0832. No radio detection was made, allowing for stringent limits to be placed on the upper flux density of any radio signals emitted during the observations. The radio flux density limits presented here are roughly a factor of three better than those found at other observatories at the same time.

As the radio emission from the three previously known magnetars is variable, the limits here may only be considered valid for the duration of our observations. Using archival pulsar search data taken with the Parkes telescope, we find no radio detection from observations in 1999 and 2007, allowing for further limits to be placed on the radio flux density of SGR 1833−0832. The limits found in this work and from other observations of SGR 1833−0832 may be found in Table 5.1.

The potential for non-detections due to intrinsic day-to-day flux density variations, combined with the uncertainty in the timescale for radio emission to turn on post outburst, makes future observations of this source warranted. Any future observing campaign would benefit from variable cadence monitoring at multiple frequencies.

Chapter 6

Summary and future work

6.1 Summary

In this thesis, we have explored the current capabilities of the Effelsberg telescope as an instrument for the discovery and exploitation of new and exciting pulsar systems. With 13 new pulsars discovered, including two previously unknown binary MSPs, this work has built upon the initial discoveries of Lorimer et al. (1999), providing clear proof of the capabilities of the Effelsberg telescope as an instrument for the discovery of new pulsars.

Through application of statistical methods to the *Fermi* LAT First Source catalogue, we selected 289 unassociated γ-ray sources that had a high probability of being previously unknown pulsars (Section 3.2). Observations of these sources resulted in the discovery of the Effelsberg telescope's first MSP, J1745+1017 (Section 3.6). Through the determination of a phase-coherent timing solution (Table 3.1), we were able to further investigate the γ-ray source in which PSR J1745+1017 was discovered, leading to the detection of γ-ray pulsations (Section 3.6.1.2). This result conclusively tied PSR J1745+1017 to the γ-ray source in which it was found, adding it to the ever growing list of radio-loud MSPs discovered through searches in unassociated γ-ray sources from the LAT instrument. As part of the above search, the positions of several known γ-ray pulsars were observed in the hope of discovering radio pulsations. With no pulsations found, we placed upper radio flux density limits on any pulsed radio emission from these sources (Table 3.3). The large number of sources observed in this search make it the most comprehensive investigation of the LAT sky at high radio frequencies.

Having shown the Effelsberg telescope (and our processing method) to be capable of detecting MSPs, we went on to describe and present the observational setup and initial

discoveries of an ongoing, all-sky search for pulsars and fast transients with the Effelsberg telescope, the High Time Resolution Universe North pulsar survey (HTRU-North). The HTRU-North uses state-of-the-art instrumentation to probe the northern sky with unprecedented time and frequency resolution (Section 4.3). Through examining the sensitivity of our observing system, both analytically (Section 4.4) and empirically (Section 4.4.2), we have shown that the survey is reaching its expected limiting flux density for all observations. Thanks in part to the specific development of new strategies for RFI removal from HTRU-North data (Section 4.6), we have, at the time of writing, discovered 12 new pulsars (Section 4.7). All discoveries are currently being timed with both the Effelsberg and Lovell radio telescopes, with all pulsars now having phase-coherent timing solutions (Table 4.3). Contained within these 12 discoveries are PSRs J1946+3414, a Galactic-disk MSP in a highly eccentric binary system (Section 4.7.3), and J2004+3427, a young pulsar with a characteristic age of < 19 kyr (Section 4.7.2). Optimistic simulations suggest that the HTRU-North survey could go on to discover in excess of 500 new pulsars (Section 4.5).

During this work targeted search observations of three objects of interest were performed; 1RXS J141256.0+792204 (Calvera), an unidentified source of pulsed X-ray emission (Section 5.1); SN 2008iz, a recent radio supernova in the M82 galaxy (Section 5.2); and SGR 1833−0832, a recently discovered magnetar in outburst (Section 5.3). No transient or periodic radio emission was detected from these sources. In each case, we have discussed the reasons for our non-detections and placed upper limits on the flux density of any potential radio emission (sections 5.1.3, 5.2.3 and 5.3.3).

6.2 Future work

6.2.1 Continuing the HTRU-North survey

The HTRU-North survey will run for many more years, with the expectation that the data taken in the survey will be re-processed several times. By considering the current state of the survey, we can examine several areas where future work may be warranted or desired.

6.2.1.1 Improving our RFI mitigation methods

At the time of writing, the HTRU-North pulsar survey (see Chapter 4) has been underway for almost two years. In this time, we have learned much about the instrumentation

used and the RFI environment present at Effelsberg. In particular, dealing with the latter has been a vital part of enabling the survey to detect new pulsars. However, the RFI excision methods currently implemented are by no means the best that could be performed. With more advanced hardware and high precision synchronisation of the backend across all beams, much more rigorous methods could be applied to the HTRU-North data.

6.2.1.2 Re-examining the Galactic pulsar distribution

Having processed 100% of the mid-latitude pointings covering the Orion-spur region (see Section 4.7.1), we can produce a *very* rough estimate of the total yield of discoveries. Extrapolating from the six pulsar discovered in this region, we estimate a total of ~ 360 new pulsars from the survey as a whole. This figure is roughly 50% of the predicted yield found through simulations of the Galactic pulsar population (see Section 4.5). As we have shown that our observing system is achieving its expected sensitivity (see Section 4.4.2), these results suggest that the model used in our simulations is not representative of the pulsar population we observe. However, it should be noted that the current number of discoveries is not yet large enough to draw any conclusive result from this discrepancy. If the discrepancy between the observed and modelled populations turns out to be real, a likely culprit would be our poor understanding of the pulsar luminosity distribution (see e.g. Faucher-Giguère and Kaspi, 2006). Increasing the number of pulsars discovered in the survey will be vital for a) investigating the differences between our observed and simulated pulsar populations, and b) comparing our results to those of similar surveys, in particular the HTRU and P-ALFA surveys, which both have overlap with the HTRU-North survey and observe at the same frequency (see Table 1.1).

6.2.1.3 Discovering the most extreme binaries in the data

The discovery of PSR J1946+3414 has shown that the HTRU-North survey is capable of detecting fascinating binary pulsar systems that test the limits of our current understanding. Short integration times make the process of searching for such systems in the high- and mid-latitude portions of the survey relatively simple, with little extra computational power required to retain sensitivity to highly accelerated signals. However, searching the 25-minute, low-latitude pointings for such systems, will present a much sterner challenge. To remain sensitive to the most extreme binary systems in the data, will require these pointings to be processed using a combination of very fast hardware and new search algorithms. In particular, if we wish to perform phase-coherent binary searches (see e.g. Eatough, 2009) of the low-latitude observations, we will most likely

have to make use of the immense computational power offered by graphics processing units and distributed computing networks, a.k.a 'citizen science'.

6.2.2 Follow-up of pulsars discovered in this work

All the pulsars discovered in this work are currently under regular observation with both the Lovell and Effelsberg radio telescopes, with PSR J1745+1017 also under regular observation with the Nançay radio telescope and the WSRT. Current timing solutions for these pulsars can be found in tables 4.3 and 3.1. Below we briefly discuss the future prospects for the two binary MSPs discovered in this work.

6.2.2.1 PSR J1745+1017

With a two year timing baseline, PSR J1745+1017 (see Section 3.6) has the most well defined properties of any pulsar discovered in this work. As a member of the recently expanded population of 'Black Widow' pulsars opened up by radio observations of *Fermi* LAT sources, further study of this source is desired. In particular, low frequency observations may be capable of observing eclipses in this system. The discovery of an eclipse in the system could, in theory, lead to an estimate for the mass-loss rate of the companion. Such a measurement would be invaluable in assessing whether the results of Arzoumanian et al. (1994) and Stappers et al. (1996) (which suggest mass-loss rates for known 'Black Widow' companions that are incompatible with evaporation on Hubble timescales) are representative of all 'Black Widow' binaries.

6.2.2.2 PSR J1946+3414

Arguably the most exciting discovery of this work is PSR J1946+3414, an MSP in a highly eccentric binary system. As discussed in Section 4.7.3, this system has the potential to shed light on the evolution of binary systems, and formation mechanisms for isolated MSPs. Despite our short timing baseline ($\sim$ 4 months), this pulsar already shows signs of becoming a good timer, with an rms timing residual of < 7 μs. As such, PSR J1946+3414 will likely make a good addition to current and future pulsar timing arrays.

The high eccentricity and good timing properties of this pulsar suggest that it should be soon possible to measure relativistic periastron advance in the system (see e.g. Lorimer and Kramer, 2005). Such a measurement will allow for strong constraints to be placed on the mass of PSR J1946+3414. A full discussion of PSR J1946+3414 will be presented in Barr et. al (in prep.).

6.2.3 Further pulsar searches with the Effelsberg telescope

The HTRU-North survey will not be the only pulsar search conducted with the Effelsberg telescope in the coming years. As seen from chapters 3 and 5, the the high sensitivity of the Effelsberg telescope makes it a strong instrument for targeted pulsar searches. This ability will soon be enhanced by the development of a new ultra-broadband receiver (UBB) system[1] with instantaneous frequency coverage from 0.6 to 3.1 GHz. The UBB will be coupled with a state-of-the-art backend, capable of coherently de-dispersing the entire bandwidth in real-time. The 80% fractional bandwidth of the receiver will allow for unprecedented study of the ISM and local environments of pulsars, as well as enabling higher-precision timing observations with the Efflesberg telescope. These observations are vital for testing theories of gravity using binary pulsars and for improving the capabilities of pulsar timing arrays.

With the new sensitivity offered by the UBB, it will be highly desirable to perform further targeted pulsar searches with the Effelsberg telescope. In particular, the ability to coherently de-disperse the band will be invaluable in removing the effects of dispersive smearing and increasing the DM depth to which we can observed MSPs. We can envisage several pulsar searches that may be undertaken in the coming years, for example:

- **Globular cluster searches**
  The ability to de-disperse observations to the central DM of a given cluster will greatly increase our ability to detect MSPs. Such a search would not require a high data rate, as only minimal frequency resolution would be needed to counteract the small range DM values between the front and back of the cluster (see e.g. Edwards et al., 2001b).

- **A low/mid-Galactic-latitude pilot search for MSPs**
  Using observations that are coherently de-dispersed to $\sim$100 pc cm^{-3}, a new type of Galactic-disk MSP search could be performed. Such a search would be more sensitive to MSPs at high DMs than current searches. As these searches would still be limited by interstellar scattering, the calculation of the optimal DM will be of great importance. The DM chosen will be dependent on the frequency observed at and the sampling rate of the backend used.

- **Further searches for radio pulsars in unassociated *Fermi* LAT sources**
  A shown in Chapter 3, observing unassociated γ-ray point sources can provide a short-cut to the discovery of MSPs. As there currently appears to be no correlation

[1] `http://cordis.europa.eu/projects/rcn/100177_en.html`

between the radio and γ-ray luminosities for pulsars, the next catalogue of unassociated *Fermi* LAT sources, the 3FGL catalogue, will, despite the lower luminosity of its sources, undoubtedly contain many pulsars. The UBBs large bandwidth has the dual effect of increasing our sensitivity to weak pulsars and reducing the possibility of missing low-DM pulsars due to interstellar scintillation. Therefore, new pulsar searches of 3FGL sources will be highly desirable.

Beyond the above ideas, the Effelsberg telescope will continue to be used to perform many searches such as those presented in Chapter 5.

6.3 The future of pulsar searching

The pulsar searches presented throughout this thesis represent the current state-of-the-art. However, technological advances in receiver and microprocessor design, coupled with vast improvements in the fields of data transport and storage, are a cause of great optimism for the future of pulsar astronomy. Much time and money has already been given over to the development of new instruments that will enable us to radically improve our understanding of the universe.

By far the most ambitious of the above instruments is the Square Kilometre Array (SKA), a telescope spread over two continents, with a collecting area of a square kilometre and continuous frequency coverage from 70 MHz to 70 GHz. The SKA's receivers are planned to have fractional bandwidths of $\sim$50%, which, when combined with the telescope's unprecedented collecting area, will give the SKA a sensitivity far in excess of any current instrumentation.

The challenges facing the SKA are daunting, with many new techniques and technologies being required to handle the immense volume of data the system will create. Beyond the sheer volumes of data, the SKA will implement several exciting new receiver and antenna designs. As these designs require thorough testing prior to construction of the SKA, several so-called 'precursor' and 'pathfinder' instruments are currently operational or in construction. Three of these instruments, MeerKAT, LOFAR and FAST, will be of particular interest for near-future pulsar searches.

6.3.1 MeerKAT

MeerKAT is a currently-under-construction telescope array in South Africa. When completed, MeerKAT will consist of 64, 13.5-m antennas and will cover frequencies of 0.6-14.5 GHz. The large collecting area and expected instantaneous bandwidth of MeerKAT

($\sim$ 750 MHz), will make it a fantastic instrument for pulsar search observations. A precursor instrument for MeerKAT, named KAT-7, was completed in 2011 and consists of seven of the antennas that will make up the final array. MeerKAT will be an important test bed for wide-bandwidth receiver technologies for the SKA.

6.3.2 LOFAR

The Low Frequency Array (LOFAR) is the first of a new generation of so-called 'software telescopes', which have no moving parts. Such telescopes consists of many array elements, which, when combined in phase, can be used to synthesise a telescope beam on the sky. LOFAR will probe the low-frequency sky (30-240 MHz) with unprecedented sensitivity, making it a great instrument for the discovery of nearby, dim pulsars. At the time of writing, LOFAR is in its science commissioning phase, and is already being used to perform several pulsar surveys. LOFAR will provide an important testing ground for aperture array technology prior to construction of the low-frequency portions of the SKA.

6.3.3 FAST

The Five-hundred-meter Aperture Spherical Telescope (FAST) represents the next generation of single-dish radio telescopes. Scheduled for completion in late 2016, FAST is a 500-m, Arecibo-like spherical reflector that is currently under construction in southwest China. However, unlike Arecibo, FAST will have an active surface capable of synthesising a parabolic reflector of 300-m diameter, giving the telescope the ability to observe down to zenith angles of $\sim 40^{\circ}$. The 70,000 m^2 collecting area of FAST will make it a peerless instrument for pulsar observations prior to the completion of the SKA. Pulsar surveys with fast are expected to be capable of detecting in excess of 5,000 pulsars (Smits et al., 2009). Most importantly, the ability of FAST to achieve very high sensitivities on very short timescales, will make it a formidable instrument for the detection of highly relativistic binary systems.

6.4 Closing remarks

Despite the advancements mentioned in the previous section, it is likely to be some time before another all-northern-sky pulsar search is performed at high radio frequencies. The main reason for this, is that the time, effort and money required to perform such a search will only be worthwhile if a significant improvement can be made over previous

searches. While it is possible that a breakthrough in receiver design will facilitate such a search, it is unlikely that this will happen prior to the completion of FAST. As such, the combination of the HTRU and HTRU-North surveys is expected to be the most sensitive all-sky search for pulsars and transients in the pre-SKA era.

Appendix A

The SigPyProc toolbox

A.1 Introduction

During the course of this work, it has been necessary to write a large amount of code to aid in the analysis of observational data from the Effelsberg telescope. In this Appendix, I present a new toolbox for the analysis of pulsar search data, SigPyProc.

A.1.1 What is SigPyProc?

SigPyProc is an object-oriented data analysis toolbox written in Python[1] and C, which provides routines for the manipulation of filterbank files and time series. As pulsar data processing is often time critical, speed is maintained through the use of compiled C libraries accessed via the Python standard library Ctypes[2] module. An additional performance increase is obtained via the use of OpenMP[3], a multi-threading library standard to most Unix systems.

A.1.2 Why do we need SigPyProc?

SigPyProc was initially intended to be an Python wrapper for the sigproc (see Section 2.2.7.2) pulsar signal-processing toolbox, but over time it has developed and become an independent project in its own right. However, with other pulsar data analysis packages already in existence, we must question the need behind another such package.

SigPyProc has several advantages over current pulsar data analysis tools:

[1] http://www.python.org/
[2] http://docs.python.org/library/ctypes.html
[3] http://openmp.org/wp/

- Straight forward and easy to follow syntax and structure.
- Economy of code.
- Abstraction from complicated data formats.
- Ideal for development.
- Opens up the vast power of Python's libraries (NUMPY, SCIPY, MATPLOTLIB, etc.)[4].
- Object-oriented structure allows for a simple plug and play system with new methods or classes.
- Can be used interactively.
- Very quick, due to the use of OPENMP.

A.1.3 Where is SigPyProc?

A working version of SIGPYPROC, together with detailed instructions on its installation, dependencies and usage, can be found at `https://github.com/ewanbarr/sigpyproc`.

A.1.4 Caveats

SIGPYPROC has been almost entirely written by myself, with contributions from Evan Keane and Sam Bates, and many useful comments and requests from members of the MPIfR pulsar group. Therefore, I accept full responsibility for any bugs in the code, of which there will, undoubtedly, be several. SIGPYPROC is very much a project in its infancy, with the possibility for several changes before it reaches an equilibrium state. I also feel it necessary to point out that although the entire code was written from scratch, I have the PRESTO and SIGPROC packages to thank for providing some of the algorithms used.

A.2 A short tutorial

Here, I will give a very brief tutorial on using SIGPYPROC interactively in the IPython[5] shell. The examples below use SIGPYPROC 0.1.2, Python 2.7.3 and IPython 0.12.1.

[4] `http://numpy.scipy.org/`, `http://matplotlib.org/`
[5] `http://ipython.org/`

A.2.1 Opening a filterbank file

Below, I give and example of how to load a filterbank file into SigPyProc.

```
In [1]: from SigPyProc.Readers import load

In [2]: myFil = load("tutorial.fil")
```

Initially we must import a method or function which allows us to access a filterbank file. In this case I use the LOAD function, which is a convenience function for loading all data types with standard file extensions (i.e. .dat, .tim, .fil, .fft, etc.). Next we create an object representing our filterbank file. In the above example, I have named this 'myFil'. This object currently contains all observational metadata, stored in the form of attributes. For example:

```
In [4]: myFil.nsamples
Out[4]: 187520

In [5]: myFil.nchans
Out[5]: 64
```

We may also obtain a brief summary of the file by typing the name of the object:

```
In [22]: myFil
Out[22]:
<class 'SigPyProc.BaseData.BaseData'>

basename                : tutorial
data_type               : Filterbank file
fch1 (MHz)              : 1510.0
filelen                 : 3000564
filename                : tutorial.fil
foff (MHz)              : -1.09
hdrlen                  : 244
machine_id              : FAKE
nbits                   : 2
nbytes                  : 3000320
nchans                  : 64
nifs                    : 1
nsamples                : 187520
source_name             : P250_DM30
```

```
telescope_id           : Fake
tsamp (s)              : 0.00032
tstart (MJD)           : 50000.0
```

The SigPyProc.BaseData.BaseData class (of which 'myFil' is an instance), contains several methods for the manipulation of the filterbank file. For example;

- dedisperse
  De-disperse the observation to a given DM.
- downsample
  Downsample the filterbank file in time and/or frequency.
- fold
  Phase-fold the filterbank file at a given period, DM and acceleration.
- getChan
  Select a single frequency channel from the filterbank file.
- readBlock
  Return a section of the observation as a 2-D array.

Below, we will take a closer look at the output of the dedisperse method.

A.2.2 De-dispersing a filterbank file

The first thing we will want to do before de-dispersing our file, is to set the number of threads available to OpenMP. To do this we use the setNthreads method. Although this step is not required, it will significantly improve the speed of the de-dispersion.

```
In [5]: myFil.setNthreads(2)
```

All methods available to 'myFil' that use OpenMP, will now have access to two CPU threads. Having set the number of threads, we can now go ahead and de-disperse our file. Here the only argument the dedisperse method requires, is the DM that we wish to de-disperse to.

```
In [6]: myTim = myFil.dedisperse(100)

Filterbank reading plan:
```

```
------------------------
Called on file:        tutorial.fil
Called by:             dedisperse
Number of samps:       187520
Number of reads:       18
Nsamps per read:       10000
Nsamps of final read:  8510
Nsamps to skip back:   55

Execution time: 0.040064 seconds
```

The DEDISPERSE method returns an instance of the SIGPYPROC.BASETIMESERIES.BASETIMESERIES class, which I have named 'myTim'. Just as with the 'myFil' object, we may obtain a summary of 'myTim' by simply typing its name.

```
In [7]: myTim
Out[7]:
<class 'SigPyProc.BaseTimeSeries.BaseTimeSeries'>

basename               : tutorial
data_type              : Timeseries file
fch1 (MHz)             : 1510.0
filelen                : 3000564
filename               : tutorial.fil
foff (MHz)             : -1.09
hdrlen                 : 244
machine_id             : FAKE
nbits                  : 32
nbytes                 : 3000320
nchans                 : 1
nifs                   : 1
nsamples               : 187465
refdm (pccm^-3)        : 100
source_name            : P: 250.000000000000 ms, DM: 30.000
telescope_id           : Fake
tsamp (s)              : 0.00032
tstart (MJD)           : 50000.0
```

We can access the raw data contained within 'myTim' in two ways. First, we can use the NDARRAY attribute, to grant access to the data in the form of a standard NUMPY array:

```
In [8]: myTim.Ndarray
Out[8]: array([ 107.,  109.,  105., ...,  105.,  109.,  103.], dtype=float32)

In [9]: myTim.Ndarray[0]
Out[9]: 107.0
```

Second, we can access the data as a CTYPES array. which may be passed as a C function argument:

```
In [10]: myTim.Cbuffer
Out[10]: <SigPyProc.Utils.c_float_Array_187465 at 0x457a560>

In [11]: myTim.Cbuffer[0]
Out[11]: 107.0
```

The 'myTim' object contains several methods for manipulation of the time series, including;

- APPLYBOXCAR
  Smooth the time series with a boxcar filter.
- DOWNSAMPLE
  Downsample the time series.
- RUNNINGMEAN
  Compute the running mean of the time series.
- RUNNINGMEDIAN
  Compute the running median of the time series (with a fast algorithm).
- RFFT
  Take the 1-D, real-to-complex DFT of the time series (using FFTW, see Section 2.2.4.2).

Below we will take a closer look at the output of the RFFT method.

A.2.3 Performing a discrete Fourier transform

Taking the DFT of 'myTim' is as simple as:

```
In [12]: mySpec = myTim.rFFT()
```

Here, 'mySpec' is an instance of the SigPyProc.BaseSpectrum.BaseSpectrum class, and contains both the complex DFT output and the formed power spectrum (shown here as Numpy arrays, but also accessible as Ctypes arrays).

```
In [13]: mySpec.fftBuffer.Ndarray          #FFTW output
Out[13]:
array([  1.96329040e+07,   0.00000000e+00,  -2.93994995e+02, ...,
        -2.38658051e+02,   2.78900000e+03,   0.00000000e+00], dtype=float32)

In [14]: mySpec.Ndarray          #Power spectrum
Out[14]:
array([    0.        ,     0.        ,     0.        , ...,  2272.41503906,
        2514.97167969,  3218.59545898], dtype=float32)
```

In this case, the power spectrum has undergone both Fourier interpolation (see Section 2.2.4.3) and brute-force suppression of the lowest frequencies (see Section 2.2.4.4).

Several methods are provided for the manipulation of the power spectrum, including:

- rednoise
  Remove an interpolated rednoise curve from the spectrum (see Section 2.2.4.4).
- sumHarms
  Perform N harmonic sums of the spectrum (see Section 2.2.4.5).
- findCands
  Identify significant signals in the spectrum.
- zapbirds
  Remove power from a list of 'bad' frequencies.
- iFFT
  Compute the 1-D, complex-to-real DFT of the spectrum (using FFTW, see Section 2.2.4.2).

A.2.4 Putting it together

Taking everything mentioned above, we can envisage an extremely minimal pulsar searching pipeline:

```
In [1]: myFil = FilReader("tutorial.fil")
```

```
In [2]: myCands = F.dedisperse(1000).seek()

In [3]: myFold = myFil.foldCand(myCands.cands[0])

In [4]: myFold.optimise()

In [5]: myFold.freeze()
```

In the above example, I first open the filterbank file by directly using the FilReader method. Next, I de-disperse the data to a DM of 1000 pc cm^{-3} and use the SEEK method. This a convenience method for performing a DFT, whitening the resulting spectrum and searching it for significant signals. I then fold the top candidate in the data using the FOLDCAND method of the 'myFil' instance. Finally, I optimise the fold (performing a series of small searches in DM and P space), before saving it in a native format using the FREEZE method of the 'myFold' instance.

A.3 Future work

SIGPYPROC was never intended to compete with the existing pulsar data analysis packages. Rather than focus on searching methodology, much of SIGPYPROC was written with the aim of providing a platform for quickly testing out new ideas and algorithms, and allow for micro-management of any raw data, particularly prior to use with existing software. As such SIGPYPROC has performed admirably, solving many small problems with data compatibility between different software packages and allowing for interactive examination of raw data in several formats. The ability of SIGPYPROC to both read and write data in the native format of PRESTO and SIGPROC, makes this package an excellent addition to any pulsar astronomers software collection.

There are still many areas in which SIGPYPROC could be improved. In particular, I hope to:

- Add support for PSRFITS format data (see Section 2.2.1).
- Add support for acceleration searching (see Section 2.2.4.7).
- Add support for the multi-beam RFI excision used in Section 4.6

Importantly, I have recently updated the code comments in SIGPYPROC such that they may be automatically parsed by the fantastic SPHINX[6] program. This will enable the

[6] `http://sphinx.pocoo.org/`

code to be very rapidly documented, providing a vital tool for any would-be contributors.

Appendix B

Observed unassociated *Fermi* LAT sources

B.1 Description

Unassociated *Fermi* LAT point sources observed as part of this work. Sources are ranked by the 2FGL logarithmic likelihood, 2FGL $R_{\rm s}$, found through application of Gaussian-mixture modelling (Lee et al., 2012) to the 2FGL catalogue. R_{95} values are the major-axes of the 95% error ellipses for each source as found in the 1FGL and 2FGL catalogues. Limiting flux densities are calculated by the method outlined in Section 3.4, with a 10% duty-cycle imposed. Both Galactic coordinates, l and b, and equatorial coordinates, R.A. and Decl., show the true pointing position of each observation.

B.2 Observations

Index	1FGL name	2FGL name	l (°)	b (°)	R.A. J2000	Decl. J2000	Offset from 2FGL (°)	1FGL R_{95} (°)	2FGL R_{95} (°)	Observations (mins)	Limiting flux density (mJy)	1FGL $R_{\rm s}$	2FGL $R_{\rm s}$
1	J1906.6+0716c	J1906.5+0720	41.13	-0.03	19:06:36	+07:16:41	0.06	0.05	0.06	32	0.10	11.9	18.2
			41.13	-0.03	19:06:36	+07:16:41	0.06			10	0.18		
			41.13	-0.03	19:06:36	+07:16:41	0.06			60	0.07		
			41.13	-0.03	19:06:36	+07:16:41	0.06			60	0.07		
2	J1819.4-1518c	J1819.3-1523	15.70	-0.05	18:19:25	−15:18:26	0.09	0.12	0.12	36	0.09	7.27	15.5
			15.70	-0.05	18:19:25	−15:18:26	0.09			26	0.11		
			15.70	-0.05	18:19:25	−15:18:26	0.09			60	0.07		
			15.70	-0.05	18:19:25	−15:18:26	0.09			10	0.18		
3	J1932.1+1914c	J1932.1+1913	54.61	0.10	19:32:10	+19:14:33	0.02	0.07	0.07	32	0.10	7.57	13.8
			54.61	0.10	19:32:10	+19:14:33	0.02			10	0.18		
4	J1846.8-0233c	J1847.2-0236	30.12	-0.14	18:46:48	−02:33:46	0.12	0.13	0.11	32	0.10	6.85	13.4
			30.12	-0.14	18:46:48	−02:33:46	0.12			10	0.18		
5	J1625.3-0019	J1625.2-0020	13.95	31.81	16:25:20	−00:19:31	0.03	0.08	0.06	32	0.10	4.36	12.2
			13.95	31.81	16:25:20	−00:19:31	0.03			60	0.07		
			13.92	31.83	16:25:13	−00:20:11	0.00			60	0.07		
6	J0224.0+6201c	J0224.0+6204	133.56	1.07	02:24:02	+62:01:00	0.06	0.07	0.06	32	0.10	11.9	12.2
			133.56	1.07	02:24:02	+62:01:01	0.06			60	0.07		
			133.55	1.09	02:24:01	+62:02:17	0.04			76	0.06		
7	J2030.9+4411	J2030.7+4417	82.30	2.84	20:30:55	+44:11:52	0.10	0.09	0.07	10	0.18	8.21	12
			82.30	2.84	20:30:55	+44:11:52	0.10			60	0.07		
			82.30	2.84	20:30:55	+44:11:52	0.10			60	0.07		
			82.30	2.84	20:30:55	+44:11:52	0.10			32	0.07		
8	J1857.9+0352c	J1857.8+0355c	37.13	0.31	18:57:60	+03:52:43	0.05	0.07	0.16	32	0.10	12.7	11.9
			37.14	0.29	18:58:06	+03:52:43	0.08			10	0.18		
9	J2030.0+3641	J2030.0+3640	76.12	-1.44	20:30:00	+36:41:02	0.01	0.06	0.04	10	0.18	9.82	11.8
10	J0308.6+7442	J0308.3+7442	131.75	14.24	03:08:37	+74:42:42	0.07	0.10	0.06	32	0.10	3.57	11.7
			131.71	14.25	03:08:16	+74:44:14	0.03			60	0.07		
11	J0608.3+2038c	J0608.3+2037	189.76	0.29	06:08:20	+20:38:07	0.00	0.09	0.11	32	0.10	4.4	9.89
			189.76	0.28	06:08:20	+20:38:07	0.00			10	0.18		
			189.76	0.27	06:08:16	+20:37:59	0.02			60	0.07		
			189.76	0.27	06:08:16	+20:37:59	0.02			60	0.07		
12	J2032.8+3928	J2033.6+3927	78.69	-0.24	20:32:48	+39:28:12	0.21	0.25	0.12	32	0.10	1.65	9.68
13	J0426.5+5437	J0426.7+5434	150.84	3.87	04:26:35	+54:37:51	0.06	0.14	0.11	32	0.10	2.99	9.38
			150.84	3.87	04:26:35	+54:37:51	0.06			10	0.18		
			150.84	3.87	04:26:35	+54:37:52	0.07			60	0.07		
			150.82	3.85	04:26:24	+54:38:17	0.10			32	0.10		
			150.82	3.85	04:26:24	+54:38:17	0.10			60	0.07		
14	J0622.2+3751	J0621.9+3750	175.84	10.99	06:22:15	+37:51:48	0.08	0.15	0.10	32	0.10	1.07	9.34
			175.84	10.99	06:22:15	+37:51:48	0.08			10	0.18		
			175.84	10.99	06:22:15	+37:51:49	0.08			60	0.07		
			175.84	10.99	06:22:15	+37:51:49	0.08			54	0.08		

			175.84	10.99	06:22:15	+37:51:49	0.08			10	0.18		
15	J1844.2-0342c	J1844.3-0343c	28.81	-0.10	18:44:15	−03:42:46	0.04	0.08	0.08	32	0.10	9.94	9.03
			28.81	-0.10	18:44:15	−03:42:46	0.04			32	0.10		
			28.83	-0.12	18:44:22	−03:42:03	0.03			60	0.07		
			28.83	-0.12	18:44:22	−03:42:03	0.03			60	0.07		
			28.81	-0.10	18:44:15	−03:42:46	0.04			10	0.18		
16	J1803.1-2147c	J1803.3-2148	8.14	0.18	18:03:12	−21:49:26	0.04	0.06	0.04	61	0.07	7.55	8.53
			8.14	0.18	18:03:12	−21:49:26	0.04			60	0.07		
			8.14	0.18	18:03:12	−21:49:26	0.04			32	0.10		
			8.14	0.18	18:03:12	−21:49:26	0.04			25	0.11		
17	J0553.9+3105	J0553.9+3104	179.08	2.65	05:53:57	+31:05:02	0.01	0.15	0.12	32	0.10	2.67	8.39
18	J2139.9+4715	J2139.8+4714	92.60	-4.04	21:39:52	+47:13:42	0.02	0.11	0.07	60	0.07	4.93	8.34
			92.60	-4.04	21:39:52	+47:13:42	0.02			32	0.07		
19	J2339.7-0531	J2339.6-0532	81.41	-62.46	23:39:43	−05:31:25	0.03	0.06	0.04	32	0.10	5.24	8.06
			81.42	-62.45	23:39:42	−05:30:51	0.03			60	0.07		
			81.42	-62.46	23:39:43	−05:31:25	0.03			60	0.07		
20	J0734.7-1557	J0734.6-1558	232.03	2.03	07:34:44	−15:57:20	0.02	0.08	0.06	32	0.10	4.61	7.86
			232.03	2.03	07:34:44	−15:57:20	0.02			32	0.10		
			232.03	2.03	07:34:44	−15:57:21	0.02			60	0.07		
			232.03	2.05	07:34:49	−15:56:26	0.05			60	0.07		
21	J1827.9-1128c	J1828.3-1124c	20.06	-0.09	18:27:59	−11:28:36	0.12	0.14	0.14	32	0.10	4.27	7.71
			20.06	-0.09	18:27:59	−11:28:36	0.12			10	0.18		
22	J2323.4+5849	J2323.4+5849	111.74	-2.12	23:23:27	+58:49:22	0.01	0.06	0.03	32	0.10	4.35	7.69
			111.74	-2.12	23:23:27	+58:49:22	0.01			32	0.10		
23	J0744.1-2523	J0744.1-2523	241.33	-0.70	07:44:09	−25:23:30	0.01	0.12	0.08	10	0.18	2.54	7.59
			241.31	-0.69	07:44:08	−25:22:09	0.03			60	0.07		
24	J1845.9-1133	J1844.9-1116	22.02	-4.05	18:45:59	−11:33:01	0.37	0.51	0.19	32	0.10	0.887	7.55
			22.19	-3.68	18:44:59	−11:13:52	0.05			60	0.07		
25	J1823.2-1336c	J1823.1-1338c	17.64	-0.07	18:23:15	−13:36:22	0.04	0.07	0.07	10	0.18	7.92	7.33
			17.60	-0.08	18:23:13	−13:38:37	0.02			59	0.07		
26	J1849.0-0055c	J1849.3-0055	31.84	0.10	18:49:05	−00:55:32	0.06	0.06	0.07	10	0.18	6.3	7.17
27	J1810.9-1905c	J1811.1-1905c	11.42	-0.08	18:10:60	−19:05:04	0.05	0.09	0.08	20	0.12	5.65	7.08
			11.42	-0.08	18:10:60	−19:05:04	0.05			10	0.18		
28	J0003.1+6227	J0002.7+6220	117.39	0.11	00:03:12	+62:27:31	0.17	0.12	0.09	32	0.10	0.444	7.04
			117.39	0.11	00:03:12	+62:27:31	0.17			10	0.18		
			117.36	0.04	00:03:06	+62:23:05	0.11			60	0.07		
29	J1653.6-0158	J1653.6-0159	16.62	24.93	16:53:41	−01:58:34	0.03	0.06	0.06	60	0.07	4.67	7.02
			16.62	24.93	16:53:41	−01:58:34	0.03			60	0.07		
			16.62	24.93	16:53:41	−01:58:34	0.03			32	0.10		
			16.62	24.93	16:53:41	−01:58:34	0.03			10	0.18		
30	J2046.0+4954	J2046.0+4954	88.42	4.24	20:46:05	+49:54:37	0.00	0.10	0.11	16	0.14	-0.996	6.87
31	J1925.0+1720c	J1924.8+1724c	52.15	0.67	19:25:06	+17:20:54	0.09	0.14	0.14	10	0.18	2.26	6.76
32	J0359.5+5410	J0359.5+5410	148.30	0.85	03:59:36	+54:10:40	0.01	0.09	0.07	32	0.10	2.59	6.69
			148.30	0.85	03:59:36	+54:10:40	0.01			10	0.18		

			148.30	0.85	03:59:36	+54:10:41	0.01			60	0.07		
33	J0541.1+3542c	J0540.3+3549c	173.73	2.74	05:41:07	+35:42:32	0.22	0.14	0.18	10	0.18	0.446	6.56
34	J1837.5-0659c	J1837.3-0700c	25.13	-0.12	18:37:34	−06:59:39	0.05	0.06	0.09	16	0.14	10.6	6.27
			25.13	-0.12	18:37:34	−06:59:39	0.05			32	0.10		
35	J1831.5-0200c	J1832.0-0200	28.86	3.51	18:31:30	−02:00:43	0.13	0.09	0.10	32	0.10	3.29	6.13
			28.86	3.51	18:31:30	−02:00:43	0.13			10	0.18		
			28.86	3.51	18:31:30	−02:00:44	0.13			60	0.07		
			28.86	3.51	18:31:30	−02:00:44	0.13			60	0.07		
36	J1849.7-0121c	J1849.9-0125c	31.52	-0.24	18:49:42	−01:21:38	0.09	0.11	0.09	32	0.10	4.9	5.94
			31.52	-0.23	18:49:42	−01:21:38	0.09			10	0.18		
37	J0541.9-0204c	J0541.8-0203c	206.72	-16.38	05:41:57	−02:04:30	0.04	0.08	0.14	10	0.18	-0.165	5.93
38	J1808.5-1954c	J1808.6-1950c	10.42	0.03	18:08:32	−19:54:16	0.06	0.13	0.08	32	0.10	8.43	5.89
			10.47	-0.01	18:08:46	−19:53:04	0.05			60	0.07		
			10.42	0.03	18:08:32	−19:54:17	0.06			60	0.07		
39	J0220.0+6257	J0221.4+6257c	132.80	1.80	02:20:01	+62:57:39	0.37	0.13	0.12	10	0.18	2.31	5.81
40	J0212.3+5319	J0212.1+5318	134.96	-7.65	02:12:20	+53:19:26	0.05	0.13	0.08	32	0.10	-0.0926	5.6
			134.96	-7.65	02:12:20	+53:19:26	0.05			60	0.07		
41	J1119.9-2205	J1120.0-2204	276.49	36.04	11:19:58	−22:05:19	0.01	0.08	0.06	32	0.10	0.917	5.46
			276.49	36.04	11:19:58	−22:05:19	0.01			32	0.10		
			276.50	36.05	11:20:2	−22:04:59	0.01			60	0.07		
			276.50	36.05	11:20:2	−22:04:59	0.01			60	0.07		
42	J1754.5-2537c	J1754.4-2538c	3.87	-0.00	17:54:34	−25:37:13	0.04	0.14	0.11	10	0.18	6.81	4.96
43	J1853.1+0032c	J1852.7+0047c	33.61	-0.14	18:53:09	+00:32:11	0.27	0.52	0.19	32	0.10	7.95	4.55
			33.61	-0.14	18:53:09	+00:32:11	0.27			2	0.39		
44	J1850.2-0019c	J1850.7-0014c	32.50	0.12	18:50:13	−00:19:44	0.16	0.10	0.19	32	0.10	5.32	4.27
45	J0605.3+3800	J0605.3+3758	174.17	8.08	06:05:19	+38:00:19	0.03	0.09	0.12	10	0.18	-0.0151	4.19
			174.17	8.08	06:05:19	+38:00:19	0.03			10	0.18		
46	J2116.8+3729	J2117.5+3730	82.73	-8.11	21:16:51	+37:29:37	0.17	0.15	0.10	16	0.14	1.22	3.73
47	J0647.3+0031	J0647.7+0032	212.00	-0.66	06:47:22	+00:31:44	0.09	0.22	0.14	32	0.10	0.801	3.72
48	J1817.6-1651c	J1817.6-1651c	14.13	-0.41	18:17:38	−16:51:37	0.00	0.15	0.20	32	0.10	9.5	3.63
			14.13	-0.41	18:17:38	−16:51:37	0.00			10	0.18		
49	J1645.0-2155c	J1645.7-2148c	358.05	15.29	16:45:09	−21:45:25	0.16	0.19	0.22	66	0.07	1.42	3.47
50	J1800.5-2359c	J1800.8-2400	6.01	-0.28	18:00:21	−23:53:52	0.16	0.08	0.07	61	0.07	8.62	3.41
			5.95	-0.37	18:00:33	−23:59:59	0.07			10	0.18		
51	J1929.0+1741c	J1928.8+1740c	52.90	0.00	19:29:04	+17:41:53	0.05	0.09	0.12	10	0.18	5.43	3.1
52	J0634.3+0402c	J0634.3+0356c	207.38	-1.96	06:34:18	+04:02:28	0.10	0.18	0.28	32	0.10	4.66	2.78
53	J2004.7+3343	J2004.4+3339c	70.77	1.17	20:04:44	+33:43:01	0.08	0.13	0.07	10	0.18	2.18	2.64
54	J2034.7+3639	J2034.9+3632	76.66	-2.23	20:34:47	+36:39:03	0.12	0.13	0.08	6	0.23	0.751	2.58
			76.66	-2.23	20:34:47	+36:39:03	0.12			32	0.10		
			76.64	-2.27	20:34:51	+36:36:43	0.08			60	0.07		
55	J1630.5+3735	J1630.3+3732	60.27	43.22	16:30:34	+37:35:52	0.07	0.12	0.08	60	0.07	0.298	2.48
			60.27	43.22	16:30:34	+37:35:52	0.07			32	0.10		
			60.27	43.22	16:30:34	+37:35:52	0.07			10	0.18		
56	J1921.2+0132	J1921.3+0131	37.73	-5.92	19:21:16	+01:32:53	0.03	0.14	0.13	32	0.10	3.28	2.37

			37.70	-5.91	19:21:11	+01:31:12	0.04			60	0.07		
			37.70	-5.91	19:21:11	+01:31:12	0.04			60	0.07		
57	J1226.0+2954	J1226.0+2953	184.92	83.77	12:26:02	+29:54:47	0.02	0.09	0.07	16	0.14	0.421	1.98
			184.91	83.79	12:26:09	+29:54:10	0.02			60	0.07		
58	J0608.1-0630c	J0607.5-0618c	213.86	-12.58	06:08:09	−06:30:32	0.26	0.40	0.19	32	0.10	-0.202	1.94
			213.86	-12.58	06:08:09	−06:30:32	0.26			32	0.10		
59	J0046.8+5658	J0047.2+5657	122.30	-5.89	00:46:51	+56:58:19	0.10	0.13	0.07	10	0.18	1.55	1.8
60	J2052.2+5059	J2051.8+5054	89.88	4.15	20:52:16	+50:59:10	0.14	0.10	0.09	16	0.14	2.09	1.61
61	J1858.1-2218	J1858.3-2218	13.54	-11.37	18:58:08	−22:18:46	0.05	0.11	0.11	32	0.10	2.73	1.26
62	J2029.2+4924	J2029.4+4924	86.38	6.12	20:29:17	+49:24:56	0.05	0.08	0.07	10	0.18	-3.91	0.91
63	J1942.7+1033	J1942.8+1033	48.25	-6.35	19:42:45	+10:33:37	0.02	0.05	0.04	60	0.07	3.33	0.35
			48.25	-6.35	19:42:45	+10:33:36	0.02			10	0.18		
64	J0423.8+4148	J0423.8+4149	159.71	-5.41	04:23:50	+41:48:57	0.01	0.03	0.04	10	0.18	2.37	0.3
65	J1916.0+1110c	J1916.1+1106	45.67	-0.31	19:16:06	+11:10:21	0.07	0.08	0.16	32	0.10	7.54	0.12
			45.67	-0.31	19:16:06	+11:10:21	0.07			10	0.18		
66	J2334.2+4319		45.67	-0.31	23:34:14	+43:19:19		0.12		10	0.18	-1.9	
67	J2321.4+1738		45.67	-0.31	23:23:56	+17:55:16		0.12		16	0.14	-2.5	
68	J2250.8+6336		45.67	-0.31	22:52:47	+63:52:52		0.14		16	0.14	0.678	
			45.67	-0.31	22:50:53	+63:36:54				32	0.10		
69	J2214.5+5949		45.67	-0.31	22:16:18	+60:04:42		0.12		16	0.14	1.07	
			45.67	-0.31	22:14:35	+59:49:42				32	0.10		
			45.67	-0.31	22:14:17	+59:50:38				60	0.07		
70	J2208.6+3903		45.67	-0.31	22:10:48	+39:17:58		0.08		16	0.14	-6.55	
71	J2133.4+2532		45.67	-0.31	21:33:28	+25:32:43		0.14		16	0.14	-0.294	
72	J2128.0+3623		45.67	-0.31	21:30:04	+36:37:01		0.13		16	0.14	-0.894	
73	J2110.6+0403		45.67	-0.31	21:13:09	+04:15:58		0.11		5	0.25	-0.976	
74	J2108.2+5246c		45.67	-0.31	21:09:51	+52:58:24		0.13		16	0.14	0.784	
75	J2104.6+2119		45.67	-0.31	21:04:39	+21:19:45		0.14		16	0.14	-0.363	
76	J2103.0-1127		45.67	-0.31	21:05:44	−11:14:59		0.08		16	0.14	-0.119	
77	J2049.1+3142		45.67	-0.31	20:51:13	+31:54:10		0.13		16	0.14	0.073	
78	J2040.4+4652		45.67	-0.31	20:40:28	+46:52:10		0.09		9	0.19	2.73	
79	J2040.0+4157c		45.67	-0.31	20:41:51	+42:07:59		0.20		32	0.10	3	
80	J2020.0+4049		45.67	-0.31	20:20:01	+40:49:07		0.10		10	0.18	1.01	
81	J1958.9+3459		45.67	-0.31	19:58:54	+34:59:51		0.12		10	0.18	1.04	
82	J1948.6+2437		45.67	-0.31	19:48:37	+24:37:44		0.13		10	0.18	-0.0103	
83	J1945.0-0724c		45.67	-0.31	19:47:42	−07:16:35		0.09		16	0.14	-2.79	
84	J1943.4+2340c		45.67	-0.31	19:43:28	+23:40:53		0.11		32	0.10	4.05	
			45.67	-0.31	19:43:28	+23:40:53				10	0.18		
85	J1940.1+2209c		45.67	-0.31	19:40:07	+22:09:55		0.15		21	0.12	5.67	
			45.67	-0.31	19:40:07	+22:09:55				10	0.18		
86	J1934.9+2031c		45.67	-0.31	19:37:09	+20:38:15		0.28		32	0.10	6.98	
87	J1930.8+1653c		45.67	-0.31	19:30:51	+16:53:10		0.14		10	0.18	5.42	
88	J1926.5+1647c		45.67	-0.31	19:26:33	+16:47:42		0.12		10	0.18	1.98	
89	J1926.1+1601c		45.67	-0.31	19:28:28	+16:07:35		0.14		32	0.10	4.79	

		45.67	-0.31	19:26:12	+16:01:22		10	0.18	
		45.67	-0.31	19:26:12	+16:01:22		10	0.18	
90	J1919.9+6633	45.67	-0.31	19:20:07	+66:39:20	0.14	16	0.14	0.716
91	J1913.2-0744	45.67	-0.31	19:15:55	−07:38:59	0.08	16	0.14	0.064
92	J1911.7+0307	45.67	-0.31	19:11:46	+03:07:46	0.12	10	0.18	-0.186
93	J1902.3+0503c	45.67	-0.31	19:02:21	+05:03:36	0.07	60	0.07	6.85
		45.67	-0.31	19:02:21	+05:03:35		32	0.10	
		45.67	-0.31	19:02:21	+05:03:35		10	0.18	
94	J1857.1+0212c	45.67	-0.31	18:59:38	+02:16:28	0.08	32	0.10	13.8
		45.67	-0.31	18:57:20	+02:06:21		61	0.07	
		45.67	-0.31	18:57:20	+02:06:21		60	0.07	
95	J1846.0-0831	45.67	-0.31	18:48:48	−08:27:44	0.11	16	0.14	0.415
96	J1844.3-0309c	45.67	-0.31	18:44:22	−03:09:25	0.07	32	0.10	5.32
		45.67	-0.31	18:44:22	−03:09:25		10	0.18	
97	J1842.0-1409	45.67	-0.31	18:42:02	−14:09:40	0.08	16	0.14	-0.362
98	J1834.3-0842c	45.67	-0.31	18:37:03	−08:40:01	0.06	32	0.10	9.65
99	J1830.1+0618	45.67	-0.31	18:30:10	+06:18:04	0.06	32	0.10	-4.27
		45.67	-0.31	18:30:10	+06:18:04		10	0.18	
100	J1830.0+0043	45.67	-0.31	18:32:34	+00:45:51	0.20	32	0.10	2.73
		45.67	-0.31	18:30:30	+00:51:04		60	0.07	
101	J1829.6-1006c	45.67	-0.31	18:29:38	−10:06:48	0.13	10	0.18	6.59
102	J1825.7-1410c	45.67	-0.31	18:25:45	−14:10:55	0.06	10	0.18	0.58
		45.67	-0.31	18:25:45	−14:10:56		60	0.07	
103	J1818.7-1557c	45.67	-0.31	18:18:43	−15:57:33	0.11	32	0.10	6.56
		45.67	-0.31	18:18:43	−15:57:33		10	0.18	
104	J1806.8-2109c	45.67	-0.31	18:06:52	−21:09:50	0.13	32	0.10	10.5
		45.67	-0.31	18:06:52	−21:09:50		10	0.18	
		45.67	-0.31	18:06:52	−21:09:50		10	0.18	
105	J1747.6-2820c	45.67	-0.31	17:47:40	−28:20:07	0.06	10	0.18	7.61
106	J1744.6-0354	45.67	-0.31	17:47:14	−03:55:51	0.11	16	0.14	0.0858
107	J1738.5-2656	45.67	-0.31	17:41:43	−26:57:39	0.15	32	0.10	5.65
108	J1735.1-0729	45.67	-0.31	17:37:50	−07:31:33	0.15	16	0.14	0.554
109	J1733.2-2628	45.67	-0.31	17:36:22	−26:30:31	0.27	32	0.10	3.79
110	J1726.2-0724	45.67	-0.31	17:26:58	−07:29:59	0.25	78	0.06	-0.278
111	J1709.8-2026	45.67	-0.31	17:12:50	−20:29:36	0.14	16	0.14	0.959
112	J1642.5+3947	45.67	-0.31	16:42:34	+39:47:38	0.06	10	0.18	-9.46
113	J1632.7-2431c	45.67	-0.31	16:35:48	−24:37:20	0.17	32	0.10	3.69
114	J1627.8-1711c	45.67	-0.31	16:30:46	−17:17:49	0.15	16	0.14	-0.425
115	J1625.8-2429c	45.67	-0.31	16:25:54	−24:29:50	0.09	10	0.18	5.85
116	J1607.5-2030	45.67	-0.31	16:10:32	−20:38:29	0.07	16	0.14	-0.507
117	J1548.7+6311	45.67	-0.31	15:49:31	+63:02:16	0.11	16	0.14	-0.178
118	J1527.6+4152	45.67	-0.31	15:29:27	+41:41:47	0.10	16	0.14	-4.29
119	J1515.5+5448	45.67	-0.31	15:16:56	+54:37:15	0.15	16	0.14	-3.87

120	J1511.9-2253	45.67	-0.31	15:14:52	−23:04:26	0.12	16	0.14	-2.03
121	J1509.7-0843	45.67	-0.31	15:09:46	−08:43:50	0.10	10	0.18	-3.93
		45.67	-0.31	15:09:46	−08:43:50		10	0.18	
		45.67	-0.31	15:09:46	−08:43:50		10	0.18	
122	J1412.6+7406	45.67	-0.31	14:13:03	+73:52:45	0.11	16	0.14	0.477
123	J1407.5-0944	45.67	-0.31	14:07:43	−09:43:29	0.14	10	0.18	-1.78
124	J1351.8-1523	45.67	-0.31	13:51:49	−15:23:35	0.10	32	0.10	-2.41
		45.67	-0.31	13:51:49	−15:23:35		10	0.18	
125	J1322.1+0838	45.67	-0.31	13:22:11	+08:38:48	0.14	10	0.18	-0.000999
126	J1301.5-2046	45.67	-0.31	13:01:33	−20:47:23	0.07	78	0.06	-10.8
127	J1258.3+2125	45.67	-0.31	12:58:21	+21:25:14	0.10	10	0.18	-9.23
128	J1138.0+4109	45.67	-0.31	11:40:42	+40:53:03	0.14	16	0.14	-1.58
129	J1112.3+0458	45.67	-0.31	11:14:58	+04:41:42	0.14	16	0.14	-0.579
130	J1110.3-1622	45.67	-0.31	11:12:51	−16:38:33	0.14	16	0.14	-2.38
131	J1101.3+1009	45.67	-0.31	11:03:56	+09:53:13	0.07	16	0.14	-3.69
132	J1040.9-1205	45.67	-0.31	10:43:26	−12:21:44	0.15	16	0.14	-1.61
133	J1034.7+7353	45.67	-0.31	10:38:40	+73:37:38	0.14	16	0.14	0.164
134	J0942.1+4313	45.67	-0.31	09:45:16	+42:59:39	0.09	16	0.14	-4.58
135	J0847.4+1517	45.67	-0.31	08:47:26	+15:16:60	0.09	10	0.18	0.218
136	J0842.2+0251	45.67	-0.31	08:42:12	+02:51:30	0.07	32, 78	0.10	-2.24
		45.67	-0.31	08:42:12	+02:51:30	0.07	78	0.06	
137	J0828.9+0901	45.67	-0.31	08:28:55	+09:01:01	0.10	10	0.18	-1.79
138	J0753.1+4649	45.67	-0.31	07:53:12	+46:49:13	0.07	10	0.18	-5.05
139	J0736.4+4053	45.67	-0.31	07:36:28	+40:53:55	0.07	10	0.18	-0.0841
140	J0731.9-1517	45.67	-0.31	07:34:13	−15:23:52	0.11	16	0.14	-0.388
141	J0724.7-2223c	45.67	-0.31	07:24:44	−22:22:60	0.10	10	0.18	0.931
142	J0709.0-1116	45.67	-0.31	07:09:02	−11:16:31	0.09	32	0.10	0.881
		45.67	-0.31	07:09:02	−11:16:31		10	0.18	
143	J0659.9+1303	45.67	-0.31	06:59:56	+13:03:08	0.12	10	0.18	-1.33
144	J0653.6+8236	45.67	-0.31	06:53:41	+82:36:26	0.07	76	0.06	-5.66
		45.67	-0.31	06:53:41	+82:36:26		76	0.06	
145	J0636.0+0458c	45.67	-0.31	06:36:01	+04:58:51	0.07	10	0.18	1.52
146	J0630.1+0622	45.67	-0.31	06:30:08	+06:22:05	0.11	10	0.18	1.24
147	J0625.7+0001	45.67	-0.31	06:25:44	+00:01:47	0.13	10	0.18	-6.05
148	J0623.5+3330	45.67	-0.31	06:23:34	+33:30:22	0.12	32	0.10	0.506
		45.67	-0.31	06:23:34	+33:30:22		10	0.18	
149	J0540.4-0737c	45.67	-0.31	05:21:47	−21:14:06	0.10	10	0.18	1.1
		45.67	-0.31	05:21:47	−21:14:06	0.10	10	0.18	
150	J0536.2-0607c	45.67	-0.31	05:36:15	−06:07:41	0.14	10	0.18	1.82
151	J0534.7-0531c	45.67	-0.31	05:37:12	−05:29:34	0.10	32	0.10	3.76
		45.67	-0.31	05:34:41	−05:32:29		60	0.07	
		45.67	-0.31	05:34:45	−05:31:19		10	0.18	
152	J0527.6+6646	45.67	-0.31	05:27:36	+66:47:31	0.11	10	0.18	-1.59

153	J0520.2+2632		45.67	-0.31	05:20:14	+26:32:34		0.09		10	0.18	-2	
154	J0513.0+4048		45.67	-0.31	05:13:02	+40:48:36		0.09		16	0.14	-1.29	
155	J0500.8+3437		45.67	-0.31	05:00:52	+34:37:01		0.09		10	0.18	-0.487	
156	J0500.1+5237		45.67	-0.31	05:00:11	+52:37:48		0.05		10	0.18	-3.28	
157	J0427.9+5556		45.67	-0.31	04:32:01	+56:03:13		0.15		16	0.14	-1.65	
158	J0427.3+2028		45.67	-0.31	04:30:19	+20:35:08		0.11		16	0.14	-3.04	
159	J0411.6+5459		45.67	-0.31	04:15:37	+55:07:18		0.14		16	0.14	-1.14	
160	J0402.2+6810		45.67	-0.31	04:07:17	+68:18:42		0.12		16	0.14	-6.39	
161	J0338.8+1313		45.67	-0.31	03:41:40	+13:23:27		0.09		16	0.14	-0.216	
162	J0336.0+7845		45.67	-0.31	03:43:12	+78:54:36		0.07		16	0.14	-1.87	
163	J0256.9+2920		45.67	-0.31	02:59:57	+29:32:52		0.12		16	0.14	-3.7	
164	J0218.8+6158c		45.67	-0.31	02:18:51	+61:58:21		0.14		10	0.18	3.26	
			45.67	-0.31	02:18:51	+61:58:21				10	0.18		
			45.67	-0.31	02:18:51	+61:58:21				60	0.07		
165	J0208.6+3522		45.67	-0.31	02:08:21	+35:17:35		0.05		76	0.06	-1.78	
			45.67	-0.31	02:08:21	+35:17:35				76	0.06		
166	J0147.4+1547		45.67	-0.31	01:47:26	+15:47:31		0.12		10	0.18	-1.71	
167	J0136.3-2220		45.67	-0.31	01:38:41	−22:05:11		0.11		32	0.10	-3.63	
			45.67	-0.31	01:36:19	−22:20:24				10	0.18		
168	J0059.6+1904		45.67	-0.31	00:59:38	+19:04:39		0.09		10	0.18	0.28	
169	J0038.6+2048		45.67	-0.31	00:38:39	+20:48:10		0.15		10	0.18	-2.02	
170	J0008.3+1452		45.67	-0.31	00:08:20	+14:52:53		0.14		10	0.18	-0.855	
171	J0000.8+6600c		45.67	-0.31	00:00:50	+66:00:07		0.11		60	0.07	2.38	
			45.67	-0.31	00:00:50	+66:00:06				60	0.07		
			45.67	-0.31	00:00:50	+66:00:06				32	0.10		
			45.67	-0.31	00:00:50	+66:00:06				10	0.18		
172	J1816.7+4509	J1816.5+4511	72.81	24.71	18:16:42	+45:09:27	0.05	0.10	0.08	16	0.14	-0.733	-0.27
			72.80	24.74	18:16:31	+45:09:07	0.05			60	0.07		
173	J0110.0+6806	J0110.3+6805	124.67	5.30	01:10:03	+68:06:36	0.07	0.08	0.05	10	0.18	0.686	-0.72
174	J0707.3+7742	J0706.5+7741	136.77	27.30	07:07:20	+77:42:07	0.19	0.10	0.09	16	0.14	-0.343	-0.92
			136.77	27.30	07:07:20	+77:42:07	0.19			16	0.14		
175	J0054.9-2455	J0055.0-2454	142.78	-87.66	00:54:56	−24:55:44	0.03	0.09	0.12	32	0.10	-0.169	-0.93
176	J0517.6+0857	J0517.5+0900	193.61	-16.20	05:17:38	+08:57:11	0.06	0.12	0.12	32	0.10	0.527	-1
			193.61	-16.20	05:17:38	+08:57:11	0.06			10	0.18		
			193.61	-16.20	05:17:38	+08:57:11	0.06			10	0.18		
177	J1745.5+1018	J1745.6+1015	34.88	19.27	17:45:31	+10:18:36	0.05	0.12	0.12	10	0.18	1	-1.08
			34.88	19.27	17:45:31	+10:18:36	0.05			76	0.06		
178	J1829.3-2423	J1829.3-2419	8.73	-6.32	18:29:19	−24:23:01	0.06	0.07	0.11	16	0.14	0.939	-1.21
179	J1926.8+6153	J1927.0+6153	93.41	19.70	19:27:31	+61:59:13	0.14	0.06	0.04	16	0.14	0.944	-1.42
			93.28	19.73	19:26:54	+61:53:01	0.05			60	0.07		
180	J1721.1+0713	J1721.0+0711	29.07	23.34	17:21:09	+07:13:06	0.04	0.12	0.14	32	0.10	0.582	-1.48
			29.07	23.34	17:21:09	+07:13:06	0.04			10	0.18		
181	J2016.2-0903	J2016.3-0904	34.36	-22.94	20:16:17	−09:03:07	0.02	0.07	0.05	16	0.14	-1.42	-1.54

			34.36	-22.94	20:16:18	−09:02:53	0.02			60	0.07		
182	J0754.4-1147	J0754.4-1147	230.77	8.24	07:54:28	−11:47:37	0.02	0.07	0.09	10	0.18	-2.9	-1.57
			230.77	8.24	07:54:28	−11:47:37	0.02			10	0.18		
183	J0009.1+5031	J0009.1+5030	116.06	-11.80	00:08:59	+50:29:58	0.05	0.12	0.05	76	0.06	-1.03	-1.63
184	J1844.1+1547	J1844.3+1548	46.28	8.71	18:44:08	+15:47:34	0.05	0.11	0.07	10	0.18	0.366	-1.66
185	J0115.7+0357	J0115.4+0358	134.54	-58.36	01:15:44	+03:57:31	0.06	0.08	0.08	10	0.18	-0.284	-1.73
186	J0018.6+2945	J0018.5+2945	114.51	-32.62	00:18:47	+29:42:49	0.08	0.07	0.10	76	0.06	-1.39	-1.76
			114.51	-32.62	00:18:47	+29:42:49	0.08			76	0.06		
187	J0902.4+2050	J0902.4+2050	206.67	37.74	09:02:24	+20:50:52	0.01	0.11	0.10	10	0.18	-4.42	-1.91
188	J1956.2-0238	J1955.9-0241	38.05	-15.60	19:56:12	−02:38:39	0.09	0.12	0.19	10	0.18	-0.669	-1.93
189	J0043.6+3424	J0043.7+3426	121.13	-28.43	00:43:45	+34:24:55	0.02	0.07	0.06	60	0.07	-1.33	-1.98
			121.12	-28.44	00:43:42	+34:24:21	0.04			10	0.18		
190	J1048.7+2335	J1048.6+2336	213.32	62.13	10:48:45	+23:35:44	0.03	0.14	0.17	16	0.14	-0.0311	-2.01
191	J2300.4+3138	J2300.6+3139	96.87	-25.55	23:00:26	+31:38:44	0.05	0.13	0.08	16	0.14	0.16	-2.09
192	J2056.7+4938	J2056.7+4939	89.30	2.74	20:56:44	+49:38:37	0.01	0.05	0.07	16	0.14	-0.447	-2.13
193	J0039.2+4331	J0039.1+4331	120.59	-19.29	00:39:13	+43:31:18	0.02	0.11	0.12	10	0.18	-1.06	-2.17
194	J1908.5-0138	J1908.8-0132	33.42	-4.55	19:08:32	−01:38:06	0.11	0.14	0.12	10	0.18	1.99	-2.18
195	J2017.9-1621	J2017.5-1618	27.21	-26.31	20:17:57	−16:21:16	0.10	0.12	0.11	16	0.14	0.519	-2.19
196	J1643.5-0646	J1643.5-0641	10.67	24.46	16:43:33	−06:46:48	0.09	0.08	0.11	16	0.14	-1.54	-2.25
197	J0038.0+1236	J0037.8+1238	117.84	-50.13	00:38:04	+12:36:38	0.06	0.10	0.07	10	0.18	-0.286	-2.28
198	J1824.6+1013	J1824.5+1013	39.06	10.63	18:24:17	+10:13:23	0.08	0.09	0.10	40	0.09	-0.714	-2.34
			39.06	10.63	18:24:17	+10:13:23	0.08			76	0.06		
199	J0333.7+2919	J0333.7+2918	160.47	-21.47	03:33:42	+29:19:38	0.02	0.05	0.07	16	0.14	-1.3	-2.36
200	J0223.0-1118	J0223.0-1118	181.04	-63.29	02:23:04	−11:18:05	0.01	0.10	0.10	16	0.14	-2.53	-2.41
201	J0137.8+5814	J0137.7+5811	129.02	-4.07	01:37:49	+58:14:57	0.05	0.13	0.10	16	0.14	0.529	-2.41
202	J1419.7+7731	J1419.4+7730	116.97	38.56	14:19:44	+77:31:27	0.06	0.07	0.11	16	0.14	-0.695	-2.45
203	J1841.9+3220	J1841.7+3221	61.52	15.97	18:41:55	+32:20:26	0.05	0.08	0.08	32	0.10	-2.41	-2.47
			61.52	15.97	18:41:55	+32:20:26	0.05			10	0.18		
204	J0746.5-0711	J0746.5-0713	225.75	8.81	07:46:34	−07:11:55	0.02	0.13	0.15	16	0.14	0.0373	-2.55
205	J0305.2-1601	J0305.0-1602	200.17	-57.10	03:05:13	−16:01:41	0.05	0.12	0.12	16	0.14	-0.482	-2.63
206	J2358.5-1809	J2358.4-1811	66.51	-74.87	23:58:31	−18:09:39	0.04	0.14	0.15	16	0.14	0.411	-2.65
207	J0721.4+0401	J0721.5+0404c	212.75	8.50	07:21:25	+04:01:46	0.05	0.13	0.23	10	0.18	-1.33	-2.65
			212.75	8.50	07:21:25	+04:01:46	0.05			10	0.18		
208	J0254.2+5107	J0253.5+5107	141.78	-7.20	02:54:16	+51:07:23	0.18	0.13	0.09	16	0.14	-0.626	-2.65
209	J1811.3+0340	J1811.3+0339	31.65	10.60	18:11:20	+03:41:08	0.03	0.07	0.08	76	0.06	0.303	-2.66
			31.64	10.58	18:11:23	+03:40:06	0.02			76	0.18		
			31.64	10.58	18:11:23	+03:40:06	0.02			10	0.18		
210	J0706.5+3744	J0706.5+3744	179.49	18.98	07:06:30	+37:44:22	0.01	0.07	0.06	10	0.18	0.404	-2.67
211	J0922.0+2337	J0921.9+2335	204.98	42.91	09:22:03	+23:37:06	0.04	0.11	0.23	32	0.10	-4.29	-2.68
212	J0758.6-1450	J0758.8-1448	233.93	7.58	07:58:38	−14:50:05	0.07	0.12	0.16	16	0.14	-3.02	-2.69
213	J1249.8+3706	J1249.9+3705	124.99	80.02	12:49:39	+37:05:53	0.07	0.16	0.10	76	0.06	-3.3	-2.73
			124.99	80.02	12:49:39	+37:05:53	0.07			72	0.06		
214	J1548.6+1451	J1548.3+1453	25.58	47.16	15:48:27	+14:53:06	0.03	0.16	0.08	76	0.06	-0.394	-2.74

215	J0248.7+5127	J0248.5+5131	140.85	-7.29	02:48:44	+51:27:22	0.09	0.10	0.11	10	0.18	-5.85	-2.75
216	J0515.9+1528	J0515.9+1528	187.71	-13.03	05:15:57	+15:27:42	0.01	0.08	0.06	10, 10	0.18	-0.97	-2.8
			187.71	-13.03	05:15:57	+15:27:42	0.01			10	0.18		
217	J1835.3+1345	J1835.4+1349	43.50	9.73	18:35:22	+13:45:55	0.06	0.12	0.15	10	0.18	0.0675	-2.91
218	J1933.3+0723	J1933.3+0722	44.35	-5.85	19:33:23	+07:23:58	0.02	0.08	0.07	32	0.10	0.0717	-2.92
			44.35	-5.85	19:33:23	+07:23:58	0.02			10	0.18		
219	J2223.3+0103	J2223.4+0104	65.22	-44.57	22:23:17	+01:04:15	0.04	0.07	0.08	74	0.06	-0.548	-2.94
220	J2042.2+2427	J2042.1+2428	67.80	-10.82	20:42:13	+24:27:48	0.02	0.10	0.10	16	0.14	-0.797	-2.94
221	J1521.0-0350	J1520.8-0349	358.14	42.45	15:21:01	−03:50:12	0.03	0.07	0.09	16	0.14	0.408	-2.94
222	J0030.7+0724	J0031.0+0724	113.92	-55.11	00:30:43	+07:24:09	0.10	0.08	0.12	4	0.28	-4.58	-2.95
			113.92	-55.11	00:30:43	+07:24:09	0.10			16	0.14		
			113.92	-55.11	00:30:43	+07:24:09	0.10			76	0.06		
			113.92	-55.11	00:30:43	+07:24:09	0.10			76	0.06		
223	J0521.6+0103	J0521.9+0108	201.29	-19.35	05:21:41	+01:03:05	0.12	0.11	0.20	10	0.18	-0.0418	-2.96
224	J2329.2+3755	J2329.2+3755	105.53	-22.15	23:29:12	+37:55:53	0.01	0.03	0.06	16	0.14	0.096	-3.01
			105.53	-22.15	23:29:13	+37:55:38	0.00			60	0.07		
225	J1811.0+1607	J1810.8+1606	43.15	16.05	18:11:04	+16:07:36	0.05	0.15	0.10	32	0.10	-2.39	-3.02
			43.15	16.05	18:11:04	+16:07:36	0.05			10	0.18		
226	J0332.0+6310	J0332.1+6309	139.94	5.74	03:32:05	+63:10:24	0.02	0.06	0.10	32	0.10	0.546	-3.05
			139.93	5.75	03:32:05	+63:11:03	0.03			60	0.07		
			139.94	5.74	03:32:05	+63:10:24	0.02			10	0.18		
227	J2014.4+0647	J2014.7+0646	48.90	-15.03	20:14:28	+06:47:19	0.07	0.12	0.12	16	0.14	-2.75	-3.08
228	J1406.2-2510	J1406.2-2510	323.60	34.68	14:06:16	−25:10:12	0.01	0.07	0.07	10	0.18	-1.69	-3.08
229	J1221.4-0635	J1221.4-0633	289.69	55.51	12:21:26	−06:35:11	0.03	0.13	0.14	16	0.14	-0.451	-3.09
230	J0814.5-1011	J0814.0-1006	231.92	13.31	08:14:34	−10:10:60	0.15	0.11	0.15	10	0.18	0.208	-3.09
231	J2146.6-1345	J2146.6-1345	40.65	-44.98	21:46:41	−13:45:12	0.01	0.07	0.05	16	0.14	-1.71	-3.12
232	J1511.8-0513	J1511.8-0513	354.62	43.11	15:11:54	−05:13:49	0.01	0.09	0.08	16	0.14	-0.416	-3.12
233	J0908.7-2119	J0908.7-2119	249.14	17.56	09:08:46	−21:19:24	0.01	0.10	0.13	32	0.10	0.224	-3.12
			249.14	17.56	09:08:46	−21:19:24	0.01			10	0.18		
234	J0251.5+5634	J0250.7+5631	138.95	-2.51	02:51:32	+56:34:51	0.20	0.14	0.12	16	0.14	0.193	-3.12
			138.95	-2.51	02:51:32	+56:34:51	0.20			16	0.14		
			138.95	-2.51	02:51:32	+56:34:51	0.20			60	0.07		
235	J1129.3+3757	J1129.5+3758	175.61	69.67	11:29:23	+37:57:24	0.04	0.13	0.15	16	0.14	0.272	-3.13
236	J1437.0+5640	J1437.1+5640	97.69	55.01	14:37:03	+56:38:01	0.05	0.03	0.06	76	0.06	-0.152	-3.15
237	J0505.9+6121	J0505.9+6116	149.00	12.16	05:05:56	+61:21:09	0.08	0.08	0.09	10	0.18	-0.862	-3.16
238	J0345.2-2355	J0345.2-2356	218.28	-50.73	03:45:47	−23:55:30	0.13	0.14	0.11	62	0.07	-1.46	-3.16
			218.23	-50.84	03:45:18	−23:55:06	0.03			16	0.14		
239	J1331.0+6957	J1330.9+7001	117.99	46.80	13:31:06	+69:57:01	0.09	0.10	0.09	16	0.14	-0.737	-3.18
240	J1323.1+2942	J1323.0+2941	55.22	82.57	13:23:06	+29:43:20	0.03	0.05	0.06	32	0.10	1.02	-3.19
			55.22	82.57	13:23:06	+29:43:20	0.03			32	0.10		
			55.22	82.57	13:23:06	+29:43:20	0.03			60	0.07		
241	J2246.3+1549	J2246.3+1549	83.96	-37.41	22:46:19	+15:49:15	0.01	0.11	0.11	16	0.14	-7.25	-3.21
242	J0609.3-0244	J0609.4-0248	210.57	-10.60	06:09:23	−02:44:37	0.07	0.10	0.09	10	0.18	0.169	-3.22

			210.57	-10.60	06:09:23	−02:44:37	0.07			10	0.18		
243	J0131.2+6121	J0131.1+6121	127.69	-1.15	01:31:18	+61:21:06	0.04	0.04	0.04	62	0.07	2.42	-3.22
			127.69	-1.15	01:31:18	+61:21:06	0.04			60	0.07		
			127.69	-1.15	01:31:18	+61:21:06	0.04			10	0.18		
244	J2014.5-0047	J2014.0-0046	42.02	-18.78	20:14:34	−00:47:08	0.12	0.09	0.12	16	0.14	-0.933	-3.24
245	J1141.8-1403	J1141.7-1404	278.50	45.49	11:41:52	−14:03:38	0.03	0.10	0.11	16	0.14	-0.911	-3.24
246	J2228.5-1633	J2228.6-1633	43.17	-55.34	22:28:31	−16:33:51	0.04	0.07	0.11	16	0.14	0.318	-3.25
247	J2004.8+7004	J2004.6+7004	103.00	19.53	20:04:45	+70:12:54	0.14	0.05	0.06	16	0.14	-0.109	-3.25
248	J2347.3+0710	J2347.2+0707	96.29	-52.35	23:47:20	+07:10:26	0.06	0.14	0.10	16	0.14	-3.87	-3.27
249	J1254.4+2209	J1254.4+2209	310.99	84.97	12:54:29	+22:09:00	0.01	0.09	0.08	16	0.14	-1.33	-3.27
250	J1256.9+3650	J1257.0+3650	116.40	80.22	12:56:58	+36:50:01	0.01	0.13	0.11	5	0.25	0.357	-3.29
			116.40	80.22	12:56:58	+36:50:01	0.01			10	0.18		
251	J0102.3+0942	J0102.2+0943	127.40	-53.06	01:02:19	+09:42:51	0.03	0.14	0.13	10	0.18	-1.69	-3.29
252	J1950.0+0904	J1949.9+0907	47.84	-8.66	19:50:05	+09:04:21	0.07	0.09	0.18	10	0.18	-4.37	-3.3
253	J1649.6+5241	J1649.6+5238	80.31	39.50	16:49:39	+52:41:35	0.05	0.09	0.11	16	0.14	0.207	-3.36
			80.31	39.50	16:49:39	+52:41:35	0.05			10	0.18		
254	J0730.0+3305	J0729.9+3304	185.90	22.08	07:30:37	+33:06:42	0.17	0.07	0.10	76	0.06	-0.0773	-3.39
			185.90	22.08	07:30:37	+33:06:42	0.17			76	0.06		
255	J0848.6+0504	J0849.0+0455	222.32	28.32	08:48:41	+05:04:49	0.19	0.14	0.15	10	0.18	-5.84	-3.4
256	J2110.3+3820	J2110.3+3822	82.48	-6.60	21:10:23	+38:20:32	0.03	0.10	0.13	15	0.14	-0.163	-3.41
257	J0334.3+6536	J0334.3+6538	138.72	7.86	03:34:23	+65:36:09	0.04	0.10	0.08	16	0.14	0.339	-3.42
258	J1249.3-2812	J1249.5-2811	302.38	34.66	12:49:23	−28:12:42	0.04	0.08	0.09	16	0.14	-3.12	-3.45
259	J1251.3+1044	J1251.2+1045	302.88	73.61	12:51:23	+10:44:31	0.03	0.11	0.16	16	0.14	-3.11	-3.48
			302.88	73.61	12:51:23	+10:44:31	0.03			76	0.06		
			302.88	73.61	12:51:23	+10:44:31	0.03			76	0.06		
260	J2134.5-2130	J2134.6-2130	28.94	-45.07	21:34:34	−21:30:21	0.01	0.08	0.11	16	0.14	0.302	-3.49
261	J0352.8+5658	J0353.2+5653	145.77	2.37	03:52:49	+56:58:03	0.14	0.08	0.16	32	0.10	-1.1	-3.52
			145.77	2.37	03:52:49	+56:58:03	0.14			10	0.18		
			145.77	2.37	03:52:49	+56:58:03	0.14			10	0.18		
262	J2352.1+1752	J2352.0+1753	103.55	-42.76	23:52:06	+17:52:08	0.03	0.09	0.10	16	0.14	-0.278	-3.53
263	J1754.3+3212	J1754.3+3212	57.74	25.39	17:54:19	+32:12:10	0.01	0.07	0.05	60	0.07	-1.6	-3.53
			57.74	25.39	17:54:20	+32:12:06	0.00			10	0.18		
264	J0239.5+1324	J0239.5+1324	159.20	-41.72	02:39:26	+13:25:25	0.03	0.06	0.10	76	0.06	-4.1	-3.55
			159.20	-41.72	02:39:26	+13:25:25	0.03			76	0.06		
265	J1421.0+5421	J1420.2+5422	98.00	58.22	14:21:02	+54:21:22	0.19	0.14	0.11	16	0.14	0.211	-3.67
266	J0409.9-0357	J0409.8-0357	195.87	-37.35	04:09:55	−03:57:23	0.02	0.08	0.10	16	0.14	-0.397	-3.68
267	J0849.3+6607	J0849.2+6606	148.91	36.45	08:49:20	+66:07:55	0.03	0.08	0.09	16	0.14	-0.105	-3.69
268	J0439.8-1857	J0439.8-1858	216.90	-37.25	04:39:52	−18:57:55	0.02	0.07	0.06	16	0.14	-0.379	-3.78
269	J1836.3+3135	J1836.2+3137	60.33	16.79	18:36:18	+31:35:20	0.03	0.05	0.13	10	0.18	-2.51	-3.83
270	J0105.7+3930	J0105.3+3930	125.94	-23.28	01:05:45	+39:30:17	0.10	0.14	0.11	10	0.18	-0.585	-3.84
271	J2310.9+0204	J2310.9+0204	79.35	-52.09	23:11:8	+02:04:55	0.04	0.09	0.08	16	0.14	-1.17	-3.92
272	J1315.6-0729	J1315.6-0730	313.41	54.88	13:15:40	−07:29:51	0.01	0.07	0.11	10	0.18	-2.06	-3.93
			313.41	54.88	13:15:40	−07:29:51	0.01			60	0.07		
273	J1154.0-0008	J1154.0-0010	273.79	59.41	11:54:02	−00:10:37	0.02	0.07	0.07	76	0.06	0.392	-3.95

			273.66	59.54	11:54:02	−00:01:37	0.14			76	0.06		
274	J1040.5+0616	J1040.7+0614	240.78	52.56	10:40:30	+06:16:39	0.07	0.12	0.10	10	0.18	-2.44	-4.14
275	J1218.4-0128	J1218.5-0122	286.11	60.32	12:18:29	−01:28:14	0.09	0.12	0.09	16	0.14	-1	-4.24
276	J0024.6+0346	J0024.5+0346	110.11	-58.43	00:24:41	+03:46:32	0.03	0.10	0.20	10	0.18	-2.8	-4.46
277	J0342.2+3859	J0342.4+3859	155.65	-12.79	03:42:15	+38:59:47	0.04	0.11	0.09	16	0.14	-0.95	-6.25
278	J1954.8+1402	J1955.2+1356	52.78	-7.19	19:54:52	+14:02:44	0.14	0.14	0.08	10	0.18	-2.73	-9.53
279	J0656.2-0321	J0656.2-0320	216.48	-0.46	06:56:17	−03:21:41	0.02	0.08	0.07	10	0.18	-7.06	-9.77
280	J0648.7-1740	J0648.7-1739	228.48	-8.53	06:48:45	−17:40:12	0.01	0.13	0.12	19	0.13	-8.82	-10.2
281	J2001.1+4351	J2001.1+4352	79.05	7.10	20:01:12	+43:51:51	0.02	0.02	0.02	10	0.18	4.5	-10.2
282	J0521.7+2114	J0521.7+2113	183.59	-8.69	05:21:47	+21:14:06	0.01	0.03	0.02	10	0.18	-2.49	-10.4
283	J0643.2+0859	J0643.2+0858	203.99	2.28	06:43:13	+08:59:58	0.02	0.07	0.07	60	0.07	-11.4	-10.8
			203.97	2.29	06:43:13	+09:00:57	0.04			10	0.18		
284	J1830.1-0425		203.97	2.29	18:32:50	−04:23:01		0.14		32	0.10	4.93	
			203.97	2.29	18:30:20	−04:22:20				60	0.07		
			203.97	2.29	18:30:11	−04:25:18				10	0.18		
285	J0102.8+5827	J0102.7+5827	124.42	-4.37	01:02:49	+58:27:59	0.02	0.09	0.06	10	0.18	-8.26	-11.8
			124.42	-4.37	01:02:49	+58:27:59	0.02			10	0.18		
286	J0048.0+2232	J0047.9+2232	121.90	-40.32	00:48:01	+22:32:26	0.01	0.09	0.08	60	0.07	-5.83	-12.7
			121.90	-40.32	00:48:01	+22:32:26	0.01			60	0.07		
			121.90	-40.32	00:48:01	+22:32:25	0.01			10	0.18		
287	J1739.4+8717	J1738.9+8716	120.01	27.93	17:39:29	+87:17:22	0.14	0.05	0.07	16	0.14	-11.9	-21
288	J2015.7+3708	J2015.6+3709	74.86	1.16	20:15:43	+37:08:24	0.02	0.04	0.04	9	0.19	-13.7	-22.6
			74.86	1.16	20:15:43	+37:08:24	0.02			60	0.07		
			74.86	1.16	20:15:43	+37:08:23	0.02			10	0.18		
			74.85	1.17	20:15:38	+37:08:25	0.03			60	0.07		
289	J1740.0+5209	J1740.2+5212	79.52	31.83	17:40:05	+52:09:38	0.06	0.07	0.06	16	0.14	-19.3	-38.1

Bibliography

B. Abbott, R. Abbott, R. Adhikari, et al. Search for gravitational waves from binary inspirals in S3 and S4 LIGO data. *Physical Review D*, 77(6):1–12, 2008. ISSN 1550-7998. doi:10.1103/PhysRevD.77.062002.

A. A. Abdo, M. Ackermann, M. Ajello, et al. *Fermi* Large Area Telescope First Source Catalog. *The Astrophysical Journal Supplement Series*, 188(2):405–436, 2010a. ISSN 0067-0049. doi:10.1088/0067-0049/188/2/405.

A. A. Abdo, M. Ackermann, M. Ajello, et al. The First *Fermi* Large Area Telescope catalog of gamma-ray pulsars. *The Astrophysical Journal Supplement Series*, 187(2):460–494, 2010b. ISSN 0067-0049. doi:10.1088/0067-0049/187/2/460.

A. Abramovici, W. E. Althouse, R. W. Drever, et al. LIGO: The Laser Interferometer Gravitational-Wave Observatory. *Science (New York, N.Y.)*, 256(5055):325–33, 1992. ISSN 0036-8075. doi:10.1126/science.256.5055.325.

A. Akmal, V. R. Pandharipande, and D. G. Ravenhall. Equation of state of nucleon matter and neutron star structure. *Physical Review C*, 58(3):1804–1828, 1998. ISSN 0556-2813. doi:10.1103/PhysRevC.58.1804.

C. Allen. *Allen's Astrophysical Quantaties*. Fourth edition, 1999.

M. A. Alpar, A. F. Cheng, M. A. Ruderman, and J. Shaham. A new class of radio pulsars. *Nature*, 300(5894):728–730, 1982. ISSN 0028-0836. doi:10.1038/300728a0.

S. B. Anderson, P. W. Gorham, S. R. Kulkarni, T. A. Prince, and A. Wolszczan. Discovery of two radio pulsars in the globular cluster M15. *Nature*, 346(6279):42–44, 1990. ISSN 0028-0836. doi:10.1038/346042a0.

J. Antoniadis, M. H. van Kerkwijk, D. Koester, et al. The relativistic pulsar-white dwarf binary PSR J1738+0333 - I. Mass determination and evolutionary history. *Monthly Notices of the Royal Astronomical Society*, 423(4):3316–3327, 2012. ISSN 00358711. doi:10.1111/j.1365-2966.2012.21124.x.

A. M. Archibald, I. H. Stairs, S. M. Ransom, et al. A radio pulsar/x-ray binary link. *Science (New York, N.Y.)*, 324(5933):1411–4, 2009. ISSN 1095-9203. doi:10.1126/science.1172740.

Z. Arzoumanian, A. S. Fruchter, and J. H. Taylor. Orbital variability in the eclipsing pulsar binary PSR B1957+20. *The Astrophysical Journal*, 426:L85, 1994. ISSN 0004-637X. doi:10.1086/187346.

J.-L. Atteia, M. Boer, K. Hurley, et al. Localization, time histories, and energy spectra of a new type of recurrent high-energy transient source. *The Astrophysical Journal*, 320:L105, 1987. ISSN 0004-637X. doi:10.1086/184984.

W. B. Atwood, A. A. Abdo, M. Ackermann, et al. The Large Area Telescope on the *Fermi* gamma-ray space telescope mission. *The Astrophysical Journal*, 697/P(2):1071–1102, 2009. ISSN 0004-637X. doi:10.1088/0004-637X/697/2/1071.

W. Baade and F. Zwicky. Cosmic Rays from Super-novae. *Proceedings of the National Academy of Sciences*, 20(5):259–263, 1934. ISSN 0027-8424. doi:10.1073/pnas.20.5.259.

D. C. Backer. Millisecond pulsars. *Journal of Astrophysics and Astronomy*, 5(3):187–207, 1984. ISSN 0250-6335. doi:10.1007/BF02714539.

D. C. Backer, S. R. Kulkarni, C. Heiles, M. M. Davis, and W. M. Goss. A millisecond pulsar. *Nature*, 300(5893):615–618, 1982. ISSN 0028-0836. doi:10.1038/300615a0.

M. Bailes, S. D. Bates, V. Bhalerao, et al. Transformation of a star into a planet in a millisecond pulsar binary. *Science (New York, N.Y.)*, 333(6050):1717–20, 2011. ISSN 1095-9203. doi:10.1126/science.1208890.

M. Bailes, S. M. Ord, H. S. Knight, and A. W. Hotan. Self-Consistency of Relativistic Observables with General Relativity in the White Dwarf-Neutron Star Binary PSR J1141-6545. *The Astrophysical Journal*, 595(1):L49–L52, 2003. ISSN 0004-637X. doi:10.1086/378939.

J. Bally, M. W. Pound, A. A. Stark, et al. G70.7+1.2: A nonthermal bubble in a globule - Nova, supernova remnant, or outflow? *The Astrophysical Journal*, 338:L65, 1989. ISSN 0004-637X. doi:10.1086/185402.

S. D. Barthelmy, T. Sakamoto, W. H. Baumgartner, et al. Swift-BAT refined analysis of the probable new Sgr 1833-0832. *GRB Coordinates Network, Circular Service*, 10528:1, 2010.

S. D. Bates, M. Bailes, N. D. R. Bhat, et al. The High Time Resolution Universe Pulsar Survey - II. Discovery of five millisecond pulsars. *Monthly Notices of the Royal Astronomical Society*, 416(4):2455–2464, 2011a. ISSN 00358711. doi:10.1111/j.1365-2966.2011.18416.x.

S. D. Bates, S. Johnston, D. R. Lorimer, et al. A 6.5-GHz multibeam pulsar survey. *Monthly Notices of the Royal Astronomical Society*, 411(3):1575–1584, 2011b. ISSN 00358711. doi:10.1111/j.1365-2966.2010.17790.x.

M. G. Bernhardt, W. Becker, T. Prinz, F. M. Breithuth, and U. Walter. Autonomous spacecraft navigation based on pulsar timing information. In *2011 2nd International Conference on Space Technology*, pages 1–4. IEEE, 2011. ISBN 978-1-4577-1874-8. doi:10.1109/ICSpT.2011.6064649.

R. J. Beswick. Radio Supernovae. *The Astrophysical Journal*, page 16, 2006.

H. A. Bethe and G. E. Brown. Evolution of Binary Compact Objects That Merge. *The Astrophysical Journal*, 506(2):780–789, 1998. ISSN 0004-637X. doi:10.1086/306265.

N. D. R. Bhat, J. M. Cordes, F. Camilo, D. J. Nice, and D. R. Lorimer. Multifrequency Observations of Radio Pulse Broadening and Constraints on Interstellar Electron Density Microstructure. *The Astrophysical Journal*, 605(2):759–783, 2004. ISSN 0004-637X. doi:10.1086/382680.

N. D. R. Bhat, S. J. Tingay, and H. S. Knight. Bright Giant Pulses from the Crab Nebula Pulsar: Statistical Properties, Pulse Broadening, and Scattering Due to the Nebula. *The Astrophysical Journal*, 676(2):1200–1209, 2008. ISSN 0004-637X. doi:10.1086/528735.

D. Bhattacharya and E. P. J. van den Heuvel. Formation and evolution of binary and millisecond radio pulsars. *Physics Reports*, 203(1-2):1–124, 1991. ISSN 03701573. doi:10.1016/0370-1573(91)90064-S.

G. S. Bisnovatyi-Kogan and B. V. Komberg. Pulsars and close binary systems. *Soviet Astronomy*, 18:217, 1974.

R. Blandford and S. A. Teukolsky. Arrival-time analysis for a pulsar in a binary system. *The Astrophysical Journal*, 205:580, 1976. ISSN 0004-637X. doi:10.1086/154315.

R. N. Bracewell. *The Fourier Transform and Its Applications*. McGraw-Hill, 3rd edition, 2000. ISBN 0-07-303938-1.

R. P. Breton, V. M. Kaspi, M. Kramer, et al. Relativistic spin precession in the double pulsar. *Science (New York, N.Y.)*, 321(5885):104–7, 2008. ISSN 1095-9203. doi:10.1126/science.1159295.

A. Brunthaler, I. Marti-Vidal, K. M. Menten, et al. The expansion of SN 2008iz in M82. In *10th European VLBI Network Symposium and EVN Users Meeting: VLBI and the New Generation of Radio Arrays*, page 6. 2010.

A. Brunthaler, K. Menten, M. Reid, C. Henkel, G. Bower, and H. Falcke. Discovery of a bright radio transient in M82: a new radio supernova? *The Astronomer's Telegram*, 2020:1, 2009a.

A. Brunthaler, K. M. Menten, C. Henkel, et al. Supernova 2008iz in M82. *Central Bureau Electronic Telegrams*, 1803:1, 2009b.

A. Brunthaler, K. M. Menten, M. J. Reid, C. Henkel, G. C. Bower, and H. Falcke. Discovery of a bright radio transient in M82: a new radio supernova? *Astronomy and Astrophysics*, 499(2):L17–L20, 2009c. ISSN 0004-6361. doi:10.1051/0004-6361/200912327.

M. Burgay, N. D'Amico, A. Possenti, et al. An increased estimate of the merger rate of double neutron stars from observations of a highly relativistic system. *Nature*, 426(6966):531–3, 2003. ISSN 1476-4687. doi:10.1038/nature02124.

M. Burgay, B. C. Joshi, N. D'Amico, et al. The Parkes High-Latitude pulsar survey. *Monthly Notices of the Royal Astronomical Society*, 292, 2006. ISSN 0035-8711. doi: 10.1111/j.1365-2966.2006.10100.x.

M. Burgay, A. Possenti, P. Esposito, et al. Upper limit on the radio emission from the soft gamma-ray repeater SGR 1833-0832. *The Astronomer's Telegram*, 2515:1, 2010.

B. F. Burke and F. Graham-Smith. *An Introduction to Radio Astronomy*. Cambridge University Press, 2009.

S. Burke-Spolaor and M. Bailes. The millisecond radio sky: transients from a blind single-pulse search. *Monthly Notices of the Royal Astronomical Society*, 402(2):855–866, 2010. ISSN 00358711. doi:10.1111/j.1365-2966.2009.15965.x.

S. Burke-Spolaor, M. Bailes, S. Johnston, et al. The High Time Resolution Universe Pulsar Survey - III. Single-pulse searches and preliminary analysis. *Monthly Notices of the Royal Astronomical Society*, 416(4):2465–2476, 2011. ISSN 00358711. doi: 10.1111/j.1365-2966.2011.18521.x.

S. Burke-Spolaor, S. Johnston, M. Bailes, et al. The High Time Resolution Universe Pulsar Survey - V. Single-pulse energetics and modulation properties of 315 pulsars. *Monthly Notices of the Royal Astronomical Society*, 423(2):1351–1367, 2012. ISSN 00358711. doi:10.1111/j.1365-2966.2012.20998.x.

W. R. Burns and B. G. Clark. Pulsar Search Techniques. *Astronomy and Astrophysics*, 2:280–287, 1969.

P. B. Cameron and S. R. Kulkarni. Near-Infrared and X-Ray Observations of the Enigmatic G70.7+1.2. *The Astrophysical Journal*, 665(2):L135–L138, 2007. ISSN 0004-637X. doi:10.1086/521077.

F. Camilo, I. Cognard, S. M. Ransom, et al. The Magnetar XTE J1810197: Variations in Torque, Radio Flux Density, and Pulse Profile Morphology. *The Astrophysical Journal*, 663(1):497–504, 2007a. ISSN 0004-637X. doi:10.1086/518226.

F. Camilo, M. Kerr, P. S. Ray, et al. PSR J2030+3641: Radio discovery and gamma-ray study of a middle-aged pulsar in the now identified *Fermi*-LAT source 1FGL J2030.0+3641. *The Astrophysical Journal*, 746(1):39, 2012. ISSN 0004-637X. doi: 10.1088/0004-637X/746/1/39.

F. Camilo, D. R. Lorimer, N. D. R. Bhat, et al. Discovery of a 136 Millisecond Radio and X-Ray Pulsar in Supernova Remnant G54.1+0.3. *The Astrophysical Journal*, 574(1):L71–L74, 2002a. ISSN 0004637X. doi:10.1086/342351.

F. Camilo, D. R. Lorimer, P. Freire, A. G. Lyne, and R. N. Manchester. Observations of 20 Millisecond Pulsars in 47 Tucanae at 20 Centimeters. *The Astrophysical Journal*, 535(2):975–990, 2000. ISSN 0004-637X. doi:10.1086/308859.

F. Camilo, R. N. Manchester, B. M. Gaensler, D. R. Lorimer, and J. Sarkissian. PSR J1124-5916: Discovery of a Young Energetic Pulsar in the Supernova Remnant G292.0+1.8. *The Astrophysical Journal*, 567(1):L71–L75, 2002b. ISSN 0004-637X. doi:10.1086/339799.

F. Camilo, C.-Y. Ng, B. M. Gaensler, et al. OUT OF THE FRYING PAN: A YOUNG PULSAR WITH A LONG RADIO TRAIL EMERGING FROM SNR G315.9-0.0. *The Astrophysical Journal*, 703(1):L55–L58, 2009. ISSN 0004-637X. doi:10.1088/0004-637X/703/1/L55.

F. Camilo, D. J. Nice, J. A. Shrauner, and J. H. Taylor. Princeton-Arecibo Declination-Strip Survey for Millisecond Pulsars. I. *The Astrophysical Journal*, 469:819, 1996a. ISSN 0004-637X. doi:10.1086/177829.

F. Camilo, D. J. Nice, and J. H. Taylor. A Search for Millisecond Pulsars at Galactic Latitudes -50 degrees ¡ B ¡ -20 degrees. *The Astrophysical Journal*, 461:812, 1996b. ISSN 0004-637X. doi:10.1086/177103.

F. Camilo, S. M. Ransom, J. P. Halpern, and J. Reynolds. 1E 1547.0-5408: A Radio-emitting Magnetar with a Rotation Period of 2 Seconds. *The Astrophysical Journal*, 666(2):L93–L96, 2007b. ISSN 0004-637X. doi:10.1086/521826.

F. Camilo, S. M. Ransom, J. P. Halpern, et al. Transient pulsed radio emission from a magnetar. *Nature*, 442(7105):892–5, 2006. ISSN 1476-4687. doi:10.1038/nature04986.

F. Camilo, S. M. Ransom, J. Penalver, et al. The Variable RadiotoXRay Spectrum of the Magnetar XTE J1810197. *The Astrophysical Journal*, 669(1):561–569, 2007c. ISSN 0004-637X. doi:10.1086/521548.

F. Camilo and F. A. Rasio. Pulsars in Globular Clusters. *Binary Radio Pulsars, Astronomical Society of the Pacific Conference Series*, 328:147, 2005.

F. Camilo, I. H. Stairs, D. R. Lorimer, et al. Discovery of Radio Pulsations from the X-Ray Pulsar J0205+6449 in Supernova Remnant 3C 58 with the Green Bank Telescope. *The Astrophysical Journal*, 571(1):L41–L44, 2002c. ISSN 0004637X. doi: 10.1086/341178.

F. Camilo, S. E. Thorsett, and S. R. Kulkarni. The magnetic fields, ages, and original spin periods of millisecond pulsars. *The Astrophysical Journal*, 421:L15, 1994. ISSN 0004-637X. doi:10.1086/187176.

G. L. Case and D. Bhattacharya. A New Σ D Relation and Its Application to the Galactic Supernova Remnant Distribution. *The Astrophysical Journal*, 504(2):761–772, 1998. ISSN 0004-637X. doi:10.1086/306089.

D. J. Champion, G. B. Hobbs, R. N. Manchester, et al. Measuring the mass of solar system plantes using pulsar timing. *The Astrophysical Journal*, 720(2):L201–L205, 2010. ISSN 2041-8205. doi:10.1088/2041-8205/720/2/L201.

D. J. Champion, M. A. McLaughlin, and D. R. Lorimer. A survey for pulsars in EGRET error boxes. *Monthly Notices of the Royal Astronomical Society*, 364(3):1011–1014, 2005. ISSN 0035-8711. doi:10.1111/j.1365-2966.2005.09660.x.

D. J. Champion, S. M. Ransom, P. Lazarus, et al. An eccentric binary millisecond pulsar in the galactic plane. *Science (New York, N.Y.)*, 320(5881):1309–12, 2008. ISSN 1095-9203. doi:10.1126/science.1157580.

S. Chandrasekhar. The Maximum Mass of Ideal White Dwarfs. *The Astrophysical Journal*, 74:81, 1931. ISSN 0004-637X. doi:10.1086/143324.

K. Chen and M. Ruderman. Pulsar death lines and death valley. *The Astrophysical Journal*, 402:264, 1993. ISSN 0004-637X. doi:10.1086/172129.

W.-C. Chen, X.-w. Liu, R.-x. Xu, and X.-d. Li. Can eccentric binary millisecond pulsars form by accretion-induced collapse of white dwarfs? *Monthly Notices of the Royal Astronomical Society*, 7, 2010. ISSN 00358711. doi:10.1111/j.1365-2966.2010.17512.x.

G. W. Clark. X-ray binaries in globular clusters. *The Astrophysical Journal*, 199:L143, 1975. ISSN 0004-637X. doi:10.1086/181869.

T. R. Clifton and A. G. Lyne. High-radio-frequency survey for young and millisecond pulsars. *Nature*, 320(6057):43–45, 1986. ISSN 0028-0836. doi:10.1038/320043a0.

I. Cognard, L. Guillemot, T. J. Johnson, et al. Discovery of two millisecond pulsars in *Fermi* sources with the Nançay radio telescope. *The Astrophysical Journal*, 732(1):47, 2011. ISSN 0004-637X. doi:10.1088/0004-637X/732/1/47.

J. W. Cooley and J. W. Tukey. An Algorithm for the Machine Calculation of Complex Fourier Series. *Mathematics of Computation*, 19(90):297–301, 1965.

J. Cordes and M. McLaughlin. Searches for fast radio transients. *The Astrophysical Journal*, 596:1142, 2003.

J. M. Cordes. Observational limits on the location of pulsar emission regions. *The Astrophysical Journal*, 222:1006, 1978. ISSN 0004-637X. doi:10.1086/156218.

J. M. Cordes, N. D. R. Bhat, T. H. Hankins, M. A. McLaughlin, and J. Kern. The Brightest Pulses in the Universe: Multifrequency Observations of the Crab Pulsars Giant Pulses. *The Astrophysical Journal*, 612(1):375–388, 2004. ISSN 0004-637X. doi:10.1086/422495.

J. M. Cordes, P. C. C. Freire, D. R. Lorimer, et al. Arecibo Pulsar Survey Using ALFA. I. Survey Strategy and First Discoveries. *The Astrophysical Journal*, 637(1):446–455, 2006. ISSN 0004-637X. doi:10.1086/498335.

J. M. Cordes and T. J. W. Lazio. NE2001.I. A New Model for the Galactic Distribution of Free Electrons and its Fluctuations. *arXiv:astro-ph/0207156v3*, page 21, 2002.

F. Crawford, M. J. Pivovaroff, V. M. Kaspi, and R. N. Manchester. A Sensitive Targeted Search Campaign at Parkes to Find Young Radio Pulsars at 20 cm. 9999:4, 2001.

J. K. Daugherty and A. K. Harding. Compton scattering in strong magnetic fields. *The Astrophysical Journal*, 309:362, 1986. ISSN 0004-637X. doi:10.1086/164608.

J. Davies and M. I. Large. A single-pulse search for pulsars. *Monthly Notices of the Royal Astronomical Society*, 149:301, 1970.

J. G. Davies, M. I. Large, and A. C. Pickwick. Five New Pulsars. *Nature*, 227(5263):1123–1124, 1970. ISSN 0028-0836. doi:10.1038/2271123a0.

J. G. Davies, A. G. Lyne, and J. H. Seiradakis. Pulsar Associated with the Supernova Remnant IC 443. *Nature*, 240(5378):229–230, 1972. ISSN 0028-0836. doi:10.1038/240229a0.

J. G. Davies, A. G. Lyne, and J. H. Seiradakis. Pulsars-Thirteen new ones discovered. *Nature Physical Science*, 244:84, 1973.

J. G. Davies, A. G. Lyne, and J. H. Seiradakis. The galactic distribution of pulsars. *Monthly Notices of the Royal Astronomical Society*, 179:635–650, 1977.

O. C. de Jager and I. Büsching. The H-test probability distribution revisited: improved sensitivity. *Astronomy and Astrophysics*, 517:L9, 2010. ISSN 0004-6361. doi:10.1051/0004-6361/201014362.

A. De Luca. Central Compact Objects in Supernova Remnants. In *AIP Conference Proceedings*, volume 983, pages 311–319. AIP, 2008. ISBN 9780735405028. ISSN 0094243X. doi:10.1063/1.2900173.

A. T. Deller. *Precision VLBI astrometry : Instrumentation, algorithms and pulsar parallax determination.* Ph.D. thesis, Swinburne University, 2009.

P. B. Demorest, R. D. Ferdman, M. E. Gonzalez, et al. Limits on the Stochastic Gravitational Wave Background from the North American Nanohertz Observatory for Gravitational Waves. *arXiv:1201.6641*, 2012.

P. B. Demorest, T. Pennucci, S. M. Ransom, M. S. E. Roberts, and J. W. T. Hessels. A two-solar-mass neutron star measured using Shapiro delay. *Nature*, 467(7319):1081–3, 2010. ISSN 1476-4687. doi:10.1038/nature09466.

J. S. Deneva, J. M. Cordes, and T. J. W. Lazio. DISCOVERY OF THREE PULSARS FROM A GALACTIC CENTER PULSAR POPULATION. *The Astrophysical Journal*, 702(2):L177–L181, 2009a. ISSN 0004-637X. doi:10.1088/0004-637X/702/2/L177.

J. S. Deneva, J. M. Cordes, M. a. McLaughlin, et al. ARECIBO PULSAR SURVEY USING ALFA: PROBING RADIO PULSAR INTERMITTENCY AND TRANSIENTS. *The Astrophysical Journal*, 703(2):2259–2274, 2009b. ISSN 0004-637X. doi:10.1088/0004-637X/703/2/2259.

R. J. Dewey, J. H. Taylor, J. M. Weisberg, and G. H. Stokes. A search for low-luminosity pulsars. *The Astrophysical Journal*, 294:L25, 1985. ISSN 0004-637X. doi:10.1086/184502.

R. C. Duncan and C. Thompson. Formation of very strongly magnetized neutron stars - Implications for gamma-ray bursts. *The Astrophysical Journal*, 392:L9, 1992. ISSN 0004-637X. doi:10.1086/186413.

R. P. Eatough. *A search for relativistic binary pulsars in the Galactic plane.* Ph.D. thesis, The University of Manchester, 2009.

R. P. Eatough, E. F. Keane, and A. G. Lyne. An interference removal technique for radio pulsar searches. *Monthly Notices of the Royal Astronomical Society*, 395(1):410–415, 2009. ISSN 00358711. doi:10.1111/j.1365-2966.2009.14524.x.

R. P. Eatough, N. Molkenthin, M. Kramer, et al. Selection of radio pulsar candidates using artificial neural networks. *Monthly Notices of the Royal Astronomical Society*, 407(4):2443–2450, 2010. ISSN 00358711. doi:10.1111/j.1365-2966.2010.17082.x.

R. Edwards, M. Bailes, W. van Straten, and M. Britton. The Swinburne intermediate-latitude pulsar survey. *Monthly Notices of the Royal Astronomical Society*, 326(1):358–374, 2001a. ISSN 00358711. doi:10.1046/j.1365-8711.2001.04637.x.

R. T. Edwards, W. van Straten, and M. Bailes. A Search for Submillisecond Pulsars. *The Astrophysical Journal*, 560(1):365–370, 2001b. ISSN 0004-637X. doi:10.1086/322772.

C. M. Espinoza, A. G. Lyne, M. Kramer, R. N. Manchester, and V. M. Kaspi. THE BRAKING INDEX OF PSR J17343333 AND THE MAGNETAR POPULATION. *The Astrophysical Journal*, 741(1):L13, 2011a. ISSN 2041-8205. doi:10.1088/2041-8205/741/1/L13.

C. M. Espinoza, A. G. Lyne, B. W. Stappers, and M. Kramer. A study of 315 glitches in the rotation of 102 pulsars. *Monthly Notices of the Royal Astronomical Society*, 414(2):1679–1704, 2011b. ISSN 00358711. doi:10.1111/j.1365-2966.2011.18503.x.

P. Esposito, G. L. Israel, L. Stella, N. Rea, and A. Tiengo. Possible pulsation period in SGR 1833-0832. *The Astronomer's Telegram*, 2494:1, 2010.

P. Esposito, G. L. Israel, R. Turolla, et al. Long-term spectral and timing properties of the soft gamma-ray repeater SGR 18330832 and detection of extended X-ray emission around the radio pulsar PSR B183008. *Monthly Notices of the Royal Astronomical Society*, 12(May):no–no, 2011. ISSN 00358711. doi:10.1111/j.1365-2966.2011.19022.x.

C. Faucher-Giguère and V. M. Kaspi. Birth and Evolution of Isolated Radio Pulsars. *The Astrophysical Journal*, 643(1):332–355, 2006. ISSN 0004-637X. doi:10.1086/501516.

A. J. Faulkner, M. Kramer, A. G. Lyne, et al. PSR J1756-2251: A New Relativistic Double Neutron Star System. *The Astrophysical Journal*, 618(2):L119–L122, 2005. ISSN 0004-637X. doi:10.1086/427776.

a. J. Faulkner, I. H. Stairs, M. Kramer, et al. The Parkes Multibeam Pulsar Survey - V. Finding binary and millisecond pulsars. *Monthly Notices of the Royal Astronomical Society*, 355(1):147–158, 2004. ISSN 00358711. doi:10.1111/j.1365-2966.2004.08310.x.

R. D. Ferdman, R. van Haasteren, C. G. Bassa, et al. The European Pulsar Timing Array: current efforts and a LEAP toward the future. *Classical and Quantum Gravity*, 27(8):084014, 2010. ISSN 0264-9381. doi:10.1088/0264-9381/27/8/084014.

R. S. Foster and D. C. Backer. Constructing a pulsar timing array. *The Astrophysical Journal*, 361:300, 1990. ISSN 0004-637X. doi:10.1086/169195.

R. S. Foster, B. J. Cadwell, A. Wolszczan, and S. B. Anderson. A High Galactic Latitude Pulsar Survey of the Arecibo Sky. *The Astrophysical Journal*, 454:826, 1995. ISSN 0004-637X. doi:10.1086/176535.

W. L. Freedman, S. M. Hughes, B. F. Madore, et al. The Hubble Space Telescope Extragalactic Distance Scale Key Project. 1: The discovery of Cepheids and a new distance to M81. *The Astrophysical Journal*, 427:628, 1994. ISSN 0004-637X. doi: 10.1086/174172.

P. C. C. Freire, C. G. Bassa, N. Wex, et al. On the nature and evolution of the unique binary pulsar J1903+0327. *Monthly Notices of the Royal Astronomical Society*, 412(4):2763–2780, 2011. ISSN 00358711. doi:10.1111/j.1365-2966.2010.18109.x.

P. C. C. Freire, S. M. Ransom, S. Bégin, et al. Eight New Millisecond Pulsars in NGC 6440 and NGC 6441. *The Astrophysical Journal*, 675(1):670–682, 2008. ISSN 0004-637X. doi:10.1086/526338.

P. C. C. Freire, N. Wex, G. Esposito-Farèse, et al. The relativistic pulsar-white dwarf binary PSR J1738+0333 - II. The most stringent test of scalar-tensor gravity. *Monthly Notices of the Royal Astronomical Society*, 423(4):3328–3343, 2012. ISSN 00358711. doi:10.1111/j.1365-2966.2012.21253.x.

P. A. Fridman and W. A. Baan. Astrophysics RF I mitigation methods in radio astronomy. 344:327–344, 2001. doi:10.1051/0004-6361.

A. S. Fruchter, D. R. Stinebring, and J. H. Taylor. A millisecond pulsar in an eclipsing binary. *Nature*, 333(6170):237–239, 1988. ISSN 0028-0836. doi:10.1038/333237a0.

F. P. Gavriil, V. M. Kaspi, and P. M. Woods. A Comprehensive Study of the XRay Bursts from the Magnetar Candidate 1E 2259+586. *The Astrophysical Journal*, 607(2):959–969, 2004. ISSN 0004-637X. doi:10.1086/383564.

N. Gehrels, G. Chincarini, P. Giommi, et al. The Swift GammaRay Burst Mission. *The Astrophysical Journal*, 611(2):1005–1020, 2004. ISSN 0004-637X. doi:10.1086/422091.

J. M. Gelbord, S. D. Barthelmy, W. H. Baumgartner, et al. GRB 100319A: Swift detection of a burst; possible Sgr. *The Astronomer's Telegram*, 10526:1, 2010.

T. Gold. Rotating Neutron Stars as the Origin of the Pulsating Radio Sources. *Nature*, 218(5143):731–732, 1968. ISSN 0028-0836. doi:10.1038/218731a0.

P. Goldreich and W. H. Julian. Pulsar Electrodynamics. *The Astrophysical Journal*, 157:869, 1969. ISSN 0004-637X. doi:10.1086/150119.

S. V. Golenetskii, V. N. Ilyinskii, and E. P. Mazets. Recurrent bursts in GBS052666, the source of the 5 March 1979 γ-ray burst. *Nature*, 307(5946):41–43, 1984. ISSN 0028-0836. doi:10.1038/307041a0.

E. V. Gotthelf and J. P. Halpern. The anatomy of a magnetar: XMM monitoring of the transient anomalous X-ray pulsar XTE J1810197. *Astrophysics and Space Science*, 308(1-4):79–87, 2007. ISSN 0004-640X. doi:10.1007/s10509-007-9327-9.

E. Göğüş, G. Cusumano, a. J. Levan, et al. DISCOVERY OF A NEW SOFT GAMMA REPEATER, SGR J18330832. *The Astrophysical Journal*, 718(1):331–339, 2010a. ISSN 0004-637X. doi:10.1088/0004-637X/718/1/331.

E. Göğüş, T. Strohmayer, C. Kouveliotou, and P. Woods. Discovery of the Spin Period of SGR 1833-0832. *The Astronomer's Telegram*, 2493:1, 2010b.

F. Graham-Smith. The radio emission from pulsars. *Reports on Progress in Physics*, 66(2):173–238, 2003. ISSN 0034-4885. doi:10.1088/0034-4885/66/2/203.

J. E. Grindlay. Detection of Pulsed Gamma Rays of $\sim 10^{12}$ EV from the Pulsar in the Crab Nebula. *The Astrophysical Journal*, 174:L9, 1972. ISSN 0004-637X. doi:10.1086/180939.

E. J. Groth. Probability distributions related to power spectra. *The Astrophysical Journal Supplement Series*, 29:285, 1975. ISSN 0067-0049. doi:10.1086/190343.

L. Guillemot, P. C. C. Freire, I. Cognard, et al. Discovery of the millisecond pulsar PSR J2043+1711 in a Fermi source with the Nançay Radio Telescope. *Monthly Notices of the Royal Astronomical Society*, 422(2):1294–1305, 2012a. ISSN 00358711. doi:10.1111/j.1365-2966.2012.20694.x.

L. Guillemot, T. J. Johnson, C. Venter, et al. Pulsed gamma rays from the original millisecond and black widow pulsars: A case for caustic radio emission? *The Astrophysical Journal*, 744(1):33, 2012b. ISSN 0004-637X. doi:10.1088/0004-637X/744/1/33.

F. Haberl. The magnificent seven: magnetic fields and surface temperature distributions. *Astrophysics and Space Science*, 308(1-4):181–190, 2007. ISSN 0004-640X. doi:10.1007/s10509-007-9342-x.

J. P. Halpern. Is Calvera a gamma-ray pulsar? *The Astrophysical Journal*, 736(1):L3, 2011. ISSN 2041-8205. doi:10.1088/2041-8205/736/1/L3.

J. P. Halpern, E. V. Gotthelf, R. H. Becker, D. J. Helfand, and R. L. White. Discovery of Radio Emission from the Transient Anomalous X-Ray Pulsar XTE J1810-197. *The Astrophysical Journal*, 632(1):L29–L32, 2005. ISSN 0004-637X. doi:10.1086/497537.

T. H. Hankins and J. a. Eilek. Radio Emission Signatures in the Crab Pulsar. *The Astrophysical Journal*, 670(1):693–701, 2007. ISSN 0004-637X. doi:10.1086/522362.

T. H. Hankins and B. J. Rickett. Pulsar signal processing. In *Methods in Computational Physics. Volume 14 - Radio astronomy*, pages 55–129. 1975.

A. K. Harding and D. Lai. Physics of strongly magnetized neutron stars. *Reports on Progress in Physics*, 69(9):2631–2708, 2006. ISSN 0034-4885. doi:10.1088/0034-4885/69/9/R03.

S. S. Hasan, R. T. Gangadhara, and V. Krishan. *Turbulence, Dynamos, Accretion Disks, Pulsars and Collective Plasma Processes*. 2008.

C. G. T. Haslam, C. J. Salter, H. Stoffel, and W. E. Wilson. A 408 MHz all-sky continuum survey. II The atlas of contour maps. *Astronomy and Astrophysics Supplement Series*, 47:1, 2, 4–51, 53–142, 1982.

J. W. T. Hessels, S. M. Ransom, V. M. Kaspi, et al. The GBT350 Survey of the Northern Galactic Plane for Radio Pulsars and Transients. In *AIP Conference Proceedings*, volume 983, pages 613–615. AIP, 2008. ISSN 0094243X. doi:10.1063/1.2900310.

J. W. T. Hessels, S. M. Ransom, I. H. Stairs, P. C. C. Freire, V. M. Kaspi, and F. Camilo. A radio pulsar spinning at 716 Hz. *Science (New York, N.Y.)*, 311(5769):1901–4, 2006. ISSN 1095-9203. doi:10.1126/science.1123430.

J. W. T. Hessels, B. W. Stappers, R. E. Rutledge, D. B. Fox, and A. H. Shevchuk. A strong upper limit on the pulsed radio luminosity of the compact object 1RXS J141256.0+792204. *Astronomy and Astrophysics*, 476(1):331–333, 2007. ISSN 0004-6361. doi:10.1051/0004-6361:20078330.

A. Hewish, S. J. Bell, J. D. H. Pilkington, P. F. Scott, and R. A. Collins. Observation of a Rapidly Pulsating Radio Source. *Nature*, 217(5130):709–713, 1968a. ISSN 0028-0836. doi:10.1038/217709a0.

A. Hewish, S. J. Bell, J. D. H. Pilkington, P. F. Scott, and R. A. Collins. Observation of a Rapidly Pulsating Radio Source. *Nature*, 217(5130):709–713, 1968b. ISSN 0028-0836. doi:10.1038/217709a0.

J. S. Heyl and L. Hernquist. A QED Model for the Origin of Bursts from Soft Gamma Repeaters and Anomalous XRay Pulsars. *The Astrophysical Journal*, 618(1):463–473, 2005. ISSN 0004-637X. doi:10.1086/425974.

A. S. Hill, D. R. Stinebring, H. A. Barnor, D. E. Berwick, and A. B. Webber. Pulsar Scintillation Arcs. I. Frequency Dependence. *The Astrophysical Journal*, 599(1):457–464, 2003. ISSN 0004-637X. doi:10.1086/379191.

G. Hobbs, a. Archibald, Z. Arzoumanian, et al. The International Pulsar Timing Array project: using pulsars as a gravitational wave detector. *Classical and Quantum Gravity*, 27(8):084013, 2010a. ISSN 0264-9381. doi:10.1088/0264-9381/27/8/084013.

G. Hobbs, W. Coles, R. N. Manchester, et al. Development of a pulsar-based timescale. *arXiv:1208.3560*, 2012.

G. Hobbs, a. Faulkner, I. H. Stairs, et al. The Parkes multibeam pulsar survey - IV. Discovery of 180 pulsars and parameters for 281 previously known pulsars. *Monthly Notices of the Royal Astronomical Society*, 352(4):1439–1472, 2004. ISSN 00358711. doi:10.1111/j.1365-2966.2004.08042.x.

G. Hobbs, D. R. Lorimer, a. G. Lyne, and M. Kramer. A statistical study of 233 pulsar proper motions. *Monthly Notices of the Royal Astronomical Society*, 360(3):974–992, 2005. ISSN 00358711. doi:10.1111/j.1365-2966.2005.09087.x.

G. Hobbs, A. G. Lyne, and M. Kramer. An analysis of the timing irregularities for 366 pulsars. *Monthly Notices of the Royal Astronomical Society*, 402(2):1027–1048, 2010b. ISSN 00358711. doi:10.1111/j.1365-2966.2009.15938.x.

G. B. Hobbs, R. T. Edwards, and R. N. Manchester. TEMPO2, a new pulsar-timing package - I. An overview. *Monthly Notices of the Royal Astronomical Society*, 369(2):655–672, 2006. ISSN 00358711. doi:10.1111/j.1365-2966.2006.10302.x.

C. J. Horowitz. Gravitational waves from low mass neutron stars. *Physical Review D*, 81(10), 2010. ISSN 1550-7998. doi:10.1103/PhysRevD.81.103001.

A. W. Hotan, W. van Straten, and R. N. Manchester. PSRCHIVE and PSRFITS : An Open Approach to Radio Pulsar Data Storage and Analysis. *Publications Astronomical Society of Australia*, 21:302–309, 2004. doi:10.1071/AS04022.

J. D. Huba. *NRL PLASMA FORMULARY*. 2011.

R. A. Hulse and J. H. Taylor. A High-Sensitivity Pulsar Survey. *The Astrophysical Journal*, 191:L59, 1974. ISSN 0004-637X. doi:10.1086/181548.

R. A. Hulse and J. H. Taylor. A deep sample of new pulsars and their spatial extent in the galaxy. *The Astrophysical Journal*, 201:L55, 1975a. ISSN 0004-637X. doi: 10.1086/181941.

R. A. Hulse and J. H. Taylor. Discovery of a pulsar in a binary system. *The Astrophysical Journal*, 195:L51, 1975b. ISSN 0004-637X. doi:10.1086/181708.

A. I. Ibrahim, C. B. Markwardt, J. H. Swank, et al. Discovery of a Transient Magnetar: XTE J1810-197. *The Astrophysical Journal*, 609(1):L21–L24, 2004. ISSN 0004-637X. doi:10.1086/422636.

G. L. Israel and L. Stella. A New Technique for the Detection of Periodic Signals in "Colored" Power Spectra. *The Astrophysical Journal*, 468:369, 1996. ISSN 0004-637X. doi:10.1086/177697.

N. Ivanova, K. Belczynski, J. M. Fregeau, and F. A. Rasio. The evolution of binary fractions in globular clusters. *Monthly Notices of the Royal Astronomical Society*, 358(2):572–584, 2005. ISSN 00358711. doi:10.1111/j.1365-2966.2005.08804.x.

N. Ivanova, C. O. Heinke, F. A. Rasio, K. Belczynski, and J. M. Fregeau. Formation and evolution of compact binaries in globular clusters â II. Binaries with neutron stars. *Monthly Notices of the Royal Astronomical Society*, 386(1):553–576, 2008. ISSN 00358711. doi:10.1111/j.1365-2966.2008.13064.x.

J. D. Jackson. *Classical Electrodynamics*. New York: Wiley, 1962. ISBN 047130932X.

B. A. Jacoby, M. Bailes, S. M. Ord, R. T. Edwards, and S. R. Kulkarni. A large-area survey for radio pulsars at high Galactic latitudes. *The Astrophysical Journal*, 699(2):2009–2016, 2009. ISSN 0004-637X. doi:10.1088/0004-637X/699/2/2009.

A. H. Jaffe and D. C. Backer. Gravitational Waves Probe the Coalescence Rate of Massive Black Hole Binaries. *The Astrophysical Journal*, 583(2):616–631, 2003. ISSN 0004-637X. doi:10.1086/345443.

F. A. Jenet, G. B. Hobbs, K. J. Lee, and R. N. Manchester. Detecting the Stochastic Gravitational Wave Background Using Pulsar Timing. *The Astrophysical Journal*, 625(2):L123–L126, 2005. ISSN 0004-637X. doi:10.1086/431220.

S. G. Johnson and M. Frigo. A modified split-radix FFT with fewer arithmetic operations. *Signal Processing, IEEE Transactions on*, 55(1):111–119, 2007.

S. Johnston and M. Bailes. New limits on the population of millisecond pulsars in the galactic plane. *Monthly Notices of the Royal Astronomical Society*, 252:177–281, 1991.

S. Johnston, M. Kramer, D. R. Lorimer, et al. Discovery of two pulsars towards the Galactic Centre. *Monthly Notices of the Royal Astronomical Society: Letters*, 373(1):L6–L10, 2006. ISSN 1745-3925. doi:10.1111/j.1745-3933.2006.00232.x.

S. Johnston, D. R. Lorimer, P. A. Harrison, et al. Discovery of a very bright, nearby binary millisecond pulsar. *Nature*, 361(6413):613–615, 1993. ISSN 0028-0836. doi: 10.1038/361613a0.

S. Johnston, A. G. Lyne, R. N. Manchester, et al. A high-frequency survey of the southern Galactic plane for pulsars. *Monthly Notices of the Royal Astronomical Society*, 255:401–411, 1992.

D. I. Jones. Pulsar state switching, timing noise and free precession. *Monthly Notices of the Royal Astronomical Society*, 420(3):2325–2338, 2012. ISSN 00358711. doi: 10.1111/j.1365-2966.2011.20238.x.

V. Kalogera, C. Kim, D. R. Lorimer, et al. The Cosmic Coalescence Rates for Double Neutron Star Binaries. *The Astrophysical Journal*, 601(2):L179–L182, 2004. ISSN 0004-637X. doi:10.1086/382155.

G. Kanbach, D. Bertsch, A. Favale, et al. The project EGRET (energetic gamma-ray experiment telescope) on NASA's Gamma-Ray Observatory GRO. *Space Science Reviews*, 49(1):69–84, 1989.

D. L. Kaplan, K. Stovall, S. M. Ransom, et al. Discovery of the Optical/Ultraviolet/Gamma-ray Counterpart to the Eclipsing Millisecond Pulsar J1816+4510. *arXiv:1205.3699*, page 10, 2012.

R. Karuppusamy, B. W. Stappers, and W. van Straten. Giant pulses from the Crab pulsar. *Astronomy and Astrophysics*, 515(13279):A36, 2010. ISSN 0004-6361. doi: 10.1051/0004-6361/200913729.

E. F. Keane. *The Transient Radio Sky*. Springer Berlin Heidelberg, 1 edition, 2012. doi:10.1007/978-3-642-19627-0_5.

E. F. Keane, M. Kramer, A. G. Lyne, B. W. Stappers, and M. A. McLaughlin. Rotating Radio Transients: new discoveries, timing solutions and musings. *Monthly Notices of the Royal Astronomical Society*, 415(4):3065–3080, 2011. ISSN 00358711. doi: 10.1111/j.1365-2966.2011.18917.x.

E. F. Keane, D. A. Ludovici, R. P. Eatough, et al. Further searches for Rotating Radio Transients in the Parkes Multi-beam Pulsar Survey. *Monthly Notices of the Royal Astronomical Society*, 401(2):1057–1068, 2010. ISSN 00358711. doi:10.1111/j.1365-2966.2009.15693.x.

E. F. Keane and M. A. Mclaughlin. Rotating radio transients. *Bulletin of the Astronomical Society of India*, 39:333–352, 2011.

E. F. Keane, B. W. Stappers, M. Kramer, and A. G. Lyne. On the origin of a highly dispersed coherent radio burst. *Monthly Notices of the Royal Astronomical Society: Letters*, 425(1):L71–L75, 2012. ISSN 17453925. doi:10.1111/j.1745-3933.2012.01306.x.

M. J. Keith, A. Jameson, W. Van Straten, et al. The High Time Resolution Universe Pulsar Survey - I. System configuration and initial discoveries. *Monthly Notices of the Royal Astronomical Society*, 409(2):619–627, 2010. ISSN 00358711. doi:10.1111/j.1365-2966.2010.17325.x.

M. J. Keith, S. Johnston, M. Bailes, et al. The High Time Resolution Universe Pulsar Survey - IV. Discovery and polarimetry of millisecond pulsars. *Monthly Notices of the Royal Astronomical Society*, 419(2):1752–1765, 2012. ISSN 00358711. doi:10.1111/j.1365-2966.2011.19842.x.

M. J. Keith, S. Johnston, M. Kramer, P. Weltevrede, K. P. Watters, and B. W. Stappers. A high-frequency search for radio pulsars in three EGRET error boxes. *Monthly Notices of the Royal Astronomical Society*, 389(4):1881–1884, 2008. ISSN 00358711. doi:10.1111/j.1365-2966.2008.13711.x.

M. J. Keith, S. Johnston, P. S. Ray, et al. Discovery of millisecond pulsars in radio searches of southern Fermi Large Area Telescope sources. *Monthly Notices of the Royal Astronomical Society*, 414(2):1292–1300, 2011. ISSN 00358711. doi:10.1111/j.1365-2966.2011.18464.x.

M. J. Keith, M. Kramer, A. G. Lyne, et al. PSR J17532240: a mildly recycled pulsar in an eccentric binary system. *Monthly Notices of the Royal Astronomical Society*, 393(2):623–627, 2009. ISSN 00358711. doi:10.1111/j.1365-2966.2008.14234.x.

M. Kerr. Improving sensitivity to weak pulsations with photon probability weighting. *The Astrophysical Journal*, 732(1):38, 2011. ISSN 0004-637X. doi:10.1088/0004-637X/732/1/38.

M. Kerr, F. Camilo, T. J. Johnson, et al. Five new millisecond pulsars from a radio survey of 14 unidentified *Fermi*-LAT gamma-ray sources. *The Astrophysical Journal*, 748(1):L2, 2012. ISSN 2041-8205. doi:10.1088/2041-8205/748/1/L2.

B. Klein. *Die Suche nach hochdispergierten Radio-Pulsaren in Richtung des Galaktischen Zentrums*. Ph.D. thesis, Rheinische Friedrich-Wilhelms-Universität Bonn, 2004.

B. Klein, S. Hochgürtel, I. Krämer, A. Bell, K. Meyer, and R. Güsten. High-resolution wide-band fast Fourier transform spectrometers. *Astronomy and Astrophysics*, 542:L3, 2012. ISSN 0004-6361. doi:10.1051/0004-6361/201218864.

J. Kocz, M. Bailes, D. Barnes, S. Burke-Spolaor, and L. Levin. Enhanced pulsar and single pulse detection via automated radio frequency interference detection in multi-pixel feeds. *Monthly Notices of the Royal Astronomical Society*, 420(1):271–278, 2012. ISSN 00358711. doi:10.1111/j.1365-2966.2011.20029.x.

R. Kothes, K. Fedotov, T. J. Foster, and B. Uyanker. A catalogue of Galactic supernova remnants from the Canadian Galactic plane survey. *Astronomy and Astrophysics*, 457(3):1081–1093, 2006. ISSN 0004-6361. doi:10.1051/0004-6361:20065062.

M. L. A. Kouwenhoven and J. L. L. Voûte. The effect of digitisation on the signal-to-noise ratio of a pulsed radio signal. *Astronomy and Astrophysics*, 378(2):700–709, 2001. ISSN 0004-6361. doi:10.1051/0004-6361:20011226.

M. Kramer, D. Backer, J. Cordes, T. Lazio, B. Stappers, and S. Johnston. Strong-field tests of gravity using pulsars and black holes. *New Astronomy Reviews*, 48(11-12):993–1002, 2004. ISSN 13876473. doi:10.1016/j.newar.2004.09.020.

M. Kramer, J. F. Bell, R. N. Manchester, et al. The Parkes Multibeam Pulsar Survey - III. Young pulsars and the discovery and timing of 200 pulsars. *Monthly Notices of the Royal Astronomical Society*, 342(4):1299–1324, 2003. ISSN 0035-8711. doi: 10.1046/j.1365-8711.2003.06637.x.

M. Kramer, a. G. Lyne, J. T. O'Brien, C. a. Jordan, and D. R. Lorimer. A periodically active pulsar giving insight into magnetospheric physics. *Science (New York, N.Y.)*, 312(5773):549–51, 2006a. ISSN 1095-9203. doi:10.1126/science.1124060.

M. Kramer, I. H. Stairs, R. N. Manchester, et al. Tests of general relativity from timing the double pulsar. *Science (New York, N.Y.)*, 314(5796):97–102, 2006b. ISSN 1095-9203. doi:10.1126/science.1132305.

M. Kramer, K. M. Xilouris, D. R. Lorimer, et al. The Characteristics of Millisecond Pulsar Emission. I. Spectra, Pulse Shapes, and the Beaming Fraction. *The Astrophysical Journal*, 501(1):270–285, 1998. ISSN 0004-637X. doi:10.1086/305790.

S. R. Kulkarni, S. N. Vogel, Z. Wang, and D. O. S. Wood. Identification of the nebula G70.7 + 1.2 as a bow shock powered by a pulsar/Be-star binary. *Nature*, 360(6400):139–141, 1992. ISSN 0028-0836. doi:10.1038/360139a0.

C. Lange, F. Camilo, N. Wex, et al. Precision timing measurements of PSR J1012+5307. *Monthly Notices of the Royal Astronomical Society*, 326(1):274–282, 2001. ISSN 00358711. doi:10.1046/j.1365-8711.2001.04606.x.

M. I. Large, A. E. Vaughan, and B. Y. Mills. A Pulsar Supernova Association? *Nature*, 220(5165):340–341, 1968a. ISSN 0028-0836. doi:10.1038/220340a0.

M. I. Large, A. E. Vaughan, and R. Wielebinski. Pulsar Search at the Molonglo Radio Observatory. *Nature*, 220(5169):753–756, 1968b. ISSN 0028-0836. doi: 10.1038/220753a0.

J. G. Laros, E. E. Fenimore, M. M. Fikani, et al. The soft γ-ray burst GB790107. *Nature*, 322(6075):152–153, 1986. ISSN 0028-0836. doi:10.1038/322152a0.

D. A. Leahy, W. Darbro, R. F. Elsner, et al. On searches for pulsed emission with application to four globular cluster X-ray sources - NGC 1851, 6441, 6624, and 6712. *The Astrophysical Journal*, 266:160, 1983. ISSN 0004-637X. doi:10.1086/160766.

K. J. Lee, L. Guillemot, Y. L. Yue, M. Kramer, and D. J. Champion. Application of the Gaussian mixture model in pulsar astronomy - pulsar classification and candidates ranking for the Fermi 2FGL catalogue. *Monthly Notices of the Royal Astronomical Society*, 424(4):2832–2840, 2012. ISSN 00358711. doi:10.1111/j.1365-2966.2012.21413.x.

P. Léna, D. Rouan, F. Lebrun, F. Mignard, and D. Pelat. *Observational Astrophysics*. Astronomy and Astrophysics Library. Springer Berlin Heidelberg, Berlin, Heidelberg, 2012. ISBN 978-3-642-21814-9. doi:10.1007/978-3-642-21815-6.

L. Levin, M. Bailes, S. Bates, et al. A radio-loud magnetar in X-ray quiescence. *The Astrophysical Journal*, 721(1):L33–L37, 2010. ISSN 2041-8205. doi:10.1088/2041-8205/721/1/L33.

J. R. Lin and S. N. Zhang. Radio Pulsars as Progenitors of Anomalous X-Ray Pulsars and Soft Gamma-Ray Repeaters: Magnetic Field Evolution through Pulsar Glitches. *The Astrophysical Journal*, 615(2):L133–L136, 2004. ISSN 0004-637X. doi:10.1086/426316.

K. Liu, E. F. Keane, K. J. Lee, M. Kramer, J. M. Cordes, and M. B. Purver. Profile-shape stability and phase-jitter analyses of millisecond pulsars. *Monthly Notices of the Royal Astronomical Society*, 420(1):361–368, 2012. ISSN 00358711. doi:10.1111/j.1365-2966.2011.20041.x.

D. Lorimer. Pulsar Searches at Effelsberg - Past, Present and Future. In *Pulsar Astronomy - 2000 and Beyond*. 2000.

D. Lorimer and M. Kramer. *Handbook of Pulsar Astronomy*, volume 300. Cambridge University Press, 1 edition, 2005. ISBN 0521828236.

D. Lorimer, M. Kramer, P. Müller, et al. A 1400-MHz pilot search for young pulsars. *Arxiv:astro-ph/9910569*, 176:169–176, 1999.

D. R. Lorimer. Binary and Millisecond Pulsars. 8, 2008.

D. R. Lorimer, M. Bailes, M. A. McLaughlin, D. J. Narkevic, and F. Crawford. A bright millisecond radio burst of extragalactic origin. *Science (New York, N.Y.)*, 318(5851):777–80, 2007. ISSN 1095-9203. doi:10.1126/science.1147532.

D. R. Lorimer, F. Camilo, P. Freire, et al. Millisecond Radio Pulsars in 47 Tucanae. In *Radio Pulsars, ASP Conference Series*, page 363. 2003.

D. R. Lorimer, a. J. Faulkner, a. G. Lyne, et al. The Parkes Multibeam Pulsar Survey - VI. Discovery and timing of 142 pulsars and a Galactic population analysis. *Monthly Notices of the Royal Astronomical Society*, 372(2):777–800, 2006. ISSN 00358711. doi:10.1111/j.1365-2966.2006.10887.x.

A. G. Lyne, C. Bassa, Z. Wang, A. Cumming, and V. M. Kaspi. Parkes 20-cm Multibeam Pulsar Surveys. *AIP Conference Proceedings*, 983(1):561–566, 2008. ISSN 0094243X. doi:10.1063/1.2900299.

A. G. Lyne, A. Brinklow, J. Middleditch, S. R. Kulkarni, D. C. Backer, and T. R. Clifton. The discovery of a millisecond pulsar in the globular cluster M28. *Nature*, 328(6129):399–401, 1987. ISSN 0028-0836. doi:10.1038/328399a0.

A. G. Lyne, M. Burgay, M. Kramer, et al. A double-pulsar system: a rare laboratory for relativistic gravity and plasma physics. *Science (New York, N.Y.)*, 303(5661):1153–7, 2004. ISSN 1095-9203. doi:10.1126/science.1094645.

A. G. Lyne, F. Camilo, R. N. Manchester, et al. The Parkes Multibeam Pulsar Survey: PSR J1811-1736, a pulsar in a highly eccentric binary system. *Monthly Notices of the Royal Astronomical Society*, 312(4):698–702, 2000a. ISSN 0035-8711. doi:10.1046/j.1365-8711.2000.03231.x.

A. G. Lyne, R. N. Manchester, N. D'Amico, et al. An eclipsing millisecond pulsar in the globular cluster Terzan 5. *Nature*, 347(6294):650–652, 1990. ISSN 0028-0836. doi:10.1038/347650a0.

A. G. Lyne, R. N. Manchester, D. R. Lorimer, et al. The Parkes Southern Pulsar Survey - II. Final results and population analysis. *Monthly Notices of the Royal Astronomical Society*, 295(4):743–755, 1998. ISSN 0035-8711. doi:10.1046/j.1365-8711.1998.01144.x.

A. G. Lyne, S. H. Mankelow, J. F. Bell, and R. N. Manchester. Radio pulsars in Terzan 5. *Monthly Notices of the Royal Astronomical Society*, 316(3):491–493, 2000b. ISSN 00358711. doi:10.1046/j.1365-8711.2000.03517.x.

A. G. Lyne, M. A. McLaughlin, E. F. Keane, et al. Unusual glitch activity in the RRAT J1819-1458: an exhausted magnetar? *Monthly Notices of the Royal Astronomical*

Society, 400(3):1439–1444, 2009. ISSN 00358711. doi:10.1111/j.1365-2966.2009.15668.x.

R. G. Lyons. *Understanding Digital Signal Processing*. Pearson Education, 3rd edition, 2010.

M. Maggiore. Gravitational wave experiments and early universe cosmology. *Physics Reports*, 331(6):283–367, 2000. ISSN 03701573. doi:10.1016/S0370-1573(99)00102-7.

W. A. Majid, C. J. Naudet, S. T. Lowe, and T. B. H. Kuiper. STATISTICAL STUDIES OF GIANT PULSE EMISSION FROM THE CRAB PULSAR. *The Astrophysical Journal*, 741(1):53, 2011. ISSN 0004-637X. doi:10.1088/0004-637X/741/1/53.

R. Manchester, A. Lyne, F. Camilo, et al. The Parkes multi-beam pulsar survey - I. Observing and data analysis systems, discovery and timing of 100 pulsars. *Monthly Notices of the Royal Astronomical Society*, 328(1):17–35, 2001. ISSN 00358711. doi:10.1046/j.1365-8711.2001.04751.x.

R. N. Manchester and G. Hobbs. A GIANT GLITCH IN PSR J17183718. *The Astrophysical Journal*, 736(2):L31, 2011. ISSN 2041-8205. doi:10.1088/2041-8205/736/2/L31.

R. N. Manchester, G. B. Hobbs, A. Teoh, and M. Hobbs. The ATNF Pulsar Catalogue. *Astron.J*, 129, 2005. doi:10.1086/428488.

R. N. Manchester, A. G. Lyne, N. D'Amico, S. Johnston, J. Lim, and D. A. Kniffen. A 5.75-millisecond pulsar in the globular cluster 47 Tucanae. *Nature*, 345(6276):598–600, 1990. ISSN 0028-0836. doi:10.1038/345598a0.

R. N. Manchester, A. G. Lyne, N. D'Amico, et al. The Parkes Southern Pulsar Survey. I. Observing and data analysis systems and initial results. *Monthly Notices of the Royal Astronomical Society*, 279:1235–1250, 1996.

R. N. Manchester, A. G. Lyne, S. Johnston, et al. Pulsar in Direction of NGC 6440. *Central Bureau Electronic Telegrams*, 4905:2, 1989.

R. N. Manchester, A. G. Lyne, C. Robinson, N. D'Amico, M. Bailes, and J. Lim. Discovery of ten millisecond pulsars in the globular cluster 47 Tucanae. *Nature*, 352(6332):219–221, 1991. ISSN 0028-0836. doi:10.1038/352219a0.

R. N. Manchester, A. G. Lyne, J. H. Taylor, J. M. Durdin, M. I. Large, and A. G. Little. The second Molonglo pulsar survey – discovery of 155 pulsars. *Monthly Notices of the Royal Astronomical Society*, 185:409–421, 1978.

O. Maron, J. Kijak, M. Kramer, and R. Wielebinski. Pulsar spectra of radio emission. *Astronomy and Astrophysics Supplement Series*, 147(2):195–203, 2000. ISSN 0365-0138. doi:10.1051/aas:2000298.

F. E. Marshall, E. V. Gotthelf, J. Middleditch, Q. D. Wang, and W. Zhang. The Big Glitcher: The Rotation History of PSR J05376910. *The Astrophysical Journal*, 603(2):682–689, 2004. ISSN 0004-637X. doi:10.1086/381567.

F. Mavromatakis, P. Boumis, J. Meaburn, and A. Caulet. A new candidate supernova remnant G 70.5+1.9. *Astronomy and Astrophysics*, 503(1):129–136, 2009. ISSN 0004-6361. doi:10.1051/0004-6361/200912211.

M. a. McLaughlin, a. G. Lyne, D. R. Lorimer, et al. Transient radio bursts from rotating neutron stars. *Nature*, 439(7078):817–20, 2006. ISSN 1476-4687. doi:10.1038/nature04440.

S. Mereghetti. The strongest cosmic magnets: soft gamma-ray repeaters and anomalous X-ray pulsars. *The Astronomy and Astrophysics Review*, 15(4):225–287, 2008. ISSN 0935-4956. doi:10.1007/s00159-008-0011-z.

D. J. Morris, G. Hobbs, A. G. Lyne, et al. The Parkes Multibeam Pulsar Survey - II. Discovery and timing of 120 pulsars. *Monthly Notices of the Royal Astronomical Society*, 335(2):275–290, 2002. ISSN 0035-8711. doi:10.1046/j.1365-8711.2002.05551.x.

R. NAN, D. LI, C. JIN, et al. THE FIVE-HUNDRED-METER APERTURE SPHERICAL RADIO TELESCOPE (FAST) PROJECT. *International Journal of Modern Physics D*, 20(06):989–1024, 2011. ISSN 0218-2718. doi:10.3109/09553002.2012.720410.

R. Narayan, T. Piran, and A. Shemi. Neutron star and black hole binaries in the Galaxy. *The Astrophysical Journal*, 379:L17, 1991. ISSN 0004-637X. doi:10.1086/186143.

D. J. Nice, A. S. Fruchter, and J. H. Taylor. A Search for Fast Pulsars along the Galactic Plane. *The Astrophysical Journal*, 449:156, 1995. ISSN 0004-637X. doi:10.1086/176041.

P. L. Nolan, a. a. Abdo, M. Ackermann, et al. *Fermi* Large Area Telescope Second Source Catalog. *The Astrophysical Journal Supplement Series*, 199(2):31, 2012. ISSN 0067-0049. doi:10.1088/0067-0049/199/2/31.

A. Noutsos, S. Johnston, M. Kramer, and A. Karastergiou. New pulsar rotation measures and the Galactic magnetic field. *Monthly Notices of the Royal Astronomical Society*, 386(4):1881–1896, 2008. ISSN 0035-8711. doi:10.1111/j.1365-2966.2008.13188.x.

J. R. Oppenheimer and G. M. Volkoff. On Massive Neutron Cores. *Physical Review*, 55(4):374–381, 1939. ISSN 0031-899X. doi:10.1103/PhysRev.55.374.

F. Pacini. Energy Emission from a Neutron Star. *Nature*, 216(5115):567–568, 1967. ISSN 0028-0836. doi:10.1038/216567a0.

W. D. Pence, L. Chiappetti, C. G. Page, R. A. Shaw, and E. Stobie. Definition of the Flexible Image Transport System (FITS), version 3.0. *Astronomy and Astrophysics*, 524:A42, 2010. ISSN 0004-6361. doi:10.1051/0004-6361/201015362.

B. B. P. Perera, M. a. McLaughlin, M. Kramer, et al. The evolution of PSR J07373039B and a model for relativistic spin precession. *The Astrophysical Journal*, 721(2):1193–1205, 2010. ISSN 0004-637X. doi:10.1088/0004-637X/721/2/1193.

E. Pfahl and A. Loeb. Probing the Spacetime around Sagittarius A* with Radio Pulsars. *The Astrophysical Journal*, 615(1):253–258, 2004. ISSN 0004-637X. doi:10.1086/423975.

E. Pfahl, P. Podsiadlowski, and S. Rappaport. Relativistic Binary Pulsars with Black Hole Companions. *The Astrophysical Journal*, 628(1):343–352, 2005. ISSN 0004-637X. doi:10.1086/430515.

M. J. Pivovaroff, V. M. Kaspi, and F. Camilo. XRay Observations of the High Magnetic Field Radio Pulsar PSR J18141744. *The Astrophysical Journal*, 535(1):379–384, 2000. ISSN 0004-637X. doi:10.1086/308848.

H. J. Pletsch, L. Guillemot, B. Allen, et al. Discovery of nine gamma-ray pulsars in *Fermi* Large Area Telescope data using a new blind search method. *The Astrophysical Journal*, 744(2):105, 2012. ISSN 0004-637X. doi:10.1088/0004-637X/744/2/105.

P. Podsiadlowski, S. Rappaport, and E. D. Pfahl. Evolutionary Sequences for Low and IntermediateMass XRay Binaries. *The Astrophysical Journal*, 565(2):1107–1133, 2002. ISSN 0004-637X. doi:10.1086/324686.

M. V. Popov and B. Stappers. Statistical properties of giant pulses from the Crab pulsar. *Astronomy and Astrophysics*, 470(3):1003–1007, 2007. ISSN 0004-6361. doi:10.1051/0004-6361:20066589.

S. Portegies Zwart, E. P. J. van den Heuvel, J. van Leeuwen, and G. Nelemans. The formation of the eccentric-orbit millisecond pulsar J1903+0327 and the origin of single millisecond pulsars. *The Astrophysical Journal*, 734(1):55, 2011. ISSN 0004-637X. doi:10.1088/0004-637X/734/1/55.

S. M. Ransom. *New search techniques for binary pulsars*. Ph.D. thesis, Harvard University, 2001.

S. M. Ransom, C. Bassa, Z. Wang, A. Cumming, and V. M. Kaspi. Twenty Years of Searching for (and Finding) Globular Cluster Pulsars. In *AIP Conference Proceedings*, volume 983, pages 415–423. AIP, 2008. ISSN 0094243X. doi:10.1063/1.2900267.

S. M. Ransom, J. M. Cordes, and S. S. Eikenberry. A New Search Technique for Short Orbital Period Binary Pulsars. *The Astrophysical Journal*, 589(2):911–920, 2003. ISSN 0004-637X. doi:10.1086/374806.

S. M. Ransom, S. S. Eikenberry, and J. Middleditch. Fourier Techniques for Very Long Astrophysical Time-Series Analysis. *The Astronomical Journal*, 124(3):1788–1809, 2002. ISSN 00046256. doi:10.1086/342285.

S. M. Ransom, J. W. T. Hessels, I. H. Stairs, et al. Twenty-one millisecond pulsars in Terzan 5 using the Green Bank Telescope. *Science (New York, N.Y.)*, 307(5711):892–6, 2005. ISSN 1095-9203. doi:10.1126/science.1108632.

S. M. Ransom, P. S. Ray, F. Camilo, et al. Three millisecond pulsars in *Fermi* LAT unassociated bright sources. *The Astrophysical Journal*, 727(1):L16, 2011. ISSN 2041-8205. doi:10.1088/2041-8205/727/1/L16.

P. S. Ray, A. A. Abdo, D. Parent, et al. Radio Searches of Fermi LAT Sources and Blind Search Pulsars. In *2011 Fermi Symposium proceedings*. 2012a.

P. S. Ray, A. A. Abdo, D. Parent, et al. Radio Searches of Fermi LAT Sources and Blind Search Pulsars: The Fermi Pulsar Search Consortium. 2012b.

P. S. Ray, M. Kerr, D. Parent, et al. Precise γ-ray timing and radio observations of 17 *Fermi* γ-ray pulsars. *The Astrophysical Journal Supplement Series*, 194(2):17, 2011. ISSN 0067-0049. doi:10.1088/0067-0049/194/2/17.

P. S. Ray and P. M. Saz Parkinson. Pulsar Results with the Fermi Large Area Telescope. In *High-Energy Emission from Pulsars and their Systems, Astrophysics and Space Science Proceeding*, page 21. 2011. doi:10.1007/978-3-642-17251-9_3.

B. J. Rickett. Radio Propagation Through the Turbulent Interstellar Plasma. *Annual Review of Astronomy and Astrophysics*, 28(1):561–605, 1990. ISSN 0066-4146. doi:10.1146/annurev.aa.28.090190.003021.

M. S. E. Roberts. New Black Widows and Redbacks in the Galactic. *arXiv:1103.0819v1*, 2011.

R. W. Romani and I.-A. Yadigaroglu. Gamma-ray pulsars: Emission zones and viewing geometries. *The Astrophysical Journal*, 438:314, 1995. ISSN 0004-637X. doi:10.1086/175076.

M. A. Ruderman and P. G. Sutherland. Theory of pulsars - Polar caps, sparks, and coherent microwave radiation. *The Astrophysical Journal*, 196:51, 1975. ISSN 0004-637X. doi:10.1086/153393.

R. E. Rutledge, D. B. Fox, and A. H. Shevchuk. Discovery of an Isolated Compact Object at High Galactic Latitude. *The Astrophysical Journal*, 672(2):1137–1143, 2008. ISSN 0004-637X. doi:10.1086/522667.

P. M. Saz Parkinson. Status and Prospects of Fermi LAT Pulsar Blind Searches. In *arXiv:1101.3096*, pages 48–51. 2011. doi:10.1063/1.3615074.

J. H. Seiradakis and D. A. Graham. A 21-cm search for periodicities in objects of special interest. *Astronomy and Astrophysics*, 85(3):353–355, 1980.

I. Shklovskii. Possible Causes of the Secular Increase in Pulsar Periods. *Soviet Astronomy*, 13:562, 1970.

M. S. Sipior, S. P. Zwart, and G. Nelemans. Recycled pulsars with black hole companions: the high-mass analogues of PSR B2303+46. *Monthly Notices of the Royal Astronomical Society*, 354(4):L49–L53, 2004. ISSN 0035-8711. doi:10.1111/j.1365-2966.2004.08373.x.

L. L. Smarr and R. Blandford. The binary pulsar - Physical processes, possible companions, and evolutionary histories. *The Astrophysical Journal*, 207:574, 1976. ISSN 0004-637X. doi:10.1086/154524.

R. Smits, D. R. Lorimer, M. Kramer, et al. Pulsar science with the Five hundred metre Aperture Spherical Telescope. *Astronomy and Astrophysics*, 505(2):919–926, 2009. ISSN 0004-6361. doi:10.1051/0004-6361/200911939.

V. Soglasnov. Amazing properties of giant pulses and the nature of pulsar's radio emission. *Proceedings of the 363. WE-Heracus Seminar on: "Neutron Stars and Pulsars"*, pages 68–71, 2007.

A. Spitkovsky. Electrodynamics of Pulsar Magnetospheres. *Young Neutron Stars and Their Environments, IAU Symposium*, 218:357, 2004.

A. Spitkovsky. High-Energy Emission from Pulsars and their Systems. pages 139–158, 2011. doi:10.1007/978-3-642-17251-9.

D. H. Staelin and E. C. Reifenstein. Pulsating Radio Sources near the Crab Nebula. *Science (New York, N.Y.)*, 162(3861):1481–3, 1968. ISSN 0036-8075. doi:10.1126/science.162.3861.1481.

I. Stairs, R. Manchester, A. Lyne, et al. PSR J1740-3052: a pulsar with a massive companion. *Monthly Notices of the Royal Astronomical Society*, 325(3):979–988, 2001. ISSN 0035-8711. doi:10.1046/j.1365-8711.2001.04447.x.

I. H. Stairs. Pulsars in binary systems: probing binary stellar evolution and general relativity. *Science (New York, N.Y.)*, 304(5670):547–52, 2004. ISSN 1095-9203. doi: 10.1126/science.1096986.

B. W. Stappers, M. Bailes, A. G. Lyne, et al. Probing the Eclipse Region of a Binary Millisecond Pulsar. *The Astrophysical Journal*, 465(2):L119–L122, 1996. ISSN 0004637X. doi:10.1086/310148.

G. H. Stokes, J. H. Taylor, J. M. Weisberg, and R. J. Dewey. A survey for short-period pulsars. *Nature*, 317(6040):787–788, 1985. ISSN 0028-0836. doi:10.1038/317787a0.

P. A. Sturrock. A Model of Pulsars. *The Astrophysical Journal*, 164:529, 1971. ISSN 0004-637X. doi:10.1086/150865.

T. M. Tauris. Spin-down of radio millisecond pulsars at genesis. *Science (New York, N.Y.)*, 335(6068):561–3, 2012. ISSN 1095-9203. doi:10.1126/science.1216355.

T. M. Tauris and E. P. J. van den Heuvel. Formation and Evolution of Compact Stellar X-ray Sources. In *Compact stellar X-ray sources*, pages 623–665. 2006.

J. Taylor. A sensitive method for detecting dispersed radio emission. *Astronomy and Astrophysics Supplement Series*, 1974.

J. H. Taylor and G. R. Huguenin. Two New Pulsating Radio Sources. *Nature*, 221(5183):816–817, 1969. ISSN 0028-0836. doi:10.1038/221816a0.

J. H. Taylor and R. N. Manchester. Galactic distribution and evolution of pulsars. *The Astrophysical Journal*, 215:885, 1977. ISSN 0004-637X. doi:10.1086/155426.

J. H. Taylor and J. M. Weisberg. Further experimental tests of relativistic gravity using the binary pulsar PSR 1913 + 16. *The Astrophysical Journal*, 345:434, 1989. ISSN 0004-637X. doi:10.1086/167917.

C. Thompson and R. C. Duncan. Neutron star dynamos and the origins of pulsar magnetism. *The Astrophysical Journal*, 408:194, 1993. ISSN 0004-637X. doi:10.1086/172580.

D. J. Thompson. Gamma ray astrophysics: the EGRET results. *Reports on Progress in Physics*, 71(11):116901, 2008. ISSN 0034-4885. doi:10.1088/0034-4885/71/11/116901.

A. N. Timokhin. A model for nulling and mode changing in pulsars. *Monthly Notices of the Royal Astronomical Society: Letters*, 408(1):L41–L45, 2010. ISSN 17453925. doi:10.1111/j.1745-3933.2010.00924.x.

R. C. Tolman. Static Solutions of Einstein's Field Equations for Spheres of Fluid. *Physical Review*, 55(4):364–373, 1939. ISSN 0031-899X. doi:10.1103/PhysRev.55.364.

R. Turolla. Isolated Neutron Stars : The Challenge of Simplicity. 2009. doi:10.1007/978-3-540-76965-1_7.

A. J. Turtle and A. E. Vaughan. Discovery of Two Southern Pulsars. *Nature*, 219(5155):689–690, 1968. ISSN 0028-0836. doi:10.1038/219689a0.

H. Umeda, K. Nomoto, S. Tsuruta, T. Muto, and T. Tatsumi. Neutron star cooling and pion condensation. *The Astrophysical Journal*, 431:309, 1994. ISSN 0004-637X. doi:10.1086/174487.

E. P. J. van den Heuvel. Late stages of close binary systems. In *Structure and Evolution of Close Binary Systems, IAU Symposium*, page 35. 1976.

J. Vasseur, J. Paul, B. Parlier, et al. Possible pulsed gamma ray emission above 50 MeV from the Crab pulsar. *Nature*, 226(5245):534–5, 1970. ISSN 0028-0836. doi:10.1038/226534a0.

A. E. Vaughan and M. I. Large. Five New Pulsars. *Nature*, 225(5228):167–168, 1970. ISSN 0028-0836. doi:10.1038/225167a0.

A. E. Vaughan and M. I. Large. Discovery of three pulsars. *Monthly Notices of the Royal Astronomical Society*, 156:27, 1972.

C. Venter, A. K. Harding, and L. Guillemot. Probing millisecond pulsar emission geometry using light curves from the *Fermi* Large Area Telescope. *The Astrophysical Journal*, 707(1):800–822, 2009. ISSN 0004-637X. doi:10.1088/0004-637X/707/1/800.

J. P. W. Verbiest, M. Bailes, W. A. Coles, et al. Timing stability of millisecond pulsars and prospects for gravitational-wave detection. *Monthly Notices of the Royal Astronomical Society*, 400(2):951–968, 2009. ISSN 00358711. doi:10.1111/j.1365-2966.2009.15508.x.

J. P. W. Verbiest, M. Bailes, W. van Straten, et al. Precision Timing of PSR J04374715: An Accurate Pulsar Distance, a High Pulsar Mass, and a Limit on the Variation of Newtons Gravitational Constant. *The Astrophysical Journal*, 679(1):675–680, 2008. ISSN 0004-637X. doi:10.1086/529576.

J. P. W. Verbiest, J. M. Weisberg, a. a. Chael, K. J. Lee, and D. R. Lorimer. On pulsar distanve measurements and their uncertainties. *The Astrophysical Journal*, 755(1):39, 2012. ISSN 0004-637X. doi:10.1088/0004-637X/755/1/39.

W. Voges and B. Aschenbach. The ROSAT all-sky survey bright source catalogue. *Astronomy and Astrophysics*, 349:389–405, 1999.

R. Voss and T. M. Tauris. Galactic distribution of merging neutron stars and black holes - prospects for short gamma-ray burst progenitors and LIGO/VIRGO. *Monthly Notices of the Royal Astronomical Society*, 342(4):1169–1184, 2003. ISSN 0035-8711. doi:10.1046/j.1365-8711.2003.06616.x.

K. P. Watters, R. W. Romani, P. Weltevrede, and S. Johnston. An atlas for interpreting γ-ray pulsar light curves. *The Astrophysical Journal*, 695(2):1289–1301, 2009. ISSN 0004-637X. doi:10.1088/0004-637X/695/2/1289.

J. M. Weisberg and J. H. Taylor. General Relativistic Geodetic Spin Precession in Binary Pulsar B1913+16: Mapping the Emission Beam in Two Dimensions. *The Astrophysical Journal*, 576(2):942–949, 2002. ISSN 0004-637X. doi:10.1086/341803.

L. Weliachew, E. B. Fomalont, and E. W. Greisen. Radio observations of H I and OH in the center of the galaxy M 82. *Astronomy and Astrophysics*, 137:335–342, 1984.

P. Weltevrede, R. T. Edwards, and B. W. Stappers. The subpulse modulation properties of pulsars at 21 cm. *Astronomy and Astrophysics*, 445(1):243–272, 2006. ISSN 0004-6361. doi:10.1051/0004-6361:20053088.

P. M. Woods and C. Thompson. Soft Gamma Repeaters and Anomalous X-ray Pulsars : Magnetar Candidates. In *Compact stellar X-ray sources*, pages 547 – 586. 2006.

J.-W. Xu, X.-Z. Zhang, and J.-L. Han. Statistics of Galactic Supernova Remnants. *Chinese Journal of Astronomy and Astrophysics*, 5(2):165–174, 2005. ISSN 1009-9271. doi:10.1088/1009-9271/5/2/007.

D. R. B. Yardley, W. A. Coles, G. B. Hobbs, et al. On detection of the stochastic gravitational-wave background using the Parkes pulsar timing array. *Monthly Notices of the Royal Astronomical Society*, 414(2):1777–1787, 2011. ISSN 00358711. doi: 10.1111/j.1365-2966.2011.18517.x.

K. Yoshita, E. Miyata, and H. Tsunemi. Discovery of a New Supernova Remnant in the Direction of G69.7+1.0. *Publications of the Astronomical Society of Japan*, 52:867–873, 2000.

S. Zane, F. Haberl, G. L. Israel, et al. Discovery of 59 ms pulsations from 1RXS J141256.0+792204 (Calvera). *Monthly Notices of the Royal Astronomical Society*, 410(4):2428–2445, 2011. ISSN 00358711. doi:10.1111/j.1365-2966.2010.17619.x.

C. M. Zhang, J. Wang, Y. H. Zhao, et al. Study of measured pulsar masses and their possible conclusions. *Astronomy and Astrophysics*, 527:A83, 2011. ISSN 0004-6361. doi:10.1051/0004-6361/201015532.

Erklärung

Ich versichere, daß ich die von mir vorgelegte Dissertation selbständig angefertigt, die benutzten Quellen und Hilfsmittel vollständig angegeben und die Stellen der Arbeit - einschlielich Tabellen, Karten und Abbildungen -, die anderen Werken im Wortlaut oder dem Sinn nach entnommen sind, in jedem Einzelfall als Entlehnung kenntlich gemacht habe; da diese Dissertation noch keiner anderen Fakultät oder Universität zur Prfung vorgelegen hat; daß sie noch nicht verffentlicht worden ist sowie, da ich eine solche Veröffentlichung vor Abschluß des Promotionsverfahrens nicht vornehmen werde. Die Bestimmungen dieser Promotionsordnung sind mir bekannt. Die von mir vorgelegte Dissertation ist von Prof. Dr. Michael Kramer betreut worden.

Unterschrift: _____

Datum: _____

Publications

Refereed:

- H. J. Pletsch, L. Guillemot, B. Allen, M. Kramer, C. Aulbert, H. Fehrmann, P. S. Ray, **E. D. Barr**, A. Belfiore, F. Camilo, P. A. Caraveo, Ö. Çelik, D. J. Champion, M. Dormody, R. P. Eatough, E. C. Ferrara, P. C. C. Freire, J. W. T. Hessels, M. Keith, M. Kerr, A. de Luca, A. G. Lyne, M. Marelli, M. A. McLaughlin, D. Parent, S. M. Ransom, M. Razzano, W. Reich, P. M. Saz Parkinson, B. W. Stappers, M. T. Wolff
  "Discovery of Nine Gamma-Ray Pulsars in Fermi Large Area Telescope Data Using a New Blind Search Method"
  The Astrophysical Journal, 744, 2, 105.

- S. Zane, F. Haberl, G. L. Israel, A. Pellizzoni, M. Burgay, R. P. Mignani, R. Turolla, A. Possenti, P. Esposito, D. J. Champion, R. P. Eatough, **E. D. Barr**, M. Kramer
  "Discovery of 59 ms pulsations from 1RXS J141256.0+792204 (Calvera)"
  MNRAS, 410, 4, 2428-2445.

Non-refereed:

- **E. Barr**
  "The Northern-sky High Time Resolution Universe Pulsar Survey"
  AIP Conference Proceedings, 1357, 52.

- C. Ng, **E. Barr**
  "Enabling PTAs for gravitational wave detection: The all-sky HTRU pulsar survey"
  Proceedings of the 25th Texas Symposium on Relativistic Astrophysics. Published online at `http://pos.sissa.it/cgi-bin/reader/conf.cgi?confid=123`, id.66.

In preparation/under review:

- **E. D. Barr**, L. Guillemot, D. J. Champion, M. Kramer, R. P. Eatough, K. J. Lee, J. P. W. Verbiest, C. G. Bassa, F. Camilo, O. Celik, I. Cognard, E. C. Ferrara, P. C. C. Freire, G. H. Janssen, S. Johnston, M. Keith, A. G. Lyne, P. F. Michelson,

P. M. Saz Parkinson, S. M. Ransom, P. S. Ray, B. W. Stappers, K. S. Wood
"Pulsar Searches of Fermi Unassociated Sources with the Effelsberg Telescope"
Submitted to MNRAS, 2012.

- **E. D. Barr**, D. J. Champion, M. Kramer, R. P. Eatough, P. C. C. Freire, R. Karuppusamy, K. J. Lee, A. G. Lyne, B. Stappers, J. P. W. Verbiest
"The Northern High Time Resolution Universe Pulsar Survey I: Initial setup and discoveries"
To be submitted to MNRAS, 2012.

- **E. D. Barr**, P. C. C. Freire, T. M. Tauris, D. J. Champion, M. Kramer, A. G. Lyne, B. Stappers
"A millisecond pulsar formed in a hierarchical triple?"
To be submitted to MNRAS, 2012.